Optimizing Oil Production in Horizontal Wells

(Water/Oil Cresting in Horizontal Wells)

Hector Ngozi Akangbou

(*B.Eng., MSc.*)

School of Computing Science and Engineering

Petroleum Technology and Spray Research Groups

University of Salford

Salford, UK

Submitted in Partial Fulfilment of the Requirements of the
Degree of Doctor of Philosophy, April 2017

TABLE OF CONTENT

LIST OF FIGURES

LIST OF TABLES

JOURNAL PUBLICATIONS

(See Appendix-A)

1. **Akangbou, H. N., Burby, M. and Nasr, G.** Effectively Optimizing Production of Horizontal Wells in Oil Reservoirs. Journal of Petroleum Science and Engineering, **Elsevier.** DOI: http://dx.doi.org/10.1016/j.petrol.2016.12.005.

2. **Akangbou, H. N., Burby, M. and Nasr, G.** Proactive Control of Cresting in Homogeneous Oil Reservoirs. Journal of Petroleum Science. **Springer.** DOI: 10.1007/s12182-017-0167-0.

3. **Akangbou, H. N.**, Burby, M and Ghasem, G., Babaie, M. Effect of impermeable barrier orientation on bottom water cresting. Journal of Engineering Technology. **American Society for Engineering Education (ASEE), Thomson Reuters**.

4. **Akangbou, H. N., Burby, M. and Nasr, G.** Water/oil cresting in horizontal well, A sensitivity Study. International Journal of Oil, Gas and Coal Technology. **Inderscience publishers.** (in press).

ACKNOWLEDGEMENT

xi

DECLARATION

"I HECTOR NGOZI AKANGBOU, declare that this thesis is submitted in fulfilment of the requirements for the degree of Ph.D. at the University of Salford. The work presented in this thesis is my own work. Any work from publications copied in the form of words or phrases in this thesis have been referenced at the point of use and properly referenced at the reference section".

Mr Hector Ngozi Akangbou

Supervisors:

………………………………

Dr Martin Burby

&

……………………………..

Prof. Ghasem G. Nasr

NOMENCLATURE

A – Area (cm^2 or m^2)

$AWACT$ – Anti-Water Coning Technology

BOP – Blow Out Preventer

CFD – Computational Fluid Dynamics

C_p – Specific heat (J/kgs)

cP – Centipoise

CT – Computed Tomography

C_2 – inertia loss coefficient

d – Density / Diameter

D – Dimension / Darcy

D_p – Mean particle diameter (m)

DWL – Downhole Water Loop

DWS – Downhole Water Sink

EOR – Enhanced Oil Recovery

E – Exponential (where, E-$1 = 0.1$, E-$2 = 0.01$, E+$2 = 10^2$ etecetera)

F – Force / Fahrenheit

FS - Full scale

FSD – Full Scale Deflection

GOC – Gas -Oil-Contact

GOR – Gas-Oil-Ratio

h_d – horizontal displacement of inclined section

HD – Horizontal displacement of well

h_T – Total fluid height in reservoir

H_r, y – Height

h_w – Height of bottom water

Hz – Hertz

ICD – Inflow Control Devices

$IGES$ – Initial Graphics Exchange Specification file

J - Joules

KOP – Kick off point

k – Effective permeability

K – Thermal conductivity

kV – Kilo volts

$k\text{-}\varepsilon$ - K-epsilon

LH – Length of horizontal section (subscripts 1 and 2 depicts case 1 and 2 respectively)

LR – Long radius

l_r – Length of lateral in reservoir

MD – Measured depth

MWD – Measurement While Drilling

MR –Medium radius

$OOIP$ – Original Oil In Place

PET – Polyethylene tetra phthalate

PIV – Particle Image Velocimetry

$PMMA$ – Poly (methyl methacrylate)

Psi – Pound square inch

$Psig$ – Pound square inch gauge

Q – Volumetric flow rate

q_T – Total fluid rate

Re – Reynold number

ROI – Region Of Interest

RPM – Revolution Per Minute

R_v – Viscous resistance

SG – Specific Gravity

SR – Short radius

$STEP$ – Standard for Exchange of Product

TVD – True vertical depth

u - Velocity

USB – Universal Serial Bus

V_d – Vertical displacement of bend

WOC – Water- Oil-Contact

WOR – Water-Oil-Ratio

w_1, - Well case 1

w_2, - Well case 2

x – horizontal length of reservoir

$\propto$ - permeability in Ergun's Equation

ε - void in Ergun's Equation

δ - Kronecker delta function

θ – Theta

ρ – density

μ – Viscosity

q^* - Heat flux

^oC – Celsius

CONVERSION TABLES

In the oil and gas industry, measurements are usually made in imperial units, however the SI unit system of measurement was applied although the imperial unit was used where necessary. The conversion factors for the units used in this thesis are listed below.

Length

1 m = 100 cm

1 Foot = 30.48 cm

1 Inch = 2.54 cm

Pressure

1 bar = 14.50 Psi = 0.986923 atm.

1 Psi = 0.068046 atm.

1 atm = 101325 pascals

Flow rate

1 cm^3/s = 1 ml/s

I ton/s = 1000 Kg/s

1 cm^3/min = 0.0000167 L/s

1 m^3/s = 1000000 cm^3

Effective permeability

1 D = 1000 millidarcy (mD)

ABSTRACT

In recent years, the application of horizontal wells has been predominant in minimizing cresting scenarios due to significant reservoir exposure of its laterals. Cresting is known to occur in horizontal wells when the pressure drop supersedes the hydrostatic pressure existing between the phases in a typical reservoir. Cresting poses problems such as uneconomic oil production rates due to increasing volumes of effluent(s) (unwanted water and or gas) produced with oil over time as well as the overall recovery efficiency of oil reservoirs.

Production optimization from crest-affected thick- and thin-oil rim homogeneous reservoirs were investigated experimentally by considering the effect of varying the inclined sections of a horizontal well at low angles of inclination (15°-30°), initial surface pressures (-4.351Psig), lateral length in reservoir (l_r, = 0.305 m) and oil viscosity (50 cP) on oil recovery, oil produced and cumulative water produced during cresting. A strong bottom aquifer and considerable gas cap were modeled at constant bottom water injection rate of 41.68 cm^3/s and at atmospheric pressure (14.7 Psi) respectively. An experimental proactive cresting control technique based on reservoir wettability, gravity segregation and effluent(s) breakthrough times were investigated for cresting control in thick- and thin-oil rim homogeneous reservoirs, using an electromagnetic valve installation. Numerical simulations were considered using Particle Image Velocimetry (PIV) to the determine the velocity of captured water cresting images and Computational Fluid Dynamics (CFD) to validate the oil withdrawal rate, Gas-Oil-Contact (GOC) and Water-Oil-Contact (WOC) by applying boundary conditions from the physical model.

From results of varying the inclined section of the horizontal well, the Short radius wells with 30° angle of inclination and ratio of vertical displacement of the inclined section to reservoir height (V_d/H_r) of 0.079 resulted in 177.75 cm^3 increment in oil recovered and reduction in cumulative water produced (258 cm^3) at a production time of 300 s in thick-oil rim reservoirs while 250 cm^3 increment in oil was observed with 356 cm^3 reduction in cumulative water produced at a production time of 495 s in thick-oil rim reservoirs with V_d/H_r, 0.063. Further increment of 108.91 cm^3 in oil produced and reduction in cumulative water produced (183.99 cm^3), was observed when cresting was controlled proactively in thick-oil rim reservoirs. From varying the inclined section of the horizontal well, increment in oil produced of 163 cm^3 and 134 cm^3 cumulative reduction in produced water were observed at V_d/H_r equals 0.079 in thin-oil rim reservoirs at a simulation time of 210 s while a lower oil increment of 6.84 cm^3 and cumulative water reduction of 10.98 cm^3 were observed in thin-oil rim reservoirs when controlled proactively. The over predicted quantitative results as high as 75.06% using the CFD model compared with experimental data were due to two-dimensional (2D) model limitations in porous media as well as the corresponding grain sizes. To exemplify, for WOC the predicted results was about 28.56% compared to experimental data at 4.5 s. The average velocity profile from PIV analysis increased steadily from 0.113 to 2.08E-15 m/s from 10 to 90 s.

CHAPTER-1

INTRODUCTION

1.1   Introduction

Cresting in horizontal wells or coning in vertical wells, is regarded as the insurgence of effluent(s) (water and or gas) through the perforation of the well, which is produced together with oil from an oil reservoir. One major cause of cresting is pressure drawdown imposed on the reservoir. In view of this, the vertical wells are produced with relatively high drawdown pressure to produce oil at commercial quantities and this has shown to manifest in high pressure around the wellbore area, thus increase the chances of coning in reservoirs susceptible to coning. In the quest to minimize the effect of coning and obviously enhance oil recovery, numerous unsuccessful oilfield methods have been proposed such as operating the production rate below a certain rate called the "critical rate" (production rate below which water-free oil can be produced), completing the well far above the Water-Oil-Contact (WOC) " interface of water and oil" and Gas-Oil-Contact (GOC) "interface between gas and oil" as possible, wellbore plugging with cement, and the creation of an artificial water barrier by injecting a crosslinking polymer or gel around the wellbore area.

The success story started with the development and application of horizontal well technology in the late 1980s to minimize cresting in both strong gas cap and bottom aquifer reservoirs susceptible to cresting by minimizing the pressure drawdown and yet maintain an economical oil production rates with a higher critical rate than in a vertical well. This is due to more reservoir exposure of horizontal well lateral, resulting in a lower pressure drop at same withdrawal rate compared to vertical wells which effectively delays cresting occurrence (Al Zarafi, 1993, Chen, 1993, Coffin, 1993, Murphy, 1990, Sherrard et al., 1987) but not preventing it.

In all cases, horizontal drilling technique involves development of a reservoir by drilling through into its extensive lateral dimension ensuring significant reservoir contact with the wellbore whereas in the vertical well, the wellbore dissects the reservoir bedding plane in a perpendicular manner, thus reservoir contact with the wellbore is limited by its effective thickness. The former is the topic of interest in this study because of the interest it has

generated in the industry today due to its variety of application. On average, a typical horizontal well is costlier and technically demanding to drill than a vertical well. However, the use of horizontal well in reservoir development has been widely accepted all over the world in recent times (Schevchenko, 2013). Horizontal wells allow access to unconventional reservoirs from different angles for optimum productivity and increased reserves, a feature not obtainable in conventional technology such as delay in water and gas coning (Schevchenko, 2013, Nurmi et al., 1995). As the average cost of constructing horizontal well is reducing the use of more sophisticated and tailored technology such as drilling and completions with coiled tubing and slim holes, there is going to be increased opportunities and acceptability of horizontal drilling. The advantages of horizontal well in development of the following reservoirs cannot be over–emphasized (Nurmi et al., 1995);

- Thin-oil rim Reservoir: a vertical well drilled into such a formation is limited by the thickness of the reservoir unlike a horizontal well placed in alike reservoir (Nurmi et al., 1995), which offer more reservoir contact for optimum drainage (Schevchenko, 2013).

- Reservoir with natural fractures: natural fractures in the reservoir occur in the direction perpendicular to the maximum stress caused by the overburden, if a horizontal well is drilled to cut across the open planes of these fractures, it provides an effective channel for reservoir communication which enhances crude oil recovery. However, misjudgement of orientation of these fracture planes could lead to early water production in the well, this underscores the importance of sound reservoir model.

- Reservoir susceptible to water and/or gas coning: fluid flow pattern in reservoirs is maximized by the using of horizontal well to delay either water and/or gas coning in oil fields but in case of high vertical permeability due to fracture planes, selective completion techniques are employed to case off unwanted zones. Pressure gradients in the wellbore area are reduced, hence significant amount of oil is evacuated before the onset of water or gas. This is one of the main advantages of horizontal wells over vertical wells.

- Lateral heterogeneous reservoirs: the issues associated with heterogeneity in vertical wells are virtually solved with horizontal wells. Horizontal wells are preferable in

draining homogeneous anisotropic reservoirs due to the presence of horizontal permeability. It can be used to produce multiple thin isolated reservoirs, which could have been uneconomical to produce independently. It offers more lateral reservoir exposure for logging thus revealing internal reservoir structure.

Regardless of the advantages of this kind of wells, the horizontal wells experience high influx of water after breakthrough (Inikori, 2002) as well as higher pressure drop as a result of frictional loss along the tubing in the horizontal well when compared to a vertical well involving a viscous oil (Schevchenko, 2013). However, more oil production is usually observed from the heel of a horizontal well with low-pressure drawdown in the horizontal section (Ratterman, 2006). This results in early cresting of water and gas towards this section of the horizontal well and this influx is greatly affected by the degree of permeability variation; causing an acceleration in early water breakthrough as well as uneven down hole inflow (Schevchenko, 2013, Halliburton, 2008). These conditions could result in an adverse effect on the sweep efficiency and reduction in hydrocarbon recovery from horizontal wells with some left over oil in the reservoir (Schlumberger, 2010).

1.2 Research contribution

This experimental study provides an in-depth procedure and findings on the effect of varying the inclined section of the horizontal well. The investigation also used electromagnetic valve to proactively control cresting effect while improving oil production and reducing the production of effluent (unwanted water).

1.3 Overall aims

The aims of the research are to:

1. Develop an experimental procedure for simulating inclined or deviated wells.

2. Model experimentally water and gas cresting occurring simultaneously in thin-oil rim and thick-oil rim homogeneous reservoirs.

3. Develop experimental techniques for optimizing oil production from homogeneous oil reservoirs with considerable gas cresting and strong bottom cresting problems in horizontal wells, using electromagnetic valve.

1.4 Objectives

The objectives of the research are to:

1. To construct physical horizontal well apparatus with varying horizontal and vertical displacements of the inclined section, at low angles of inclination.

2. To utilise the constructed horizontal well apparatus to investigate its effect on oil recovery, oil produced and cumulative water produced in thin- and thick-oil rim reservoirs

3. To devise an experimental proactive cresting control technique in horizontal well via electromagnetic valve.

1.5 Thesis outline

The thesis consists of six chapters covering:

- **Chapter 2** presents a survey of literatures. This chapter covers the definition, brief history and classification of horizontal wells geometry. The basic phases in drilling and constructing a typical horizontal well are also presented. The problems associated with reservoirs affected by cresting problems are also covered.

- **Chapter 3** gives a detailed description of the water and gas-cresting rig apparatus and set up. All measurements and tests including effective permeability test for all phases involved and total porosity of the reservoir are presented. The procedure for the rig operation is highlighted. Finally, proactive cresting control mechanisms for higher oil recovery and oil produced are discussed for thin- and thick-oil rim reservoirs.

- **Chapter 4** provides an elaborate and precise discussion of results and findings from this study.

- **Chapter 5** is the numerical modeling of water and gas cresting using the commercial ANSYS-CFD package, for validation of experimental data. The procedure and setting in modeling cresting is presented. Water-cresting velocity was evaluated by processing images obtained from video recording of the cresting process using PIV.

- **Chapter 6** is a summary of the presented work in this study. The main contributions are also highlighted with recommendations for future work.

CHAPTER-2

LITERATURE REVIEW

2.1　Overview

The reasons for the choice of horizontal well in development of isotropic reservoir was enumerated for which the cardinal objective is to create more reservoir contact with the wellbore for enhanced productivity and reduction or delay of bottom water cresting or overlying gas cresting for maximum oil recovery (Peng and Yeh, 1995) before Enhanced Oil Recovery (EOR) is adopted as usually the case. For this, horizontal well was found to perform better than vertical well in a homogeneous medium. Stage by stage process of developing a reservoir using horizontal technology is presented for general knowledge with the view of making an informed choice based on friability, homogeneity and cresting potential of the reservoir rocks. Furthermore, various literatures which have discussed water or gas cresting/coning or where both occurred together were examined and presented herein to gain an insight into coning/cresting development, from the initial rise of bottom water and/or gas cap from the GOC and WOC through to the maximum water and/or gas cone/crest height before hitting the bottom or top of the well and eventual entry into the wellbore of the horizontal well.

2.2　Definition of horizontal well

Horizontal wells illustrated in Figure 2-1 can be seen as an exaggerated "J" shape (Curtis 2011). A widely accepted definition of a horizontal well is yet to be seen in literature, however, the quote below seems more suitable in describing the peculiar features of a horizontal well. "Horizontal drilling is the process of drilling and completing production of a well that begins as a vertical or inclined linear bore which extends from the surface to a subsurface location just above the target oil and gas reservoir called the "kick-off point," then bears off on an arc to intersect the reservoir, at the "entry point," and, thereafter, continues to a near-horizontal attitude tangent to the arc, to substantially or entirely remain within the reservoir until the desired bottom location is reached" (EIA, 1993).
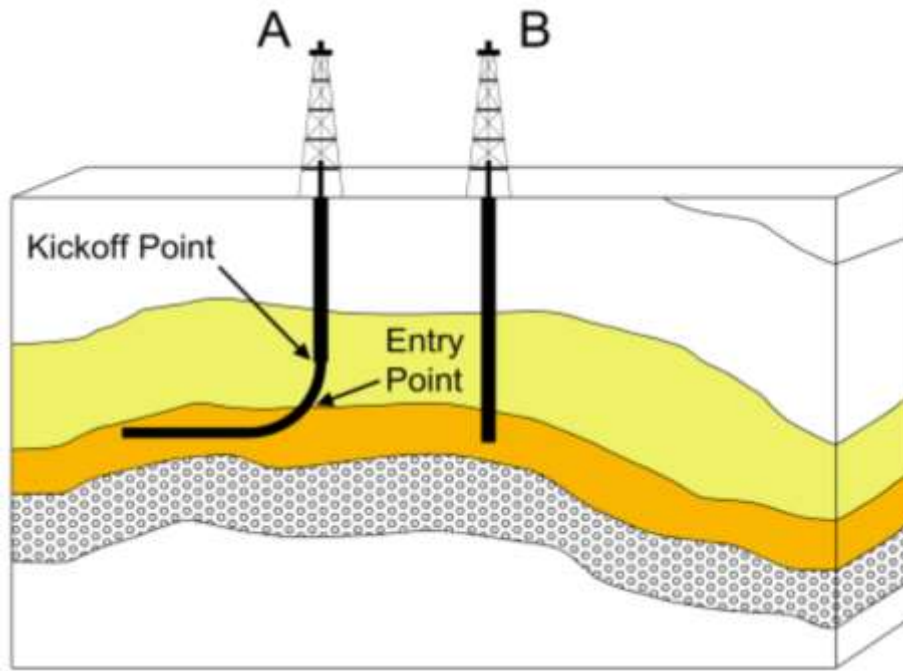
Figure 2-1: Typical shape of horizontal well (A) (EIA, 1993)

Since most reservoir have extensive lateral dimensions than vertical dimensions, it makes much sense to make a horizontal wellbore into the reservoir parallel to its area of extensive dimension for optimum contact (as shown in Figure 2-1) with reservoir compartments than would have been possible with conventional vertical wells. The objective of this is to exploit some specific physical properties of the reservoir for effective reservoir drainage.

2.3 Brief history of horizontal wells

The idea of horizontal wells is very ancient. Over 2000 years ago, the earliest horizontal well was drilled in the form of horizontal ground water wells in Iran (Figure 2-2) to increase water production. In the western dessert of Egypt, more than 2500 years ago, this similar technique was used to increase flow from the fractured Nubian sandstone (Jubralla et al., 1995, Samuel and Gao, 2007).
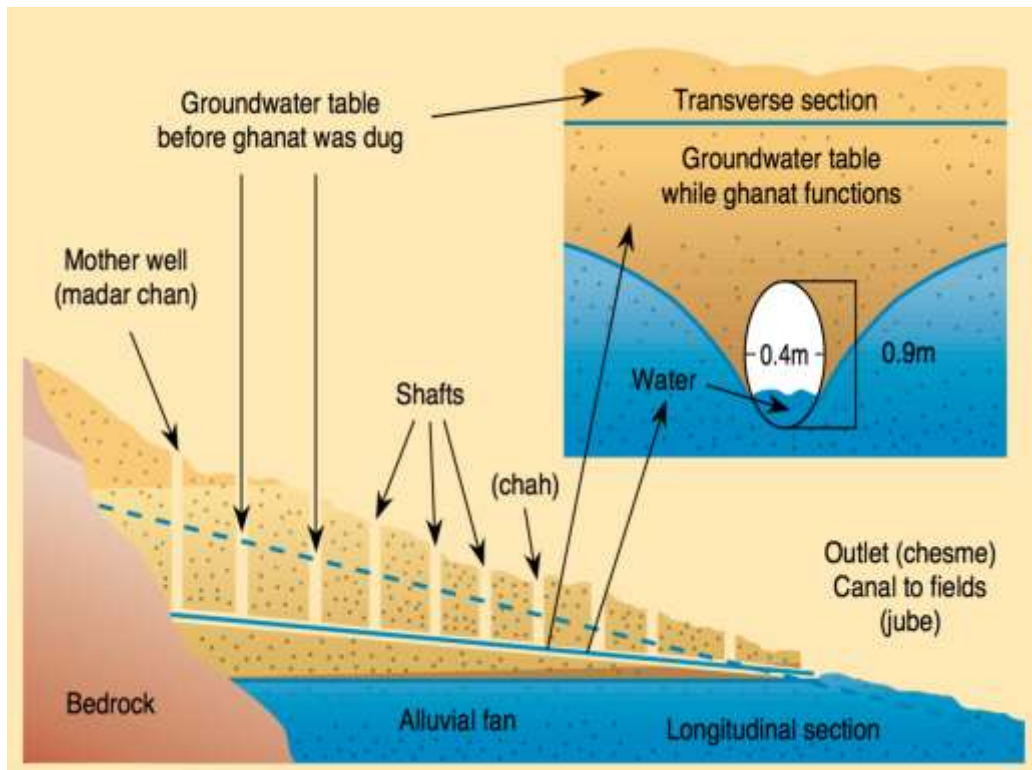
Figure 2-2: History of water production using Horizontal wells (Jubralla et al., 1995)

In the 1920s, the first United States patent for horizontal wells was issued, although the modern concept of the short-radius drilling, can be traced as far as 1891, when John Smalley Campbell was issued the first United States patent (Patent Number 459,152) for the use of flexible shafts to rotate drilling bits (EIA, 1993). In 1929, the horizontal well drilled near Texon, Texas was the first of its kind to be recorded (EIA, 1993, Curtis, 2011). In 1957, China exploited this technology, after it was drilled by the soviet union in 1944 in the Franklin Heavy Oil field, Venango county, Pennsylvania, 500 feet in depth (EIA, 1993, Yost et al., 1987). Due to technology limitations in the early 19th century, few horizontal wells were drilled and completed (Peng and Yeh, 1995). However, in the mid-1980s, horizontal wells were considered economically viable as a result of advancements in directional drilling, Measurement While Drilling (MWD) survey and other drilling and completion technologies (Peng and Yeh, 1995)

Commercialization of horizontal wells began in the early 1980s, with tests carried out between 1980 and 1983 by Elf Aquitaine. Four horizontal wells were known to be drilled in European fields, Two wells in the Lacq Superieur Oil Field and one Castera Lou Oil Field both located in Southern France while and the fourth was drilled in the Rospo Mare Oil Field located in Italy (EIA, 1993). British Petroleum undertook early production in the

7

Alaska Prudhoe Field in a successful attempt to minimize effluents (water and gas) insurgence into the Sadlerochit reservoir. Due to the successful commercialization of this technology, this has led to its domestic application in over 50 offshore areas mainly applied to crude oil in the United States. In 1990, many horizontal wells greater than 1000 were drilled worldwide, 850 of them were targeted at Texas' Upper Cretaceous Austin Chalk Formation alone. As low as 1 percent of the domestic horizontal wells drilled were completed for gas, as compared to 45.3 percent of all successful wells (oil plus gas) drilled. A fraction of 0.062 out of 0.547 of all successful wells completed for oil was horizontal wells. Through the 20th century, well over 20,000 horizontal wells have been drilled in 69 countries (Figure 2-3), with most of the horizontal wells drilled in the United states (10,966) and seconded by Canada.
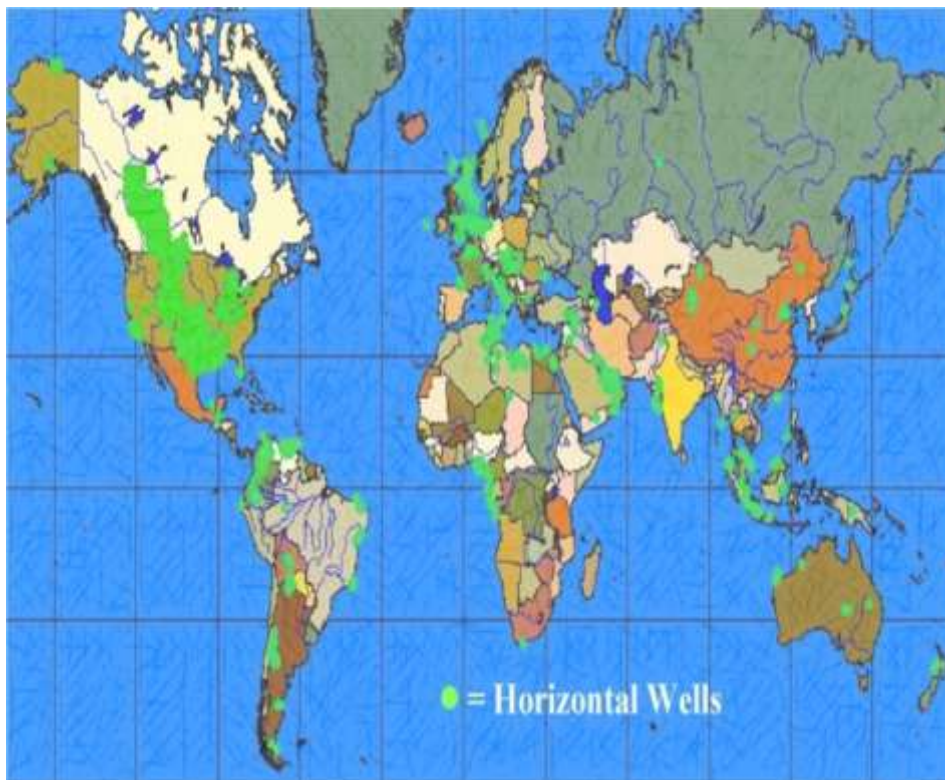
Figure 2-3: Drilled horizontal wells worldwide (Carr and Gerlach, 2001)

2.4   Basic Phases in Drilling or Constructing Horizontal Wells

The various stages in drilling or constructing a standard horizontal well is described by Chesapeake-Energy (2011) and is below:

At the initial stage, the drilling site is prepared to meet all the required standards of health and safety. A heavy duty industrial drill bit is then mounted at the end of drill pipe, as the

bit grinds away a mixture of water and chemicals called mud is pumped into the hole to cool the bit and flush the cuttings to the surface. The drill bit and steel casing used at this stage is the largest in terms of diameter. This hole is drilled for the first 50-80ft prior to cementing the conductor casing. The importance of this conductor casing is for ground stability around the drilling rig and wellhead as well as isolating the well from water wells if present. The mud also clips on the wellbore, keeping it intact. Similar to drilling a vertical well the horizontal well is drilled to just under the deepest fresh water zone (1000-1200ft in measured depth). The drill pipe and bit are then withdrawn (Figure 2-4) and stored for future use.
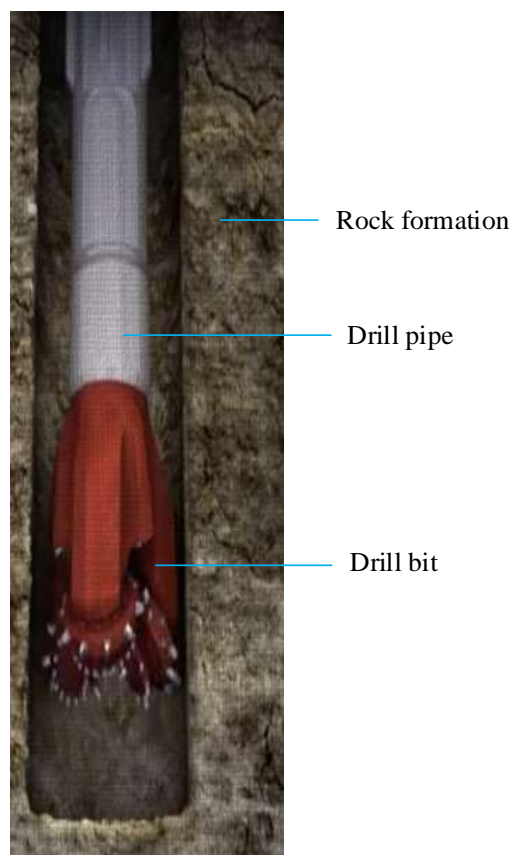
Figure 2-4: Drill bit in rock formation (Chesapeake-Energy, 2011)

Surface casing "a second layer of steel casing" is inserted into the drilled hole through the conductor casing to isolate the fresh water zone and also serves as a foundation for the Blow Out Preventer (BOP) "a set of high-pressure safety valves and seals attached to the top of the casing that protects the well pressure and prevents surface releases" and to protect well integrity. Cement is then pumped down the casing and out through the opening from the shoe at the bottom of the casing, as illustrated in Figure 2-5. It is then forced up between the

casing and the hole, sealing off the wellbore from the fresh water. The cementing process prevents any further contamination of the fresh water aquifer. The BOP is usually installed after the surface casing has been properly cemented. A small diameter sized casing and bit are lowered down the hole to drill through the plug and cement and continue the vertical section of the well to the natural gas target area but above the planned horizontal leg.

Drilling below the surface casing involves the use of drilling mud (synthetic thickeners). The drilling mud helps to lift the rock cuttings to the surface, stabilize the drilling hole, cool the drill bit and control downhole pressure. Up to this point the process is the same as drilling a vertical well. At this point a pressure transient test to obtain as much information about the reservoir can be performed (Peng and Yeh, 1995).
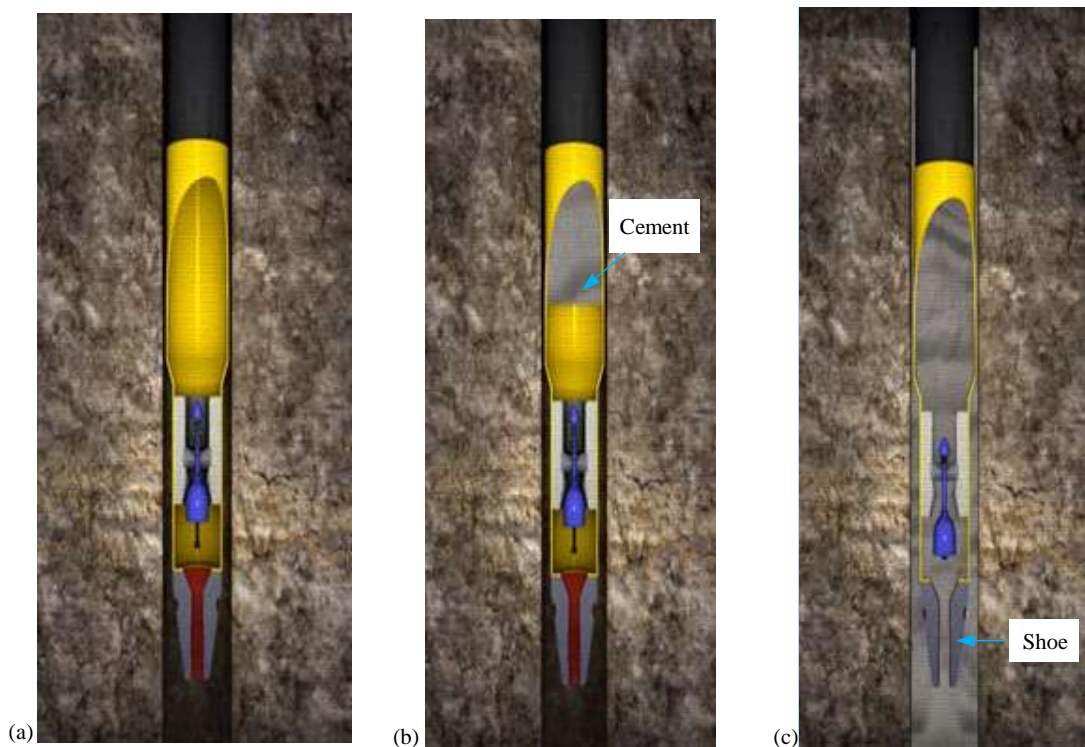
Figure 2-5: Illustration of cement pumped through the shoe (Chesapeake-Energy, 2011)

The pipe and bit are again pulled out of the hole and a down hole motor with MWD instrument is lowered back into the hole to begin the angle building process (Figure 2-6). The distance to make a curve from the top to where the well becomes horizontal is just under a quarter of a mile.
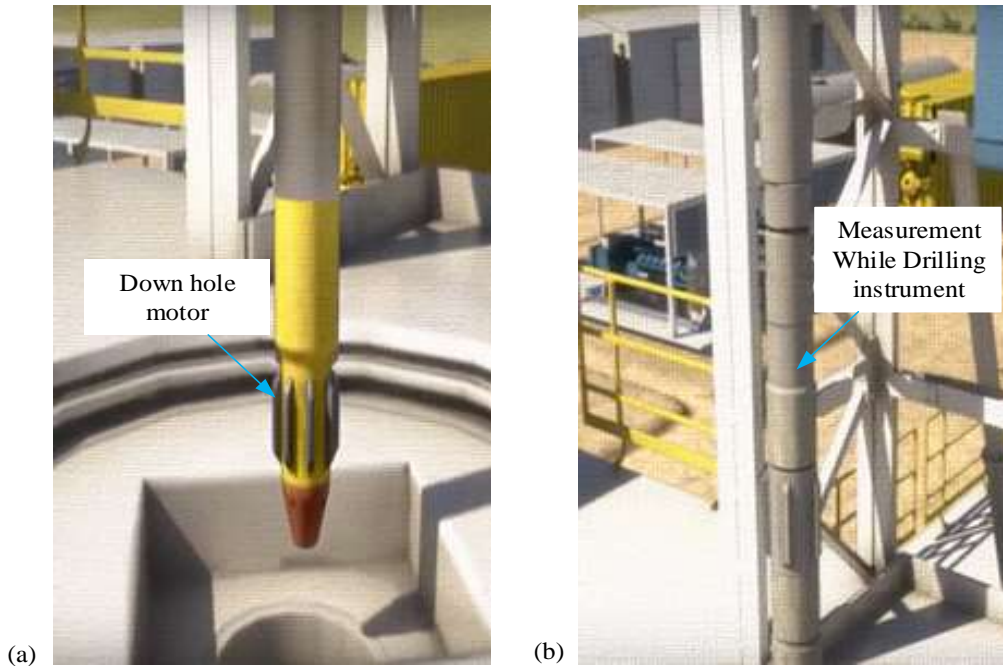
Figure 2-6: (a) Downhole motor (b) Measurement While Drilling instrument (Chesapeake-Energy, 2011)

Once this curve is completed, drilling begins on the well's horizontal section called the "lateral". The pipe used to drill the well, measures 30 ft. in length and weighs approximately 495 pounds each. At various stages in drilling, the pipe is taken out of the hole for tool and bit changes and returned down the hole, a process called "tripping pipe". One the targeted distance is reached; the drill pipes are removed from the wellbore one last time. The production casing is now inserted into the full length of the well bore. Cement is again pump down the casing and out through the hole in the casing shoe, forcing the cement up between the casing and the wall of the hole, filling the open space known as the annulus. Casing the well is a very important process because it permanently secures the wellbore and it prevents hydrocarbons and other fluids from sipping out into the formation as they are brought out to the surface. A cross section of the well below surface shows seven protective layers (Figure 2-7) from ascending order of drilling:

- Cement
- Conductor casing
- Cement
- Surface casing
- Drilling mud
- Production casing
- Production tubing

11
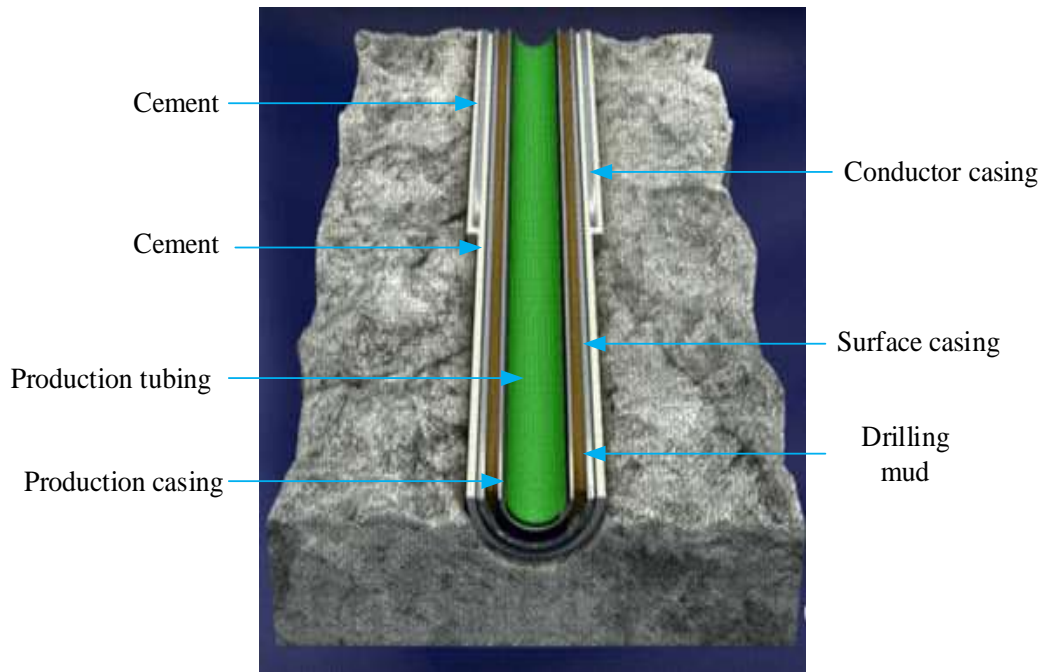
Figure 2-7: Cross section of well showing protective layers (Chesapeake-Energy, 2011)

A wellhead is installed afterwards. The well is then pressure tested for its integrity for continued drilling prior to perforating the lateral section using a perforating gun at approximately 1000 ft., lowered by wire line into the casing of the targeted section of the horizontal leg. An electric current is sent down the wire line to the perforating gun and this initiates a charge that shoots small holes through the casing and cement. The perforating gun is then pulled out of hole and crude oil flows into the well through the perforations. At this point, production can be initiated which allows the flow of crude oil to the surface. Finally, a Christmas tree is installed and other necessary surface equipment.

2.5 Terminologies Used in Drilling Conventional and Non-Conventional Wells

This section describes the terms used to describe horizontal wells. These include the measured depth (MD), True Vertical Depth (TVD), Horizontal Displacement of well (HD), Kick Off Point (KOP), Build section or inclined section, angle of inclination, horizontal or lateral section, bridge block. Figure 2-8 Shows a detailed summary of the key sections of a completed horizontal well.

- **Measured Depth:** This term is abbreviated as MD, and is used to illustrate the total length of the horizontal or vertical well from the surface to the bridge block. The lengths of the pipes are usually measured on the derrick or while the pipes are placed on the pipe rack prior to screwing together and inserting into the wellbore. This is

because once the pipes are screwed and sent into the wellbore, they would have undergone stress and tension hence precision in measured depth measurement will be impossible. This term is important to drillers to know how much pipe is required for the well.

▪ **True Vertical Depth:** This term has an alternate form, TVD. The term describes the vertical distance or displacement from the surface to extreme of the horizontal or vertical well. For the case of vertical wells, the MD will be the same as the TVD. This term is important for determining the bottom hole pressure, partly due to the fluid hydrostatic head in the wellbore. This length is usually shorter than the Measured Depth for horizontal wells.

▪ **Horizontal displacement of well**: This term is usually used for horizontal wells. This refers to the horizontal distance of a horizontal well from the point of insertion to the point of completion.

▪ **Bridge block**: The bridge block is usually inserted if a closed-hole completion is used. This ensures flow into the wellbore is only through the perforation of the well.

▪ **Kick Off Point**: This is the point in depth of a vertical hole at which deviation from the vertical is started. This term abbreviated as KOP, is usually used for inclined are deviated wells.

▪ **Build or inclined section**: this is the term used to describe the section of inclined or deviated wells, from the kick off point to the point at which the well becomes horizontal.

▪ **Angle of inclination**: this is the angle in degrees when the well deviates from the vertical. The higher the angle of inclination, the higher the tendency of interference effect occurring at the junction especially in multilateral wells. This effect describes the turbulence and flow efficiency at the junction of the well.

▪ **Vertical and horizontal displacement of the inclined section**: In this research, this term is used to describe the physical properties of the inclined section in terms of length. The vertical displacement of the inclined section refers to the vertical displacement in length of the inclined section. In other words, the vertical

displacement from the KOP to the point at which the inclined section becomes horizontal. On the contrary, the horizontal displacement of the inclined section is the horizontal distance from the KOP to the point at which the inclined section becomes horizontal.
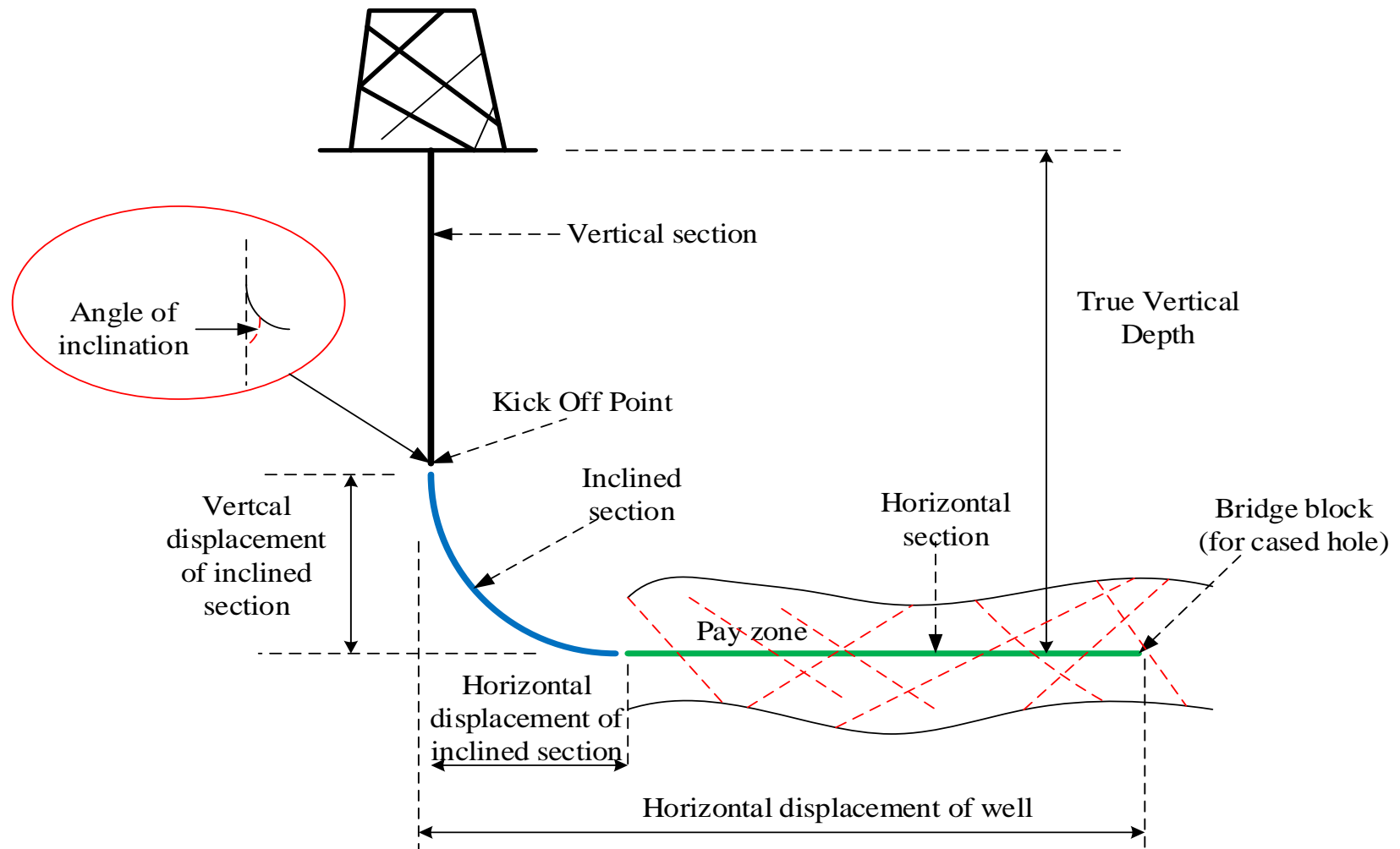
Figure 2-8: Basic sections of horizontal wells (Choudhary, 2011)

2.5.1 Types of horizontal wells and their uses

Horizontal well classification is based on their importance and technology needed for a given purpose. A system of categorization was established to take care of horizontal well with regards to the radius of the arc made by the wellbore as it's drilled from the vertical to horizontal directions. There are short-radius, medium-radius and long-radius horizontal wells as illustrated in Table 2-1 and Figure 2-9.

a) Short radius (SR) horizontal wells

Short radiuses well are drilled at build rates "positive change in angle of inclination over a fixed length" of 1.5 to 3 degree/foot with arc of 3 to 40-foot radius. They are commonly drilled in a non-friable formation with an open case completion. Short-radius horizontal wells are commonly used to re-enter existing vertical well where the steel casing of an old well allows for attainment of a higher departure angle so that short radius profile can more quickly attain horizontality, and thereby rapidly reach or remain within a pay zone in small lease blocks. This has certain benefits like lower capital cost, smaller suction head for down hole production pump and MWD is frequently not required if long horizontal sections are not drilled. Current difficulty to the use of a short radius horizontal well is that the target formation should be suitable for an open hole or slotted liner completion, since adequate tool don't exist to reliably do the producing zone isolation, remedial, stimulation or logging work in short radius holes.

b) Medium radius (MR) horizontal wells

Medium radius horizontal wells allow the use of larger wellbore diameters, near-conventional bottom hole assemblies, and more sophisticated and complex completion methods. It requires the use of MWD system, which increases well, cost, and allows for logging activities. Medium radius holes are perhaps the most popular option currently. It has build rate of 8 to 20 per foot used to drill from vertical to conventionally sized lateral. Control over build rate is achieved by varying motor size and borehole size. The tools are slightly modified to endure increased bending and buckling.

c) Long radius (LR) horizontal wells

Long radius horizontal wells are mostly used for shore based operations. These holes employ conventional drilling tools and completion techniques, and often used steerable

downhole motors. Have a relatively low curvature and a final horizontal section, which runs, along the top of a reservoir. They are characterized by their low build rates.

Table 2-1: Classification and summary of Horizontal well (Jubralla et al., 1995)

Well Type	Build Rate (ft.)	Radius (ft.)	Diameter (in.)	Length (ft.)	MWD	Direction control	Drilling method	Completion
Long Radius	1 to 6°/100	1500	8	70	Yes	Yes	Directional	Open hole
Medium Radius	8 to 20°/100	200	6	20	Yes	Yes		
Short Radius	1.5 to 3°/	15	6	5	No	Difficult		
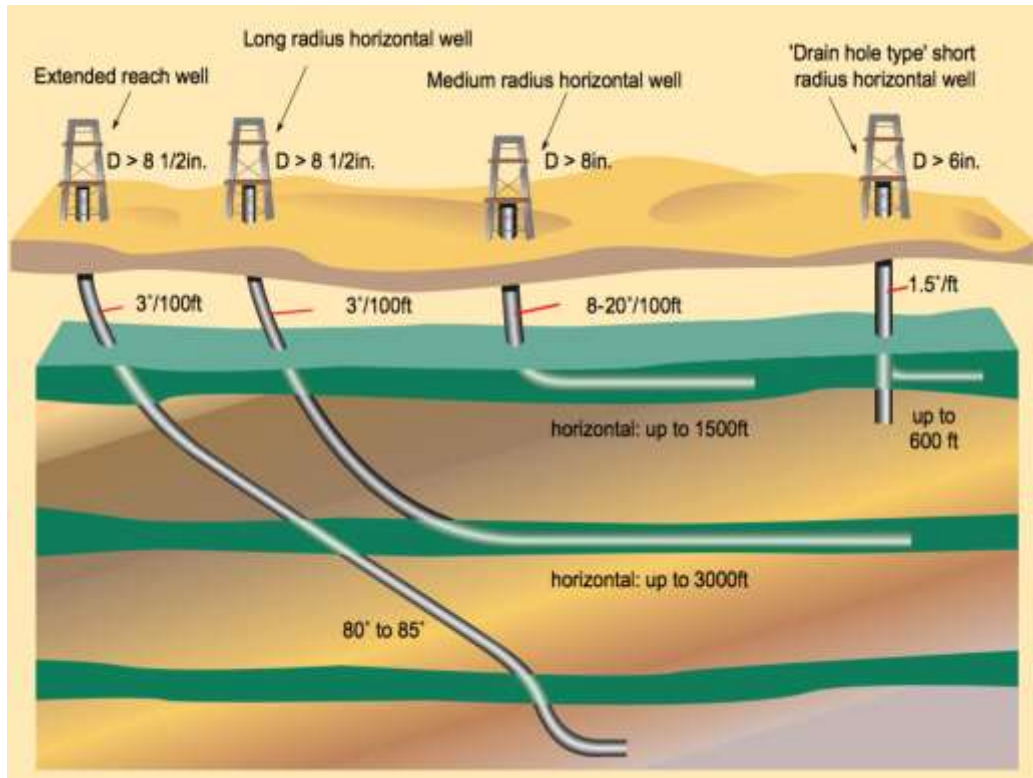
Figure 2-9: Types of horizontal wells (Jubralla et al., 1995)

2.6 Reservoir Drive Mechanism

The energy that drives the hydrocarbon present in the reservoir towards the well depicts the type of reservoir drive mechanism. This describes a reservoir at its primary stage of recovery. A reservoir may naturally have sufficient energy to push hydrocarbons to the surface but a decline in pressure is often experienced accompanied by a reduction in hydrocarbon produced. At this point, an artificial mechanism may be applicable. The various reservoir drive mechanism that exist include water drive (edge or bottom water drive), gas drive (gas cap or solution gas drive), combination drive and gravity drainage (Schlumberger, 2016d).

2.6.1 Water drive

This type of drive mechanism is known as the most efficient (Schlumberger, 2016d) (Figure 2-10) and characterized by an active aquifer that drives the hydrocarbon to the wellbore and to the surface. Strong water drive is also known to be more effective in oil reservoirs than in gas reservoirs. The water drive could be edge or bottom oriented, determined by the nature of the reservoir geometry (AAPG, 2016a) as shown in Figure 2-10.

19
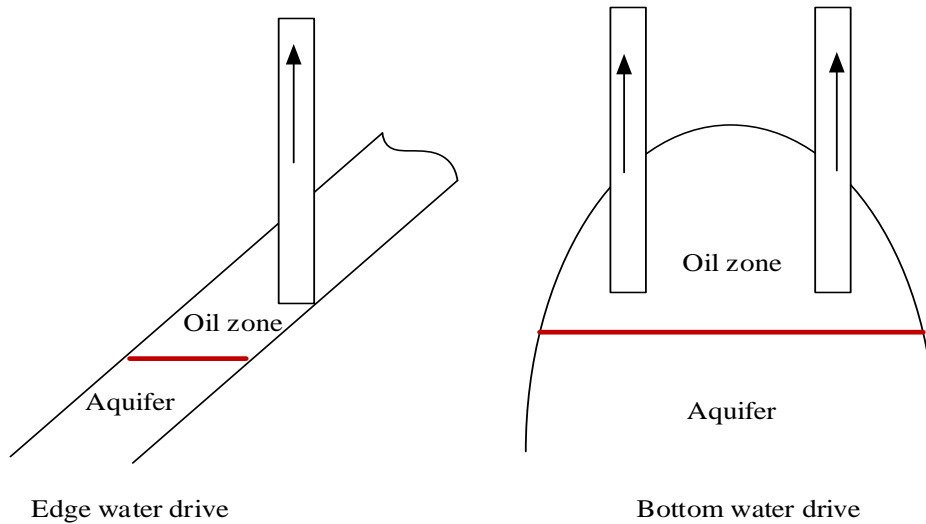
Figure 2-10: Edge and bottom water drive mechanism (AAPG, 2016a)

The disadvantage of this reservoir drive is in displacing oil over time along its path towards the perforations of the well. This results in a phenomenon known as coning or cresting. Hence depletion of reservoir pressure is experienced with the degree depending on the strength of the bottom or edge water aquifer and withdrawal rate. Increasing Water-Oil-Ratio (WOR) is often experienced until considered economically unviable. A partial or weak water drive exists, with little or no water production. This is due to little or no expansion of the partial water. A typical decline curve for strong bottom water drive is illustrated in Figure 2-11. In this figure, it can be observed that the decline curve for the partial water drive is more concaved than that of the strong bottom water drive. This is due to a weaker expansion of the aquifer as the hydrocarbon is depleted, hence a weaker support to oil production. The oil recovery for this kind of reservoirs is between 35-75%, depending on the field management, sweep efficiency of rising water and aquifer strength (AAPG, 2016a). The permeability and size of the aquifer as well as the withdrawal rate of the reservoir determine the production rate (AAPG, 2016a).
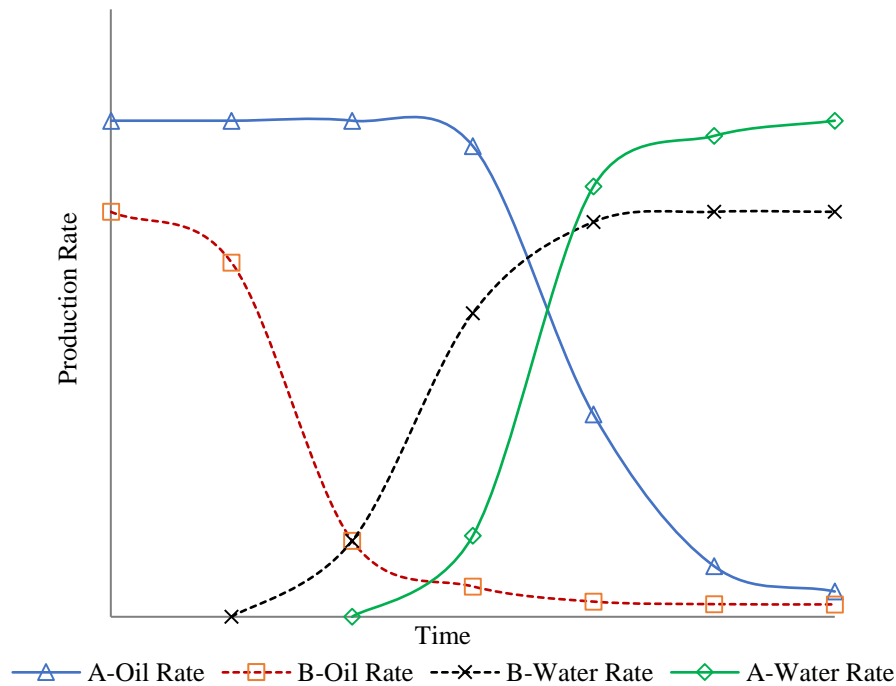
Figure 2-11: Typical decline curve for a wellbore draining a reservoir system with a strong water drive (A) and a partial water drive (B) (AAPG, 2016b)

2.6.2 Gas cap drive

An initial gas cap serves as the source of the reservoir energy. A gradual pressure drop is experienced in these kinds of reservoirs when compared to the solution gas drive mechanism due to the gas cap expansion during oil depletion. However, when the GOC gradually reaches the perforation of the well, a significant increase in the Gas-Oil-Ratio (GOR) is observed partly due to the viscosity of the gas and for this reason have the highest GOR amongst all drive mechanisms (Figure. 2-12). The increasing GOR is described as coning in vertical wells and cresting in horizontal wells. Oil recovery for this type of reservoir is often between 20 to 40% of the Original Oil In Place (OOIP), depending on the size of the initial gas cap, structure of the reservoir geometry and field management (AAPG, 2016a). A cross sectional view and map view of a typical gas cap drive mechanism is illustrated in Figure 2-12.
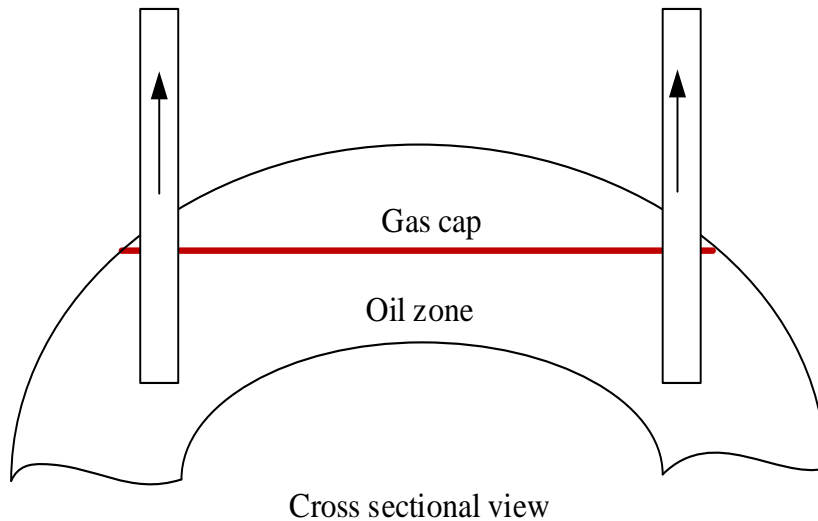
Figure 2-12: Gas cap drive mechanism (AAPG, 2016a)

2.6.3 Solution gas drive

The mechanism of the solution gas drive depends on the gas present. Due to pressure, gaseous hydrocarbons are formed in this type of drive mechanism, although they might initially appear in liquid form. Solution gas drive may be either saturated or under saturated depending on the source pressure (Odeh, 1986). In a saturated state the reservoir is at bubble point "the pressure and temperature condition at which the first bubble of gas comes out of solution" (Schlumberger, 2016b) while in an undersaturated state the reservoir is above the bubble point. During oil production, the reduction in reservoir pressure causes the oil to shrink thereby releasing the solution gas, the primary source of this drive mechanism.

During oil production, reservoir pressure declines quickly if the reservoir was initially undersaturated due to smaller compressibilities of oil, water and rock whereas the reverse is the case when the reservoir is initially saturated. The recovery of oil is usually between 5-30%. In undersaturated reservoirs, less than 5% of oil is recovered of the Original Oil In Place (OOIP). However, oil recovery can be improved by placing the well far away to reduce the GOR over time thereby conserving the reservoir energy. This type of reservoir drive mechanism is illustrated in Figure 2-13.
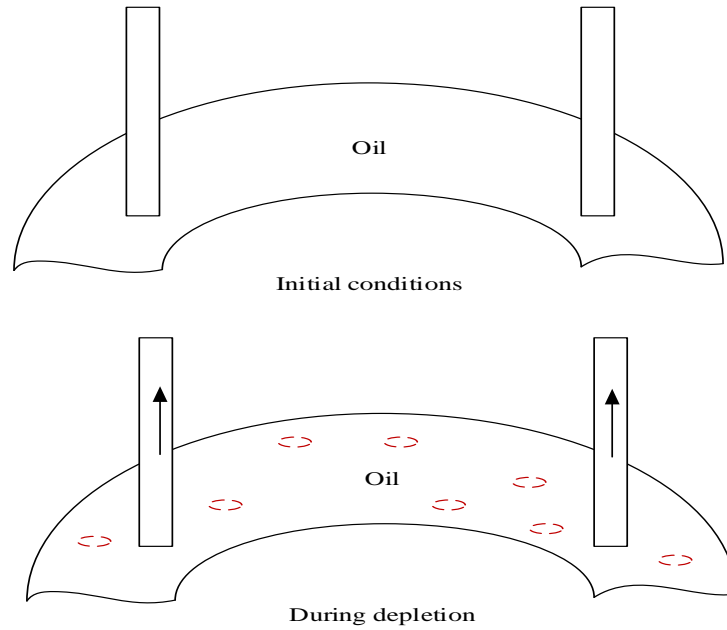
Figure 2-13: Solution drive mechanism (AAPG, 2016a)

2.6.4 Combination drive

This reservoir drive mechanism involves more than one drive mechanism to oil production. A typical example is an oil reservoir with an active aquifer and initial gas cap (Figure 2-14). Production and oil recovery from this kind of reservoir drive will depend on the dominant drive such that in a reservoir with considerable gas cap and strong bottom aquifer, the production trend will reflect that of a typical bottom water drive but with increasing WOR and GOR. Therefore, oil recovery can be improved by considering if it's a depletion or displacement drive present
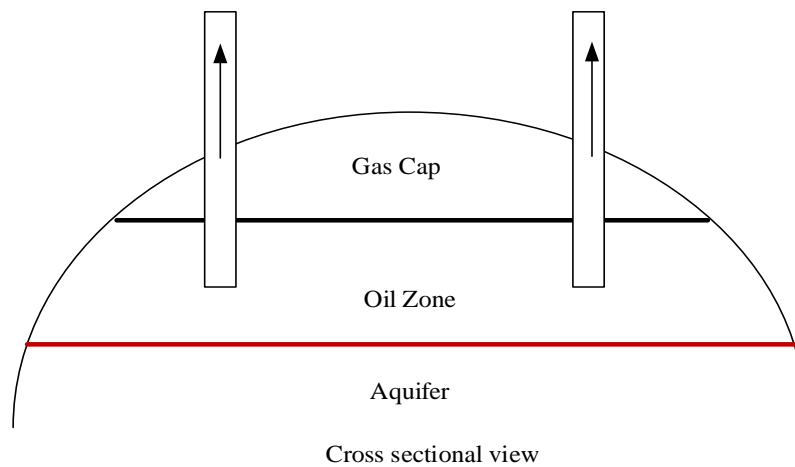
Figure 2-14: Combination drive mechanism (AAPG, 2016a)

2.6.5 Gravity drainage

In this type of reservoir drive mechanism; the reservoir fluids segregate by differences in densities (Figure 2-15). Gravity drainage is considered a secondary drive mechanism and occurs in combination with one or more primary recovery mechanism(s). Gravity drainage is effective in thick-oil reservoirs with high vertical permeability. The production rate for this type of drive mechanism is usually below field rates. However, its efficiency depends on time and could perform better than primary drive mechanisms (AAPG, 2016a).
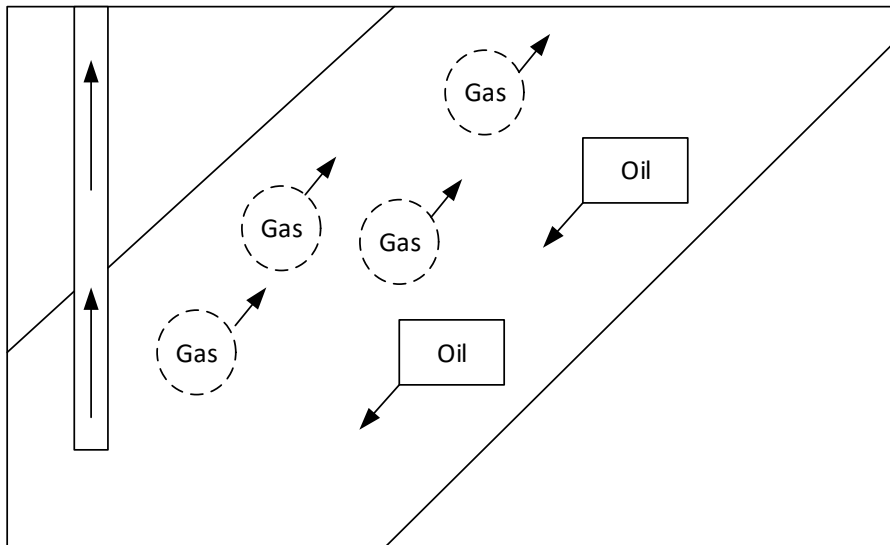
Figure 2-15: Gravity drainage (AAPG, 2016a)

2.7 Homogeneity and heterogeneity

In reservoir engineering, the term homogeneity is used to describe a reservoir with uniform rock or reservoir grain distribution. A homogeneous reservoir could be either isotropic "due to similar reservoir grains" or anisotropic "due to irregular reservoir grains structure" (Figure 2-16). In the latter case, the irregular grain structure when arranged in an even distribution will form a homogeneous layer in a rather heterogeneous rock sample. Higher interconnected pore spaces are another characteristic of a typical homogeneous reservoir when compared to a heterogeneous case.

Anisotropic   Isotropic   Anisotropic
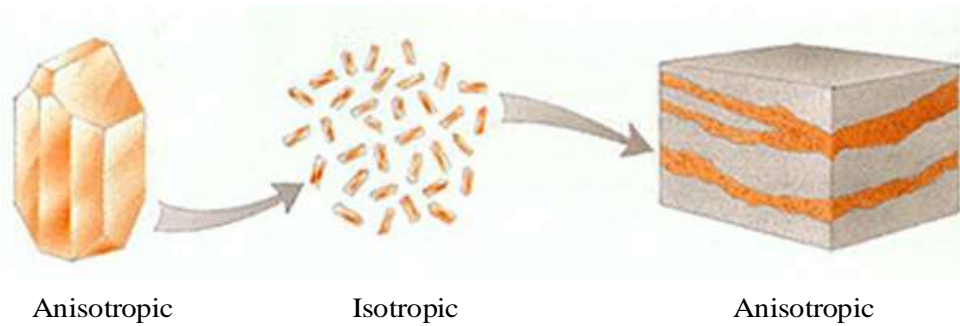
Figure 2-16: homogeneous and heterogeneous reservoir (Schlumberger, 2016a)

On the contrary, reservoir heterogeneity refers to a reservoir that have a mixture of different reservoir grain sizes, distribution and packing, which could either, be isotropic or anisotropic in orientation. For this reason, this type of reservoir is usually characterized by low interconnected pore spaces when compared to a homogeneous reservoir. In this regard, similar grains may be present in a reservoir but could have varied vertical orientation and distribution. The four possible scenarios of isotropy/anisotropy and heterogeneity/homogeneity are illustrated in Figure 2-17.
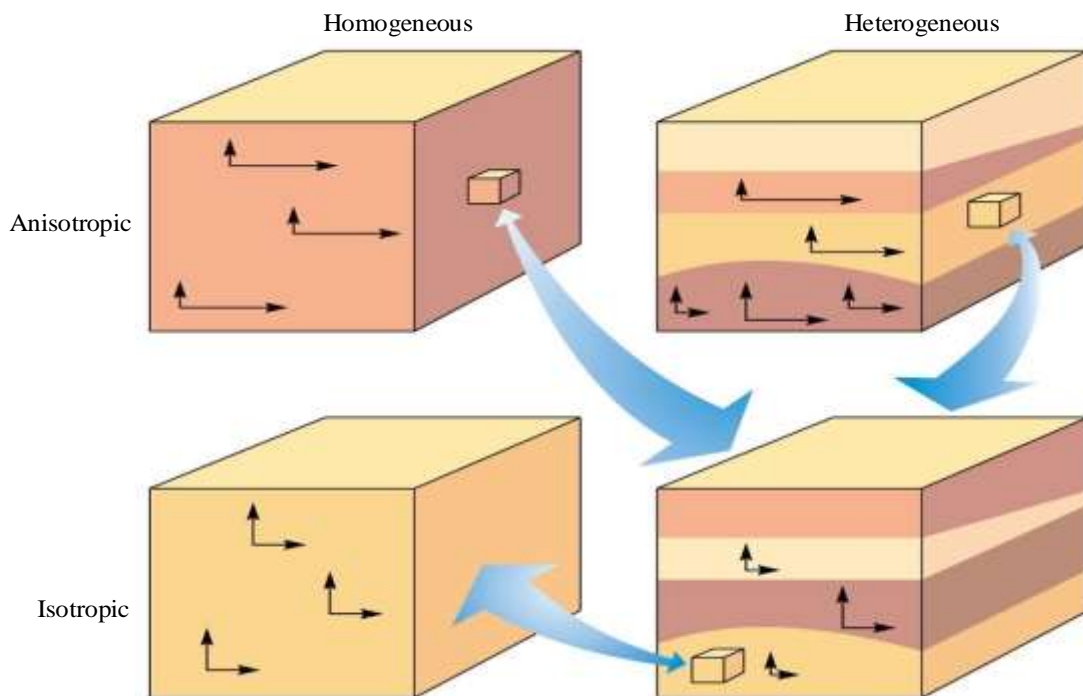
Figure 2-17: Four possible conditions for reservoir isotropy/anisotropy and heterogeneity/homogeneity (Schlumberger, 2016c)

2.8   Water and or Gas Cresting Problems

Naturally, the reservoir exists at static condition with the gas, oil and water separated by gravity, in order of their density differences (Balazs et al., 2009, Beveridge et al., 1970, Singhal, 1996). Due to the lower viscous nature of water and gas compared to oil, no restriction to flow is imposed by the reservoir rocks and thus a phenomenon called coning/cresting could occur. Coning in vertical wells (conical in shape) and cresting (crest-like shape) in horizontal wells is defined as the phenomenon in which an underlying bottom water moves upward or overlying gas cap moves downward against gravity into the completion interval through the perforations of a producing oil well. This is a problem associated with oil production in reservoirs underlain by strong aquifers (in terms of water coning/cresting), a common scenario in major hydrocarbon provinces of the world. However, some reservoirs have weak aquifers thus, produce little or no water during oil production. In the former scenario, the reservoir is subjected to rapid water or gas migration towards the completion zone, a resultant effect of high-pressure drop around the wellbore area. The WOC and GOC are first defined at static condition as illustrated in Figure 2-18 (top left) before the commencement of oil production.
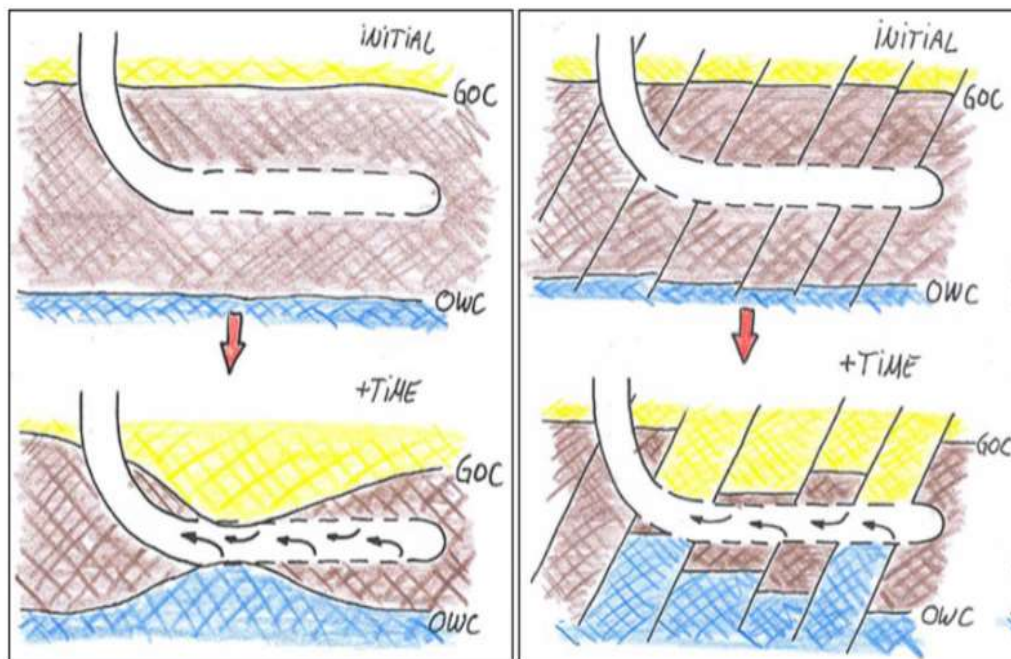
Figure 2-18: Cresting in homogeneous reservoirs (left) and heterogeneous reservoir (right) (Porturas et al., 2009, Schevchenko, 2013)

The closer the interface is to the wellbore, the earlier water or gas breakthrough time "the time for water and or gas to breakthrough into the well" is expected (Schevchenko, 2013).

Soon after production starts, the original plane interfaces between bottom water and oil and the overlying gas and oil become distorted rapidly as a result of pressure drawdown (Permadi and Jayadi, 2010, Schlumberger, 2016) as shown in Figure 2-18 (bottom left and right), to form a respective upward and downward protruded geometry reflecting the imbalance in the hydrostatic and static reservoir pressures. Therefore, this natural phenomenon occurs naturally when the pressure drop exceeds the hydrostatic pressure that occurs between the oil and water (water cresting / coning), oil and gas (gas coning / cresting) or oil, water and gas if occurring simultaneously. It is this protruded geometry that is called coning with regards to a vertical well whereas it is called cresting in horizontal wells and highly deviated wells, affected by the fluid properties involved (Schevchenko, 2013, Schlumberger, 2016).

Alternatively, coning can be said to occur when the viscous force of the unwanted fluids exceeds the gravitational force and if an equilibrium is not met, this can result in the influx of these unwanted fluids into the wellbore (Saad et al., 1995, Umnuayponwiwat and Ozkan, 2000). More so, this can be simply regarded as occurring when the viscous (as a result of fluid removal from the reservoir) and gravitational force (as a result of density difference between the fluids involved) around the near well bore becomes unstable (Shadizadeh and Ghorbani, 2001, Smith and Pirson, 1963, Umnuayponwiwat and Ozkan, 2000). Coning poses adverse effects in terms of overall oil productivity, operating and handling cost of the water or gas produced and possibly the early shutting in of wells, and some cases results in increased water disposal and environmental effects such as the Iranian oil fields (Shadizadeh and Ghorbani, 2001).

Due to increase in these effluents, production could be terminated leaving behind high percentage of oil in the reservoir. If this occurs, more money could be spent to recover the oil left by using improved or secondary recovery techniques (Verga et al., 2005). Coning is rate specific in the sense that it occurs at very high production rates and thus above the critical flow rate "the rate at which water or gas is not produced with oil". Coning can negatively affect the productivity of a well, influence the degree of depletion and the overall recovery efficiency of the oil reservoirs (Salavatov and Ghareeb, 2009), scale deposition and wettability in the case of water coning (Ehlig-Economides et al., 1996).

Horizontal wells can be used in cases where coning in vertical wells are adversely affected by coning (Ehlig-Economides et al., 1996). Due to the length of exposure of the horizontal

27

well to the reservoir compared to a vertical well, there is a less pressure drawdown for a given rate of production. For this reason, horizontal wells have been a preferred candidate in situations of water and gas coning (Peng and Yeh, 1995).

Although horizontal wells are effective in strong bottom water drive reservoirs, cresting can be delayed by:

- Producing at reduced oil rate resulting in reduced oil productivity.

- Improving the productivity of the well, using horizontal well instead of vertical wells to produce the formation.

- Partially penetrating the well at the top of the reservoir in the case of water coning, at the bottom of the reservoir in the case of gas coning, and close to the centre of the pay zone in the case of simultaneous water and gas coning, due to higher mobility of gas compared to water and after careful consideration of the water coning and gas coning velocities (Singhal, 1993, Singhal, 1996).

- Recompleting the well at a different elevation to increase the distance between the GOC or WOC and the perforated interval and infill drilling (Hatzignatiou and Mohamed, 1994).

The factors that affect cresting in horizontal wells are oil zone thickness, mobility ratio, horizontal to vertical permeability anisotropy, well productivity and production rates (Hatzignatiou and Mohamed, 1994, Verga et al., 2005). Overcoming the buoyancy forces by the pressure drawdown at the fluid entry point in the well is very important for coning behaviour (Singhal, 1996). Conventional oil field practices exist with the objective of maximizing reserves and delaying coning / cresting: placing wells adjacently in the pool such that their cones / crest do not interfere with each other, helps drain the pool more efficiently thus increase oil recovery factor. However, in modern industry practices this impairment to production can be avoided by perforating wells as far above the oil WOC as possible in water-oil reservoirs, perforating low in the oil column away from the GOC in gas-oil reservoir (Salavatov and Ghareeb, 2009).

Nevertheless, there have been success in reducing coning / cresting with polymers and gels (Dai et al., 2011, Kantzas et al., 1994, Law and Jossy, 1996, Thakur and Tachuk, 1974,

White et al., 1973, Zaitoun et al., 1992, Albonico et al., 1994, Lakatos et al., 1998, Surguchev, 1998, Shirif, 2000, Zaitoun and Pichery, 2001, Ghahfarokhi et al., 2006, Vasquez et al., 2006, El-karsani et al., 2014, Al-Muntasheri et al., 2010, Salavatov and Ghareeb, 2009, Brown, 1984) and a more recent and novel approach using down hole water-sink technology (DWS) where water is produced separately from the oil using dual packers (Shirman and Wojtanowicz, 2000). In addition, Howard and Fast (1950) introduced the idea of injecting a "pancake" of cement just below the completion interval to prevent the vertical/upward flow of water into the wellbore while Peng and Yeh (1995) recommended cementing and perforating horizontal wells. Notwithstanding, the first step in mitigating coning lies in obtaining a complete geological description of the reservoir and aquifer as possible ignorance could lead to calamitous decisions (Singhal, 1993, Singhal, 1996).

Recham (2001) investigated water and gas coning problems using numerical simulation, involving an extensive parametric sensitivity analysis of various fluid and reservoir properties with the aim of developing a new predictive correlation needed to calculate break through time and optimum oil rate for maximum recovery for both vertical and horizontal wells.

Benamara and Tiab (2001) proposed a numerical gas coning technique to investigate the effect of different parameters [oil flow rate, horizontal permeability, vertical to horizontal permeability ratio (vertical anisotropy ratio), porosity, oil reservoir thickness, perforated thickness for vertical wells and well length for horizontal wells, height below perforations for vertical wells and height below the drain hole for horizontal wells, oil density, gas density, oil viscosity, gas viscosity, reservoir size and gas cap to oil zone ratio] in the Gas-Oil-Ratio (GOR) behaviour after breakthrough. The authors concluded that coning tendency is worse in low horizontal permeability reservoirs and is restricted in reservoirs with low vertical anisotropy ratio, which delays this phenomenon. Also, they stated that low gas-oil mobility ratios result in high oil recovery with low coning tendency. More so, they proved that horizontal wells prevent or at least delay coning and fine grid simulator models are required to accurately simulate coning problems.

Mungan (1979) conducted a numerical and laboratory study of water coning in a layered model using a pie-shaped cylindrical sand pack having radial symmetry. In his experiment, he observed that oil recovery decreased for higher oil viscosity and injecting polymer solution at the oil water contact, delayed the insurgence of water into the wellbore.

29

Verga et al. (2007) studied water coning (vertical wells) and water cresting (horizontal wells) by performing an extensive comparison between the most used analytical models and the estimates obtained by numerical methods. They adopted a radial model for studying water coning phenomena and a bi-dimensional cross section for describing water cresting, while adjusting the production rate with close observation of the change in water cut. The authors then carried out a sensitivity analysis on all formation and fluid properties and their effect on water coning and cresting formation, and their results showed that these parameters affect coning and cresting formation.

Aggour and Kandil (2001) carried out an experimental investigation to study horizontal well performance with single and multiple orthogonal fractures in bottom water drive reservoirs. In their experiment, the physical model (reservoir) was packed with glass beads yielding a porosity of 0.36. Kerosene and distilled water were used as the oil and water respectively.

Singhal (1993, 1996) presented the various available methods of mitigating coning, encompassing those with and without field results. These methods include: placing of barriers to restrict movement of water and gas around the well, such as introducing water, oil, gas, gels, polymers, foams or cementing agents to reduce the effective permeability or relative permeability (illustrated in Figure 2-19). In addition, modifying flow pressure around the wells was achieved by introducing additional perforation in the gas zone or separate completion intervals in same well and by reverse coning of oil into water or gas zone; reduction in operating cost through subsurface water separation and disposal of the separated water in the same well (illustrated in Figure 2-20).
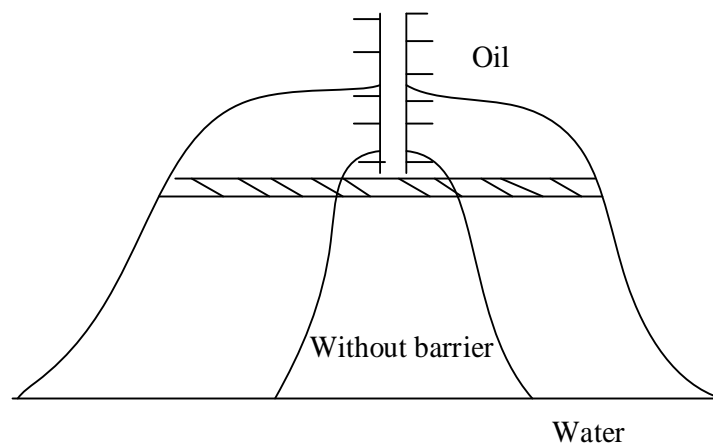
Figure 2-19: Water coning in the presence of a barrier (Singhal, 1993, 1996)
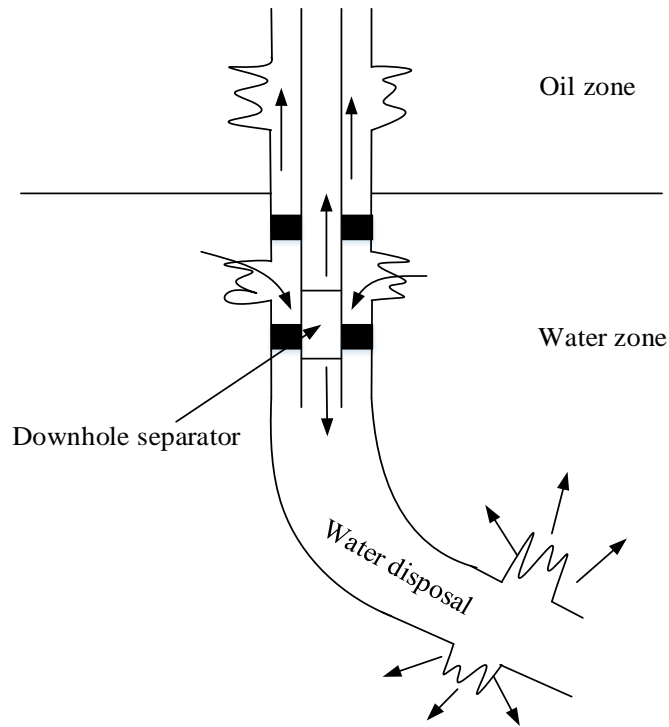
Figure 2-20: Down hole separation and water disposal (Singhal, 1993, 1996)

Ehlig-Economides et al. (1996) studied several new drilling and completion techniques to enhance production of oil in reservoirs by comparison and evaluation. From their study, they concluded that the total oil recovered is independent of the production rate and the term "critical rate" does not exist in cases of strong bottom water / aquifer for all completion methods due to material balance concept. They also stated that large reservoir area thickness and high effective permeability are critical factors that affect the performance of horizontal wells, although they are better candidates in the presence of strong bottom water.

Balazs et al. (2009) investigated water and gas coning in horizontal producing wells using an experimental model. The sole aim of their research was to provide fluid mechanics-based engineering guidelines for optimizing the productivity in horizontal wells. They stated that it is important to forecast water and/or gas coning properly in Computational Fluid Dynamics (CFD) modeling, for validation of the experimental results and serving as basis for preventing and minimizing coning effects. In their experimental set-up as shown in Figure 2-21, a transparent Plexiglas was used for visibility of the coning behaviour while the water was colored using food paint prior to filling in the tank to avoid a non-homogeneous mixture. The Plexiglas tank was filled with polystyrene beads to serve as the

31

porous media in the reservoir, while sunflower was preferred over gasoline due to the polystyrene bead dissolution in it.
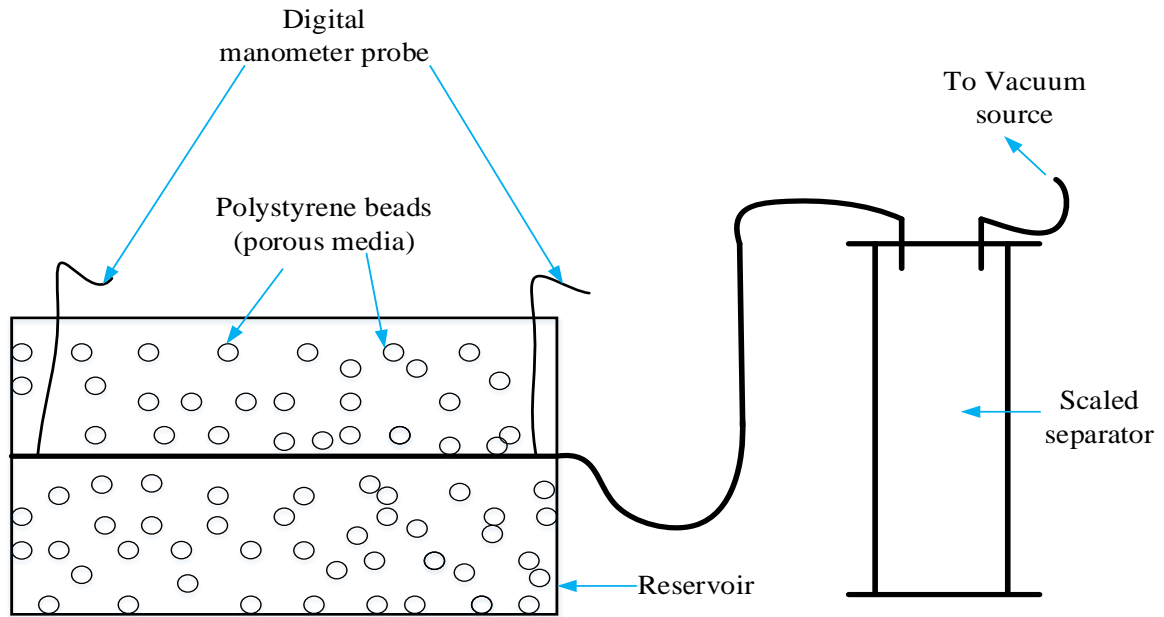
Figure 2-21: Water coning experimental set up (Balazs et al., 2009)

The sunflower oil was extracted through exchangeable perforated pipes while the level controller tube at the bottom of the vessel was used to ensure water supply from the outer communicating vessel during oil production. In the experimental set up two control valves were used to serve as start / stop of production and adjustment of mass flow rate of production. Prior to the start of the experiment, the authors filled the transparent Plexiglas with the polystyrene beads, then pumped in water from the bottom while the oil was pumped from the top. The well bore model as shown in Figure 2-21 was connected to a scaled separator and a vacuum source was connected to the scaled separator that has a constant negative, adjustable pressure. Fluid flow out of the Plexiglas tank was facilitated due to the depression created by the vacuum. The pressure gradient was measured with two probes and a digital manometer. From their experiment, it was observed that water or gas insurgence into the wellbore depended on the starting position of the upper and lower phase border, the production mass flow rate and water supply intensity. Figure 2-22 illustrates the coning phenomena development over time for water coning (Figure 2-22(b)) and gas coning (Figure 2-22(a)); read from digital photographs.
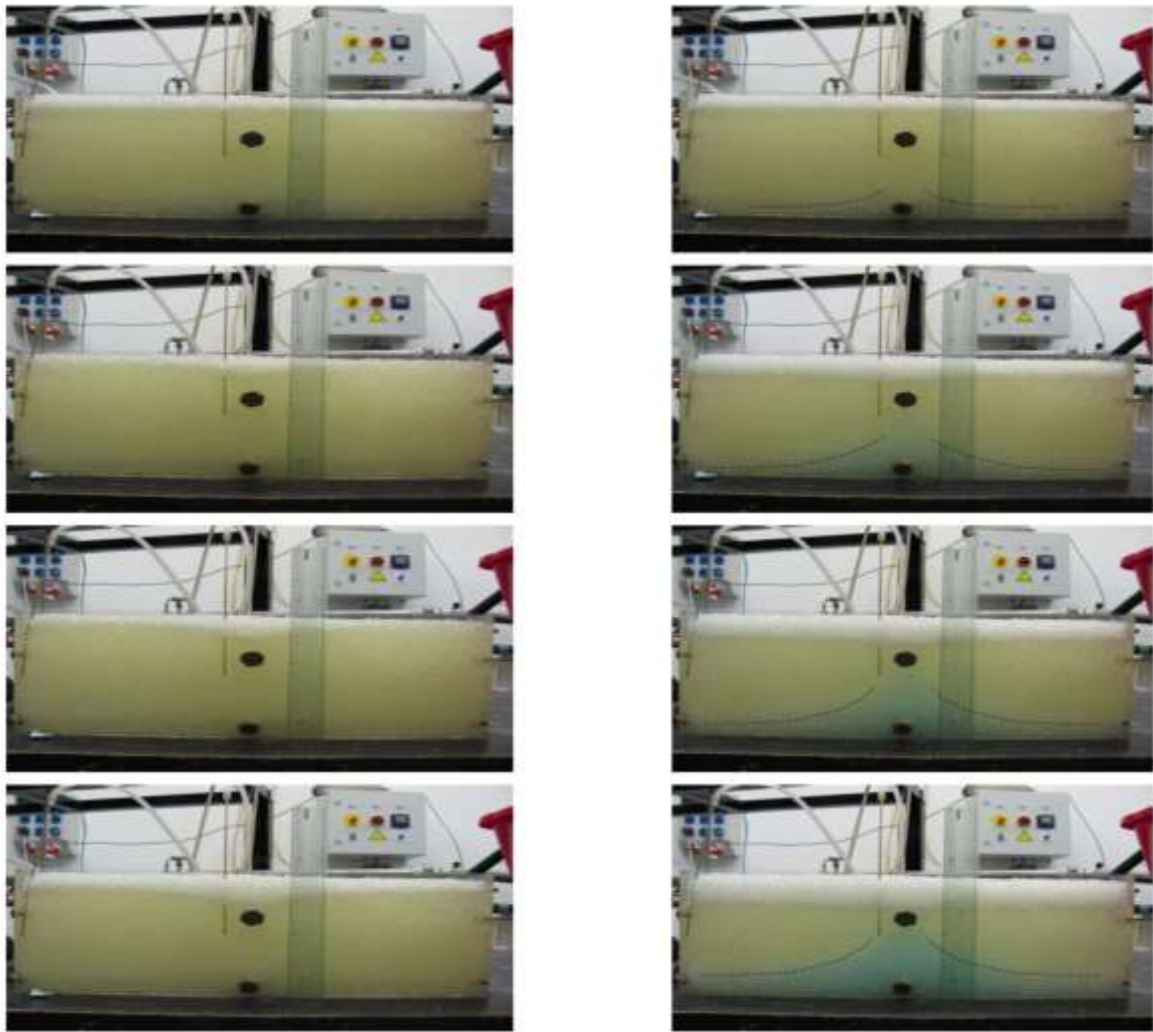
Figure 2-22: (a) Gas coning and (b) water coning (Balazs et al., 2009)

Schevchenko (2013) conducted a laboratory experiment on water coning to better understand the oil/ water flow behaviour in the gap towards a drainage hole, representing reservoir fluid inflow into the well tubing through the Inflow Control Device (ICD). His experiment rig was designed for flow visualisation and phase measurements levels and oil viscosity and density.

However, the use of ICDs can control fluids inflow but cannot stop the influx of water entirely, as shown in Figure 2-23 (top), while Figure 2-23 (bottom) shows the inevitable rise in the WOC, gradually approaching the production tubing regardless of the ICD installed. He conducted analysis involving key parameters that affect water coning; phase interface distance from the orifice, oil viscosity, density, surface tension, annulus width, total flow

rate and orifice cross sectional area. He concluded that coning, in this case water coning depends on fluids flow rate and on annulus width.
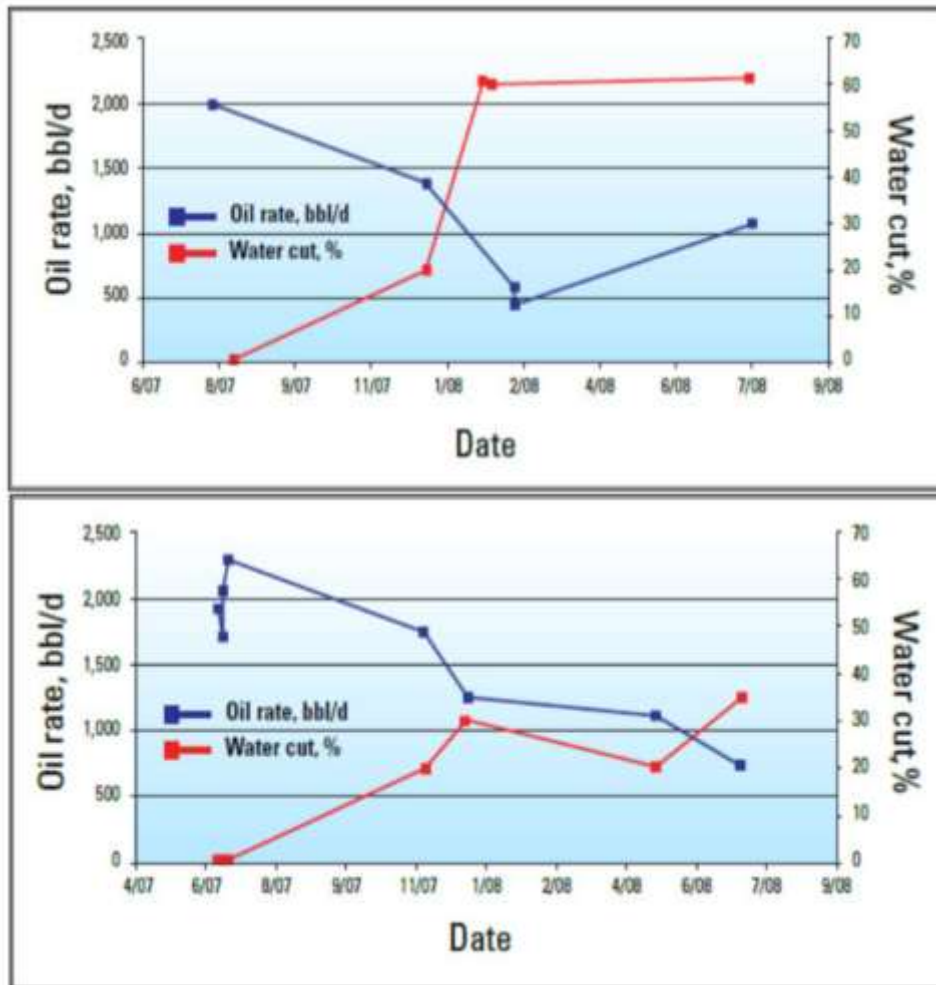
Figure 2-23: Production profile with no ICDs (top) and with ResFlowTM ICD (bottom). Baram field, east Malaysia (Schlumberger, 2010)

Karp et al. (1962) investigated the use of horizontal barriers for controlling water coning. After a series of analysis using different cement as barriers, they concluded that barriers are effective ways of solving water coning problems for all reservoir conditions but will be ineffective for reservoirs having high viscous crude oil, low effective permeability or small oil zone thickness.

Permadi et al. (1995) studied the behaviour of water cresting under horizontal wells to better understand its formation and growth, before and after water breakthrough. This was undertaken using a physical model with variation in oil column thickness, oil viscosity and well length. From their observations, the direction of cresting formation moved in opposite

34

direction to fluid flow in the well bore having a sharper curve for shorter well length with reference to the right and left flanks. In their attempt to achieve 99% water cut, they noticed that the bottom water never reached the tip end of the well. The phenomena increased with well length and oil viscosity but decreased slightly with oil column thickness. In this regard, the authors suggested a non-open hole completion be used for horizontal wells, with more holes perforated at the end of the horizontal well.

Aulie et al. (1995) investigated cresting behaviour towards horizontal wells with both bottom and edge water drive. This behaviour was investigated using a laboratory model depicted in Figure 2-24. In their laboratory model, the flow rate and pressure of water supplied from a tap was measured using a rotameter and pressure regulator respectively. For bottom water drive, the water was injected through points 1 and 2 in their model. The oil (paraffin) was dyed for more visibility and initially used to fill the model leaving only a thin layer at the bottom for water. The water was supplied at constant rate and pressure while producing oil through outlet 3. The cresting behaviour was monitored with a video camera displayed on a screen and observed picture-by-picture.
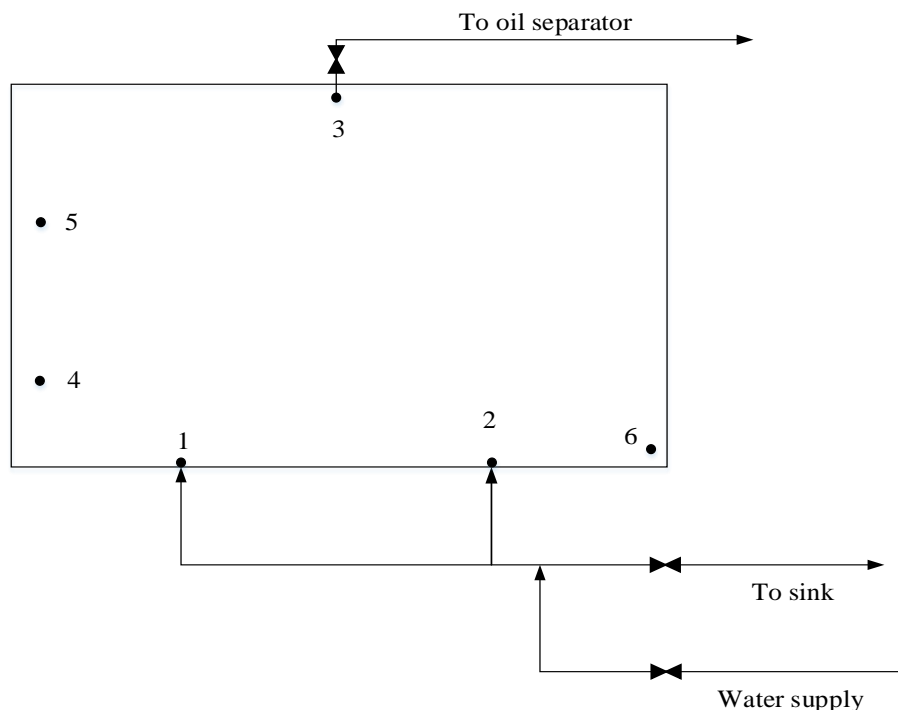
Figure 2-24: Schematic of laboratory model (Aulie et al., 1995)

Beattie and Roberts (1996) carried out numerical parametric study to identify factors that contribute to water production into a vertical well in a naturally gas fractured reservoir. The

parameters involved in their study were offtake rate, aquifer size, capillary pressure, residual gas saturation, matrix permeability, fracture permeability, vertical flow barriers, fracture spacing, completion interval position, vertical/horizontal permeability ratio. A simulation base case was first run and afterwards varying parameters individually to determine the effect on the water production performed this analysis. They stated that shutting-in the well for several days to allow the water level in the fractures to recede did not yield a sufficiently low water production. From their analysis, it was concluded that:

- High vertical permeabilities due to the presence of natural fractures favour the development of water cone, gas production rates and recovery efficiency are not significantly affected by water coning if wells are not shut-in (to cap or stop oil production) due to water disposal costs or liquid loading, operating conditions and reservoir properties conducive to water coning behaviour in single porosity formations such as high offtake rates, large aquifer thickness, short distance between initial water contact and perforations influence the water coning behaviour in naturally fractured reservoirs.

- In a similar manner, imbibition of water from fractures to the matrix has a significant influence on water coning behaviour. Reservoir properties, which restrict the degree of invasion of the matrix blocks such as wide fracture spacing, favour rise of the water level in the fractures toward the well.

Kuo (1983) carried out a rigorous sensitivity analysis of water coning behaviour to reservoir parameter using a numerical simulator with the purpose of providing engineers an easy to use model on a hand-held calculator; to calculate the critical rate, water breakthrough time and water cut performance after breakthrough. This correlation was developed from the study of parameters such as the effect of vertical permeability, effect of perforated interval, effect of mobility ratio and the effect of production rate.

Permadi (1996) performed a sensitivity study on the effect of well placement and end point mobility ratio on the performance of horizontal well in a bottom water drive. They observed and concluded that these parameters strongly affect the performance of a horizontal well in a bottom water drive.

Freeborn et al. (1990) undertook a case study of water cresting in South Jenner pool, a thin-oil rim reservoir with thick bottom water. Medium and long radii wells of 420 m and 1042 m horizontal displacements respectively were drilled to determine their inflow performances compared to a vertical well in the presence of bottom water. When the production results were reviewed it was observed by Freeborn et al. (1990) that the maximum production rate was highest for the long radius well however they indicated that the possible causes of poor performance of the short radius well was due to the cemented completion in the pay zone and the ineffectiveness of jet perforation in penetrating drilling damage. In addition, the water cut over time for each well was not reported. The authors also numerically investigated different placement of the horizontal well from the top of the reservoir and observed that there was a decline in oil reserves produced when the well is closer to the WOC and water cresting is more likely to occur faster due to the upward water flood provided by the bottom water.

Coats et al. (1970) investigated the effect of completion interval [5 inches and 20 inches (in) perforation] in a gas reservoir upon water arrival time and productivity index. This study was possible using a single well two-dimensional reservoir simulator model to simulate both homogeneous and highly stratified heterogeneous reservoir models. From their results, they concluded that the longer the perforation interval, the higher the productivity index while perforation interval has effect on the water arrival time and water cut in both homogeneous and heterogeneous reservoir models, producing at the same withdrawal rate.

Wojtanowicz et al. (1991) investigated the performance of a producing oil well, with and without tail pipe (often included in a typical completion design). This was possible by using a novel water control method in a producing oil well. This method involved the use of dual completion, above and below the oil water contact. The completion above the water oil contact was done in the oil zone which produced oil while the rise of the water cone during oil production was controlled by the completion placed in the water zone, described as the tailpipe water sink. This method was expensive but successful in decreasing the production of bottom water at increased oil production rate.

Luhning et al. (1990) developed a simple and straight forward process to overcome the excessive effluent (unwanted water) production called the Anti-Water Coning Technology (AWACT) with experimental, numerical and field trials. This process involves the use of

natural gas slug and chemical blend as a stimulant to inhibit the formation of coning. Their process could increase the oil recovery while decreasing the production of water.

Smith and Pirson (1963) investigated the effect of fluid injection to control the production of bottom water in both oil and gas producing wells. They investigated the effect of the point of fluid injection, injected fluid viscosity, length and location of the completion interval, thickness of the water and oil zones. Success was reported when the viscosity of the injected fluid was higher than that of the oil reservoir. This process when combined with other coning/ cresting control methods such as impermeable barriers or cement produced negligible results.

Boyun and Lee (1993) presented an analytic solution capable of estimating critical rate with consideration given to limited wellbore penetration of the vertical well on the well's oil productivity. Their solution showed that wellbore penetration in the oil zone is less than one third the overall thickness of the oil zone.

Wu et al. (1995) performed numerical simulation to investigated the feasibility of horizontal well application to reduce unwanted water production and increase oil recovery in the Amber field. From their study, they reported that higher production of oil was observed at the early stages of oil production but performs better when placed in the gas zone, aiding in a reduction of produced unwanted water with increase in oi recovery. However, placement of the horizontal well was below the WOC; produced the highest water at highest oil recovery.

Swisher and Wojtanowicz (1995) presented a dual completion method capable of producing water-free oil at high rates, higher than conventional completion type. The mechanism behind this method was based on providing equal pressure drop to act towards gravity to prevent the upward distortion of the WOC. In their study the tail pipe water sink completion was adopted and proven with field application.

Wojtanowicz et al. (1999) investigated the performance of the Downhole Water Sink (DWS) compared to conventional completion method. Their study involved numerical and experimental analysis. From their results, 30% increase in oil recovery was observed compared to the conventional completion. However, at early stages, the cumulative water

cut was higher using DWS. The flaw of this technique lies in handling of high volumes of unwanted water produced independently to the surface for water coning scenario.

Jin and Wojtanowicz (2011) presented the Downhole Water Loop (DWL) method for coning control. This method contrasts the DWS such that the produced water is recycled from the water sink installation without depletion of the water drive. The effectiveness of this technique is because recycling of water has been proven to have very strong beneficial effect on performance of a well. Despite the advantages, the DWL is affected by oil viscosity, thickness of the bottom water, well penetration, reservoir anisotropy and relative permeability of the oil.

Van Golf-Racht (1994) numerically investigated water coning in fractured reservoir using vertical wells aimed at determining the main characteristics of the coning mechanisms in a fractured reservoir. Their key contribution is including the production of oil along with water to graphically represent and analyse the correlation between water cut and total fluid produced for different modeled scenarios. The author demonstrated that in conventional and fractured reservoirs, the critical rate is controlled by the same parameters and thus, same forces govern flow. They stated that the water cut level depends on the ratio of the height of the bottom water to the total fluid height in the reservoir $\left(h_w / h_T \right)$, even at high production rates.

Dai et al. (2011) presented a novel technique of controlling water coning in a horizontal well. Their technique is based on the principle of density segregation among active fluids, water and oil, which have been investigated using a physical model (Figure 2-25) and applied successfully in the field with good results. It is pertinent to know that this method was applied to a reservoir with 100% water cut and after treatment resulted in an oil increase of 16.3-27.4 tonnes per day and an average decrease in water cut of 6%-9% in one-year after treatment.
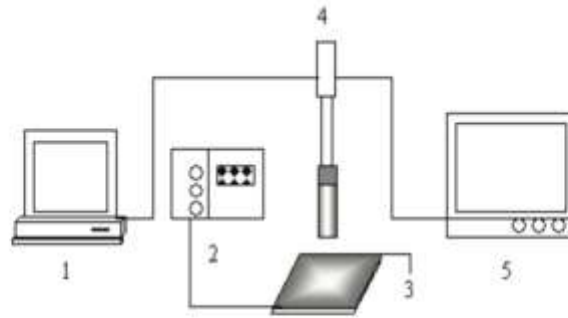
Figure 6. Visual physical simulation device
1—computer, 2—syringe pump, 3—model, 4—video camera, 5—TV
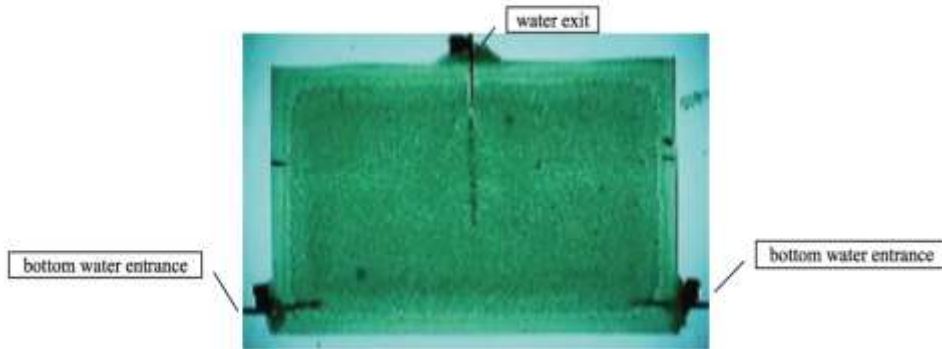
Figure 2-25: The model of thin reservoir with bottom water (Dai et al., 2011)

This technique involves the use of polymer gel, which is injected after brine, which has a density higher than oil and accumulates in the water-oil transition zone to protect the polymer gel from entering the water zone. Gelant having a higher density than oil but less dense than brine, was then injected into the high effective permeability zone to reduce the flow of water than oil. Over-displacing fluids succeeded this, which displaces the gelant out of the water-coning channel and reduce reservoir pollution. Fresh water, a displacing fluid was then used to displace the over-displacing fluid out of the percolation zone. The well was then shut-in to allow for gelation to build-up gel packer. These steps are illustrated in Figure 2-26. However, another treatment is required once water coning is experienced and consumes time due to the steps involved and the wait for gelation period.
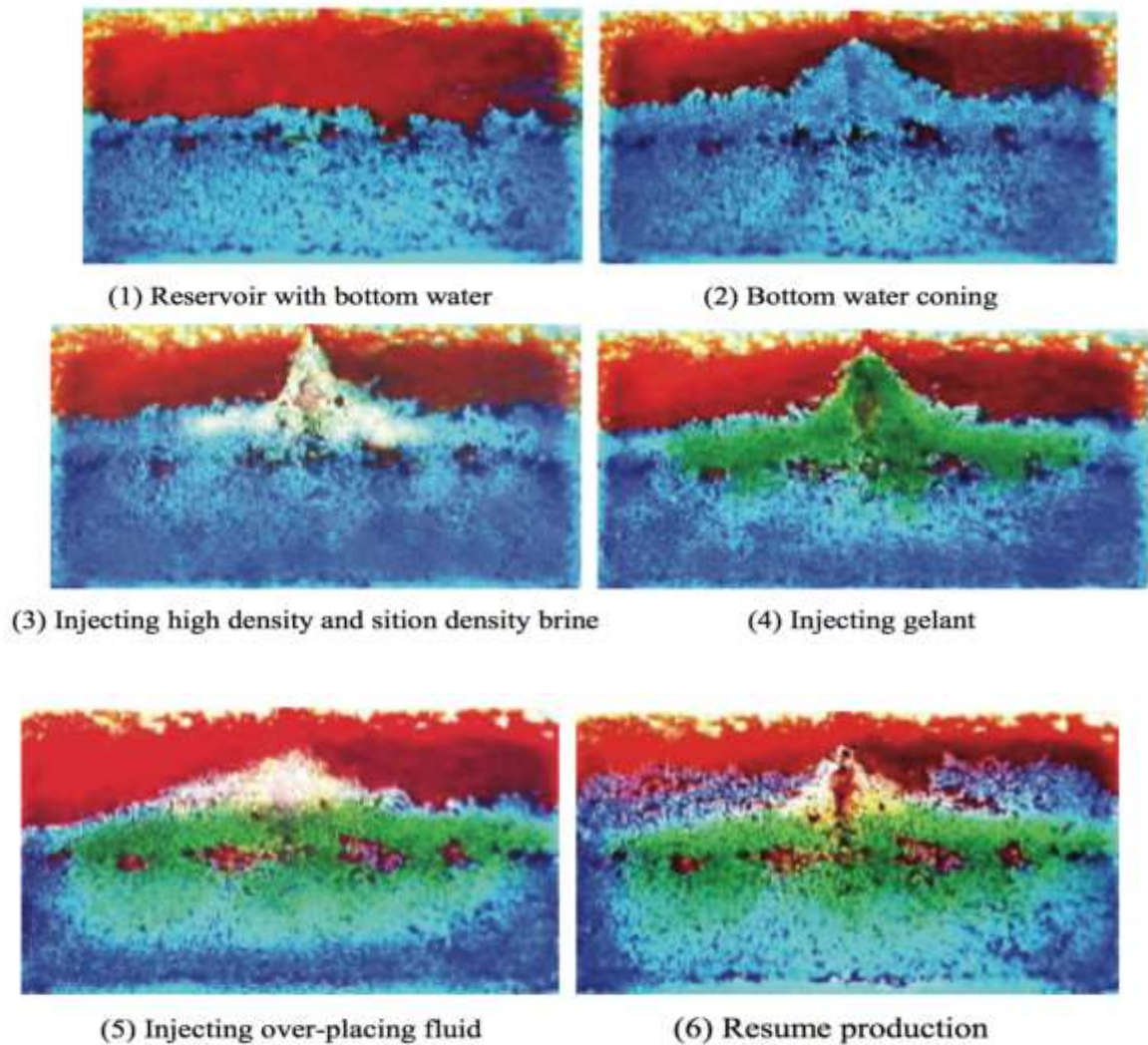
Figure 2-26: Visual physical simulation experiments (Dai et al., 2011)

Wu et al. (1995) performed a field study of horizontal well design in reducing water coning. This study was done in Amber field, a thin-oil rim reservoir with gas-cap and bottom water using a coarse-grid numerical model. Sensitivity analysis was further performed for horizontal wells to assess the effect of vertical position, well length and liquid offtake rate. From their results, they observed that water coning is reduced using longer horizontal wells due to lower drawdown; higher sweep efficiency is attainable with longer horizontal wells at longer fluid contact. More so, placing the horizontal wells in the WOC resulted in higher oil recovery but greater water cut. Water coning does not increase after a threshold is reached, the vertical position of the horizontal well has less effect on gas production due to high mobility, oil production reduces as gas is being produced, making it a major contributing factor to oil production and well length is considered important when placed close to the WOC.

Smith and Pirson (1963) employed physical and analytical method to investigate the effect of fluid injection to control water coning in oil and gas wells. The factors investigated in their study were the oil thickness, the point of fluid injection, viscosity of the injected fluid, the relative thickness of the oil and water sections and the position and length of the completion interval. The overall effect of the investigated parameters in terms of water-oil ratio was also evaluated. The authors reported that the net WOR can be reduced by fluid injection, which depended greatly on the investigated parameters. The injection fluid in this case could be either water or oil and if less than the reservoir connate water, this injected fluid will not be lost, thereby reassuring the use of valuable oil.

Great success in reducing or suppressing water production was reported by Smith and Pirson (1963) when the reservoir oil was less viscous than the injected fluid or when there is low effective permeability at the area of fluid injection. However, the use of cement pancakes or impermeable barriers proved less efficient. However, it was observed that the cone shape and injection profiles in the analytic, radial and experimental models were very similar. Fuel oil colored blue using an oil-soluble dye and water were used in their investigation. It was pertinent to note that for injection purposes, the fuel oil was mixed with viscous mineral oil. They concluded that without fluid injection, the shape of the cone does not depend on the withdrawal rate of the oil and for maximum efficiency of water cone suppression, the injection point should be far down to achieve a high net oil production.

Muskat and Wyckoff (1935) discussed important characteristics of water coning mechanism; the water cone height increase with increase in oil production and at 50-75% of the water cone height to the bottom of the well instability is attained, the apex of the water cone at stability is very sensitive to pressure differential such as a slight increase in oil production. They stated that water production can be eliminated from thin-oil rim reservoirs when the well produces at low or uneconomical rates basically below the critical rate, irrespective of the oil zone thickness, the well with minimum penetration results in a lower WOR while a 15-20% penetration is considered negligible in terms of WOR. They also stated that production by swabbing could result in considerable amount of water, which can be eliminated by steady state flow condition at same or higher oil production rate. (Muskat and Wyckoff, 1935) stated that the gas coning has the same mechanism except in is inverted cone shape. They considered gas coning favourable to control due to a greater density difference between oil and gas compared to that of oil and water.

Rajan and Luhning (1993) proposed an anti-water coning effect by gas injection such as nitrogen, methane and carbon dioxide. As the gas migrates towards the well perforation in the form of a "blanket", this increases the free-gas saturation, effecting a three-phase region. This process reduces the relative permeability of water and oil, and if the gas is soluble in oil, this will reduce the viscosity and increase the mobility of the oil, leading to a greater sweep of the oil by the gas. However, they stated that this method is not feasible for live-oil, which already contains significant dissolved gas. Rajan and Luhning (1993) also investigated plugging of pore by in-situ formation of viscous water in oil emulsion with acidic gas injection. Their study was performed both numerically and experimentally. The physical model used for their investigation was a 150 cm cylindrical or radial cell test facility.

Khan (1970) carried out an experimental study on water coning similar to that performed by Caudle and Silberberg (1965), Soengkowo (1969) using a pie shaped model. The study was focused on thin-oil rim homogeneous reservoir type. The porous media was modeled using graded sand consolidated with epoxy resin for the oil zone and unconsolidated sand with different mesh sizes in the water zone. The different sand types were used to simulate mobility ratios and allow residual oil saturation effects. However, the oil and water used in his experiment were miscible although having different viscosities and density and colour. The coning development process for each case of the experiment was made possible using transparent plastic. From this study, it was observed that: the influx of oil in the coning region depends on the oil production rate, the mobility ratio is an important parameter in water coning process. For a mobility ratio, higher than unity, the water cone height rises faster to the well perforation while having a lesser initial radial spread when compared to a mobility ratio less than unity, characterized by an initial radial spread in all directions prior to a gradual increase in water cone height towards the well, there is significant increase in water cut with increase in production rate.

Permadi et al. (1997) performed a laboratory experiment to study water-coning behaviour with a "stinger" (having a smaller diameter than the liner) inserted in the horizontal section of the well, aimed at investigating the displacement efficiency of the water cone and the performances of the stinger after breakthrough. This was possible using a physical model. The model was made of Plexiglas for effective visualisation of the water coning process while changing the lengths of the stinger. The oil viscosity and the oil column thickness

were also varied. The results indicate that a steeper profile of the water cone shape was seen for a no-stinger well although a higher oil to water ratio was achieved initially. More so, they observed that the use of stinger enabled effective pressure drop distribution in the horizontal well section, having an optimum length of 0.3 the length of the horizontal wellbore section irrespective of the mobility ratio and oil column thickness. However, the contribution of the inclined section of the well was neglected.

Ozkan and Raghavan (1990) focused on predicting the breakthrough time for water and gas coning by developing an approximate analytic model. In their study, they considered both horizontal and vertical wells. They concluded that a longer breakthrough time could be achieved using a horizontal well due to lower pressure drop in the reservoir when compared to vertical wells.

Jiang and Butler (1998) investigated the effect of different flow rates and viscosity ratios on the stability of the Water-Oil interface to a horizontal well. More so the shape of the water-oil interface and oil recovery was analysed under unstable flow condition. This was performed using a physical model. The model was made of Perspex plates for visibility of the coning process. Water was injected from the bottom using a calibrated syringe while oil was fed from the top to achieve a WOC; where the water and oil are separated by density differences. The oil and water were dyed with contrasting colours to enable a clearer water-oil interface. The coning process was captured using a 35-mm camera.

From their study, it was observed that at breakthrough the oil recovery decrease with flow rate and viscosity ratio. However, oil recovery was high at higher flow rates when multiple fingers are formed. This is because of more sweep efficiency offered by the water. The viscosity ratio between the displaced fluid and displacing fluid determines the water cut. More so, a sharper cone is achieved at higher withdrawal rates.

Aziz et al. (1973) investigated numerically the effect of horizontal permeability, vertical permeability and bottom water influx on the WOR. The simulation strategy was such that the withdrawal rate equals the bottom water influx. Arguably, their results show that higher WOR is attained at lower water influx. This is not true because it has recently been proven that at lower water influx, there will be lower mobility ratio and as such a lower WOR and vice versa.

Graue and Filgate (1971) numerically studied water coning in the Kaybob South Beaverhill Lake Gas Field in West Central Albert. Their investigation was because of the drastic effect of water coning in nearby fields. Vertical and horizontal permeabilities as well as oil withdrawal rate were varied to investigate the effect of the input data on critical rate. The vertical and horizontal permeabilities were found to have effect on the critical rate.

Thakur and Flores (1974) numerically studied the effect of oil viscosity and withdrawal on WOR in a heterogeneous and anisotropic reservoir. One significant observation from their study showed that higher withdrawal rates results in higher WOR.

2.9   Chapter Summary and Motivation of research

Most research on water and gas cresting have focused on critical rates, breakthrough times, its delay and prevention, but very few have considered the inclined section at low angles of inclination for optimization purposes for horizontal wells in oil reservoir faced with cresting problems.

An optimum geometry for deviated or inclined wells for improved oil recovery in cresting scenarios is very important, since cresting will occur at some point despite producing at the critical rate (Leemhuis et al., 2007). Investigations in use of horizontal wells in reducing cresting effects but have only considered the effect of varying the lateral lengths and measured depths of inclined or deviated wells without considering the effect of the steepness (varying inclined section) on its performance. Therefore, a novel procedure for mimicking inclined or deviated wells was developed and presented in this thesis. Varying the inclined section was possible using compression and pneumatic fittings. The modeled inclined sections can be fitted to the lateral and main bore sections with ease, using these fittings thereby allowing a change in MD, TVD, HD, vertical and horizontal displacements of the inclined sections at preferred angles of inclination.

This study was also motivated by the work of Beattie and Roberts (1996) who, carried out numerical parametric study to identify factors that contribute to water production into a vertical well in a naturally gas fractured reservoir. They stated that shutting-in the well for several days to allow the water level in the fractures to recede did not yield a sufficiently long period of low water production to be continued for a long term. Therefore, this thesis also sets out to investigate the feasibility of using a simple and inexpensive electromagnetic valve surface installation to proactively control cresting in a homogeneous reservoir

characterized by both strong bottom aquifer and considerable gas cap drive mechanisms. The mechanism of producing lower volumes of cumulative water at higher oil recovery ratios "ratio of volumes of oil recovered from an oil reservoir to the initial oil in place" in homogeneous oil reservoirs with considerable gas cap and strong bottom aquifer was the goal. The mechanism of this procedure is principled on gravity segregation, wettability consideration and density difference (acting against existing viscous and gravitational forces during cresting).

Cresting behaviour is usually modeled using the ECLIPSE reservoir simulation software. However, it is impossible to validate physical models due to insufficient data from the physical model. To date, the limited information on the use of CFD to quantitatively and qualitatively validate cresting exist. Therefore, in this thesis, the use of CFD in modeling and validating water and gas cresting occurring simultaneously in an oil reservoir, using data from an experimental model will be ascertained which encompasses performing sensitivity analysis on the effect of porosity, pressure drop and production time on oil production rate, WOC and GOC.

An introductory section on cresting or coning problems encompassing its cause and effect in oil and gas reservoirs were presented. In addition, a thorough review of past researches relating to optimization in crest or cone-affected reservoirs as well as its control were presented in details. Finally, a section highlighting the research perspective was presented.

CHAPTER-3

APPARATUS, EXPERIMENT SET UP, PROCESSING AND DATA ACQUISITION

3.1 Introduction

The purpose of this Chapter is to present detailed information on the apparatus used for the design of the water and gas-cresting rig. The equipment used in the data collection and measurement processes are described individually with application reasons such as specifications to fit the rig design process. The procedures involved in safe operation of the water and gas-cresting rig is also presented in a stepwise manner. A summary of the experimental procedures, processing and data acquisition have been presented.

3.2 Apparatus and Experimental Set up

The cresting apparatus used in this investigation comprises of a simulated reservoir illustrated in Figure 3-1(a). Figure 3-1(a) illustrates the reservoir, horizontal well and the section of the horizontal well which was the focus in this research, varied at 15-30° angles of inclination. The reservoir was made of clear Poly (methyl methacrylate) [PMMA] or acrylic with a density of 1180 kg/m^3. Clear PMMA was the preferred material for good cresting visibility (Balazs et al., 2009). The reservoir was assumed to have a free surface "imaginary surface open to the atmosphere" at the top as shown in Figure 3-1(b) for purposes of easy filling of the clear PMMA with porous media (reservoir grains) and gas cresting modeling. As can be seen in Figure 3-1(b), the reservoir was rectangular shape with interior dimensions of 0.45 m x 0.10 m x 0.43 m. The reservoir fluids used were silicone oil, water and air (gas). Note that the reservoir was generally considered to be water-driven because the bottom water injection rate was generally greater than the cumulative liquid withdrawal rate. This injection rate was maintained throughout the experiment through water inlet points 1 and 2 shown in Figure 3-1(b).
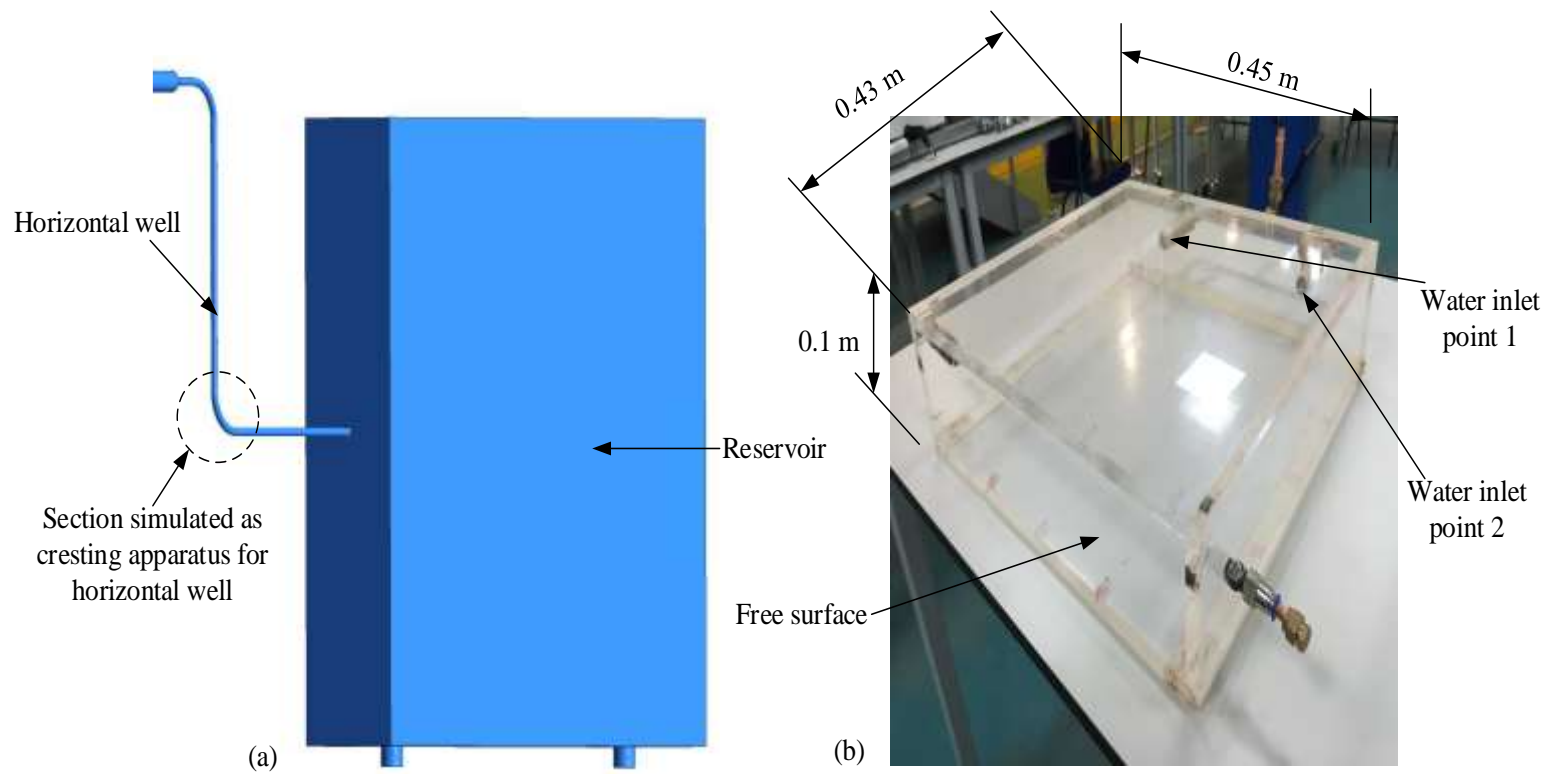
Figure 3-1: Reservoir design
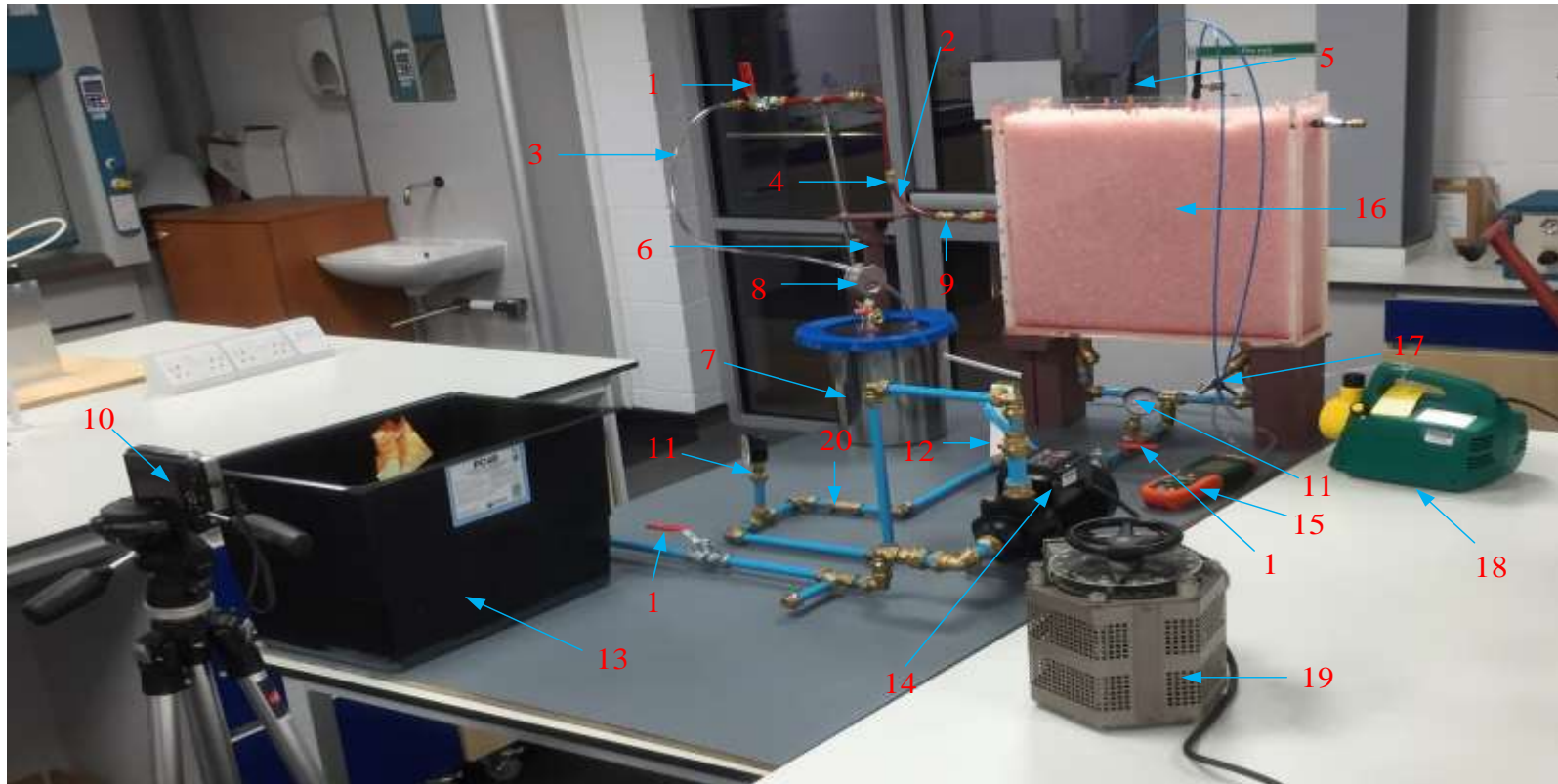
1- Ball valve,   2- Horizontal well,   3- Flexible tube,   4- Pneumatic fitting,   5- Digital manometer pressure tapping,   6- Clamp,   7- Vacuum chamber,   8- Vacuum gauge,   9- Compression fitting,   10- Digital camera,   11- Pressure gauge,   12- Rotameter,   13- Water storage tank,   14- Centrifugal pump,   15- Digital manometer,   16- Reservoir,   17- Drain,   18- Vacuum pump,   19- Variac transformer, 20- Non-return valve

Figure 3-2: Complete assembly of the Water and gas-cresting rig
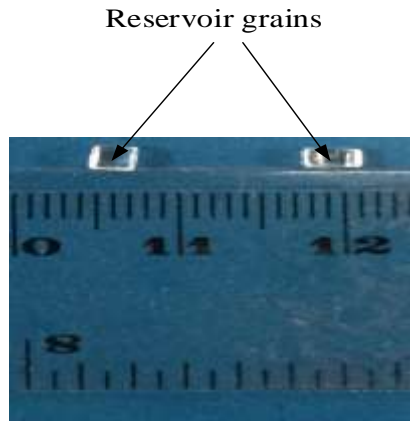
Figure 3-3: Reservoir grain measurement

The overall water and gas cresting apparatus shown in Figure 3-2 includes vacuum chamber (7) which was controlled by a Stanhope-Seta Vacuum pump, Model #22422-6P (18). The Vacuum pump (18) was the source of the pressure differential necessary to instigate cresting and can produce up to 14.50×10^{-5} Psig maximum vacuum. The flow rate of the pump is 700 cm^3/s, consuming 120 W of power. Air and other gases are taken out of the vacuum chamber (7) using a vacuum pump (18). This results in a low-pressure area inside the vacuum chamber. For oil to be produced, there must be a pressure drop between the reservoir and the surface. In this case, the vacuum acts as the low-pressure domain, hence effecting an outflow of fluid from the reservoir to the vacuum chamber. The material (vacuum chamber) was made up of stainless steel and directly connected to the reservoir (16) and the vacuum pump (18). A glycerine-filled vacuum gauge (8) was attached to the vacuum chamber, which reduces condensation, atmospheric corrosion inside the gauge and is suitable for use with Silicone oil, water and air (gas). The vacuum gauge (8) was used to control the pressure in the vacuum chamber (7), with a reading range from 0 to -14.50 Psig. To simulate a homogeneous reservoir, the acrylic tank illustrated in Figure 3-1(b) was thus filled with same-sized Polyethylene terephthalate (PET) polymer pellets (reservoir grains), measuring 0.002 m x 0.002 m x 0.003 m as shown in Figure 3-3. A variable area rotameter (12) was used to measure the bottom water injecting rate through the bottom water inlet points 1 and 2 as shown in Figure 3-1(b). The FL-2052 was designed to operate at a maximum pressure of 100Psi with an accuracy of $\pm$ 5% full scale (FS). A 0-60 Psi FLOWFIT pressure gauge (11) was used for measuring the water delivery pressure to the variable area rotameter (12). The accuracy of the pressure gauge was $\pm$ 2.5 Full Scale Deflection (FSD).

50

A EP2M model centrifugal pump (14) was used to pump water from the water storage tank (13) to the bottom of the reservoir. The centrifugal pump (14) has a 45m delivery head and a flow rate of 666.67 cm^3/s. Due to the high flow rate of the centrifugal pump relative to the size of the experiment, a Variac transformer RS Pro 1 phase 480 VA Variac (19) was connected directly to reduce the Revolution Per Minute (RPM) of the centrifugal pump (14). For accuracy of experimental results, the Variac scale was maintained at scale reading of 142 (160 cm^3/s) throughout the experiment and further regulated using the variable area rotameter (12). An Extech HD700 differential manometer (15) was used to measure the differential pressure in the reservoir (16) during experimental runs with the aid of the digital manometer pressure tapping (5). The two pressure tappings from the manometer were placed at a fixed position near the perforation area of the wellbore throughout the duration of the experiment. The accuracy of the manometer was $\pm$ 0.3% FS. The water and gas-cresting behaviour of the water and gas was recorded using a COOLPIX S9100 digital camera (10) to enable the process to be analysed frame by frame. Ball valves (1) were used to abruptly turn on and shut-off production of oil or injection of bottom water by simply rotating its handle. At the end of each experimental run, the reservoir phases (oil and water) left behind was drained off through the drain (17). The flexible tube (3) provided a connection between the horizontal well and the vacuum chamber while pneumatic fitting (4) and compression fitting (9) connected the vertical and lateral sections of the horizontal well respectively. The horizontal well (2) was held in place and adjusted when necessary by the clamp (6). The non-return valve (20) was installed to prevent damage of the centrifugal pump (14) and variable area rotameter (12) from possible back-pressure that could result during rig operation.

Figure 3-4 show the apparatus set up for water and gas-cresting control. A normally closed type solenoid valve (electromagnetic) (2) was used for instances of water and gas-cresting control. In such instances, the normally closed solenoid valve installed at the surface of the horizontal well (3) controlled oil production while the ball valve (1) ensured that the horizontal well (3) is open to production from the reservoir (4).

1- Ball valve,   2- Solenoid (electromagnetic) valve,
3- Horizontal well,   4- Reservoir
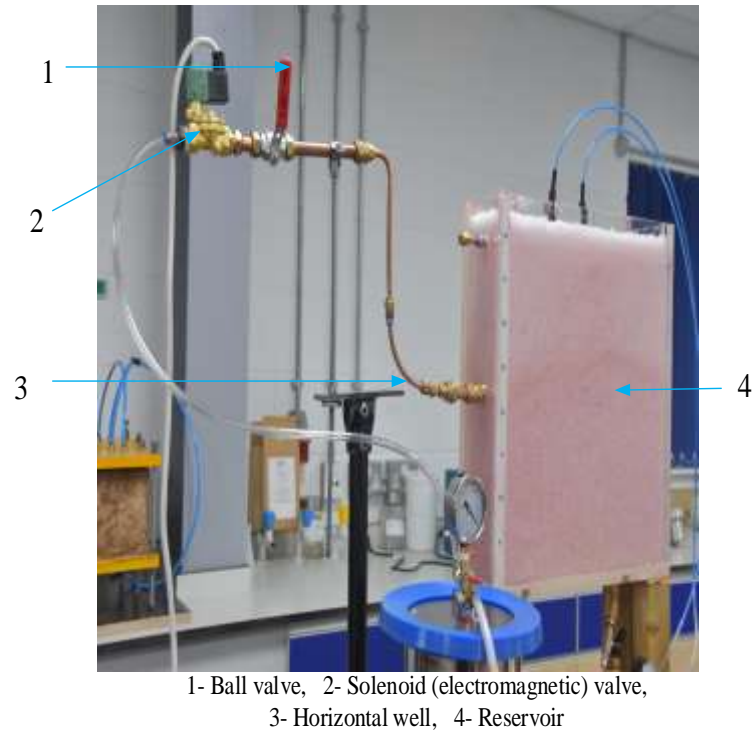
Figure 3-4: Water and gas-cresting rig showing electromagnetic valve

The flow diagram of the water and gas-cresting rig apparatus set up illustrated in Figure 3-2 and partly in Figure 3-4 is shown in Figure 3-5. In this diagram, the water line represents the direction of water injection through the bottom water inlet points 1 and 2 (Figure 3-1(b)) while the oil/water/gas line depicts the direction of flow of the reservoir phases during oil production.
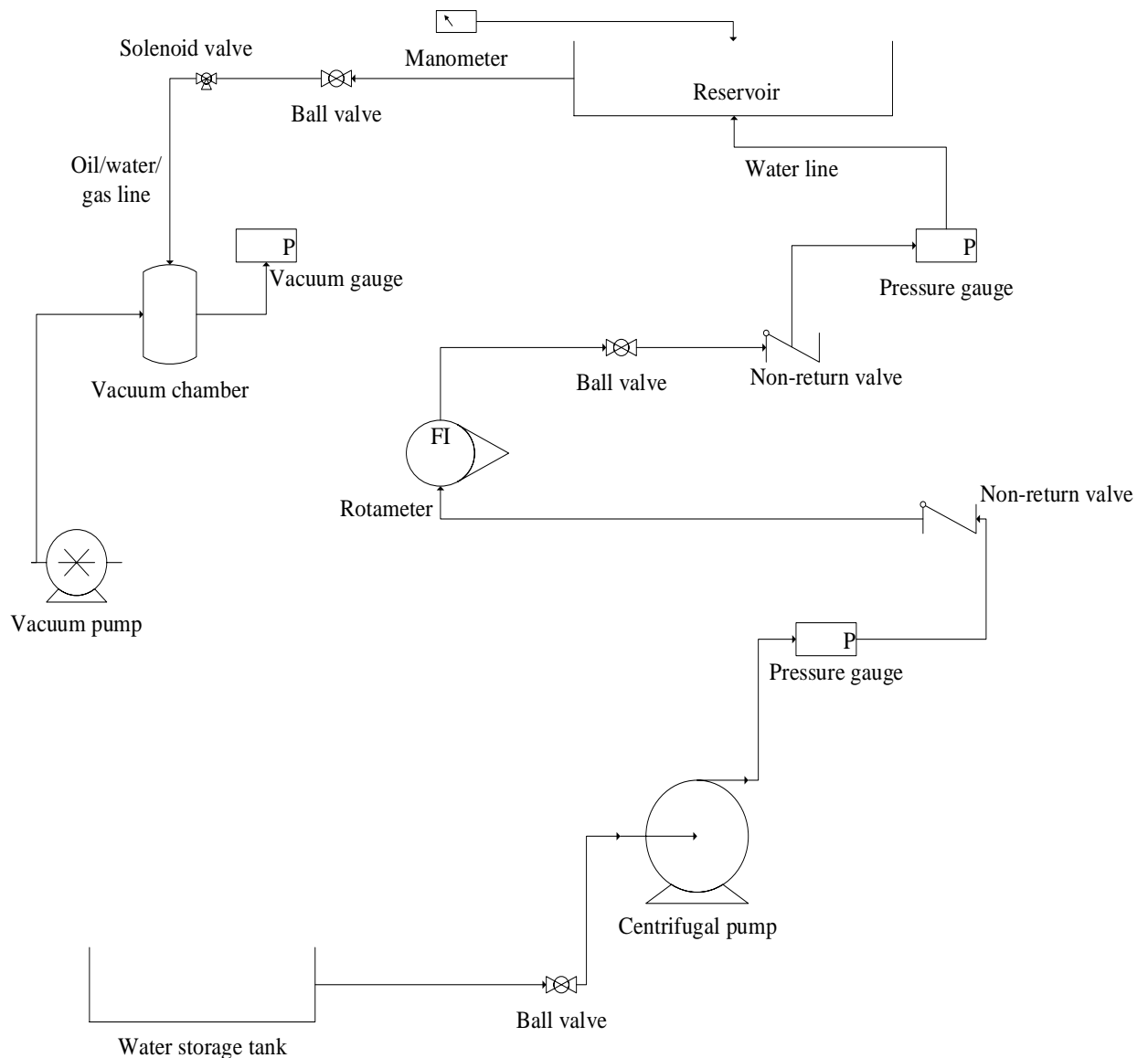
Figure 3-5: Flow diagram of experimental set-up

3.2.1   Horizontal well design

The horizontal well and its sections illustrated in Figures 3-1(a), 3-2, 3-6 and 3-7. were constructed using copper pipe. The horizontal well had an outer diameter (OD) of 0.008 m and internal diameter (ID) of 0.006 m. As shown in Figure 3-6, the lateral section exposed to the reservoir measured 0.305 m ($0.67x$ the reservoir length) and 0.251 m ($0.56x$ the reservoir length) used for sensitivity analysis. The perforation hole (1) sizes, 0.002 m OD were drilled at four perforation holes per cross section to instigate a radial flow of reservoir fluids into the wellbore. Since the completion system used for the horizontal well was a

closed-hole completion type, a bridge block (3) was used and as such flow of the reservoir fluids will be only through the perforations of the well. The opposite end of the lateral section of the horizontal well was compression fitted to the inclined section (2). The distance from the bridge block (3) to the first perforation in all cases was 0.04 m while the distance between the two-perforation areas of the lateral section of the wellbore was 0.05m.
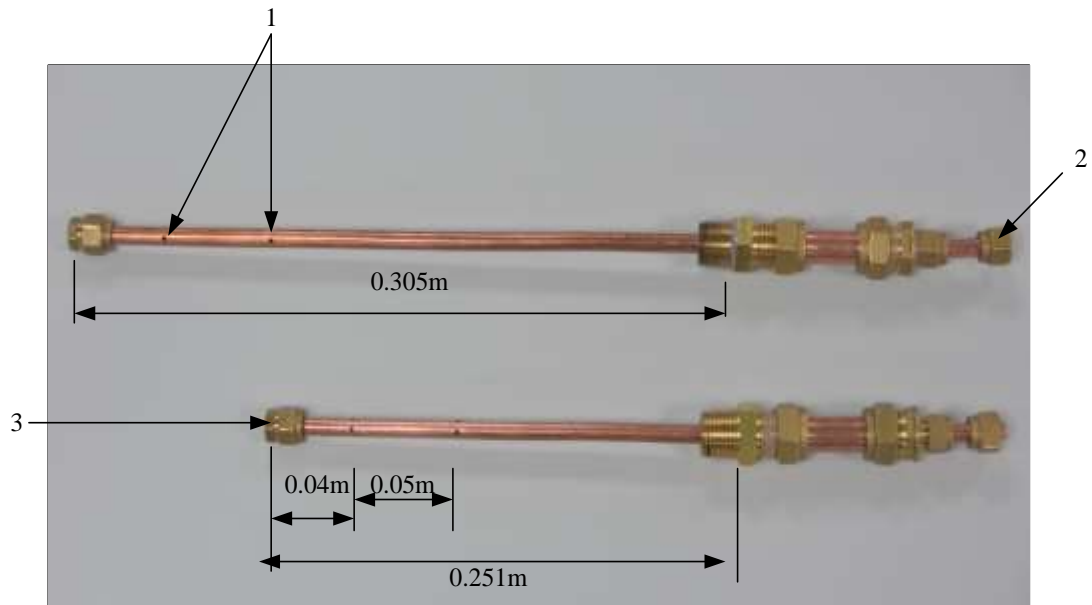
1- Perforations,   2- Connection to inclined section of well,   3- Bridge block

Figure 3-6: Different lengths of lateral section of horizontal well showing the perforations and bridge blocks

The constructed inclined sections showing connection points to the vertical and horizontal sections of a horizontal well, constructed at 15°-30° angles of inclination are illustrated in Figure 3-7. A comprehensive summary of the dimensions for the different geometries of the horizontal well models used in this investigation, such as the Measured Depth (MD), True Vertical Depth (TVD), Horizontal displacement of the inclined section (H_d), the ratio of the Vertical Displacement of the inclined section to reservoir height (V_d / H_r) and length of horizontal lateral section (LH), are illustrated in Tables 3-5 and 3-6. The radius of arc *r*, for each inclined section was calculated using Equation 3.1. The horizontal well cases were categorized based on calculated radius of arc, into either short, medium or long horizontal wells. As shown in Table 3-2, Cases-1A, 1B and 2A were considered long radii, Cases-3A, 2B and 1C, medium radii wells, while Cases 3C, 3B and 2C were short radii wells. The symbols in Tables 3-1 and 3-2 are illustrated in Figure 3-8. Figure 3-8 also shows cresting occurring simultaneously at Time (T) greater than (>) 0 s at both the GOC and WOC. For each experimental run, the cases illustrated in Figure 3-7 (also denoted by H_d and V_d sections

in Figure 3.8) will be varied for the horizontal well during water and gas-cresting (at GOC and WOC > 0 s). Varying the inclined sections at constant main bore (1) and lateral length outside reservoir (4) will result in change in TVD (2).

$$l = \frac{\theta}{360^o} \, x \, 2\pi r \qquad (3.1)$$

Where,

l = Length of arc in m

θ = Angle in degrees (°)

r = Radius of arc in m

π = 3.142
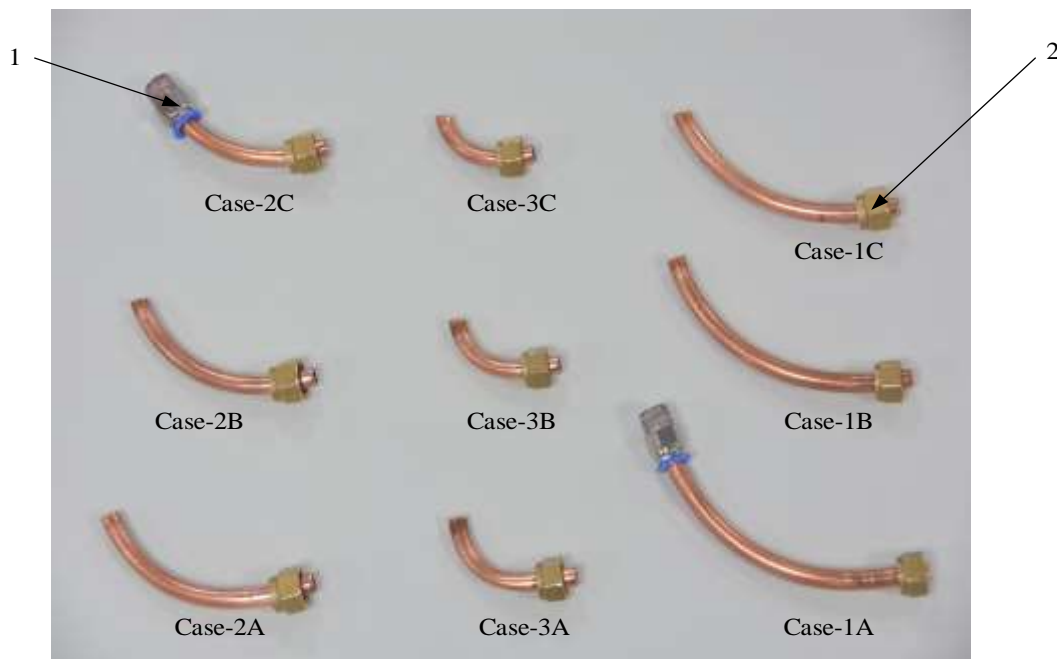
1- Pneumatic fitting to vertical section of well, 2- Connection to horizontal section of well

Figure 3-7: Constructed inclined sections of horizontal well

Table 3-1: Geometry and dimensions of horizontal wells [E-1 (m)]

Cases	Angle of inclination (Degrees)	Measured Depth (MD)		TVD	Build section Measurement		V_d/H_r	Main bore	Lateral length outside reservoir
		MD_1	MD_2		V_d	H_d			
Case-1A	15	7.18	6.64	2.17	0.77	1.02	0.179	1.40	1.68
Case-1B	23	7.01	6.47	2.03	0.63	0.93	0.147	1.40	1.68
Case-1C	30	6.90	6.36	1.94	0.54	0.85	0.126	1.40	1.68
Case-2A	15	6.83	6.29	1.90	0.50	0.80	0.116	1.40	1.68
Case-2B	23	6.76	6.22	1.87	0.47	0.78	0.109	1.40	1.68
Case-2C	30	6.64	6.10	1.74	0.34	0.73	0.079	1.40	1.68
Case-3A	15	6.48	5.94	1.72	0.32	0.49	0.074	1.40	1.68
Case-3B	23	6.40	5.86	1.69	0.29	0.44	0.067	1.40	1.68
Case-3C	30	6.34	5.80	1.67	0.27	0.41	0.063	1.40	1.68

Table 3-2: Geometry and dimensions of horizontal wells continued [E-1 (m)]

Cases	Length of horizontal lateral section (LH)		Horizontal departure of well		Length of lateral inside reservoir (l_r)		Arc length (l)	Arc radius (r)/well type
	LH_1	LH_2	HD_{w1}	HD_{w2}	l_{r1}	l_{r2}		
Case-1A	4.19	4.73	5.21	5.75	3.05	2.51	1.05	4.02 (LR)
Case-1B	4.19	4.73	5.12	5.66	3.05	2.51	0.88	2.23 (LR)
Case-1C	4.19	4.73	5.04	5.58	3.05	2.51	0.78	1.49 (MR)
Case-2A	4.19	4.73	4.99	5.53	3.05	2.51	0.70	2.68 (LR)
Case-2B	4.19	4.73	4.97	5.51	3.05	2.51	0.63	1.59 (MR)
Case-2C	4.19	4.73	4.92	5.46	3.05	2.51	0.51	0.98 (SR)
Case-3A	4.19	4.73	4.68	5.22	3.05	2.51	0.35	1.34 (MR)
Case-3B	4.19	4.73	4.63	5.17	3.05	2.51	0.27	0.70 (SR)
Case-3C	4.19	4.73	4.60	5.14	3.05	2.51	0.21	0.40 (SR)

MD (MD_1/MD_2) = main bore + l + lr

HD (HD_{WI}/HD_{W2})

lr (lr_1/lr_2)

GOC at T = 0 s

GOC at T > 0

WOC at T > 0

WOC at T = 0

LH (LH_1/LH_2)
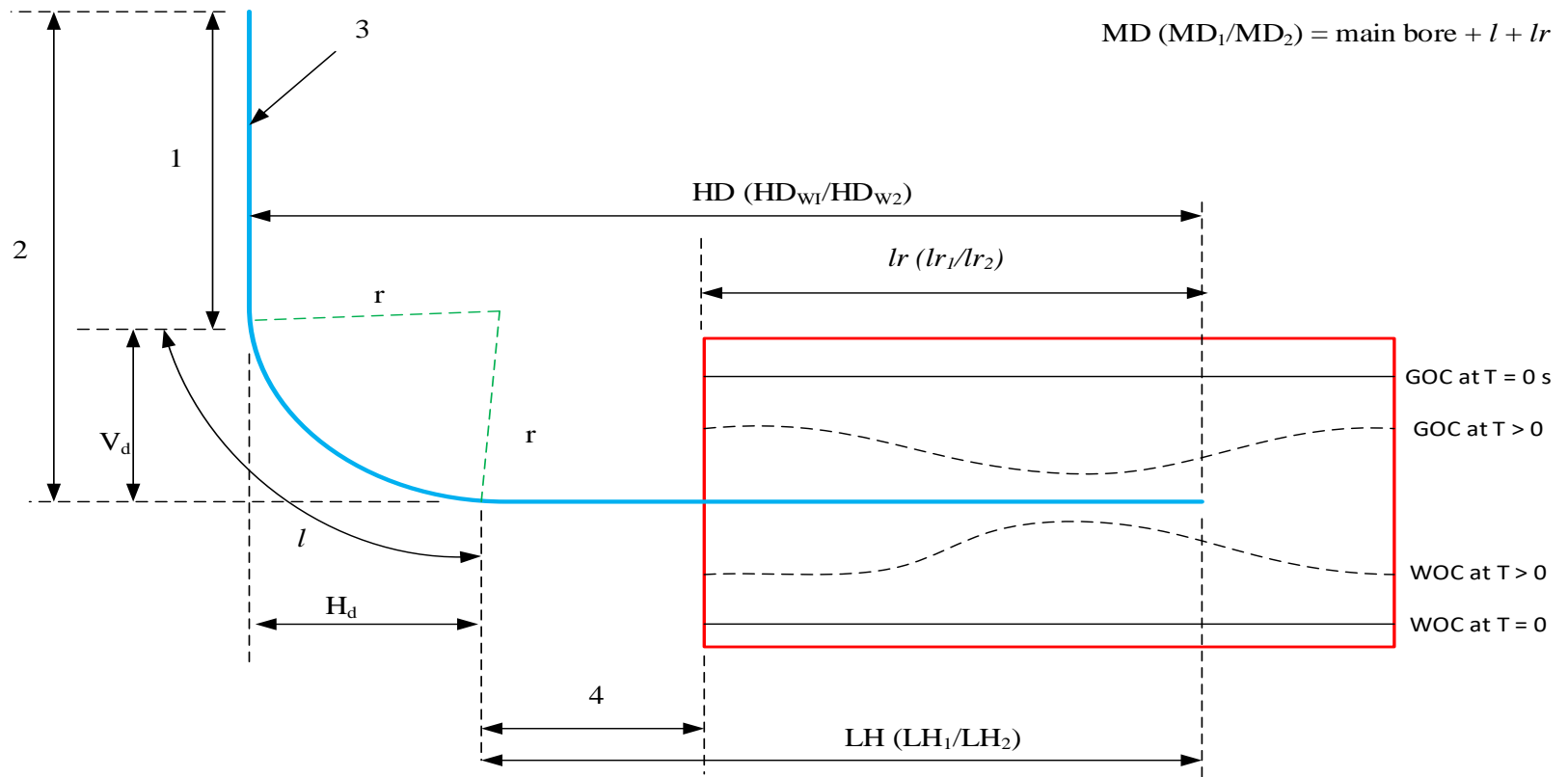
1- Main bore,   2- TVD,   3- Horizontal well,   4- Lateral length outside reservoir

Figure 3-8: Illustration of symbols that define the horizontal wells cases

58

3.3 Procedures for the Apparatus

The most important apparatus of the water and gas-cresting rig in Figure 3-2 was the reservoir also shown in Figure 3-9. Prior to the reservoir setup, the preferred horizontal well lateral section to be exposed to the reservoir described in Figure 3-6 was fitted to the reservoir. The reservoir was then filled with the reservoir grains. The reservoir fluids of interest: Fluorescein dyed water was first pumped through the bottom water inlet points 1 and 2 (described in Figure 3-1(b)) to the required WOC.

Next, Silicone oil (Dyed/undyed) a non-flammable oil, was introduced through and across the free surface in little volumes at intervals to achieve a rather uniform WOC as shown in Figure 3-9. This was continued until the desired GOC was reached. The modeled GOC used in this study were at 0.37 m and 0.28 m from the base of the reservoir while the WOC were at 0.03 m and 0.10 m. Hence a thin-oil rim homogeneous reservoir (oil column thickness of 0.18 m) and thick oil-rim homogeneous reservoir (oil column thickness of 0.34 m) were modeled as shown in Figure 3-9.
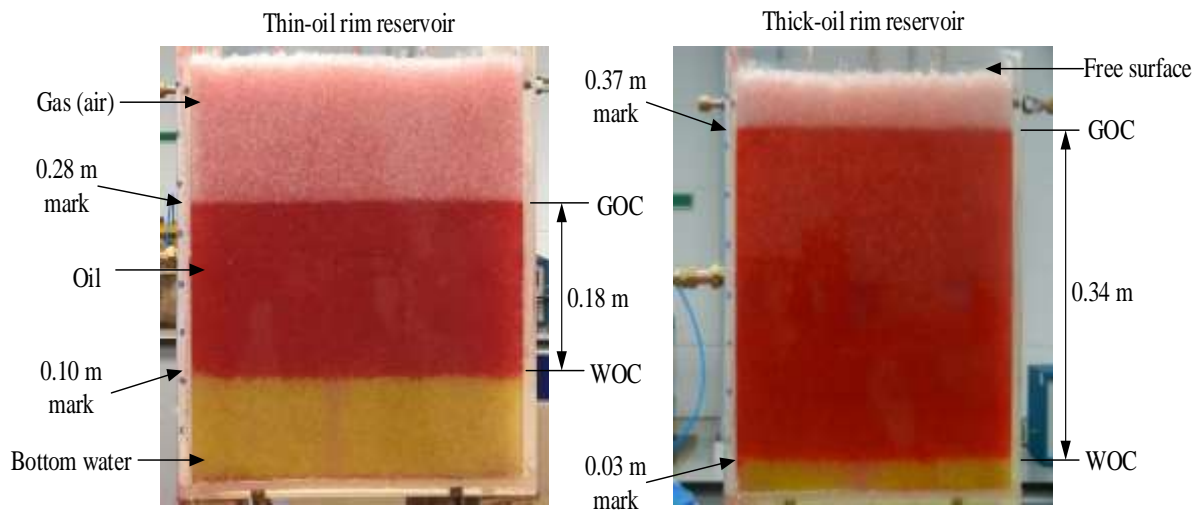
Figure 3-9: Reservoir set-up

The following procedures were conducted during the operation of the apparatus shown in Figure 3-2.

  a) *Procedure for the rig operation (Section 3.3.1)*

  b) *Procedure for determination of polymer pellets density (Section 3.3.3)*

  c) *Procedure for reservoir homogeneity determination (Section 3.3.4)*

i. Procedure for reservoir homogeneity determination (High interconnected pore spaces) (Section 3.3.4(a))

3.3.1 Procedure for the rig operation

1. A test for water leakages was performed and areas with water leakage were repaired.

2. The water storage tank was filled to a marked line in the tank prior to start of the experiment so that there would be adequate water available to be pumped through the system for the duration of one experimental run, as well as preventing damage to the centrifugal pump.

3. The vacuum pressure was then set at an initial outlet pressure, which is high enough to instigate cresting, -4.351, -7.25 and -10.15 Psig, while ensuring that the ball valve was at the close position during setting.

4. The water mass flow rate was set at 0.03 Kg/s during reservoir set-up. At -4.351 Psig, the cumulative liquid production rate for all cases was less than the water injection rate of 41.68 cm^3/s, depicting a strong bottom aquifer and considerable gas cap in the reservoir. Steps 1-3 were repeated in all experimental cases.

5. Production was started by opening the ball valve above the reservoir while synchronically starting the digital timer and opening ball valve below the reservoir for constant water injection.

6. During production, the variation in pressure drop (difference between the pressure read from the digital manometer (with probes placed at fixed points, 0.18 m from top-left and right edges respectively and depth of 0.22 m in the reservoir) were pressure from vacuum gauge) recorded thrice until 495 s and 210 s for the thick and thin-oil rim reservoirs respectively.

7. For accuracy, each experimental case was repeated thrice with good repeatability and the average liquid produced taken for each case. This was repeated for different lateral lengths in the reservoir, oil viscosity, WOC, GOC, different inclined section (different horizontal well measured depth).

8. At the end of each experiment, the cumulative produced liquid was transferred from the vacuum chamber into graduated cylinder for determining the volumes of oil and water produced.

3.3.2 Assumptions

The main assumptions of the simulation are:

- The WOC and GOC interfaces were assumed to be straight lines.
- Capillarity experienced at the different inclined sections was assumed to be negligible.
- The reservoir was assumed to have a free top surface.
- Time was assumed not critical for cresting control procedure.
- The extra length provided by the solenoid valve was considered negligible.

3.3.3 procedure for determination of polymer pellets density

Polymer pellets were used as the porous media. The density of the pellets was calculated as follows using buoyancy method illustrated in Figure 3-10:

1. An empty measuring beaker was weighed and recorded on a precision balance to two significant figures.

2. Next a volume of dry polymer pellet was poured in the beaker and weighed on a precision balance to two significant figures.

3. Another beaker was filled up to the 200-ml mark (1) with tap water.

4. The measured dry polymer pellet was then poured into the measuring beaker containing water. There was a significant rise in the water level (2), which is equivalent to the volume of polymer pellets.

(a)   (b)

1- Initial volume of water,   2- Volume of water displaced
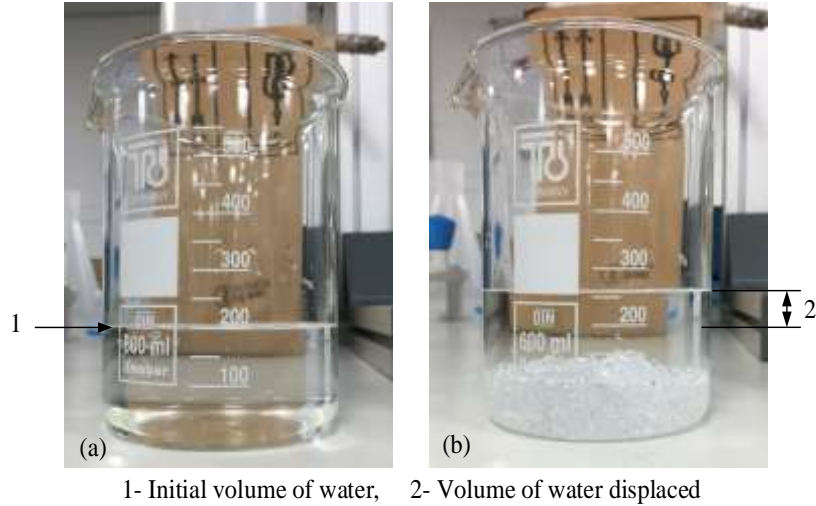
Figure 3-10: Determination of polymer pellet density using fluid displacement technique

5. The estimated density (1302 kg/m^3) of the polymer pellets were calculated using Equation 3.2.

$$\rho_{polymer\ pellet} = \frac{m_{bs} - m_b}{V_l}$$ (3.2)

Where,

ρ = Density in kg/m^3,

m_{bs} = Total mass of beaker and pellets in kg,

m_b = Total mass of beaker in kg

V_l = Volume of displaced fluid (clear water) in m^3.

3.3.4   Procedure for reservoir homogeneity determination

Although the size and arrangement of the reservoir grains used in this work does not mimic a typical homogeneous reservoir, it was considered homogeneous based on the same grain sizes as shown in Figure 3-11 and high degree of interconnected pore spaces. The reservoir grain size shown in Figure 3-3 was used because of the 0.002 m perforation hole sizes of the horizontal well illustrated in Figure 3-6. This will prevent the reservoir grains from being sucked-up with oil during oil production. The high-interconnected pore spaces were determined by first filling a cylindrical shaped vessel with the similar reservoir grains to replicate a typical core sample (Figure 3-11).

Figure 3-11: Homogeneous reservoir grains

A Computed Tomography (CT) scan was then performed with the GE Phoenix v|tome|x high-resolution CT Scanner (Figure 3-12).
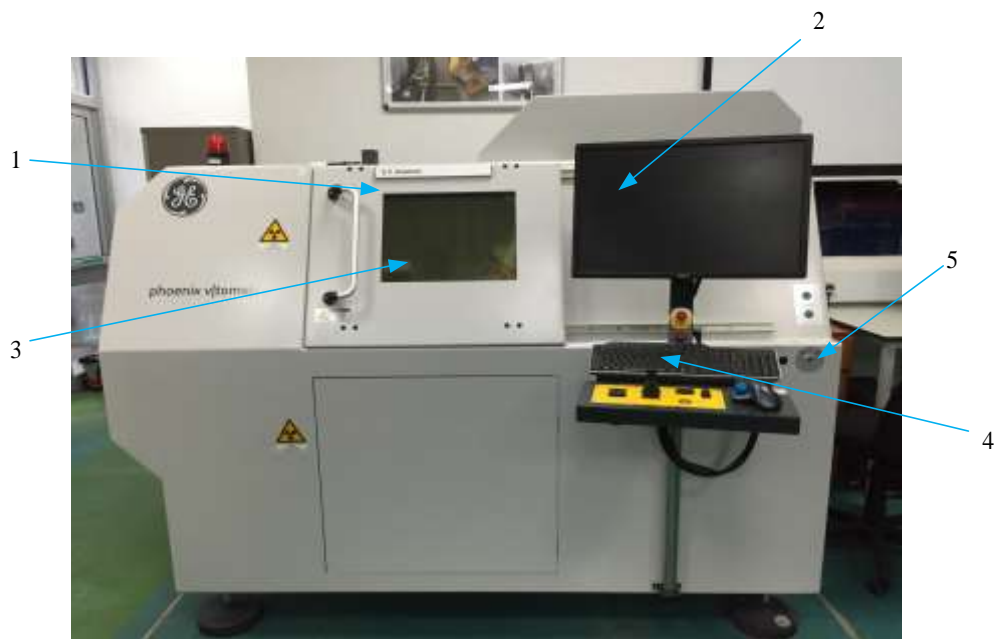
1- Sliding door, 2- Screen, 3- Sample manipulator and x-ray tube enclosure, 4- Control console, 5- On/off/stand-by switch

Figure 3-12: GE Phoenix v|tome|x high-resolution CT-Scanner

a) **Procedure for reservoir homogeneity determination (High interconnected pore spaces)**

1. The first step was to switch on the CT scanner (5) and personal computer where data processing will be done.

2. The reservoir grains sample was then inserted in the CT scanner through the sliding door (1).

3. The datos|x acquisition software   was opened and a new project was created.

4. Using the control console (4) and screen (2), the sample was positioned in the sample manipulator and x-ray tube enclosure (3) for scanning. As shown in Figure 3.13, the sample was tilted for effective penetration of the x-ray through the sample.

5. The X-ray was then turned on under the X-ray control window (highlighted blue in Figure 3-13 and live image pressed, after ensuring the sliding door was closed properly. The region of interest (ROI) was then selected.
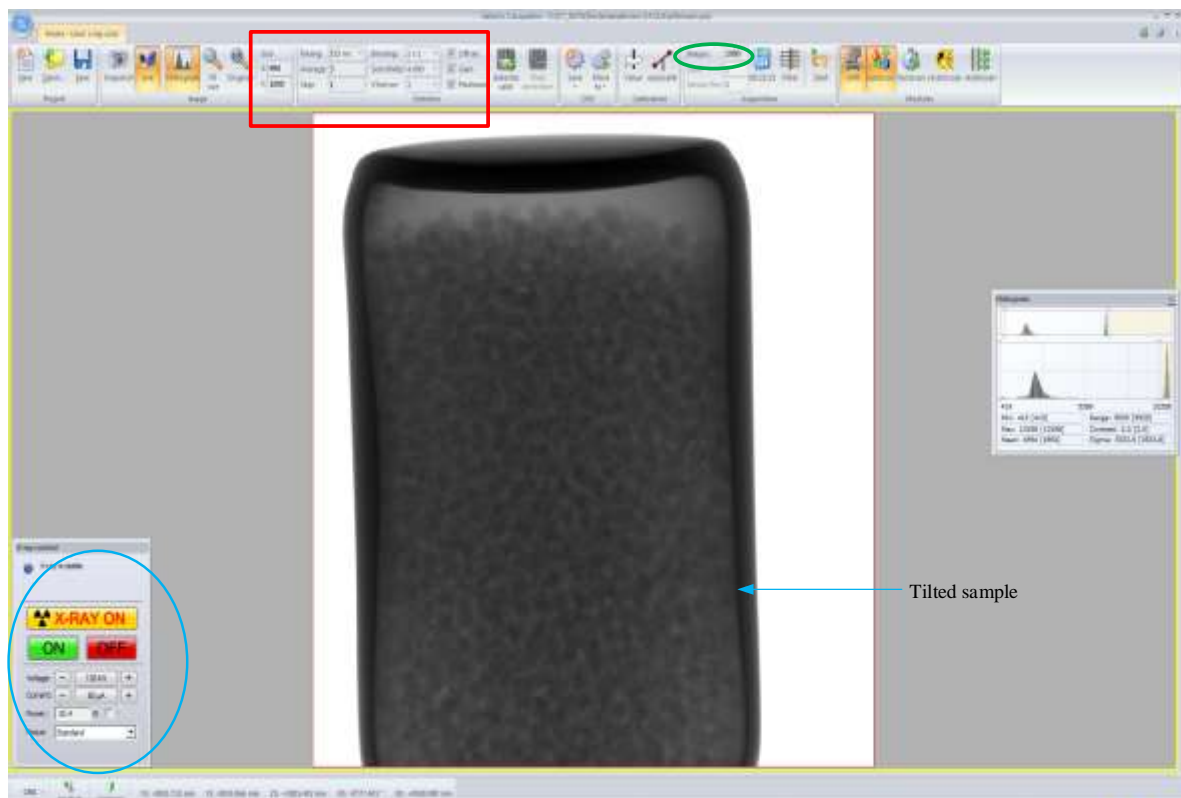
Figure 3-13: CT set up for sample

6. The settings highlighted blue, red and green in Figure 3.13 were then applied:

- Voltage – 130 kV
- Current – 70 µA
- Power – 10.4 W

64

- Focus – Standard
- Timing – 333 ms
- Images – 1000
- Average – 3
- Skip – 1
- Sensitivity – 4.000
- VSensor – 1
- Binning – 1x1

7. The CT scanner was run for a duration of 2700 s. The datos|x reconstruction was opened and the pca-file loaded. A Free-ray stability check was performed on the grey value in the first and last image. The scan|optimiser was used to correct system drifts and then reconstruction was run and result shown in Figure 3-14. Figure 3-14 illustrates a slice through sample (1) of the reservoir grains (3) showing the interconnected pore spaces (2).
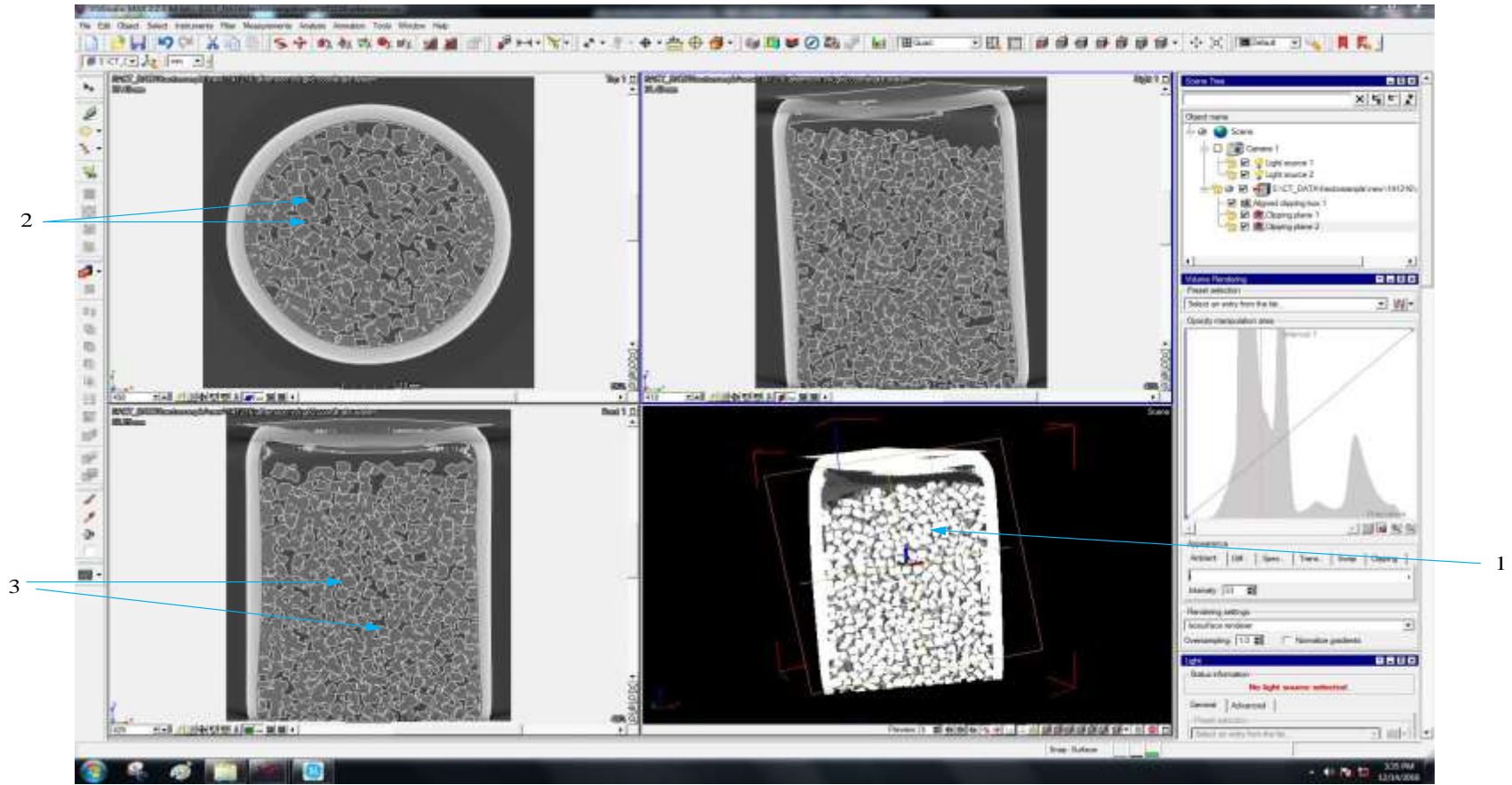
1- Slice through sample,   2- Interconnected pore spaces, 3- Reservoir grains

Figure 3-14: A slice through CT scan result of reservoir grains sample showing high-interconnected pore spaces

3.4 Measurements and data processing methods

3.4.1 Measurements

The following measurements were conducted:

a) *Density measurement*

    i. Density of silicone oil

    ii. Density of dyed tap water

b) *Viscosity measurement*

    i. Measuring viscosity of silicone oil and water

c) *Effective permeability determination*

    i. Effective permeability of reservoir fluids

d) *Total porosity*

a) Density measurement

i. Density of silicone oil

For visibility of cresting process pure silicone oil was colored with Oil Red O, a fat-soluble reddish-brown hydrophobic (water-repellent) dye shown in Figure 3-15. Little quantities of this chemical were mixed with large volume of clear silicone oil (3.15 g/$18,000$ cm^3), which was insufficient to affect its viscosity and density of the pure silicone oil. For higher accuracy of experimental data obtained, the water was poured until the 100-ml mark on the beaker was reached on eye level prior to weighing the sample (weight of fluid) and determining its density (Table 3-3).

Oil Red O
powder

Figure 3-15: Oil Red O

Table 3-3: Average weight and density of Silicone oil

Fluid in beaker	Average weight (kg)	Density (kg/m^3)
Silicone oil (50 cP)	0.38017	972
Silicone oil (100 cp)	0.28305	972

ii.   Density of dyed tap water

The water used in this study was dyed with Fluorescein sodium dye (Figure 3-16), an orange colored hydrophobic (water-repellent) dye and for visibility of the cresting process. During dissolution in water, the colour of the water changes to dark green in colour. Fluorescein is also known as colour additive. Fluorescein is a fluorescent dye and is derived from benzene and its derivatives and contains 4 aromatic rings of carbon. The experimental results for averaged weight and density of the dyed water are shown in Table 3-4.

Table 3-4: Average weight and density of dyed water

Fluid in beaker	Average weight (g)	Density (kg/m^3)
Dyed water	0.28565	998

Fluorescein powder
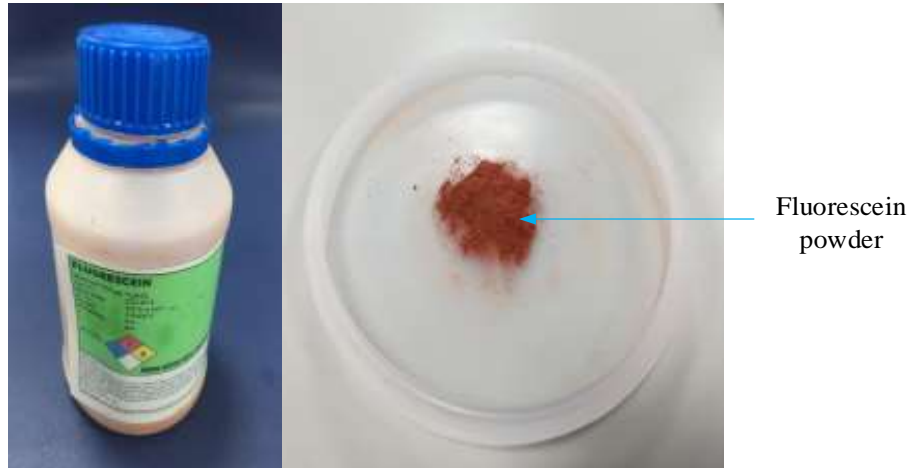
Figure 3-16: Fluorescein Sodium Dye

b) Viscosity

Viscosity of any substance can be defined as the degree of resistance to motion when acted upon by a shear or tensile stress. The viscosity of a substance is dependent on the nature of the bond between neighbouring particles such that a loose bond means a very low resistance to motion of the substance when compared to substance characterized by tightly interconnected particles. In other words, the thicker the fluid, the higher the viscosity (Symon, 1971). Movement of a substance on a surface is because of the movement of neighbouring particles at different velocities.

Viscosity is dependent on the surrounding temperature and pressure. When a viscous fluid is heated, the resistance to flow reduces significantly dependent on the heat intensity. This is because of an increase in velocity and decrease in contact time of neighbouring particles. The effect of increase in temperature in gases is a bit awkward in the sense that this results in an increase in thickness of the gas due to higher collision of its particles at such temperatures. In contrast, viscosity is independent on pressure. However, in some liquids under extreme pressure a change in viscosity is noticeable.

The viscosities of water (dyed) and silicone oil (dyed and non-dyed) were determined using the OFITE Model 800 8-Speed Electronic Viscometer illustrated in Figure 3-17. It is extensively used due to high precision measurement of rheological properties of fluids. Hence the flow characteristics of water (dyed) and silicone oil (dyed and non-dyed) were determined using this apparatus. In other to determine the viscosities of the above-named fluids, it was pertinent to first calibrate the viscometer.

69
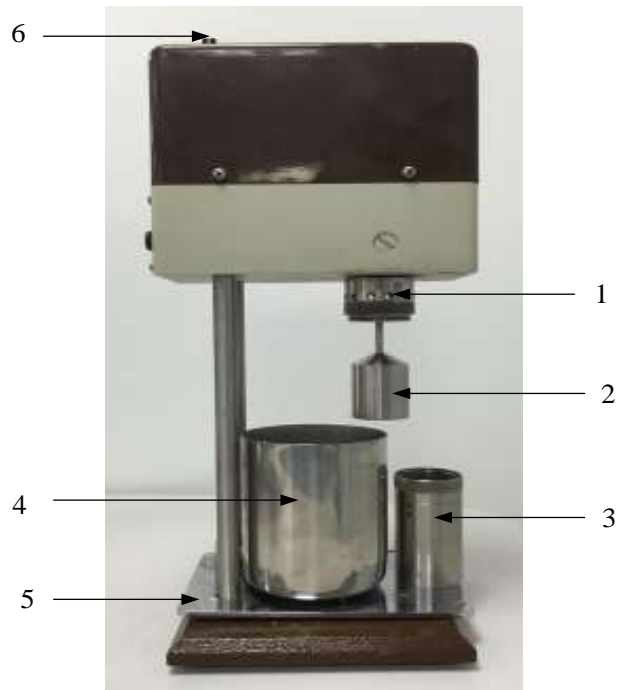
1- Rotor,   2- Bob-enclosing the splash guard,
3- Sleeve,   4- Cup,   5- platform
Figure 3-17: Electronic viscometer

i.   Measuring viscosity of silicone oil and water

After successful calibration of the viscometer if necessary, viscosity measurement can then be performed on the fluids of interest. The procedure involved in measuring the viscosity using the OFITE Model 800 8-Speed Electronic Viscometer illustrated in Figure 3-17, for water and silicone oil is as follows:

1. The reservoir fluid (oil/water) is filled to the specified mark in the cup (4).

2. The cup was then fitted on the platform (5) and raised so that the bob enclosing the splash guard (2) and sleeve (3) connected to the rotor (1) is immersed into the cup (4). The Then fluid sample was then stirred for 10 seconds by turning the knob (6) to the STIR setting.

3. The knob (6) was then rotated to a speed of 600 RPM. The dial readings and temperatures were recorded when stable. The viscosities of the measured fluids are summarised in Table 3-5.

Table 3-5: Viscosity values of fluids at 20°C

Fluid	Dynamic viscosity (cP)
Dyed tap water	1.00
Silicone oil	50, 100

c) Effective permeability determination

Permeability can be defined at the ease with which fluids or gases pass through a sample having pores spaces. The effective permeability of the reservoir fluids (atmospheric air at 20°C) were determined using steady state tests and using Darcy's linear flow Equation (Equation 3.3).

$$Q = \frac{kA(P_2 - P_1)}{\mu L}$$

(3.3)

Where,

Q = Flow rate in cm³/s

μ = Viscosity of the phase in cP

k = Effective permeability in Darcy

P_2 = Upstream Pressure in atm.

P_1 = Downstream pressure in atm.

L = Length of flow in cm

A = Cross-sectional area of flow in cm²

h = Height of the flow length in cm

π = 3.142

i. Effective permeability of reservoir fluids

Figure 3-18 demonstrates how the effective permeability for gas (air) was determined. Compressed air was used as the source gas delivered at an upstream pressure (1) read from the in-line air regulator (2) to the top–inlet of the Fancher sample holder (3). The downstream pressure (5) from the bottom-outlet of the sample holder was read from the

pressure gauge at an airflow rate read from the airflow meter (4). Similar set up was used for oil and water effective permeability determination. The values of these permeabilities in exponential, (e) millidarcy for the different grains are summarised in Table 3-6.

1- Upstream pressure (P2), 2- In-line-Air regulator, 3- Fancher core/sample holder,
4- Air flow meter, 5- Downstream pressure (P1)

Figure 3-18: Set up for effective permeability of the reservoir grains to gas

Table 3-6: Data for steady state permeability test and effective permeability estimation for grain size, 0.003 m x 0.002 m x 0.002 m

Reservoir phases	Q (cm^3/s)	μ (cP)	A (cm^2)	L (cm)	P_2 (Pa)	P_1 (Pa)	k (E+4 mD)
Gas	87	0.018	39.67	3.8	0.68046	0.646437	0.441
Oil	0.12	50	39.67	3.8	1.36092	0.816552	0.106
Water	8.33	1.00	39.67	3.8	1.36092	1.088736	0.293

d) Total porosity

Total porosity, usually represented in fraction or percentage is a measure of the pore volume or spaces to the total volume of a representative sample of the material or medium. This is represented by the ratio of the pore volume (volume of empty vessel minus the volume of the porous media) to the total volume of the empty vessel in fraction or percentage represented in Equation 3.4.

Figure 3-19 demonstrates how the total porosity of the reservoir was determined. The total porosity was determined by first weighing the reservoir grains prior to pouring into the clear PMMA as illustrated in Figure 3-20. Figure 3-20 demonstrates how the reservoir grains (2)

where poured into the reservoir (1). The data were then inputted into Equation 3.4 to determine its dimensionless value (porosity) in fraction.
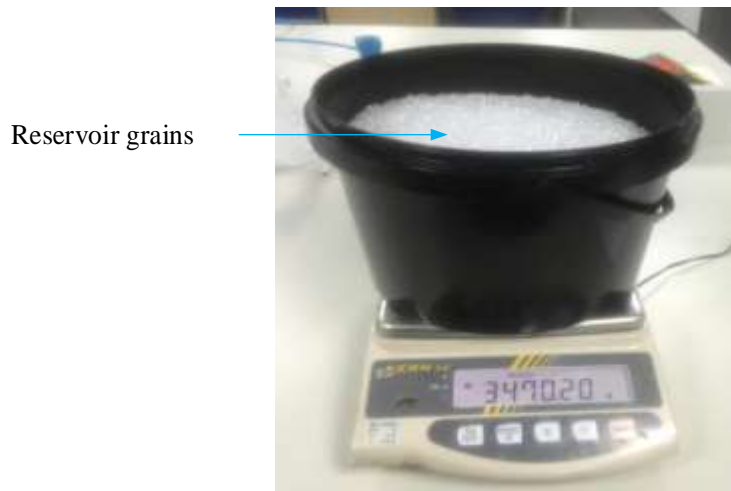
Figure 3-19: Weighing the PET pellets (reservoir grains) on a precision balance
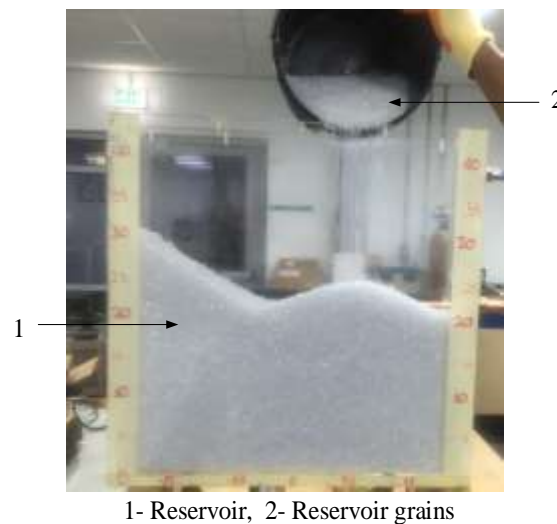
1- Reservoir, 2- Reservoir grains

Figure 3-20: Filling the tank with measured PET pellets

$$\emptyset = \frac{v - v_s}{v} = \frac{v_p}{v} \tag{3.4}$$

Where,

$\emptyset$ = Total porosity in fraction

v = Total or bulk volume of material in m^3

v_p = Volume of void space or pore volume in m^3

v_s = Total volume of porous materials in m^3

Therefore, the total porosity for homogeneous and heterogeneous reservoirs respectively were estimated as follows:

The volume of the tank, v (m) = 0.45 x 0.1 x 0.45 = 0.0198 m^3
Volume of polymer pellets in tank = 0.01601358 m^3
Therefore, total porosity

$$\emptyset = \frac{v - v_s}{v} = \frac{0.0198 - 0.01601358}{0.0198}$$

$$= \frac{0.00378642}{0.0198}$$

$$= 0.191$$

3.4.2 Data processing methods

a) *Horizontal well placement and scaling*

b) *Dimensional analysis*

   i.   Reynolds number

c) *Wettability*

d) *Proactive cresting control*

a) Horizontal well placement and scaling

The placement of the horizontal well is directly related to its performance especially in oil reservoirs with cresting severity. For instance, placement of the horizontal lateral section closer to the WOC of a strong bottom drive reservoir results in early influx of unwanted water and early shut-in of the well due to earlier reservoir pressure depletion. Since the bottom aquifer in this case/scenario is strong and the gas cap is considered weak, the well was placed at a distance from the WOC and GOC such that both water and gas is produced at approximately the same time of 140 seconds, depending on the production rate from in cases.

As shown in Figure 3-21, the horizontal lateral exposed to the reservoir was fixed at $0.67x$ the length of the reservoir (0.305 m or 0.251 m depending on the length used) and $0.5y$ (0.225 m) the height of the reservoir. For scaling purposes, the arc lengths, Vertical and Horizontal Displacements of the inclined section as well as the ratio of Vertical to reservoir height were plotted against Measured Depth of the horizontal wells as illustrated in Figures 3-22 to 3-26 respectively. Figure 3-22, illustrates a plot of the horizontal wells lengths of arc against the measured depth. In this figure, the measured depth is seen to increase linearly with increase in length of arc. In Figure 3-23, an increase in Horizontal and Vertical Displacement of the inclined section results in increase in measured depth of the horizontal wells. The measured depth is seen to increase with an increase in the ratio of vertical displacement and reservoir height as depicted in Figure 3-24. Figure 3-25 illustrates the plot of Horizontal Displacement of the inclined section versus Angle of inclination. As seen in this figure, the horizontal displacements of the inclined section decrease geometrically with increase in inclination angle. In Figure 3-26, the vertical displacement is seen to decrease with an increasing angle of inclination. Figures 3-22 to 3-26 can simply be interpolated to match field conditions.
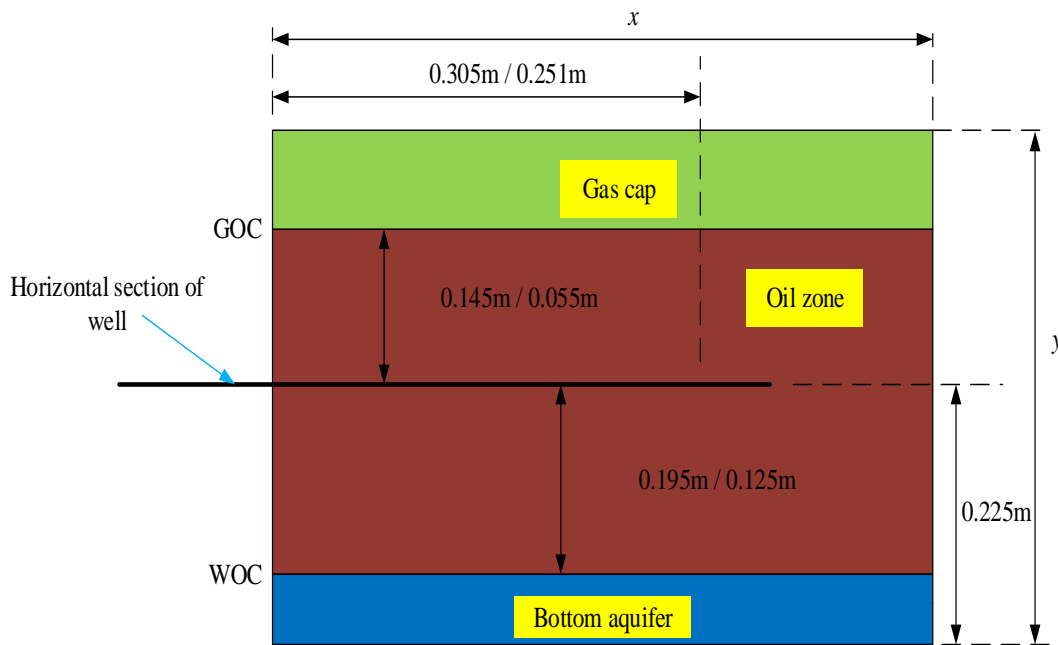
Figure 3-21: Schematic of horizontal well placement in reservoir
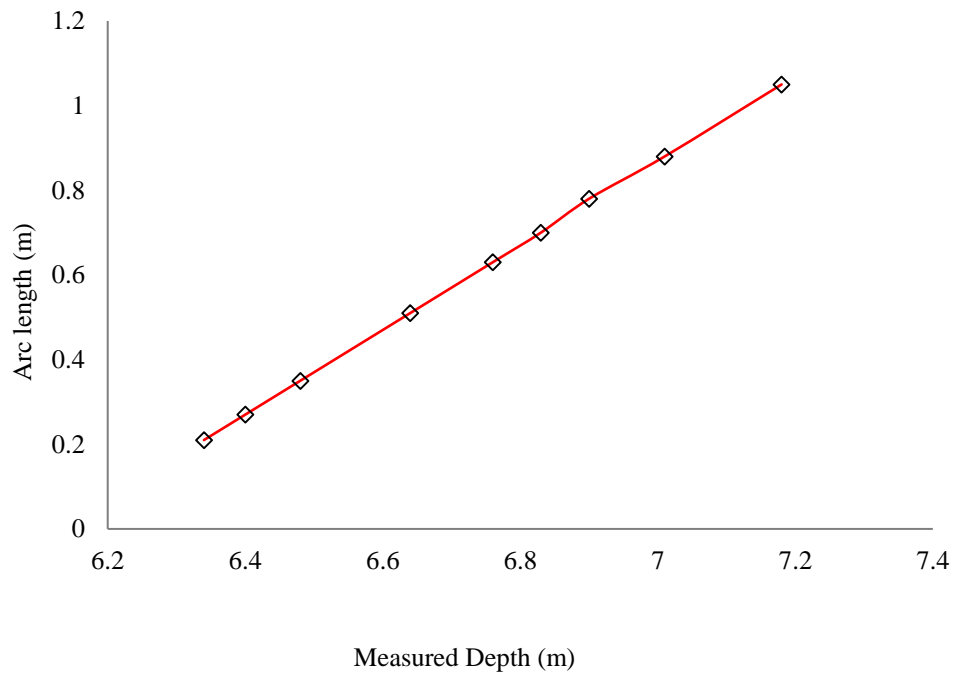
Figure 3-22: Plot of arc lengths versus measured depth
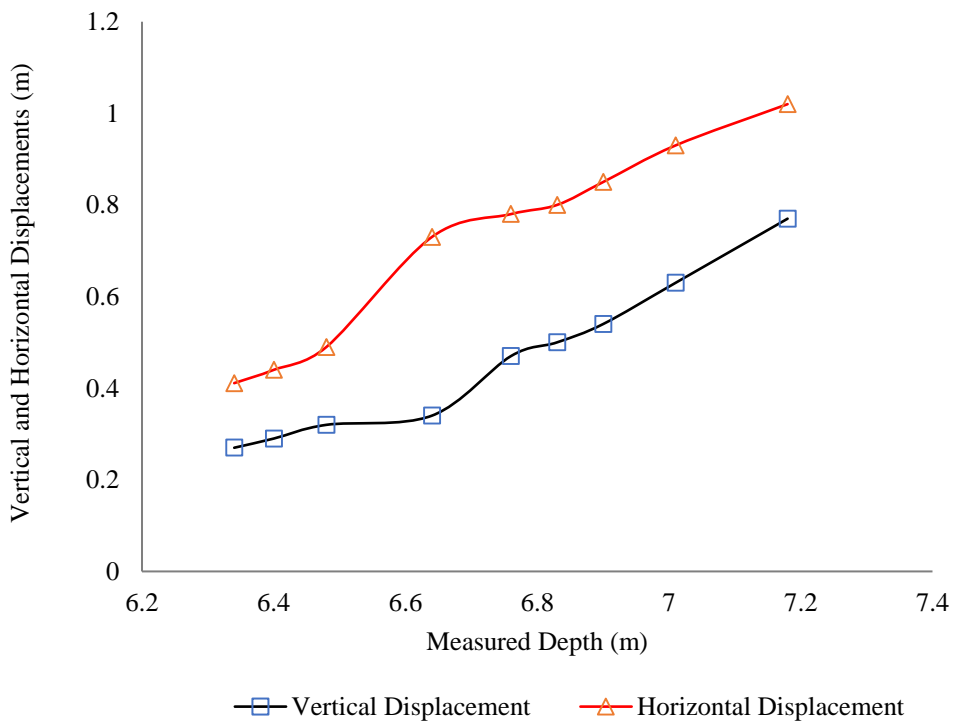
Figure 3-23: Plot of vertical and horizontal displacements of inclined section of wells against measured depth
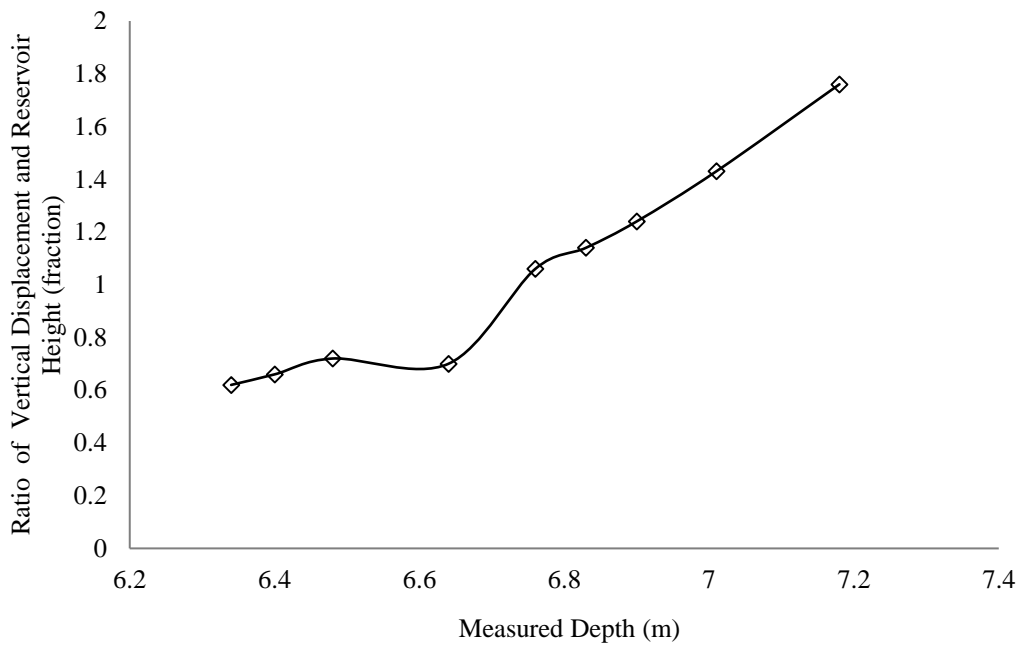
Figure 3-24: Plot of ratio of vertical displacement and reservoir height versus measured depth
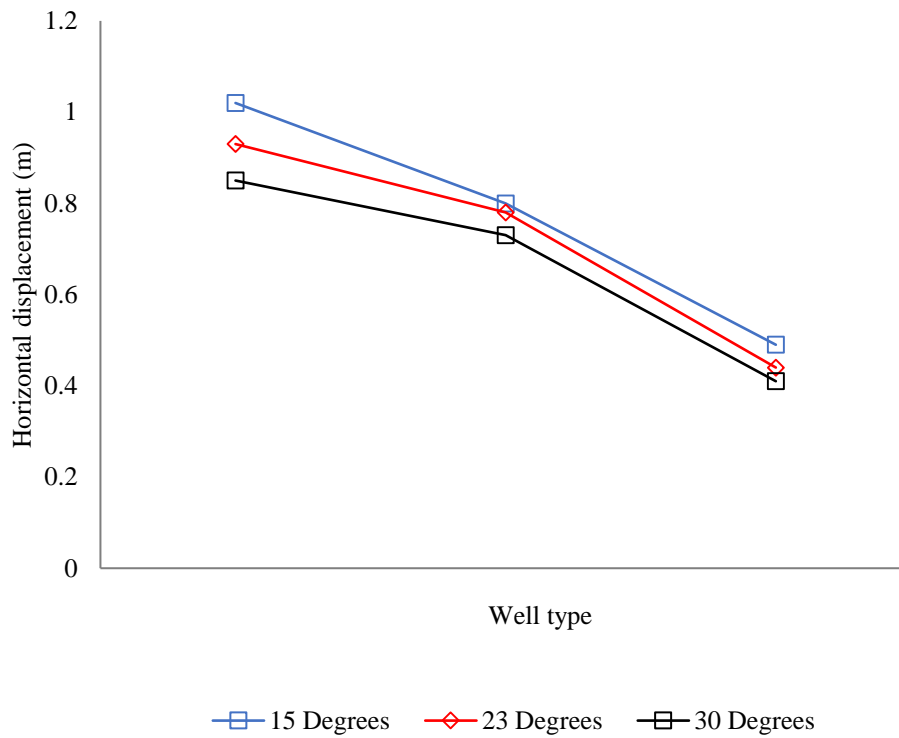
Figure 3-25: Plot of horizontal displacement versus angle of inclination
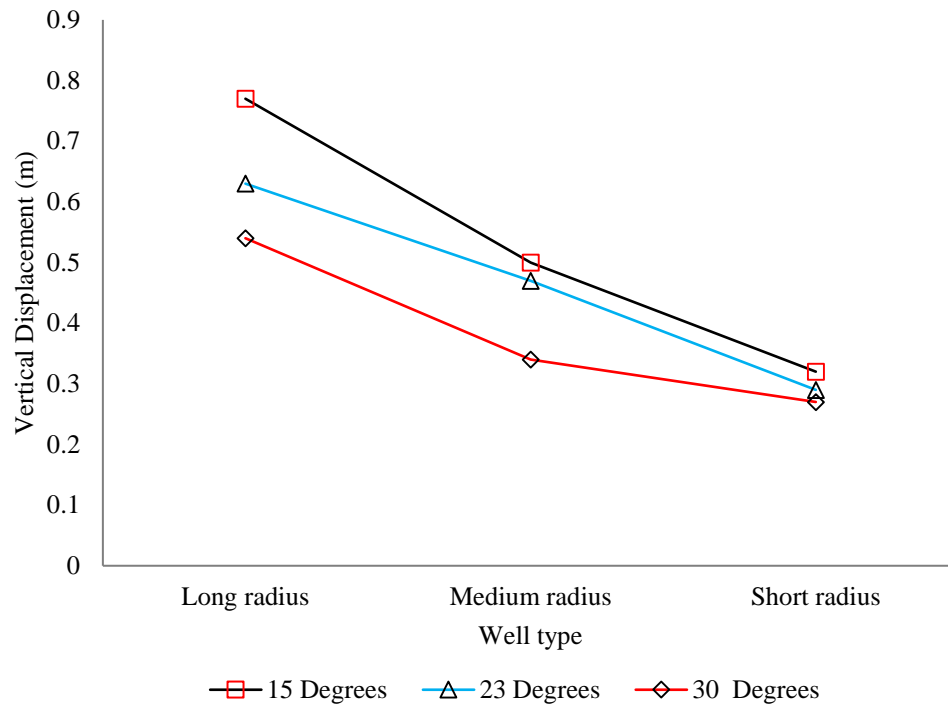
Figure 3-26: Plot of vertical displacement versus angle of inclination

b) Dimensional analysis

Dimensional analysis is an analysis performed in Engineering and Science to show the correlation between different physical quantities. This is possible using fundamental dimensions (length, time, mass and electric charge) and units of measure (such as kilograms). Since cresting is a fluid flow problem, Reynolds number (Re) was applied in this study.

i. Reynolds number

Reynolds number is a dimensionless number usually applied to determine the fluid flow regime prediction whether laminar, partially turbulent or turbulent. This dimensionless number has been applied for generalization of results from the scaled model used in this study. Since fluid flow in this study is through a pipe (horizontal well), Equation 3.5 was used to estimate the Reynolds number. The Reynolds numbers for all horizontal well cases summarised in Table 3-7 were less than 2000 ($R_e < 2000$) specifically < 1, hence depicting laminar flow due to dominant viscous forces to forces of inertia.

A correlation between the Reynolds number and measured depths of all horizontal well cases as well as the effect of change in oil production rate (change in outlet/surface pressure) on the Reynolds number for Cases-1A, 2B and 3B is illustrated in Figure 3-27. As shown

in Figure 3-27, Reynolds number is dependent of the measured depth of horizontal wells and the initial pressure at the surface. However, Reynolds number is seen to increase with increase in oil withdrawal rate or increase in pressure drop for Cases-1A, 2B and 3B. As expected, similar trend can be observed for the plot of TVD against *Re*. Figure 3-27 shows that the Reynolds number increases with an increase in the true vertical depth of the horizontal wells.

$$Re = \frac{\rho_o D_i Q_o}{\mu_o A}$$ (3.5)

Where,

A = Cross-sectional area of the pipe in m^2

Q_o = Calculated cumulative oil flow rate in m^3/s

D_i = Inside diameter of the pipe in m

μ_o = Viscosity of the oil in N-s/m^2

ρ_o = Density of the oil in kg/m^3

Re = Reynolds number in dimensionless unit

π = 3.142

Table 3-7: Effect of oil withdrawal rates and measured depth on Reynolds number at 300 seconds (E-2)

Cases	Well type	TVD (m)	Measured depth (m)	Reynolds number (Dimensionless)		
				-4.351 Psig	-7.25 Psig	-10.15 Psig
Case-1A	LR	21.70	71.80	37.11	39.24	40.32
Case-1B	LR	20.30	70.10	36.41		
Case-1C	MR	19.40	69.00	36.20		
Case-2A	LR	19.00	68.30	35.33		
Case-2B	MR	18.70	67.60	36.86	37.24	38.86
Case-2C	SR	17.40	66.40	37.78		
Case-3A	MR	17.20	64.80	35.79		
Case-3B	SR	16.90	64.00	37.33	37.79	39.79
Case-3C	SR	16.70	63.40	36.66		
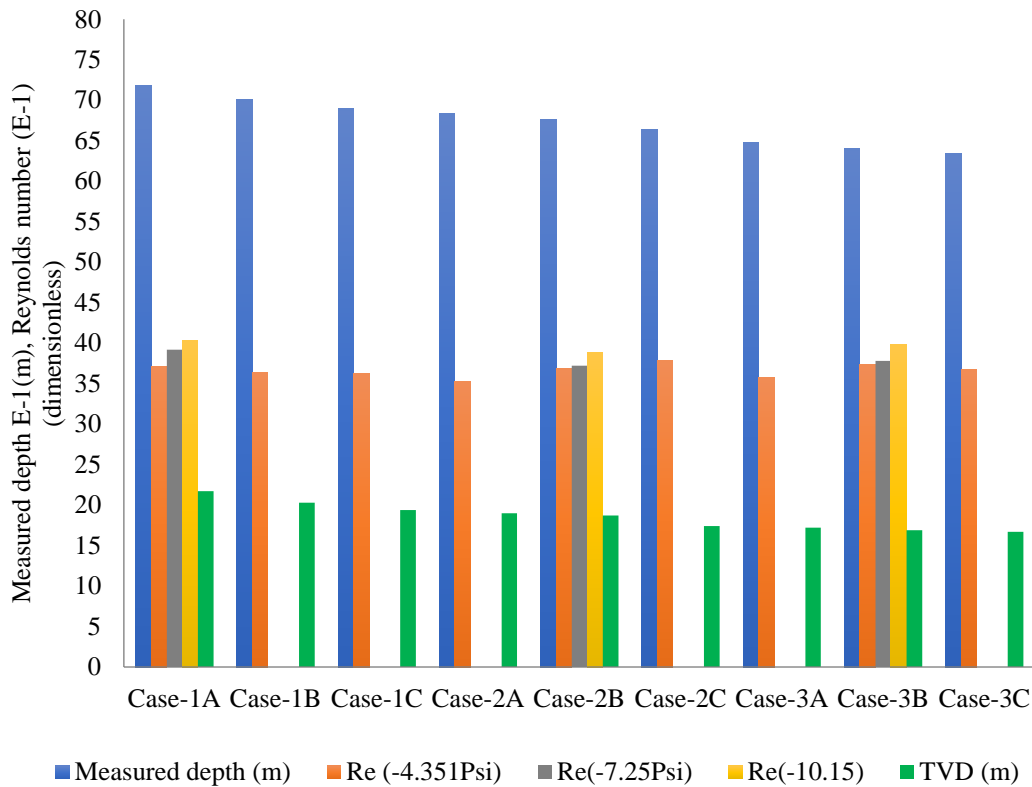
Figure 3-27: Effect of measured depth, TVD and oil withdrawal rate on Reynolds number at 300 s

c) Wettability

Reservoir wettability is the tendency of a reservoir fluid in the presence of other immiscible fluid to spread on the reservoir rock or grains (Crocker and Marchin, 1988, Galleguillos-Silva et al., 2017, Tarek, 2001). Wettability is known to affect the production of hydrocarbons from pores and hence affects productivity and oil recovery during primary and enhanced oil recovery stages. A typical reservoir could be either oil or water-wet in nature characterized by the nature fluid displacement and the concave (water-wet, (θ) < 90º) or convex shape [oil-wet, theta (θ) > 90º] formed in a capillary tube during tests (Abdallah et al., 2007). Similar experimental procedure was demonstrated to determine the wettability of the reservoir modeled. After setting up the reservoir fluids in the porous media (Figure 3-29(a)), a capillary tube was inserted close to one side of the beaker (Figure 3-29(b)). As shown in Figure 3-29(b), the convex shape observed with downward vertical displacement of water by oil in the capillary tube at θ > 90º due to interfacial tension, demonstrates that the reservoir grains have higher affinity to oil, hence an oil-wet reservoir. Therefore, it is expected that during cresting, bottom water will move more rapidly through the oil-wet regions leading to less oil recovery ratios from the oil-wet regions in the reservoir due to capillarity.

80
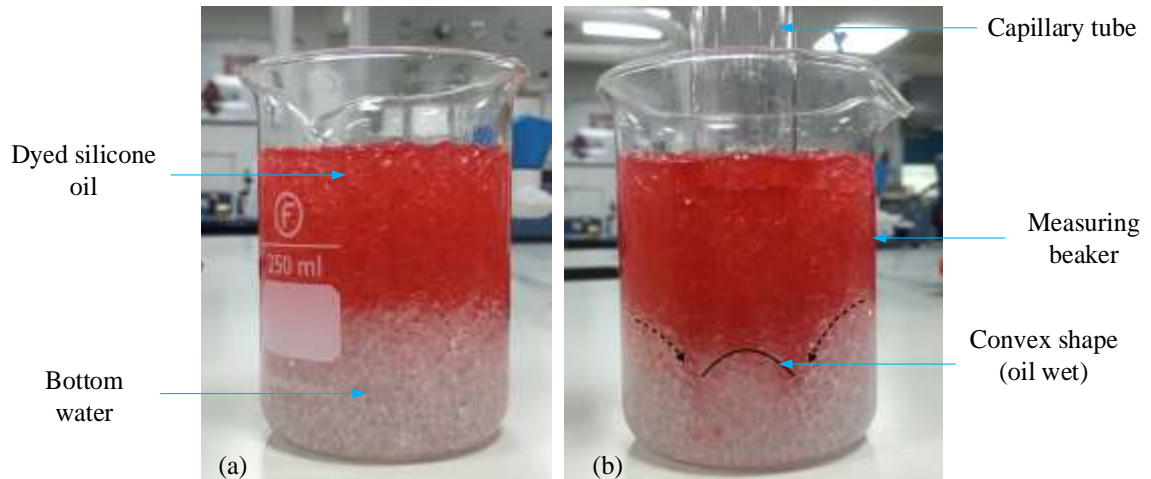
Figure 3-28: (a) Before wettability test (b) During wettability test

d) Proactive Cresting Control

Unlike varying the effect of the inclined section described in *Section 3.2.1*, sets of experiments were performed to investigate the effect of gravity and wettability consideration on oil recovery, oil produced and cumulative water produced after temporary shutting-in a horizontal well in a homogeneous reservoir affected by cresting problems. However, the procedure for the rig operation was like that described in *Section 3.3.1*, but in this case an electromagnetic valve was installed. In this study, initial pressure loss prior to temporary shut-ins was negligible for comparison with a base case horizontal well. Time was also assumed not a critical factor to allow for comparison between simulated cases. The experimental effluents breakthrough times for the thick-oil rim (0.34 m oil column thickness) and thin-oil rim reservoirs (0.18 m oil column thickness) were approximately 140 and 63 seconds respectively as illustrated in Figure 4-28. The observed breakthrough times are in good agreement with analytical, theoretical and numerical simulations using field data, such that the closer the WOC and GOC to the well the faster the effluent(s) breakthrough time(s) at same oil production rate reported previously by (Peng and Yeh, 1995, Schevchenko, 2013, Papatzacos et al., 1991, Omeke et al., 2010).
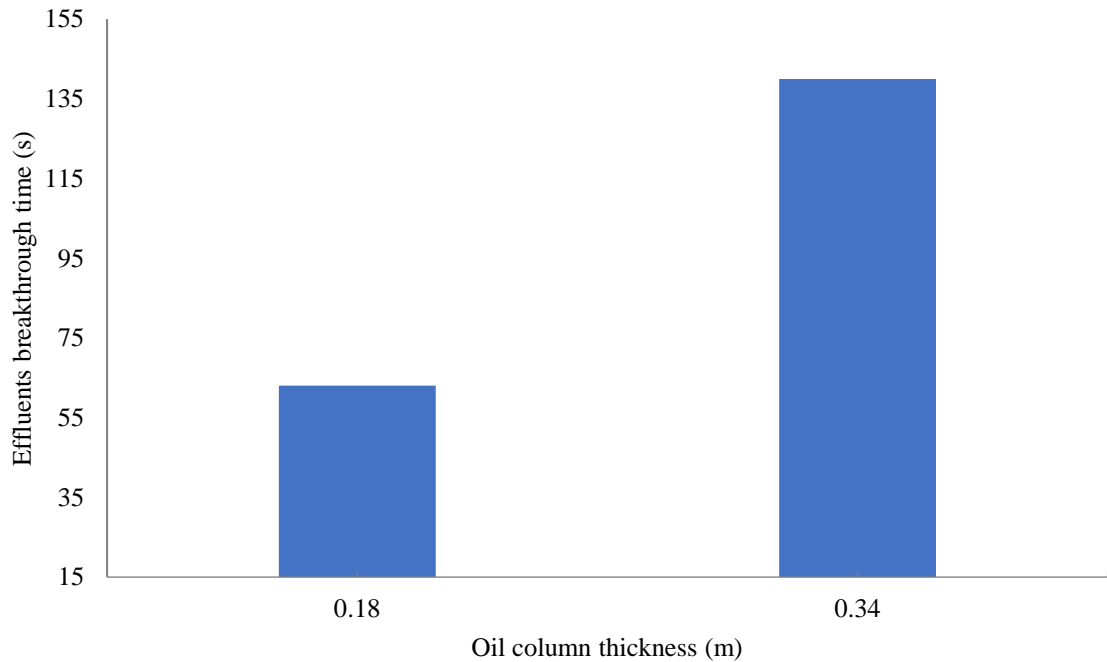
Figure 3-29: Plot of effluent(s) breakthrough time versus oil column thickness at 495 s (thick-oil rim reservoir), 210 s (thin-oil rim reservoir) and $l_r = 0.305$ m

As shown in Table 3-8, Cases 1 and 7 had uninterrupted production for the duration of 495 and 210 seconds respectively, whereas cases 2-6, 8 and 9 had one shut-in each, half the water and gas breakthrough time (approximately 70 seconds for the thick-oil rim reservoir and 31 seconds for the thin-oil rim reservoir). The extra length provided by the solenoid valve was assumed to be negligible on the liquid produced for comparison with a base case horizontal well dimension. The production time for the thin-oil rim reservoir was 210 seconds due to high volumes of water produced.

Similar procedure from the thick-oil rim investigation was applied. Therefore, case 7 had uninterrupted production for a period of 210 seconds controlled by a ball valve while Cases 8-9 were controlled by a pre-programmed electromagnetic valve. The results for these investigations were reported in terms of oil recovered, cumulative water and liquid produced at the same production times. Cases 1 and 7, regarded as the base case horizontal well for this study represents Case-3C ($l_r = 0.305$ m) described in Table 3-1 and 3-2 in Chapter 3. The reservoir types used in this investigation were thick and thin-oil reservoirs; with the oil sandwiched between a strong bottom aquifer and considerable gas cap drive.

Table 3-8: Summary of cases at different breakthrough times, shut-in times and production times

Case		Oil column thickness (m)	Breakthrough time (s)	Half the breakthrough time (s)	Shut-in time (s)	Production time (s)
Case 1	Thick-oil rim reservoir	0.34	Approximately 140	Approximately 70	0 (uninterrupted)	495
Case 2	Thick-oil rim reservoir	0.34	Approximately 140	Approximately 70	960	495
Case 3	Thick-oil rim reservoir	0.34	Approximately 140	Approximately 70	2700	495
Case 4	Thick-oil rim reservoir	0.34	Approximately 140	Approximately 70	5400	495
Case 5	Thick-oil rim reservoir	0.34	Approximately 140	Approximately 70	7200	495
Case 6	Thick-oil rim reservoir	0.34	Approximately 140	Approximately 70	9000	495
Case 7	Thin-oil rim reservoir	0.18	Approximately 63	Approximately 31	0 (uninterrupted)	210
Case 8	Thin-oil rim reservoir	0.18	Approximately 63	Approximately 31	960	210
Case 9	Thin-oil rim reservoir	0.18	Approximately 63	Approximately 31	2700	210

3.5 Accuracy and Errors

The accuracy of this experiment is affected by factors such as pressure readings, volume measurements of the produced liquids and horizontal well length and flow rates. The cumulative volumes and flow rates of produced liquids, were measured using a graduated cylinder having an accuracy of ± 10 cm^3. The digital manometer used for measuring the reservoir pressure had an accuracy of the manometer was $\pm 0.3\%$ FS. The metric rule used for the horizontal well and reservoir grains measurement had an accuracy of ± 1 mm. During steady state permeability tests the water and gas flow meter used for volumetric flow rate measurement (downstream pressure), as illustrated in Figure 3-18 had an accuracy of $\pm 2.5\%$ FSD while the in-line oil flow meter used for upstream pressure oil pressure was $\pm$ 5% FS in accuracy.

The in-line air flow meter illustrated in Figure 3-18, used for the upstream source gas pressure measurement had an accuracy of $\pm$ 4% FS. During determination of pellet density by buoyancy method, the used laboratory beaker illustrated in Figure 3-10 had an accuracy of $\pm$ 5%. The OFITE Model 800 8-Speed Electronic Viscometer (Figure 3-17) used for the viscosity determination of the reservoir fluids had a speed accuracy of 0.1 RPM. During rig operation, the rotameter used had an accuracy of $\pm$ 5% FS while the pressure and vacuum gauges were $\pm$ 2.5% FSD and 6% in accuracy. The results for each experimental run was repeated twice for higher accuracy of cumulative water and oil produced.

3.6 Summary

The description of apparatus, experiment setup, measurement and data processing, diagrammatic illustrations of the water and gas-cresting rig used in this study were determined and presented in this section. The apparatus used in this study were detailed with specifications and usage. Majority of the test data obtained agreed with already known theoretical and experimental results.

The results obtained from this section are presented and extensively discussed in the next Chapter. This encompasses the presentation and discussion of results obtained from experimental runs for thin- and thick-oil rim reservoir cases at the same operating condition. The presented results will include the effect of varying the inclined section, effect of oil viscosity, effect of lateral length in the reservoir and effect of pressure drop (thick oil rim reservoir only) and effectiveness of the presented proactive control procedure in horizontal wells on the oil recovery, oil produced and cumulative water produced.

CHAPTER 4

RESULTS AND DISCUSSION

4.1 Introduction

From results presented in Chapter 3, the tested effective permeability of the reservoir grains to oil, water and gas were 0.106E+4 mD, 0.441E+4 mD and 0.293E+4 mD respectively. The total porosity of the reservoir was estimated as 19.1%. The viscosities of the reservoir phases were 50 cP and 100 cP for the silicone oil, 1 cP for the Fluorescein dye water and 0.018 cP for the gas. The densities of the water and oil phases were 998 kg/m^3 and 972 kg/m^3 respectively. The density of the reservoir grain was 1302 kg/m^3. Due to its density being greater than that of water and silicone oil, the reservoir grains will settle to the bottom when immersed in silicone oil and/or water phases. The same sized measured reservoir grains and the high-interconnected pore spaces obtained from the CT-scan was used to consider the reservoir to be homogeneous.

The horizontal well cases were categorised into either short, medium or long horizontal wells based on calculated radius of arc as shown in Table 3-2. Hence, Cases-1A, 1B and 2A were considered long radii, Cases-3A, 2B and 1C, medium radii wells, while Cases 3C, 3B and 2C were short radii wells. The bottom aquifer was modeled at constant water injection rate of 41.68 cm^3/s while gas cresting was modeled at atmospheric pressure (14.7 Psi) through the free surface illustrated in Figure 3-1(b). The effluents break through times for thin- and thick-oil rim reservoirs were 63 s and 140 s respectively. The difference in breakthrough times between the thick- and thin-oil reservoir cases was due to the oil column thickness difference at the same reservoir and operating condition.

The results from horizontal well and reservoir scaling shown from Figures 3-22 to 3-26 indicate that the measured depth increase linearly with increase in length of arc. The horizontal and Vertical Displacement of the inclined section increase with increase in measured depth of the horizontal wells. The measured depth increase with an increase in the ratio of vertical displacement and reservoir height. The horizontal displacements of the inclined section decrease geometrically with increase in inclination angle while the vertical displacement is seen to decrease with an increasing angle of inclination. The Reynolds

number for the horizontal well cases at initial vacuum pressures at the outlet of -4.351 Psig, -7.25 Psig and -10.15 Psig were generally regarded as laminar flow regimes (Re < 2000) at a duration 300 s. However, the Reynolds number increased with increase in oil withdrawal rate. From wettability test, the reservoir was classified as oil-wet in nature due to the convex shape of the WOC after test.

In this Chapter, the experimental results are presented in order to ascertain the novel procedures of experimentally modeling deviated or inclined wells, as well as proactively controlling cresting behaviour in a reservoir affected by cresting problems. The results of the experiments described and performed in Chapter 3 are categorized into two major categories for easy comparison as shown below:

1) ***Thick-oil rim reservoir simulated at 300 s and 495 s (Section 4.2).***

    i. Effect on cumulative liquid production rate at 300 s (*Section 4.2.1*).

    ii. Effect of pressure drop increase on cumulative liquid withdrawal rate at 300 s (*Section 4.2.2*).

    iii. Effect of varying inclined sections on oil recovery at 300 s (*Section 4.2.3*).

    iv. Effect of oil viscosity and lateral length on cumulative oil recovered at 495 s (*Section 4.2.4*).

    v. Effect of oil viscosity and lateral length on cumulative water produced 495 s (*Section 4.2.5*).

    vi. Effect of oil viscosity and lateral length on cumulative water cut 495 s (*Section 4.2.6*).

    vii. Effect of lateral length on pressure drop at 495 s (*Section 4.2.7*).

    viii. Effect of increase in production time on oil recovery and cumulative water cut 300 s and 495 s (*Section 4.2.8*).

    ix. Proactive cresting control at 495 s (*Section 4.2.9*).

      a. Effect on oil recovery and oil produced (*Section 4.2.9.1*).

b. Effect on cumulative water produced (*Section 4.2.9.2*).

c. Effect on cumulative liquid produced (*Section 4.2.9.3*).

2) ***Thin-oil rim reservoir simulated at 300 s and 495 s (Section 4.3).***

i. Effect of oil viscosity and lateral length on cumulative oil recovered at 210 s (*Section 4.3.1*).

ii. Effect of oil viscosity and lateral length on cumulative water produced at 210 s (*Section 4.3.2*).

iii. Effect of lateral length on pressure drop at 210 s (*Section 4.3.3*).

iv. Proactive cresting control at 210 s (*Section 4.3.4*).

a. Effect on oil recovery and oil produced (*Section 4.3.4.1*).

b. Effect on cumulative water produced (*Section 4.3.4.2*).

c. Effect on cumulative liquid produced (*Section 4.3.4.3*).

The first step in this investigation was to observe water and gas cresting occurring simultaneously. Figure 4-1(a) shows the reservoir at static condition with the reservoir fluids (oil, water and gas) arranged in order of density differences and gravity (Balazs et al., 2009, Beveridge et al., 1970, Singhal, 1996) prior to oil production, while Figure 4-1(b) to 4-1(d) show the simulations at 55, 90 and 180 seconds respectively for Case-1A at operating pressure -4.351 Psig (vacuum pressure). In Figure 4-1(a), the black dotted lines represent the initial Water-Oil-Contact and Gas-Oil-Contact respectively, whereas the distorted lines and crest-like shapes represents water and gas cresting occurring simultaneously in Figure 4-1(b) to 4.1(d). At the end of each physical simulation, the produced liquid for each case were transferred from the vacuum chamber to a storage for measurement after two hours (to allow enough time for the produced water and oil to be separated by density difference). Although water and gas cresting were simulated simultaneously, only liquid (water and oil) produced were measured because the gas produced could not be quantified.

Time = 0 second   Time = 55 seconds   Time = 90 seconds   Time = 180 seconds
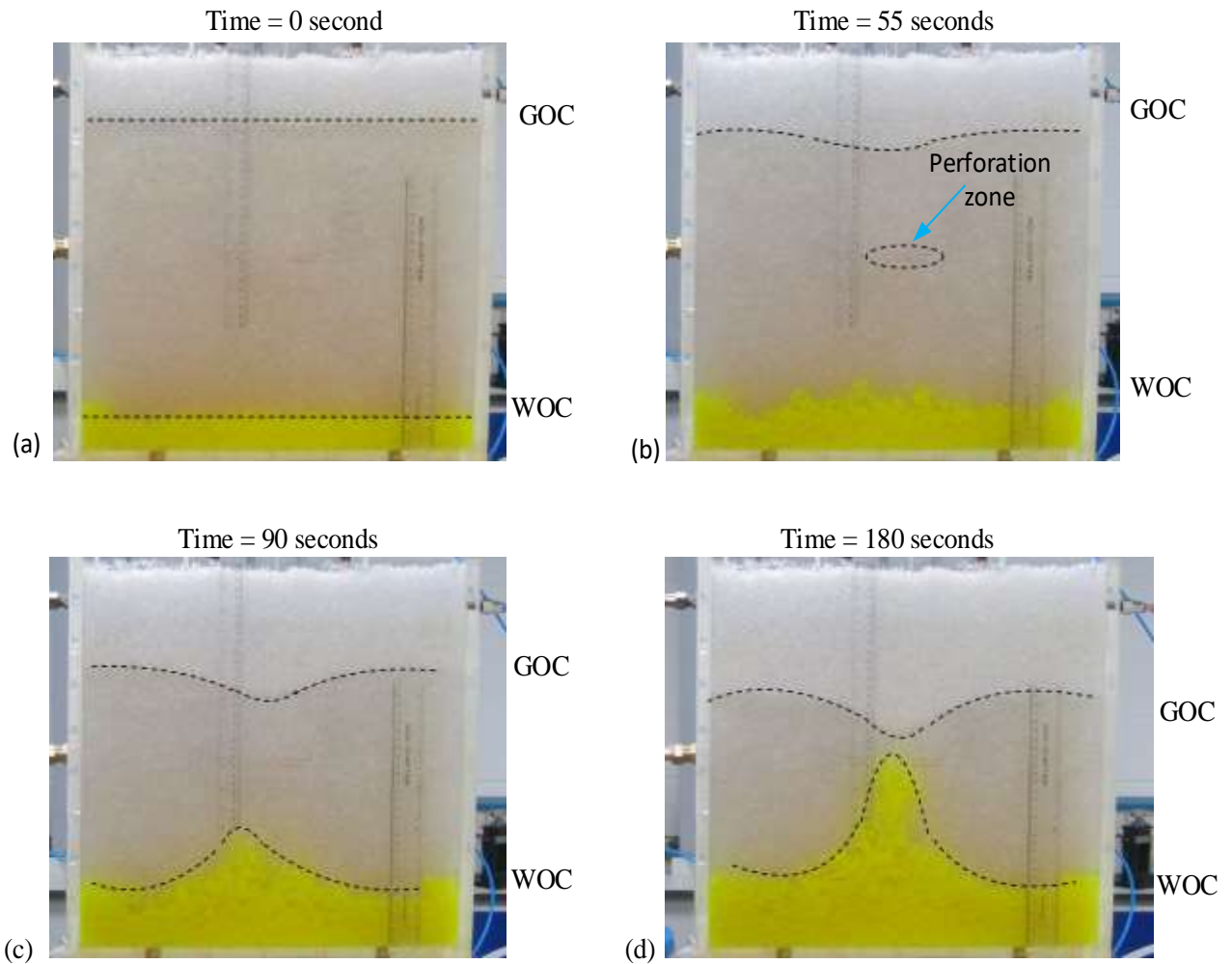
Figure 4-1: (a) reservoir at static condition for Case-1A (b) Water and Gas cresting occurring simultaneously at 55 s for Case-1A 1A (c) Water and Gas cresting occurring simultaneously at 90 s for Case-1A 1A (d) Water and Gas cresting occurring simultaneously at 180 s for Case-1A

4.2 Thick-oil rim reservoir

4.2.1 Effect on cumulative liquid production rate at 300 s

Since no individual flowmeter capable of measuring the flow rates of oil and water were installed, the flow rates were determined from the cumulative liquid (oil and water) produced. Table 4-1 illustrates the summary of the cumulative liquid production rates for thick-oil rim reservoir at 300 s, lateral length in the reservoir, 0.305 m and viscosity of 50 cP in cubic centimeters per second (cm^3/s) for all cases at operating pressure of -4.351 Psig. Figures 4-2 to 4-5 show a comparison of the cumulative liquid production rates for long radii wells, medium radii and short radii wells respectively. As shown in Figure 4-2, Case-1A resulted in a higher liquid production rate and cumulative volume of oil produced per

second. Oil was produced at a highest cumulative rate of 8.91cm^3/s, while water was produced at the lowest cumulative rate at 3.70 cm^3/s. Case-2A had the lowest oil production rate (8.48 cm^3/s) and highest water production rate (4.05 cm^3/s). This is due to a shorter well length when compared with Cases-1A and 1B, which explains the fact that at the same operating condition the shorter the well length, the faster the water breakthrough time. Hence, Case-1B succeeded Case-2A with a cumulative water production rate of 3.76 cm^3/s.

Figure 4-3, follows similar trend for cumulative water production rate depicted in Figure 4-2. In Figure 4-3, Case-3A being the shortest in measured depth is seen to have the highest cumulative water production at a rate of 4.27 cm^3/s and lowest oil production rate at 8.59 cm^3/s. Unlike Case-2A, Case 3A with a measured depth of 6.48E-1 m was most significant in terms of cumulative liquid production rate for medium radii wells. However, Case-2B is seen to have higher cumulative oil production rate of 8.85 cm^3/s with considerable cumulative water production rate of 3.83 cm^3/s. Hence, at a production time of 300 s, Case-2B would be recommended for higher cumulative oil production rate, if medium wells are used.

Table 4-1: Cumulative liquid production rate at 300 s

Cases	Well type	Cumulative oil produced (cm^3)	Cumulative oil rate (cm^3/s)	Cumulative water rate (cm^3/s)	Cumulative water produced (cm^3)	Total cumulative liquid rate (cm^3/s)
Case-1A	LR	2671.78	8.91	3.70	1110	12.61
Case-1B	LR	2622.02	8.74	3.76	1128	12.50
Case-1C	MR	2605.80	8.69	3.56	1068	12.25
Case-2A	LR	2543.80	8.48	4.05	1215	12.53
Case-2B	MR	2671.78	8.85	3.83	1149	12.68
Case-2C	SR	2622.02	9.07	3.41	1023	12.48
Case-3A	MR	2605.80	8.59	4.27	1281	12.86
Case-3B	SR	2543.80	8.96	3.56	1068	12.52
Case-3C	SR	2671.78	8.80	3.91	1173	12.71
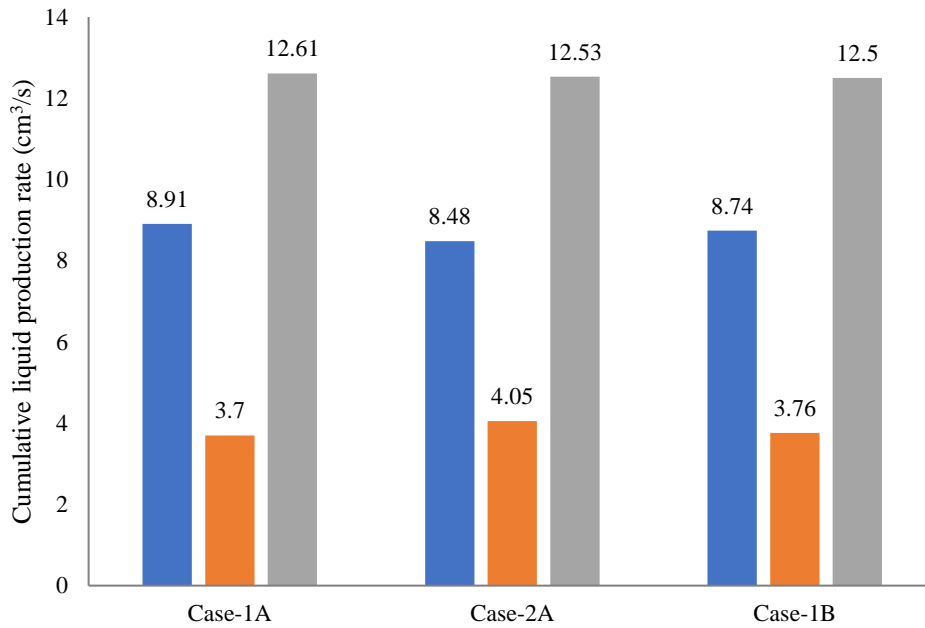
Figure 4-2: Cumulative liquid production rate comparison for long radii wells at 300 s
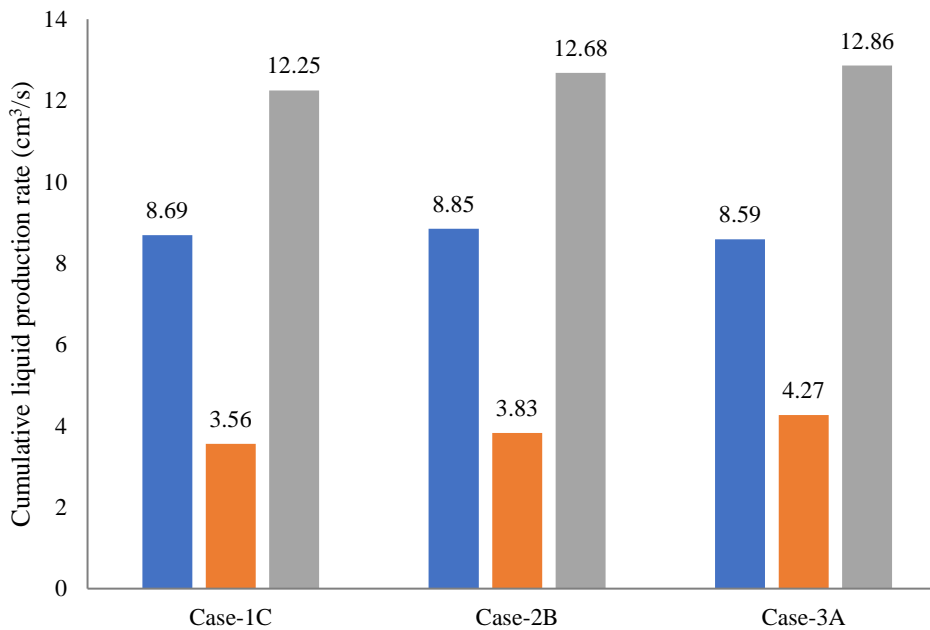
Figure 4-3: Cumulative liquid production rate comparison for medium radii wells at 300 s

In Figure 4-4, the cumulative liquid production rates for Cases-2C, 3B and 3C have higher overall cumulative liquid production rate when compared to medium and long radii wells. This is expected, due to the shorter lengths of wells having slightly lower pressure drop compared to longer lengths of wells. Figure 4-4 shows that Case-2C produced oil at highest

cumulative rate of 9.07 cm^3/s. Case-2C also produced water at the lowest rate (3.41 cm^3/s). More so, Case-2C a short radius horizontal well is seen to have performed best when compared to both the long and medium radii horizontal wells, which contradicts the results presented by Freeborn et al. (1990). However, the result from this study clarifies the reason presented by Freeborn et al. (1990) for the poor performance of short radii wells. As earlier stated, the reason for the poor performance of the short radius well was due to completion mechanism and perforation jet issues. In this case the possible result of the poor performance of the long and medium radii wells could be due to longer arc lengths (longer horizontal and vertical displacements of the inclined region), resulting in a slightly higher-pressure drop, as well as the more time for the mobility of the fluid(s) to be affected by gravitational pull.

A closer observation has been given to the results obtained from Freeborn et al., (1990) regarding the performances of the long and medium radii wells with the same completion mechanism. They reported that the long radius well performed better at higher production rates than the medium radius well. This is in contrast with the results presented here. From the results, it was observed that the shorter the length of the well, the higher the liquid production rate, hence the medium radius wells performed better having higher average oil recovery ratios compared to long radius wells. This is because of the uniform pressure distribution along the entire length of the longer radius wells resulting in lower pressure drop and hence lower production rates.
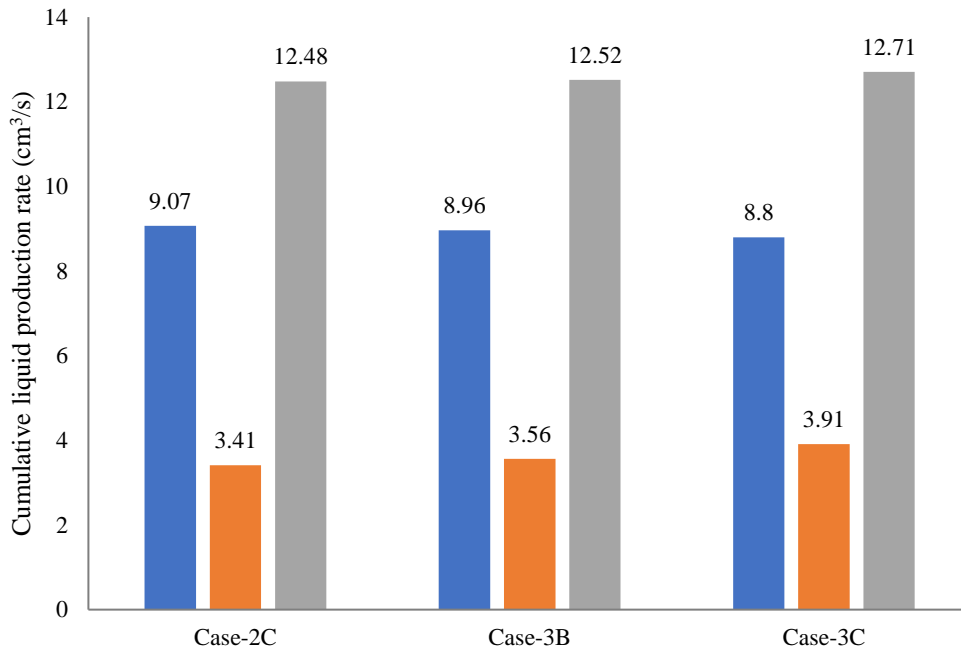
Figure 4-4: Cumulative liquid production rate comparison for short radii wells at 300 s

The performance of horizontal wells depends on its length and as such a percentage difference of 6.51% was observed for cumulative oil production rate between Case-2C and Case-2A, whereas significant percentage difference of 20.14% was observed between Case-2C and Case-3A for cumulative water production rate. In Figures 4.2 - 4.5, the water and oil cumulative production rates were very close in all cases, due to very close difference in pressure drop resulting from slight differences in measured depths between the horizontal wells. Thus, a longer production time, greater than 300 seconds could yield significant difference between all cases.

Figure 4-5 shows a comparison of oil and water flow rates for all horizontal well cases at a simulation time of 300 s. In this figure, Case-2C is seen to have the highest oil production rate (9.07 cm^3) and lowest water production rate (3.41 cm^3). Case-2A is seen to have the lowest oil production rate (8.48 cm^3) whilst Case-3A has the highest water production rate of 4.27 cm^3.
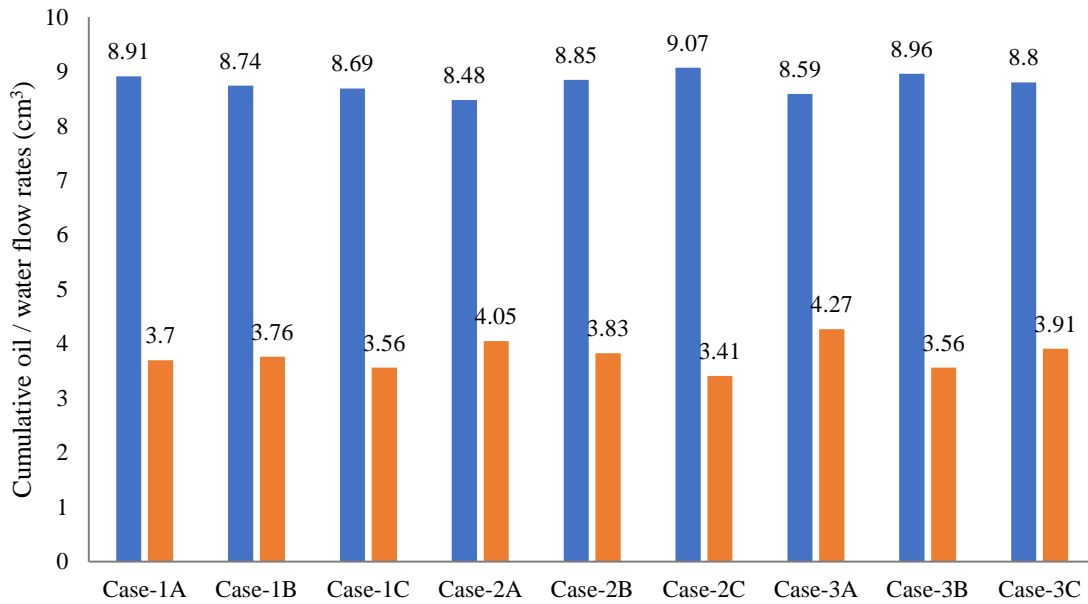
Figure 4-5: Comparison in oil/water for short, medium and long radii horizontal wells at a duration of 300 s

4.2.2 Effect of pressure drop increase on cumulative liquid withdrawal rate at 300 s

Table 4-2 is a summary of the effect of increase in pressure drawdown on the cumulative liquid withdrawal rate at 300 seconds, simulated at different withdrawal rates by varying the outlet pressure at the surface. Figures 4-6 to 4-8 show the pressure drops increment for Case-1A, case-2B and Case-3B respectively. In Figure 4-6, an increasing in pressure drop resulted in increasing in both water and oil production rates. For an overall increase in pressure drop of -5.80 Psig, an increase of 7.95% and 1.86% in oil and water cumulative production rates respectively. As expected, Figures 4-7 and 4-8 produced at higher oil and water cumulative production rates; as observed in Figure 4-6. Hence for Case-2B an increase of 5.15% (cumulative oil production rate) and 10.30% (water cumulative production rate) was observed while there was an increase of 6.18% and 9.21% in oil and water cumulative production rates respectively for Case-3B.

A sensitivity analysis was performed that demonstrated that an increase in pressure drop results in an initial increase in oil produced but accompanied with higher volumes of unwanted water. In other words, at higher withdrawal rates, higher cumulative WOR over the same production time will be obtained. From the analysis, the longer radius well (Case-1A) performed best at a cumulative oil production rate of 9.68 cm^3/s and least cumulative water production rate at 3.70 cm^3/s. The reason is that longer wells have a higher pressure drop along their length when compared to shorter wells at the same operating condition, which delays cresting effect and hence are recommended for economic reasons, where high

production rates are necessary. The close oil and water flow rate values shown in Table 4-2 and Figures 4-6 to 4-8 were due to insufficient pressure at the surface to effect significant differences in flow rate between the cases investigated.

Table 4-2: Effect of pressure drop on cumulative liquid withdrawal rate at 300 s

Cases	Well type	Pressure at surface (-) (Psig)	Cumulative liquid production rate	
			Oil (cm^3/s)	Water (cm^3/s)
		4.351	8.91	3.70
Case-1A	LR	7.25	9.42	3.76
		10.15	9.68	3.77
		4.351	8.85	3.83
Case-2B	MR	7.25	8.94	4.20
		10.15	9.33	4.27
		4.351	8.96	3.55
Case-3B	SR	7.25	9.07	3.80
		10.15	9.55	3.91
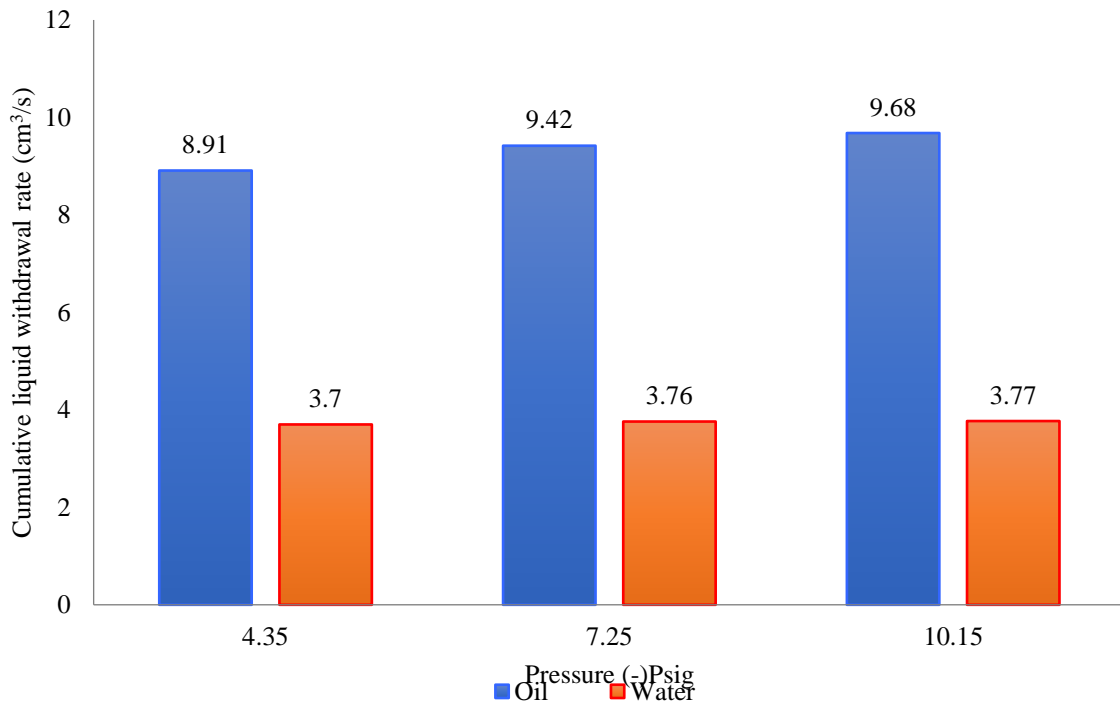
Figure 4-6: Effect of increase in pressure drop on cumulative liquid withdrawal rate (Case-1A) at 300 s
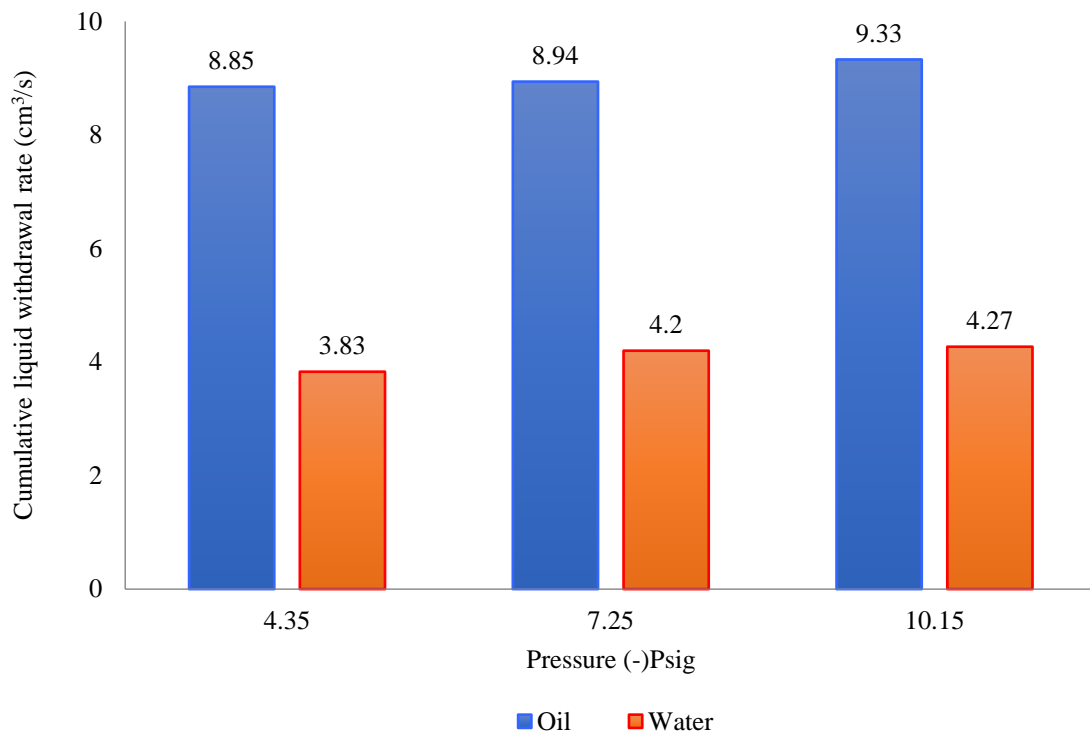
Figure 4-7: Effect of increase in pressure drop on cumulative liquid withdrawal rate (Case-2B) at 300 s
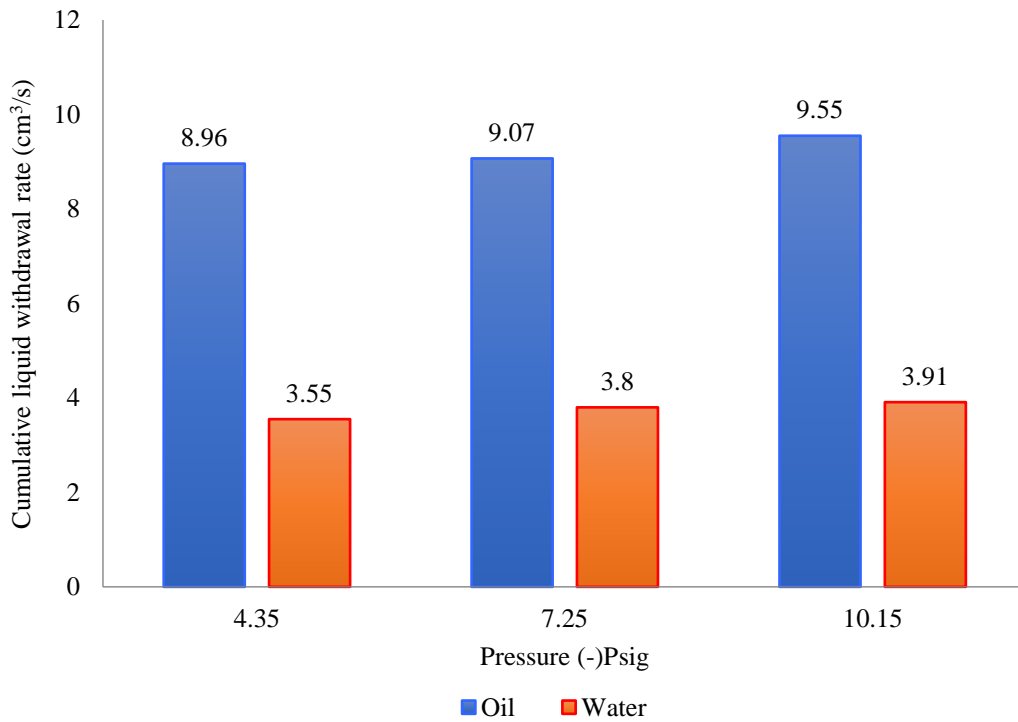
Figure 4-8: Effect of increase in pressure drop on cumulative liquid withdrawal rate (Case-3B) at 300 s

4.2.3 Effect of varying inclined sections on oil recovery at 300 s

Table 4-3 shows a summary of the oil recovery ratio in percentage for the different cases used in this investigation. Figure 4-9 illustrates the data contained in Table 4-3 for a production time of 300 seconds. From the plot, it can be clearly seen that Case-2C, a medium radius well at 30° angle of inclination and 0.73E-1 m horizontal displacement of the inclined section resulted in the highest oil recovery ratio of 38.73%, preceded by Case-3B (0.44 m horizontal displacement of the inclined section and 0.70 m short arc radius) having an oil recovery of 38.26%, while the lowest oil recovery ratio of 36.20% was obtained from Case-2A (long radius 2.68E-1 m and horizontal displacement of the inclined section, 0.80 m). However, the short radii well (Cases-2C, 3C and 3B) had the highest average oil recovery of 38.18%, whereas the long radii and medium radii wells had 37.18% and 37.19% respectively. Therefore, for a production time of 300 seconds, drilling shorter radii horizontal wells characterized by a lower measured depth and higher fluid mobility (due to lower pressure drop) is recommended for water cresting problems, as this could also be economical in the overall length of pipe used during drilling. However, this may not be the case for longer production times. Interestingly, a percentage difference in oil recovered between the best case (Case-2C) and the case with lowest performance (Case-2A) was 6.53%. However, for longer production times, larger difference in oil recovered may be obtained.

Table 4-3: Oil recovery at 300 s

Case-1A	Well type	Original oil in place (cm^3)	Oil (cm^3)	Oil recovery (%)
Case-1B	LR	7027.24	2671.78	38.02
Case-1C	LR	7027.24	2622.02	37.31
Case-2A	MR	7027.24	2605.80	37.08
Case-2B	LR	7027.24	2543.80	36.20
Case-2C	MR	7027.24	2655.25	37.79
Case-3A	SR	7027.24	2721.55	38.73
Case-3B	MR	7027.24	2577.98	36.69
Case-3C	SR	7027.24	2688.32	38.26
Case-1A	SR	7027.24	2638.87	37.55
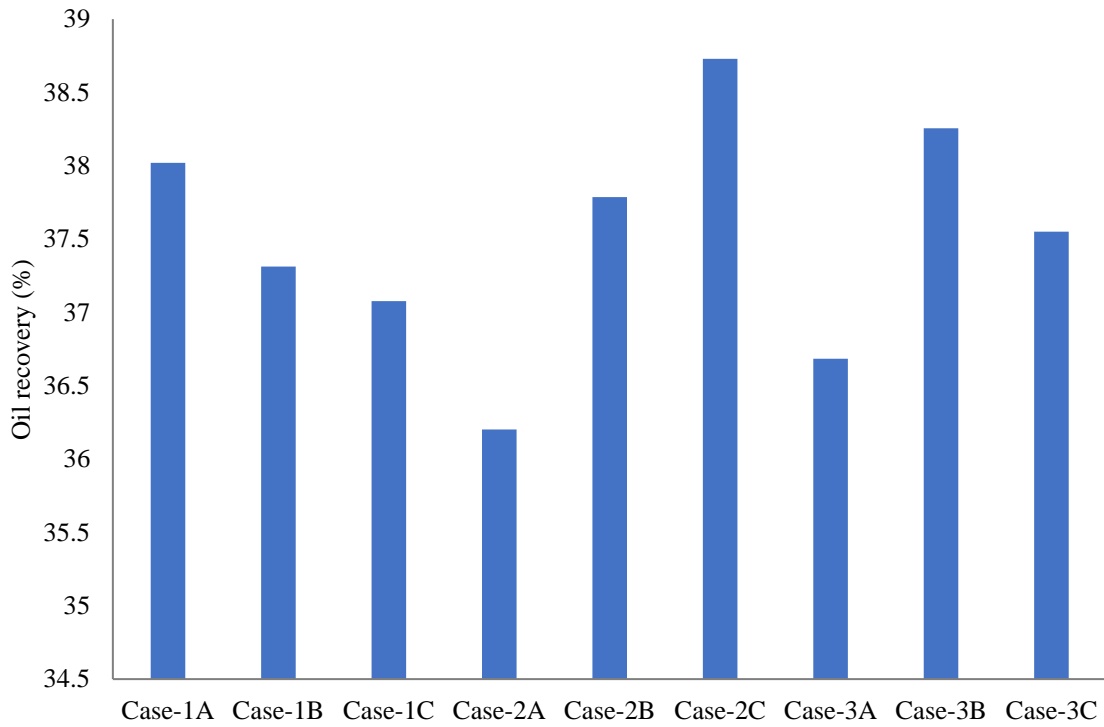
Figure 4-9: Oil recovery for different horizontal well geometries at 300 s

From the results presented in *Sections 4.2.1 to 4.2.3*, it is evident that there are differences in the cumulative oil, water production rates and oil recovery for all cases. This is due to differences in measured depths as a result of variations in horizontal and vertical displacements of the inclined section between all horizontal well cases. Hence at the same operating pressure, variation in pressure drop along the lengths of all horizontal wells is expected. Higher cumulative liquid production rate is highest for shorter radii wells (Cases-2C, 3C and 3B) due to shorter well lengths when compared to medium (Cases-1C, 2B and 3A) and longer radii (Cases-1A, 2A and 1B) wells. The lower pressure drop values along its length at some point in time during production is also a contributing factor. The same principle is expected for medium and long radii wells but at increasing pressure drop values along their lengths, highest in the later cases.

4.2.4   Effect of oil viscosity and lateral length on cumulative oil recovered at 495 s

Table 4-4 is a more concise summary of the effect of a change in oil viscosity and l_r for all horizontal well cases in a thick-oil rim reservoir. Figure 4-10 is a plot of the experimental data shown in Table 4-4. In Figure 4-10, at a simulation time of 495 seconds, Case-3C a short medium radius well achieved the highest oil recovered from the reservoir, at the same operating condition irrespective of the oil viscosity. On the contrary, Case-1A a long radius

well performed worst. This is as a result of its longer measured depth when compared to other horizontal well cases, hence higher pressure drop along its entire length and lower flow velocity of reservoir fluid. However, the higher the viscosity of oil, the lower the oil production rate as such the effect of viscosity on oil recovered is seen to decrease for all horizontal well cases in Figure 4-10. For all horizontal well cases, the shorter the lateral length in reservoir (l_r = 0.251 m), the higher the oil produced at the same operating condition. This was due to the longer diagonal-like movement of bottom aquifer with time towards the perforation of the shorter lateral well length in reservoir when compared to the shorter vertical-like movement of the bottom aquifer in longer lateral cases.

Table 4-4: Effect of oil viscosity and lateral length on oil recovered at 495 s

Cases	Well type	[50cP, l_r (0.305 m)] (cm^3)	[100cP, l_r (0.305 m)] (cm^3)	[50cP, l_r (0.251 m)] (cm^3)	[100cP, l_r (0.251 m)] (cm^3)
Case-1A	LR	2716.3	1705	3061	2060
Case-1B	LR	2728	1718.2	3071	2062
Case-1C	MR	2753	1743	3100	2089
Case-2A	LR	2700	1799	3043	2146
Case-2B	MR	2811.5	1908	3158.4	2259
Case-2C	SR	2930	2025	3282	2387.6
Case-3A	MR	2740	2215	3483	2590
Case-3B	SR	2911	2380	3646.5	2751.5
Case-3C	SR	2950	2416	3701	2803
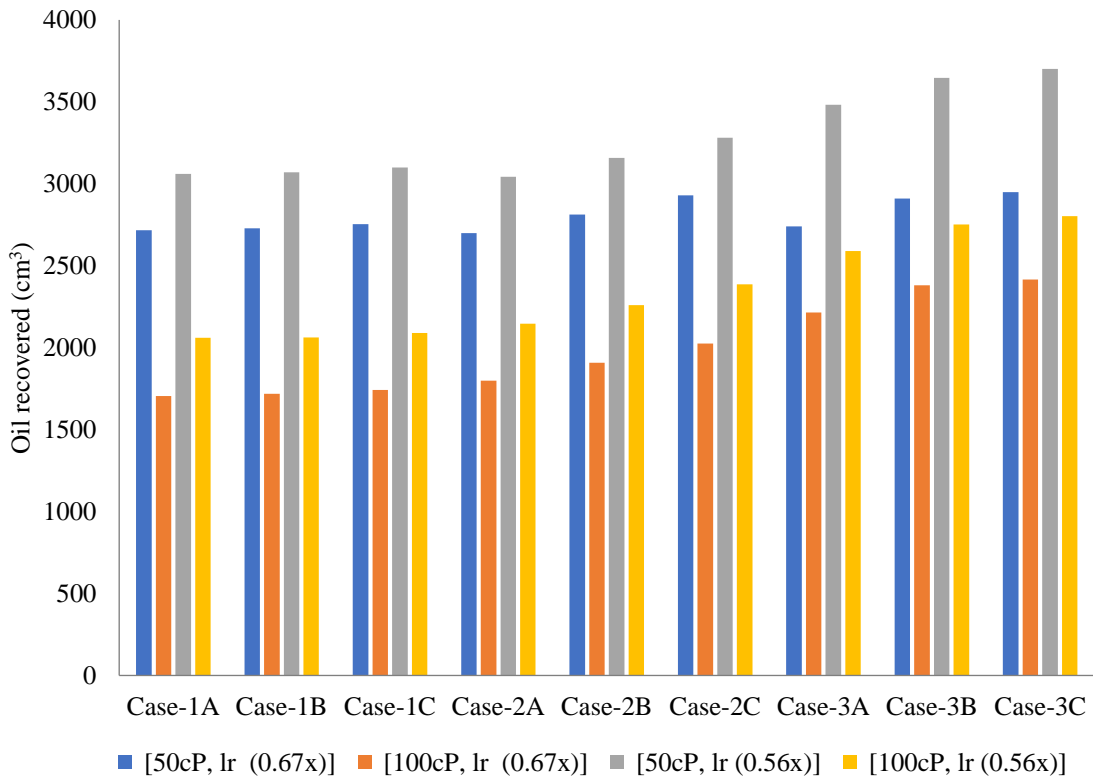
Figure 4-10: Effect of oil viscosity and lateral length on oil recovered at 495 s

As shown in Figure 4-10, the shorter radii wells (Cases-2C, 3B and 3C) had a higher average oil recovered in all scenarios at the same production time when compared to the medium and large radii wells. This was due to shorter overall well length accompanied by a lower overall pressure drop during oil production, resulting in higher overall liquid withdrawal rate. Hence the shortest radius well, Case-3C performed best in its category with 2950 cm^3 and 2416 cm^3 of oil recovered for longer lateral lengths in the reservoir and 3701 cm^3 and 2803 cm^3 for shorter lateral lengths in the reservoir. The shorter radius wells were found to be more effective in reservoirs with higher oil viscosity (100 cP); 29.43% ($l_r = 0.305$ m) and 26.51% ($l_r = 0.251$ m) was estimated between the best and worst horizontal well cases whereas 8.48% ($l_r = 0.305$ m) and 17.78% ($l_r = 0.251$ m) was observed for oil viscosity of 50 cP.

4.2.5 Effect of oil viscosity and lateral length on cumulative water produced 495 s

The effect of an increase in oil viscosity and lateral length in reservoir on the cumulative water cut and produced water, for thick-oil column reservoir is summarised in Table 4-5. Figure 4-11 illustrates a plot of all data in Table 4-5. Figure 4-11 shows that for the

horizontal well cases an increase in oil viscosity and a reduction in lateral length in the reservoir results in an increase in cumulative water produced.

In Table 4-5 and Figure 4-11, it can be seen that at the same lateral well length in reservoir but an increase in oil viscosity, higher cumulative water was produced. In all cases, it was observed that for an increase in oil viscosity from 50 to 100 cP, the cumulative water produced increased greater than 1.5 times in volume of oil. This was due to the lower oil mobility in the horizontal wells for higher oil viscosity and as such resulted in a significant increase in water influx especially after water breakthrough. As expected, the shorter radii horizontal wells had the highest average cumulative water produced succeeded by the medium and long radii wells respectively for different oil viscosity and lateral lengths in reservoir. The higher overall pressure drop experienced in longer radii wells, is the known reason for the lower cumulative produced water. In all cases, the highest difference in percentage between the worst (Case-3C) and best case (Case-1A) was 19.15% for (50 cP, l_r = 0.305 m) succeeded by 13.94% (100cP, l_r = 0.305 m), 12.76% (50cP, l_r = 0.251 m), and 9.41% (100 cP, l_r = 0.251 m).

Table 4-5: Effect of oil viscosity and lateral length in reservoir on cumulative water produced at 495 s

Cases	Well type	[50cP, lr (0.305 m)] (cm^3)	[100cP, lr (0.305 m)] (cm^3)	[50cP, lr (0.251 m)] (cm^3)	[100cP, lr 0.251 m)] (cm^3)
Case-1A	LR	1503	2353	2864	4014
Case-1B	LR	1541	2397	2911	4058
Case-1C	MR	1581	2436	2973	4123
Case-2A	LR	1608	2466	3004	4154
Case-2B	MR	1642	2512	3043	4190
Case-2C	SR	1715	2588	3121	4270
Case-3A	MR	1777	2649	3194	4345
Case-3B	SR	1785	2658	3205	4353
Case-3C	SR	1859	2734	3283	4431
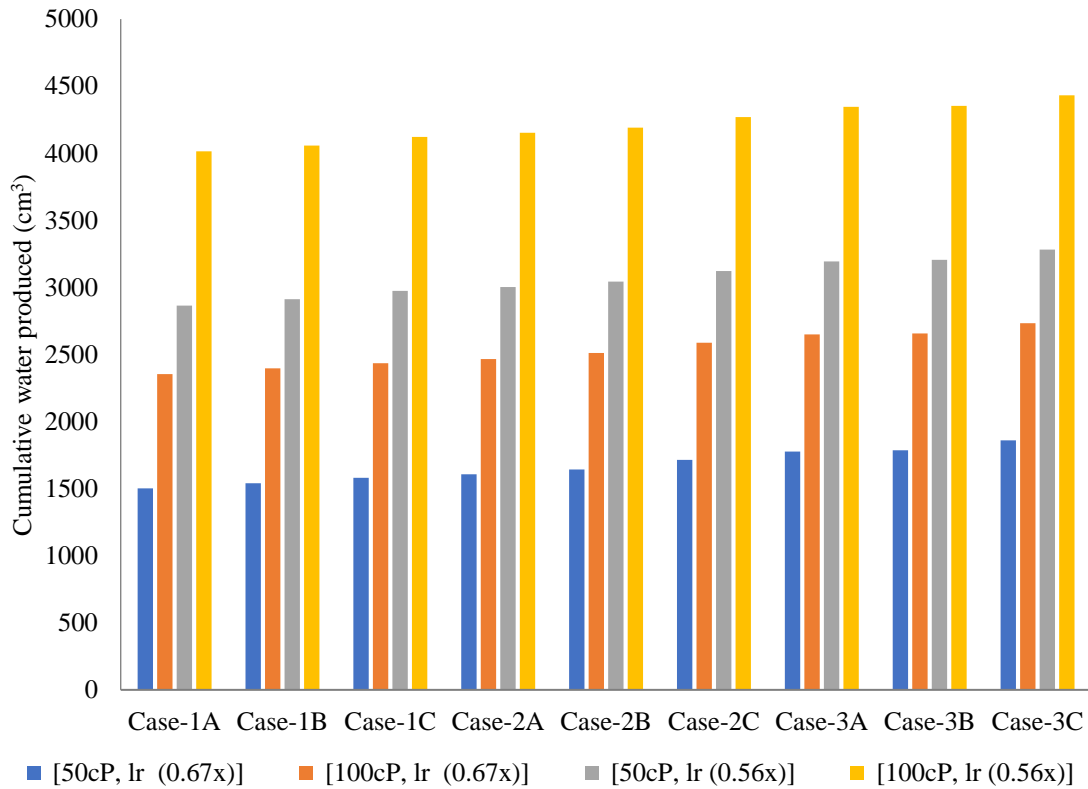
Figure 4-11: Effect of oil viscosity and lateral length on cumulative water produced at a duration of 495 s

4.2.6 Effect of oil viscosity and lateral length on cumulative water cut 495 s

Table 4-6 and Figure 4-12 represent the effect of change in oil viscosity and lateral length for thick-oil rim reservoir on cumulative water cut. The cumulative water cut was calculated using Equation 4.1.

$$Water\ cut = \frac{cumulative\ water\ produced\ (cm^3)}{oil\ plus\ cumulative\ water\ produced\ (cm^3)}\ x\ 100\% \qquad (4.1)$$

As shown in Figure 4-12, cumulative water cut increases with increase in oil viscosity and shorter lateral length in reservoir for all cases. In all horizontal well cases, the cumulative water cut is seen to be lowest for oil viscosity of 50cP and l_r = 0.305m and highest in reservoir with 100 cP oil viscosity and l_r = 0.251 m.

103

Table 4-6: Effect of oil viscosity and lateral length on cumulative water cut at 495 s

Cases	Well type	[50cP, l_r (0.305 m)] (%)	[100cP, l_r (0.305 m)] (%)	[50cP, l_r (0.251 m)] (%)	[100cP, l_r (0.251 m)] (%)
Case-1A	LR	35.62	57.98	48.33	66.08
Case-1B	LR	36.10	58.25	48.66	66.31
Case-1C	MR	36.48	58.29	48.95	66.37
Case-2A	LR	37.33	57.82	49.68	65.94
Case-2B	MR	36..87	56.83	49.07	64.97
Case-2C	SR	36.92	56.10	48.74	64.14
Case-3A	MR	39.34	54.46	47.83	62.65
Case-3B	SR	38.01	52.75	46.78	61.27
Case-3C	SR	38.66	53.09	47.01	61.25
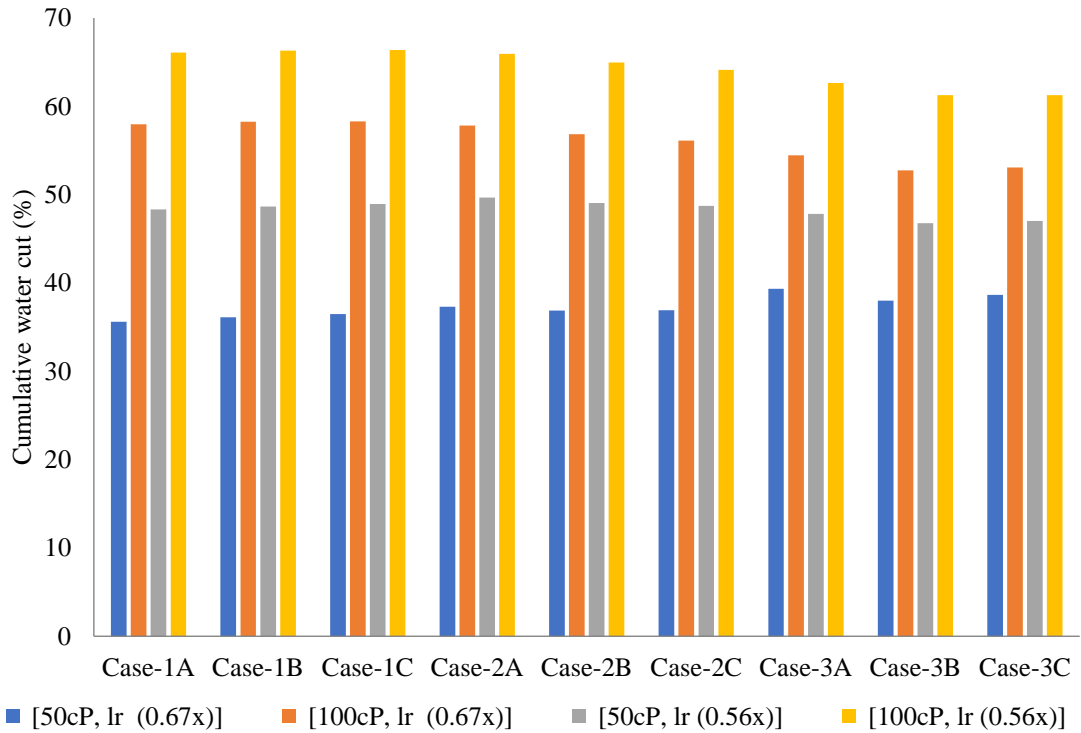
Figure 4-12: Effect of oil viscosity and lateral length on cumulative water cut at 495 s

Although the cumulative water produced increase with a shorter well length in the reservoir, the cumulative water cut was independent on the measured depth of the horizontal well but rather depended significantly on the cumulative oil recovered from the reservoir. Significant cumulative water cut was observed in the reservoir with higher oil viscosity (100 cP) and longer radii wells compared to short and medium radii wells. The unwanted water dominates production at post breakthrough times due to its lower viscosity compared to the oil, having higher velocity at the same operating pressure. Hence, the highest cumulative water cut was observed in Case-1C for oil viscosity of 100 cP and shorter lateral (0.251 m) while the least was observed in Case-3A (50cP, l_r = 0.305 m). In addition, the total cumulative water cut was found to be highest for medium radii well category, 66.37% [Case-1C; 100 cP, l_r = 0.251 m) while for long and short radii wells the total cumulative water cut were 66.31% [Case-1B; 100 cP, l_r = 0.251 m) and 64.14% (Case-2C; 100 cP, l_r = 0.251 m)] respectively.

4.2.7 Effect of lateral length on pressure drop at 495 s

Tables 4-7 and 4-8 are summaries of the experimental data for pressur^e drop for thick-oil rim reservoirs in all horizontal well cases during oil production and represented graphically in Figures 4-13 to 4-14. The pressure drop values were derived by subtracting the pressure at the surface (measured using a vacuum gauge) from the reservoir pressure (measured using digital manometer) at varying time steps. Figure 4-13 illustrate pressure drop plot for thick-oil column reservoir with l_r = 0.305 m while Figure 4-14 illustrate pressure drop plot for thick-oil column reservoir with l_r = 0.251 m respectively. In Figures 4-13 and 4-14, it can be observed that there is a gradual decline in pressure drop with oil production time. These Figures show that pressure drop depends on the Measured depth of the horizontal well, such that the longer the horizontal well, the higher the pressure drop and vice versa. This means that in general, the shorter the lateral length in the reservoir the higher the cumulative liquid produced expected.

Table 4-7: Pressure measurements at 495 s for 0.305 m length of lateral in thin-oil rim reservoir versus time (50 cP, oil viscosity) (E-1)

Time (s)	Case-1A (LR)	Case-1B (LR)	Case-1C (MR)	Case-2A (LR)	Case-2B (MR)	Case-2C (SR)	Case-3A (MR)	Case-3B (SR)	Case-3C (SR)
0	43.37	43.37	43.37	43.37	43.37	43.37	43.37	43.37	43.37
150	42.21	41.92	41.63	41.34	41.19	40.9	40.61	40.46	40.18
300	40.61	40.47	40.32	40.03	39.74	39.45	39.16	39.02	38.87
450	36.99	36.7	36.41	35.97	35.53	34.95	34.81	34.52	34.23
495	33.36	33.21	32.92	32.34	32.05	31.76	31.62	31.33	31.18
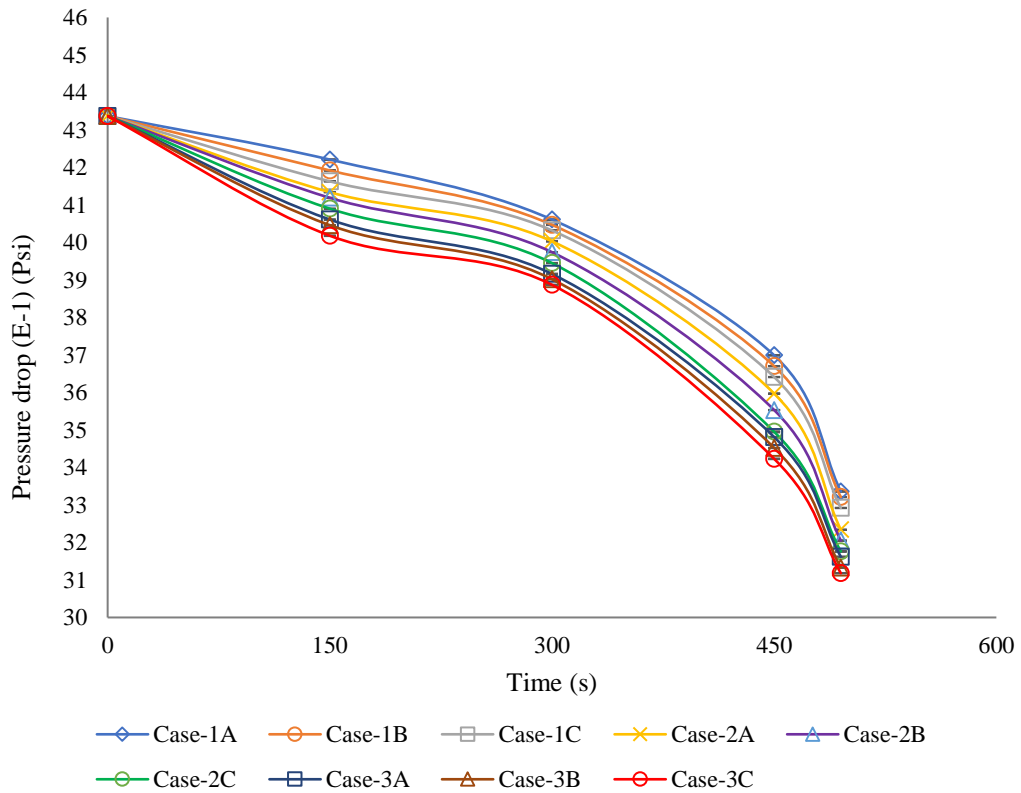
Figure 4-13: Pressure measurements at 495 s for 0.305 m length of lateral in thin-oil rim reservoir versus time (50 cP, oil viscosity) (E-1)

Table 4-8: Pressure measurements at 495 s for 0.251 m length of lateral in thin-oil rim reservoir versus time (50 cP, oil viscosity) (E-1)

Time (s)	Case-1A (LR)	Case-1B (LR)	Case-1C (MR)	Case-2A (LR)	Case-2B (MR)	Case-2C (SR)	Case-3A (MR)	Case-3B (SR)	Case-3C (SR)
0	43.37	43.37	43.37	43.37	43.37	43.37	43.37	43.37	43.37
150	41.63	41.19	40.9	40.61	40.32	39.89	39.6	39.31	39.02
300	38.58	38.29	38	37.56	37.28	36.99	36.7	36.4	36.11
450	33.5	33.36	33.07	32.63	32.34	32.05	31.76	31.47	31.18
495	30.46	27.56	27.12	26.69	26.54	26.25	25.96	25.82	25.67
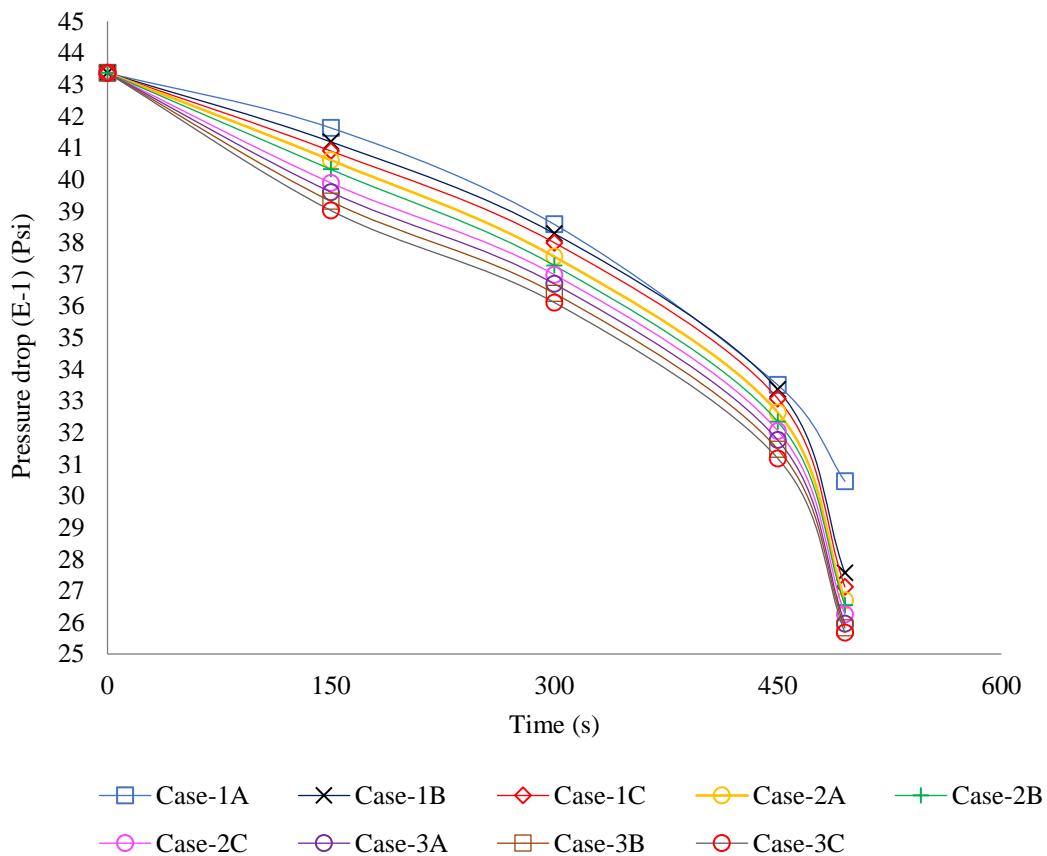
Figure 4-14: Pressure measurements at 495 s for 0.251 m length of lateral in thin-oil rim reservoir versus time (50 cP, oil viscosity) (E-1)

107

4.2.8 Effect of increase in production time on oil recovery and cumulative water cut 300 s and 495 s

Table 4-9 represent the set of data obtained for oil recovery at 300 s and 495 s at oil viscosity of 50cP. Figure 4-15 is a plot of the data shown in Table 4-9. As shown in Figure 4-15, increments in oil recovered for all horizontal well cases over time was observed. Table 4-9 shows that higher percentages of oil were recovered between 300 s and 495 s in the short radii category. This trend was succeeded by the medium radii category and lastly the long radii wells. As illustrated in Table 4-9 and Figure 4-15, the best case (Case-3C) is seen to have an increment of 10.55%, whilst the worst case (Case-1A) had an increment of 1.63%. However, the small percentage increment in oil recovered is due to the water (effluent) dominating oil production upon insurgence into the wellbore (post break-through).

Table 4-9: Effect of oil production time on oil recovery at 300 s and 495 s at oil viscosity of 50 cP

Cases	Well type	Oil recovery at 300 s (%)	Oil recovery at 495 s (%)	Increment in oil recovery (%)
Case-1A	LR	38.02	38.65	1.63
Case-1B	LR	37.31	38.82	3.89
Case-1C	MR	37.08	39.17	5.34
Case-2A	LR	36.2	38.42	5.78
Case-2B	MR	37.79	40.01	5.76
Case-2C	SR	38.73	41.69	7.10
Case-3A	MR	36.69	38.99	5.90
Case-3B	SR	38.26	41.42	7.63
Case-3C	SR	37.55	41.98	10.55
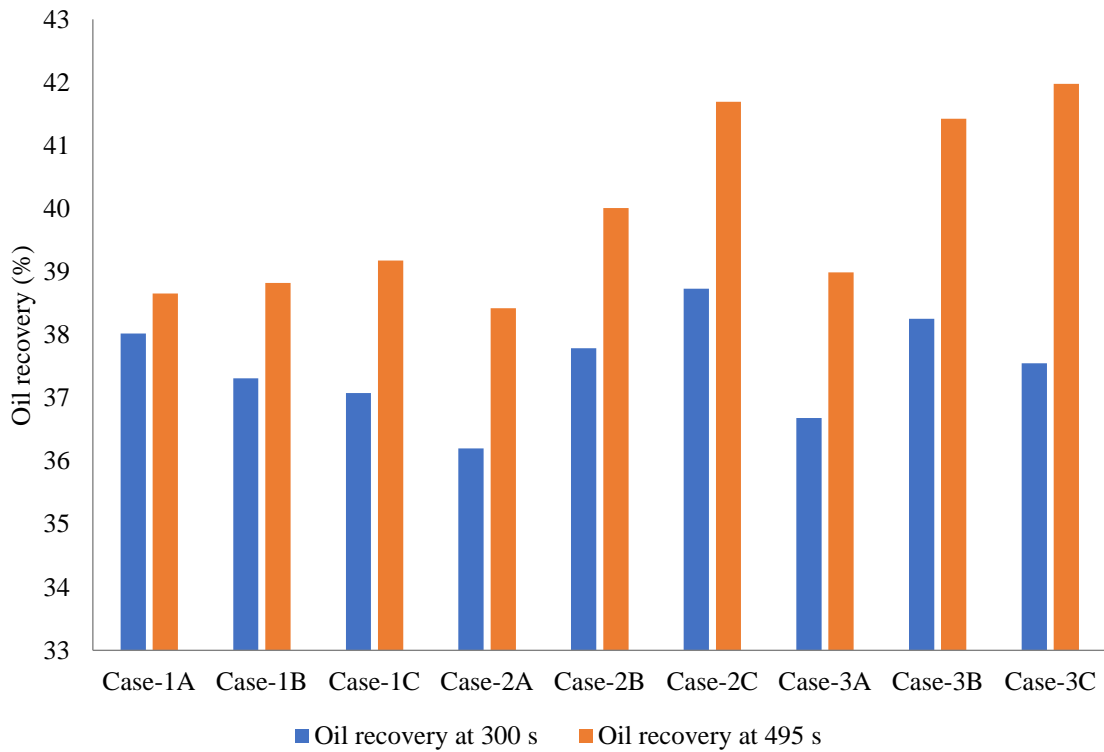
Figure 4-15: Effect of increase in oil production time on oil recovery at 300 s and 495 s at oil viscosity of 50 cP

Figure 4-16 represents the plot for sets of data, as illustrated in Tables 4-10. Table 4-10 summarizes the data for the effect of oil production time on the cumulative water cut at 300s and 495 s at oil viscosity of 50 cP. Table 4-10 also show the increments in cumulative water cut in percentage for all cases. As shown in Figure 4-16, rather high percentage increment in cumulative water cut was observed in all cases. This is due to dominating effluent (water) production after breakthrough since the nature of the aquifer was strong. From the results in Table 4-10 and Figure 4-16, the short radii well category have highest average cumulative increment in cumulative water cut (23.89%), compared to the long and medium radii categories of 15.86 % and 19.18% respectively.

Table 4-10: Effect of oil production time on cumulative water cut at 300 s and 495 s at oil viscosity of 50 cP

Cases	Well type	Cumulative water cut at 300 s (%)	Cumulative water cut at 495 s (%)	Increment in cumulative water cut (%)
Case-1A	LR	29.35	35.62	17.55
Case-1B	LR	30.08	36.10	16.68
Case-1C	MR	29.07	36.48	20.36
Case-2A	LR	32.32	37.33	13.35
Case-2B	MR	30.21	36.87	21.56
Case-2C	SR	27.32	36.92	26.00
Case-3A	MR	33.20	39.34	15.61
Case-3B	SR	28.43	38.01	25.26
Case-3C	SR	30.77	38.66	20.41
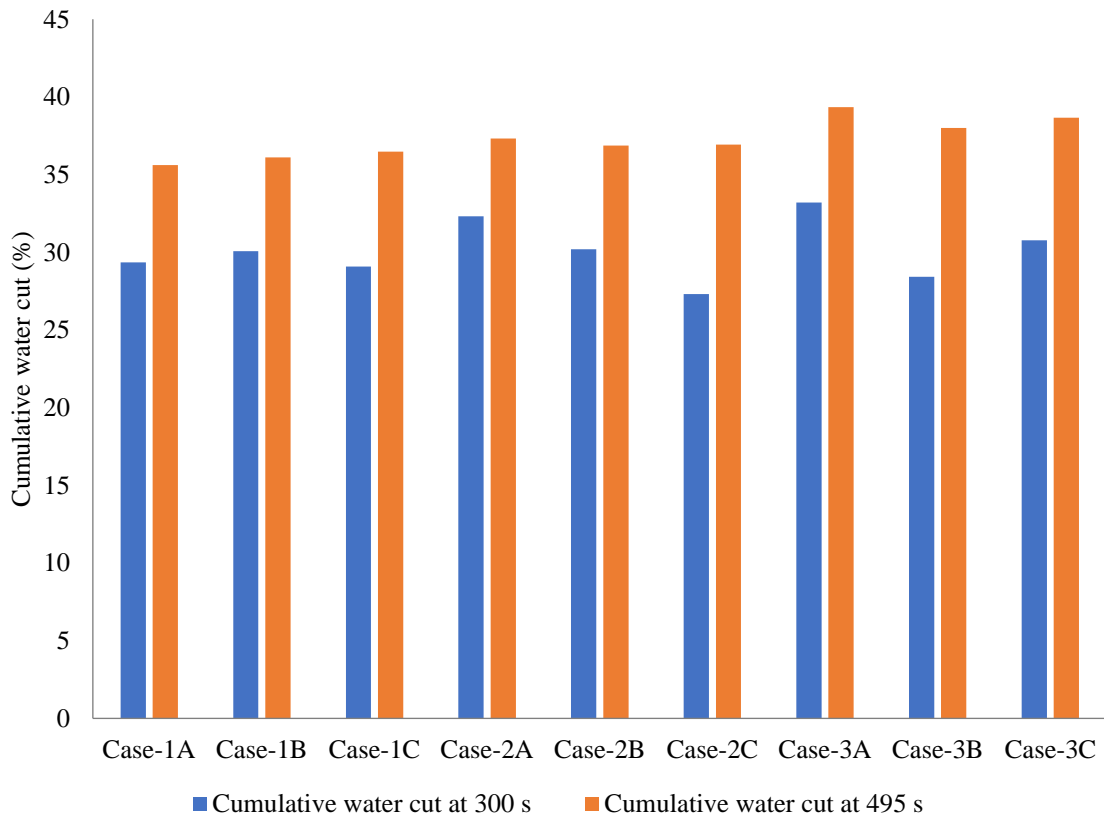
Figure 4-16: Effect of oil production time on cumulative water cut at 300 s and 495 s at oil viscosity of 50 cP

110

4.2.9 Proactive cresting control at 495 s

4.2.9.1 Effect on oil recovery and oil produced

Figure 4-17 depicts oil recovery results and oil produced for Cases 1-6 in Table 4-11 show a more detailed summary of Table 4-11. In this figure, Case 1 had the least oil recovery of 41.98%. This was due to the dominant drive mechanism in the simulated reservoir (water drive), hence the oil recovery ratio had similar trend to a typical water drive mechanism with an oil recovery ratio between 35-75% (Tarek, 2001, AAPG, 2016a) . For Case 2, an incremental oil recovery of 0.47% was achieved compared to the base case (Case 1) for a shut-in time of 960 s. At a shut-in time of 9000 s (Case 6), 1.55% increment in oil recovery was observed compared to Case 1. The relatively low oil recovery results obtained for Cases 1-6 could be due to the presence of some volumes of trapped water between pore spaces during shut-ins). However, Case 2 is seen to have 1.11% increment in produced oil compared to Case 1 for a shut-in time of 960 s. Similarly, Cases 3-6 are seen to have 2.35%, 3.24%, 3.51% and 3.56% increments in oil produced at 2700, 5400, 7200 and 9000 shut-in times respectively over Case 1. Hence, a steady increase in both oil recovery and oil produced were observed from Case 2 to Case 6, with increase in shut-in time. This is as a result of high-interconnected pore spaces and as such good tendency of oil displacement by water is possible. Due to the low total porosity (19.1%) and limited size of the reservoir, a rather low increase in produced oil (3.56%) was observed between Cases 1 and 6.

Table 4-11: Oil recovery and oil produced results at 495 s

Case	Well type	Original Oil In Place (cm^3)	Shut-ins (s)	Non-Dimensional number of shut-in times	Cumulative oil produced (cm^3)	Incremental oil produced, %	Oil recovery (%)	Incremental oil recovery, %
Case 1	SR	7027.34	0	x	2950		41.98	
Case 2	SR	7027.34	960	6.86x	2982.91	1.11	42.45	0.47
Case 3	SR	7027.34	2700	19.29x	3020.91	2.35	42.99	1.01
Case 4	SR	7027.34	5400	38.57x	3048.57	3.24	43.38	1.40
Case 5	SR	7027.34	7200	51.43x	3057.32	3.51	43.51	1.53
Case 6	SR	7027.34	9000	64.29x	3058.91	3.56	43.53	1.55
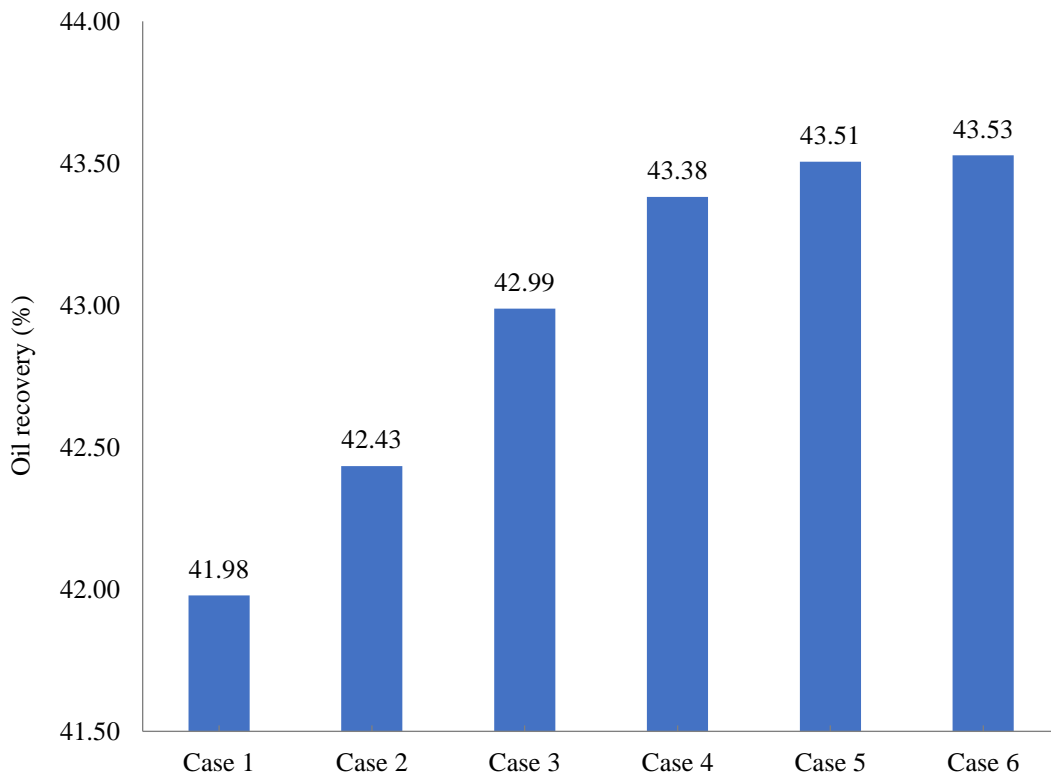
Figure 4-17: Oil recovery versus shut-in time at 495 s

4.2.9.2 Effect on cumulative water produced

Table 4-12 shows a summary of the cumulative water produced for thick-oil rim reservoir cases at a production time of 495 seconds. Figure 4-18 is a plot of the summarised data in Table 4-12. Figure 4-18 shows that the highest volume of water (1859 cm^3) produced was for Case 1 and the least for Case 6 (1675.01 cm^3). Lower volumes of unwanted water are shown to decrease with longer shut-in times. However, in between shut-ins the cumulative water reduced with time while attaining new WOC levels. Decrements of 4.87% (between Cases 2 and1), 2.65% (Cases 3 and 2), 2.02% (between Cases 4 and 3), 0.62% (between Cases 5 and 4) and 0.1% (Cases 6 and 5) were realized in between shut-in times for cumulative produced wanted water. The decrease in water produced was due to a reduction in available pores spaces over time for oil displacement. However, 9.90% reduction in cumulative water produced was observed between Cases 1 and 6. The insufficiently low water production reported by Beattie and Roberts (1996) was possibly due to the available interconnected pore spaces in the fractured reservoir, shape and height of the water cone experienced in vertical wells. In

horizontal wells, a crest-like shape was observed so a higher tendency to recede is possible in oil reservoirs with high-interconnected pore spaces such as that used in this study.

Table 4-12: Cumulative Water produced at 495 s

Cases	Well type	Cumulative water produced (cm^3)	Reduction in the cumulative water produced, %
Case 1	SR	1859	
Case 2	SR	1768.56	4.87
Case 3	SR	1721.78	7.38
Case 4	SR	1687.06	9.25
Case 5	SR	1676.56	9.81
Case 6	SR	1675.01	9.90
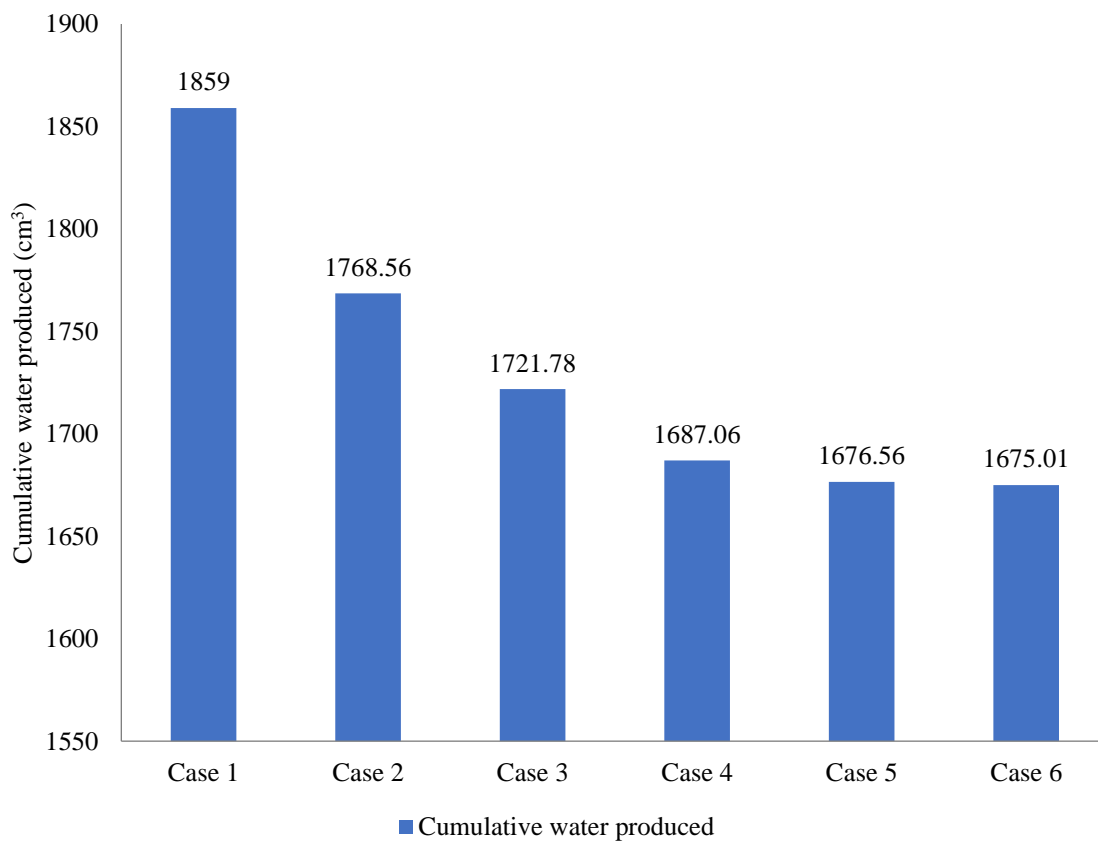
Figure 4-18: Cumulative water produced versus shut-in time after at 495 s

4.2.9.3 Effect on cumulative liquid produced

Figure 4-19 is a plot of the data for thick-oil rim reservoir summarised in Table 4-13 for the cumulative liquid in cubic centimeters produced over a period of 495 seconds. From the plot, the cumulative liquid produced is seen to decrease with increase in shut-in time. Table 4-13 shows that there is a general reduction in cumulative liquid produced. However, higher volumes of oil in cubic centimeters are produced with reducing volumes of water produced in cubic centimeters from Cases 1-5. The percentage difference in cumulative liquid produced between Cases 1 and 2, Cases 2 and 3, Cases 3 and 4, Cases 4 and 5 were 1.20%, 0.19%, 0.15%, and 0.04% respectively. The cumulative liquid produced between cases 5 and 6 have same volume if approximated. The percentage difference in the cumulative liquid produced between. The decline in the cumulative liquid produced was affected by gravity and density difference in the reservoir.

Table 4-13: Cumulative liquid produced at 495 s

Cases	Well type	Cumulative oil (cm^3)	Cumulative water produced (cm^3)	Cumulative liquid produced (cm^3)	Reduction in the cumulative liquid produced, %
Case 1	SR	2950	1859	4809	
Case 2	SR	2982.91	1768.56	4751.47	1.20
Case 3	SR	3020.91	1721.78	4742.69	1.38
Case 4	SR	3048.57	1687.06	4735.63	1.53
Case 5	SR	3057.32	1676.56	4733.88	1.56
Case 6	SR	3058.91	1675.01	4733.92	1.56
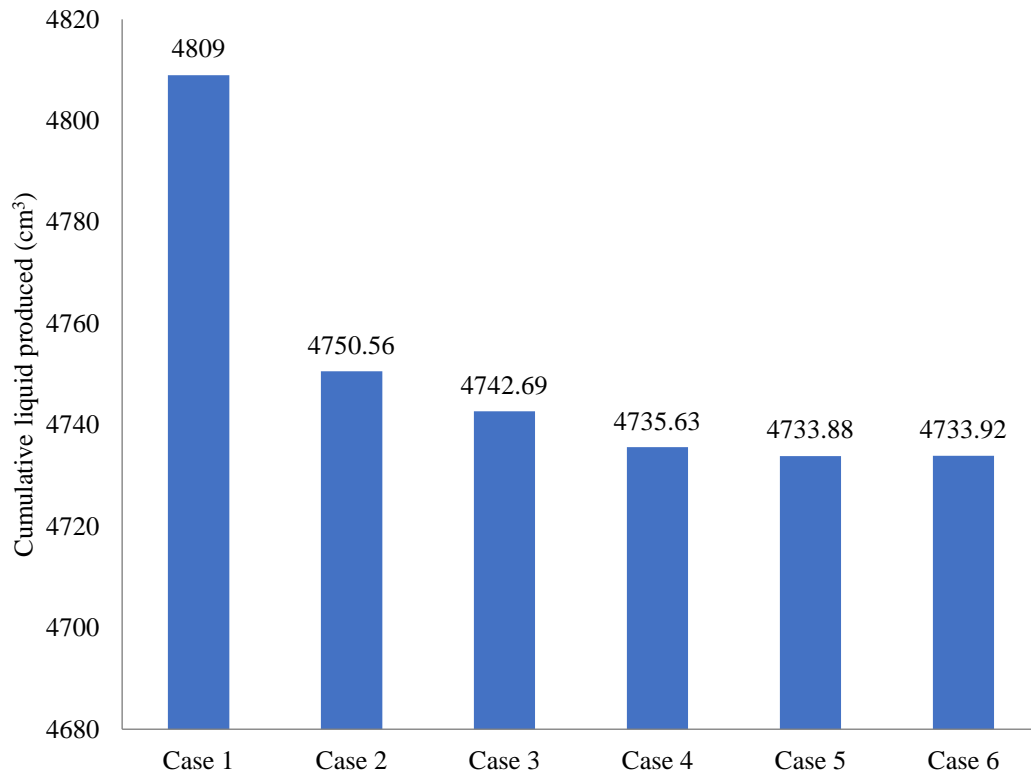
Figure 4-19: Cumulative liquid produced versus shut-in time after at 495 s

4.3   Thin-oil rim reservoir

4.3.1   Effect of oil viscosity and lateral length on cumulative oil recovered at 210 s

Table 4-14 summarizes the effect of a change in oil viscosity and lateral length in reservoir for all horizontal well cases for a thin-oil rim reservoir. A plot of the experimental data shown from Table 4-14 is illustrated in Figure 4-20. Figure 4-20 shows that at the same initial operating and reservoir pressure, an increase in oil viscosity results in a reduction of oil recovered from the reservoir. More so, greater than one-half the volume of oil was recovered for twice the oil viscosity. Figure 4-20 also shows that the shorter well length in reservoir (0.251 m) for all horizontal well cases produced slightly more oil compared to the long lateral length. This was due to a shorter simulation time and obviously the longer horizontal displacement between the water injection point 2 (illustrated in Chapter 3, Figure 3-1(b)) and perforations of the well. The diagonal shape of the crest towards the perforation of the horizontal wells is a major contributing factor as shown in Figure 4-21(b). Figure 4-20 and Table 4-14 show that for this type of oil reservoirs, Case-1C produced the lowest oil [(488cm^3) 13.29% in oil recovery (100 cP, l_r (0.305 m)] in all cases, while Case-2C a short

radius well resulted in the highest oil recovered (1035 cm^3) in all scenarios. This is possibly due to the geometry of the horizontal well, its inclined section (ratio of vertical displacement to the reservoir height), angle of inclination and its measured depth.

The results presented here contradicts that presented by Freeborn et al. (1990). In their study, a numerical simulation was the method of study known to have higher percentage error due to assumptions compared to an experimental approach as presented in this study. Also noticeable in Table 4-14 is that there is a general decrease in oil recovered in all cases for an increase in oil viscosity from 50 cP to 100 cP, which is in good agreement with the work of Mungan (1979).

Table 4-14: Effect of oil viscosity and lateral length on oil recovered at 210 s

Cases	Well type	Original Oil In Place (cm³)	[50 cP, l_r (0.305 m)]		[100 cP, l_r (0.305 m)]		[50 cP, l_r (0.251 m)]		[100 cP, l_r (0.251 m)]	
			Oil recovered (cm³)	Oil recovery (%)	Oil recovered (cm³)	Oil recovery (%)	Oil recovered (cm³)	Oil recovery (%)	Oil recovered (cm³)	Oil recovery (%)
Case-1A	LR	3672.67	957	26.06	575	15.66	970	26.41	585	15.93
Case-1B	LR	3672.67	970	26.41	590	16.07	985	26.82	602	16.39
Case-1C	MR	3672.67	838	22.82	488	13.29	849	23.11	498	13.56
Case-2A	LR	3672.67	979	26.66	628	17.10	991	26.98	637	17.34
Case-2B	MR	3672.67	855	23.28	505	13.75	860	23.42	517	14.08
Case-2C	SR	3672.67	1001	27.26	652	17.75	1035	28.18	693	18.87
Case-3A	MR	3672.67	875	23.83	526	14.32	890	24.23	553	15.06
Case-3B	SR	3672.67	980	26.68	631	17.18	995	27.09	641	17.45
Case-3C	SR	3672.67	984.3	26.80	637	17.34	1005	27.36	649	17.67
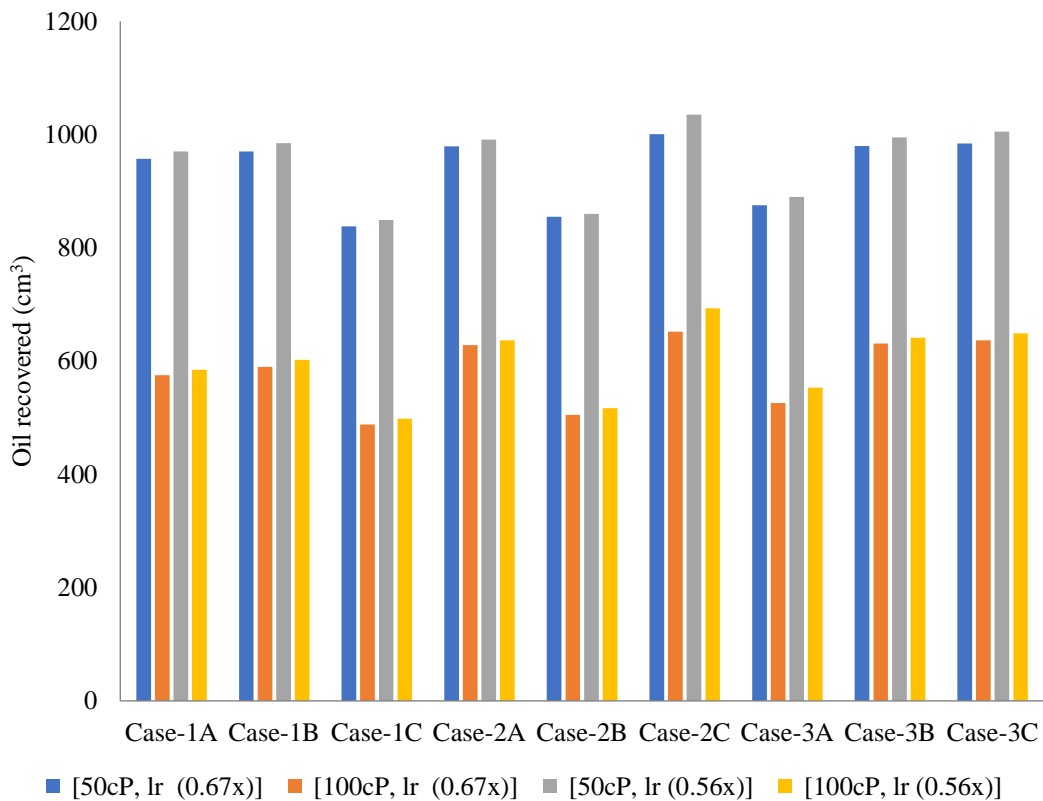
Figure 4-20: Effect of oil viscosity and lateral length on oil recovered at 210 s
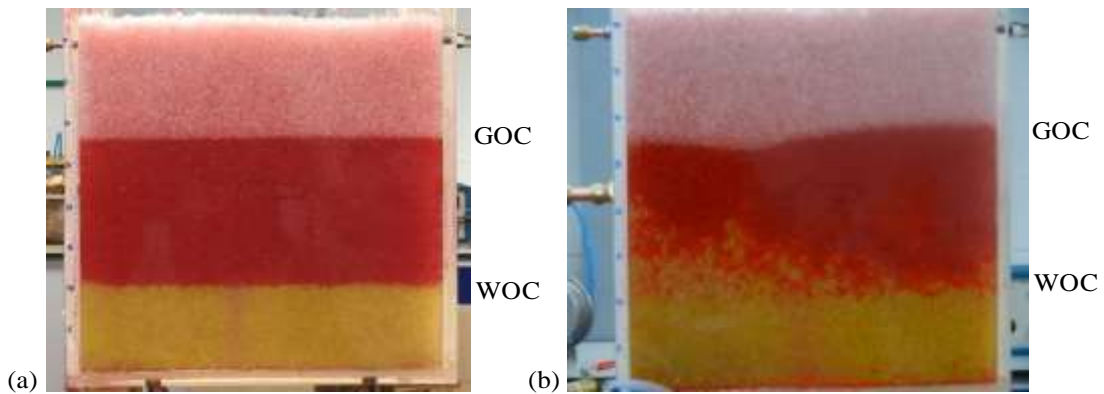
Figure 4-21: (a) thin-oil rim reservoir at static condition ($l_r = 0.251$ m) (b) diagonal-like cresting towards the well's perforation for thin-oil rim reservoir at 75 s (($l_r = 0.251$ m)

4.3.2 Effect of oil viscosity and lateral length on cumulative water produced at 210 s

Table 4-15 summarizes the effect of an increase in oil viscosity and change in lateral length in a thin-oil rim reservoir. The results were reported for cumulative water cut and produced water represented graphically in Figure 4-22. In Figure 4-22, the cumulative water produced and water cut generally increase with an increase in oil viscosity

As shown in Table 4-15 and Figure 4-22, for the same lateral well length in reservoir and increase in oil viscosity, higher cumulative water produced is observed in all horizontal well scenario. In all cases, twice the increase in oil viscosity resulted in volumes greater than one-half the cumulative water produced owing to the lower oil velocity in the horizontal wells with an increase in oil viscosity at the same operating pressure. Figure 4-22 also show that at the same oil viscosity, the cumulative water produced was independent of the measured depth of the horizontal well; although short radii horizontal wells are expected to have a rather higher water produced compared to long and medium radii well, this was not the case. The inconsistency in cumulative water produced experienced in the different horizontal wells was a function of the horizontal distance of the perforation from water inlet point 2 as shown in Figure 3-1(b) and oil viscosity for this kind of reservoirs. Hence, in all cases, the short radii horizontal wells had the least cumulative water produced (761.3 cm^3), succeeded by 823 cm^3 and 844 cm^3 for medium and long radii wells respectively at an oil viscosity of 50 cP and l_r = 0.251 m. The difference in percentage between the worst case (Case-1C) and best case (Case-2C) was 15.14% (50 cP, l_r = 0.305 m), 15.68% between Case-3C and 1A (100cP, l_r = 0.305 m), 15.81% between Case-1C and Case-2C (50 cP, l_r = 0.251 m), and 12.11% between Case-1C and 2C (100 cP, l_r = 0.251 m).

Table 4-15: Effect of oil viscosity and lateral length on cumulative water produced at 210 s

Cases	Well type	[50 cP, lr (0.305 m)] (cm^3)	[100 cP, lr (0.305 m)] (cm^3)	[50 cP, lr (0.251 m)] (cm^3)	[100 cP, lr 0.251 m)] (cm^3)
Case-1A	LR	840	1140	830	1128
Case-1B	LR	856	1159	846	1146
Case-1C	MR	885	1188	879	1181
Case-2A	LR	865	1210	856	1158
Case-2B	MR	861	1204	855	1153
Case-2C	SR	751	1317	740	1038
Case-3A	MR	763	1329	750	1043
Case-3B	SR	778	1343	769	1064
Case-3C	SR	785	1352	775	1071
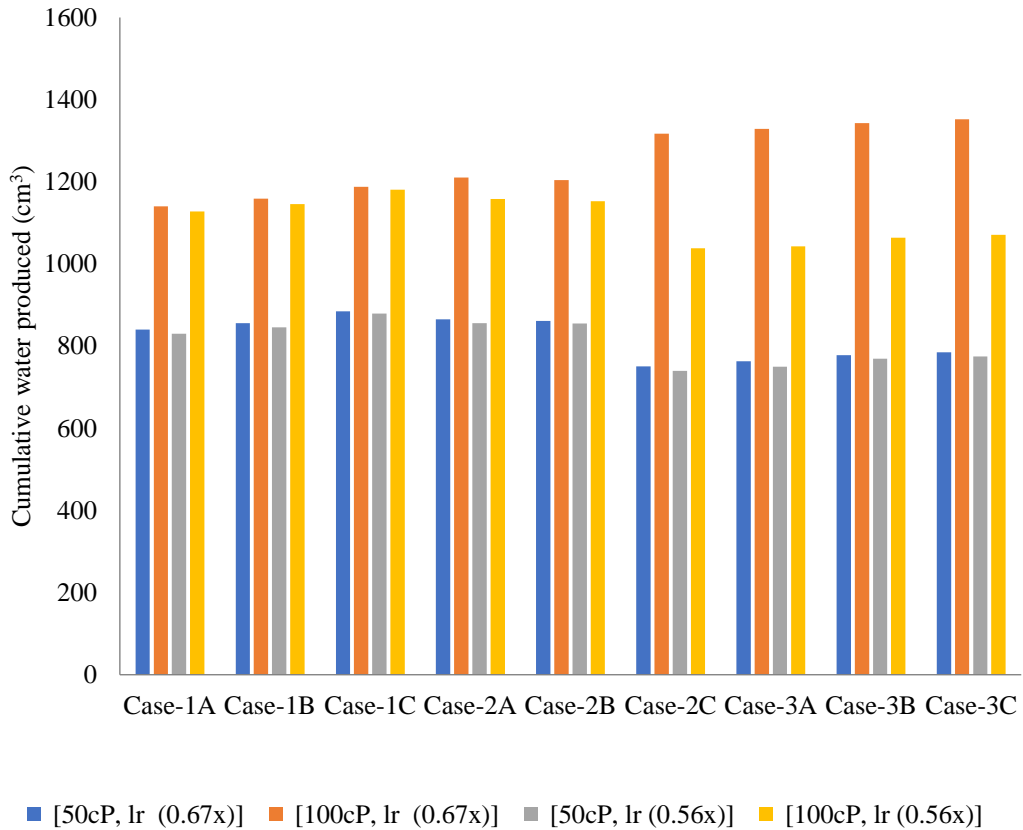
Figure 4-22: Effect of oil viscosity and lateral length on cumulative water produced at a duration of 210 s

4.3.3 Effect of oil viscosity and lateral length on cumulative water cut at 210 s

Figure 4-23 illustrates the experimental data shown in Table 4-16. It can be seen in this Figure 4-23 that the cumulative water cut generally increases with an increase in oil viscosity and a reduction in lateral length in reservoir. This is because unwanted water dominates production after breakthrough and due to its lower viscosity compared to the oil, higher volumes of water influx is expected. However, the shorter lateral well length in the reservoir did not always result in a higher cumulative water cut in all horizontal well scenarios. The cumulative water cut is seen to be lowest (44.37%) in Case-3C (50 cP, l_r = 0.305 m) due to higher initial oil production rate (higher velocity of the oil flow due to lower oil viscosity) while the highest cumulative water cut was 71.64% Case-3A (100 cP, l_r = 0.305 m) due to lower initial oil production rate. Therefore, the cumulative water cut depends on the oil produced and cumulative water produced.

121

Table 4-16: Effect of oil viscosity and lateral length on cumulative water cut at 210 s

Cases	Well type	[50cP, *lr* (0.305 m)] (%)	[100cP, *lr* (0.305 m)] (%)	[50cP, *lr* (0.251 m)] (%)	[100cP, *lr* (0.251 m)] (%)
Case-1A	LR	46.75	66.47	46.10	65.85
Case-1B	LR	46.88	66.27	46.20	65.56
Case-1C	MR	51.36	70.88	50.87	70.34
Case-2A	LR	46.91	65.83	46.35	64.51
Case-2B	MR	50.18	70.45	49.85	69.04
Case-2C	SR	42.86	66.89	41.69	59.97
Case-3A	MR	46.58	71.64	45.73	65.35
Case-3B	SR	44.25	68.03	43.59	62.41
Case-3C	SR	44.37	67.97	43.54	62.27
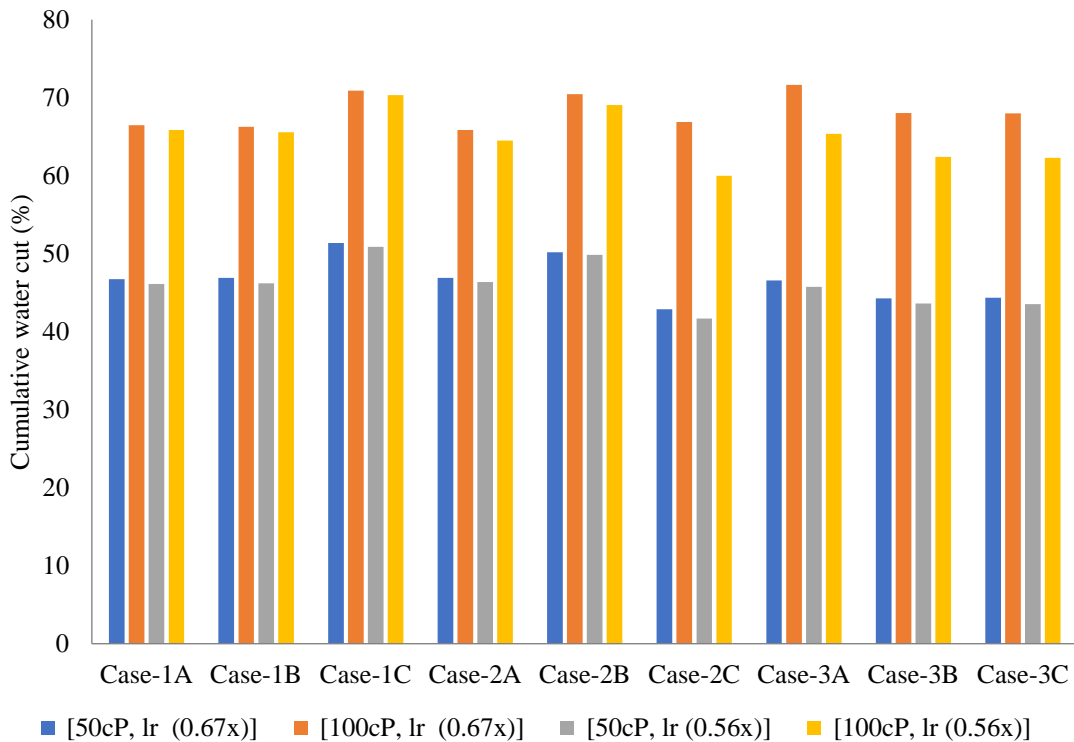
Figure 4-23: Effect of oil viscosity and lateral length on cumulative water cut at 210 s

4.3.4 Effect of lateral length on pressure drop at 210 s

Figures 4-24 and 4-25 illustrate pressure drop plot for thin-oil column reservoir with $l_r =$ 0.305 m and 0.251 m respectively represented in Tables 4-17 and 4-18. Lower pressure drop was observed in Figures 4-24 and 4-25 compared to Figures 4-13 and 4-14 respectively is due to shorter reservoir pressure depletion time caused by faster influx of gas into the wellbore through the perforations. The reason for the quick depletion in reservoir pressure is due the closeness of the GOC to the perforation, a characteristic of the thin-oil rim reservoir drilling mechanism, which results in production of high cumulative water cut and or Gas cut values at short oil production times.

Table 4-17: Pressure measurements at 210 s for 0.305 m length of lateral in thin-oil rim reservoir versus time (50 cP, oil viscosity) (E-1)

Time (s)	Case-1A (LR)	Case-1B (LR)	Case-1C (MR)	Case-2A (LR)	Case-2B (MR)	Case-2C (SR)	Case-3A (MR)	Case-3B (SR)	Case-3C (SR)
0	43.37	43.37	43.37	43.37	43.37	43.37	43.37	43.37	43.37
50	42.06	41.63	41.05	40.47	40.18	40.03	39.89	39.6	39.16
100	41.77	41.48	41.05	40.18	39.6	39.31	39.02	38.73	38.44
150	41.19	40.76	40.47	39.45	39.16	38.73	38.58	38.29	38
210	39.16	38.29	37.71	37.28	36.99	36.7	36.4	36.11	35.97
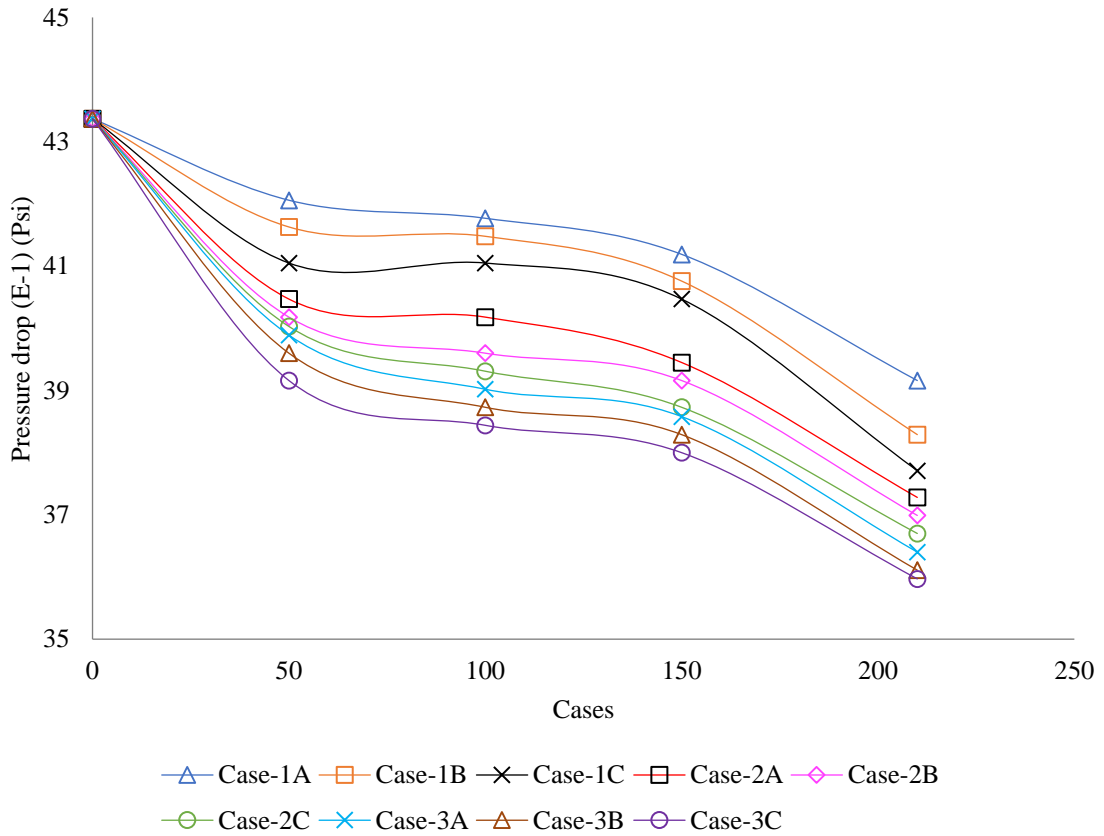
Figure 4-24: Pressure measurements at 210 s for 0.305 m length of lateral in thin-oil rim reservoir versus time (50 cP, oil viscosity) (E-1)

Table 4-18: Pressure measurements at 210 s for 0.251 m length of lateral in thin-oil rim reservoir versus time (50 cP, oil viscosity) (E-1)

Time (s)	Case-1A (LR)	Case-1B (LR)	Case-1C (MR)	Case-2A (LR)	Case-2B (MR)	Case-2C (SR)	Case-3A (MR)	Case-3B (SR)	Case-3C (SR)
0	43.37	43.37	43.37	43.37	43.37	43.37	43.37	43.37	43.37
50	41.36	41.05	40.61	40.03	39.74	39.74	39.6	39.31	39.16
100	41.36	40.9	40.47	39.74	39.31	39.02	38.87	38.58	38.44
150	40.32	39.89	39.6	38.87	38.58	38.15	37.86	37.71	37.42
210	38.87	38.58	38.44	36.14	35.87	35.2	35	34.82	34.63
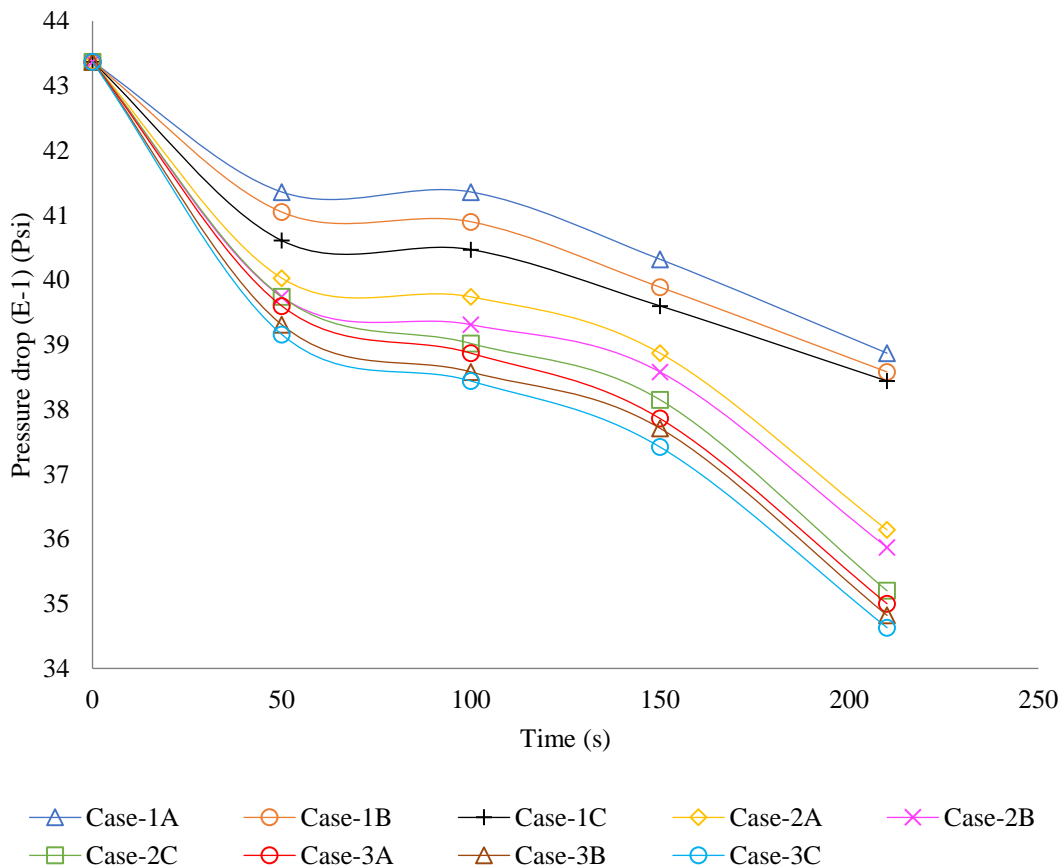
Figure 4-25: Pressure measurements at 210 s for 0.251 m length of lateral in thin-oil rim reservoir versus time (50 cP, oil viscosity) (E-1)

4.3.5 Proactive cresting control at 210 s

4.3.5.1 Effect on oil recovery and oil produced

Figure 4-26 shows a plot of results for thin-oil rim reservoir cases summarised in Table 4-19. Production in Case 7 was uncontrolled as illustrated in Table 3.8 (Chapter 3) and is seen to have the lowest oil recovered among all cases (26.80%). The low oil recovery compared to the thick-oil rim reservoir was due to the thin-oil column, thereby having lower effluents breakthrough times, where water production dominates production after breakthrough. Interestingly, for an increase in shut-in times from 960 to 2700 seconds for Cases 8 and 9, increments in oil recovery and oil produced from the base case (Case 7) were negligible (0.19% and 0.7% respectively). Unlike the results presented in Figure 4-17 (thick-oil rim reservoir), the negligible results and same oil produced and oil recovery observed between Cases 8 and 9 as shown in Figure 4.26, are possibly due to the closeness of the new WOC to the perforation zone regardless of its high-interconnected pore spaces. The closeness could mean less pore spaces available for oil displacement. The closer the WOC is to the

125

perforation, the faster the pressure drop will supersede the hydrostatic pressure at that contact (Schevchenko, 2013). The size of the reservoir, low total porosity (19.1%) and the significantly short water crest height (due to initial WOC and column thickness) are contributing factors for the low performance in this type of reservoir.

Table 4-19: Oil recovery and cumulative oil produced results at 210 s

Case	Well type	Original Oil In Place (cm^3)	Shut-ins (s)	Non-Dimensional number of shut-in times	Oil produced, (cm^3)	Incremental oil produced (%)	oil recovery, %	Incremental oil recovery (%)
Case 7	SR	3672.67	0	x	984.30		26.80	
Case 8	SR	3672.67	960	6.86x	991.14	0.7	26.99	0.19
Case 9	SR	3672.67	2700	19.29x	991.14	0.7	26.99	0.19
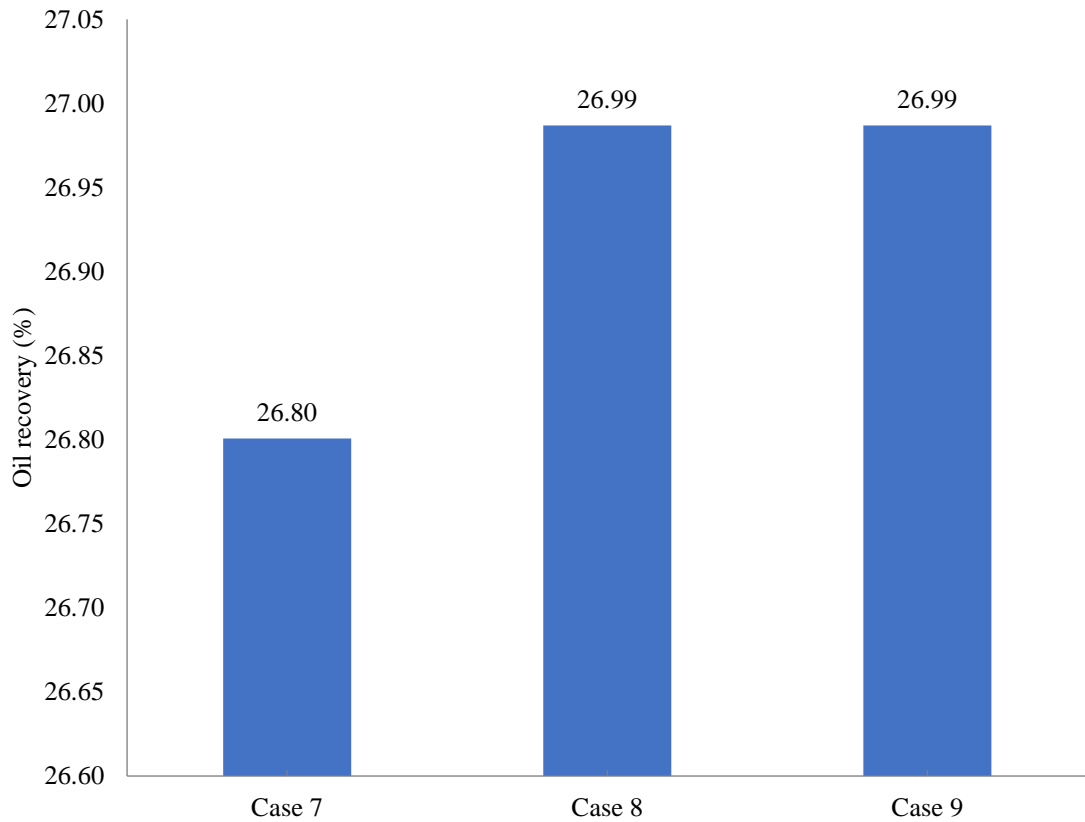
Figure 4-26: Oil recovery versus shut-in time at 210 s

4.3.5.2 Effect on cumulative water produced

A summary of the cumulative water produced at production time of 210 s for thin-oil rim reservoir cases is shown in Tables 4-20. It can be seen that Case 9, the uncontrolled production case (Case 7) had the highest produced water among all cases at 975.08 cm^3 of oil succeeded by Cases 8 and 9 at 965.30 cm^3 and 964.10 cm^3 respectively. Decrements in percentages of cumulative water produced (1.0% and 1.13%) were observed with increased shut-in times (0-2700 s) from Cases 7-9, possibly due to decreasing available pores for oil displacement by gravity and density. The low reduction in produced water between Cases 7 and 9 over increasing shut-in times was due to the closeness of the WOC to the perforation zone and hence a shorter water breakthrough time.

Table 4-20: Cumulative Water produced at 210 s

Cases	Well type	Cumulative water produced (cm^3)	Reduction in the cumulative water produced, %
Case 7	SR	975.08	
Case 8	SR	965.30	1.00
Case 9	SR	964.10	1.13
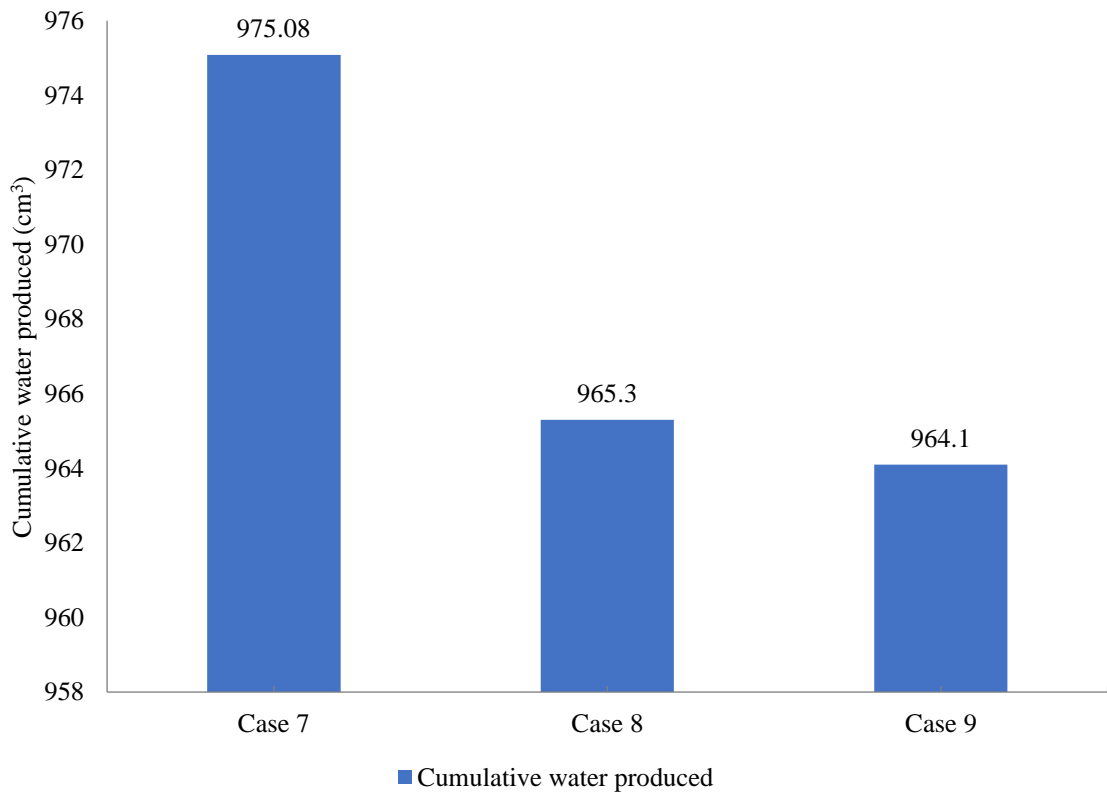
Figure 4-27: Cumulative water produced versus shut-in time at 210 s

4.3.5.3 Effect on cumulative liquid produced

Table 4-21 presents a summarised data for the cumulative liquid in volumes of produced at 210 seconds for thin-oil rim homogeneous reservoir. Figure 4-28 is a graphical representation of Table 4-21. A similar trend to that shown in Figure 4-19 is seen to occur in Figure 4-28. Therefore, with an increase in shut-in time, lower cumulative liquid was produced from Case 7 (1959.38 cm^3) to Case 9 (1955.24 cm^3). Lower percentages in

between shut-ins were realized. Case 7 and 8 had 0.15% reduction whereas Cases 8 and 9 was 0.01%.

Table 4-21: Cumulative liquid produced at 210 s

Cases	Well type	Cumulative oil produced (cm^3)	Cumulative water produced (cm^3)	Cumulative liquid produced (cm^3)	Reduction in the cumulative liquid produced, %
Case 7	SR	984.30	975.08	1959.38	
Case 8	SR	991.14	965.30	1956.44	0.15
Case 9	SR	991.14	964.10	1955.24	0.21
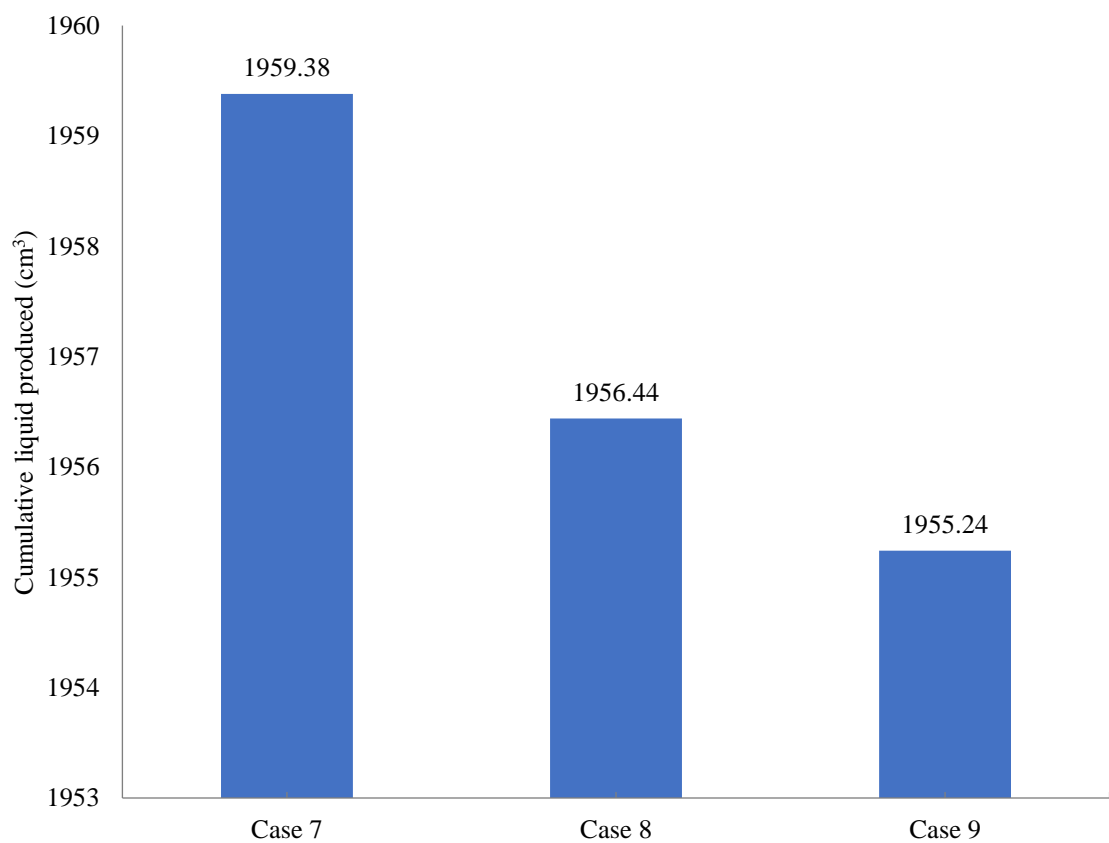
Figure 4-28: Cumulative liquid produced versus shut-in at 210 s

4.4 Summary

This Chapter studied how to optimise production in horizontal wells when drilling oil from an oil reservoir underlain by strong bottom aquifer and overlain by considerable gas cap. In this section, results were compared between the different horizontal well cases described in Chapter 3, Tables 3-1 and 3-2 as well as effect of change in oil viscosity, WOC and GOC on their performance. Results were also presented and discussed on proactive cresting control considering the reservoir wettability and the effluent breakthrough times.

Sections 4.2.1 to 4.2.8 and *Sections 4.2.9.1 to 4.2.9.3* discusses the effect of varying inclined sections of a horizontal well and proactive cresting control in thick-oil rim reservoirs respectively at different simulation times of 300 s and 495 s. In *Section 4.2.1*, the results of the effect of varying inclined section on liquid production rate at 300 s was discussed. From the results presented in *Section 4.2.1*, higher cumulative oil flowrates ($9.07cm^3$/s) and lowest cumulative water flow rate ($3.41 \ cm^3$/s) was realised at 300 s using a short radius category horizontal well (Case-2C described in Chapter 3, Tables 3-1 and 3-2). The presented results contradicted that presented by Freeborn et al, (1990) who stated that a long radius well produced at higher oil withdrawal rates.

Section 4.2.2 discussed the effect of pressure drop increase on the cumulative liquid production rate at 300 s. It was found that increase in pressure drop results in increase in oil withdrawal rate for all experimental cases investigated (Cases-1A, 2B and 3B described in Chapter 3, Tables 3-1 and 3-2) at the same oil production time of 300 s. However, this increase in oil withdrawal rates were accompanied with higher cumulative water production rates illustrated in Table 4-2, due to higher mass flow rate at higher pressure drop.

Section 4.2.3 discussed the effect of varying inclined sections on oil recovery at 300 s. It was found in Figure 4-9 that higher oil recovery (38.73%) and oil produced (2721.55 cm^3) at 300 s was realised in Case-2C ($V_d/H_r = 0.079$ as shown in Table 3-1 in Chapter 3), a short radius well category. Due to higher pressure drop along the length of a longer radius well, substantial differences in oil recovery (2.53%) and oil produced (177.75 cm^3) were observed when compared with Case-2A (worst case), a long radius well. More so, the steeper the inclined section of the well, the higher the mass flow rate.

The effect of oil viscosity and lateral length on cumulative oil recovered at production time of 495 s was discussed in *Section 4.2.4*. From the results presented, it was observed that the

oil produced for all horizontal well cases decreased more than 1.5 times with increase in oil viscosity from 50 cP to 100 cP. At l_r = 0.251 m, higher oil cumulative were produced compared to a base case (l_r = 0.305 m) for all horizontal well cases. This was due to a longer horizontal distance of the water inlet points 1 and 2 described in Chapter 3, Figure 3-1(b) from the perforation zone of the well at l_r = 0.251 m. It was observed that 3.33% increase in oil recovery and 250 cm^3 of oil produced were observed between the best case (Case-3C) and worst case (Case-2A).

The results presented in *Section 4.2.5* showed that for an increase in oil viscosity from 50 cP to 100 cP volume of cumulative produced water greater than one-half was observed as illustrated in Table 4-5 at a simulation time of 495 s. Due to the lower viscosity and higher density of water compared to oil illustrated in Chapter 3, *Sections 3.3.1a and 3.3.1b(i)*, higher volumes of water were produced after breakthrough into the well. As shown in Figure 4-11, the short radii wells category (Cases-2C, 3B and 3C described in Tables 3-1 and 3-2 in Chapter 3) resulted in higher cumulative water produced due to higher mass flow rate compared to the long (Cases-1A, 1B and 2A described in Tables 3-1 and 3-2 in Chapter 3) and medium radii (Cases-1C, 2B and 3A described in Tables 3-1 and 3-2 in Chapter 3) categories at any point in production time. In Table 4-5, Case-1A (best case) had lowest cumulative produced water at 1503 cm^3 at 50 cP and l_r = 0.305 m with volumetric increment of 356 cm^3 observed in Case-3C (worst case).

In *Section 4.2.6*, the presented results showed that with increase in oil viscosity and shorter lateral length in reservoir (l_r = 0.251 m), increase in water cut was observed as shown in Figure 4-12. Figures 4-13 and 4-14 in *Section 4.2.7* showed that pressure drop in a horizontal well depends on the measured depth of the horizontal well at simulation time of 495 s. In *Section 4.2.8*, it was observed that with increase in oil production time from 300 s to 495 s, increment in oil recovery was observed for all horizontal well cases as illustrated in Figure 4-15. Higher increments in oil recovered were observed in the shorter radii wells, with Case-3C having increments as high as 10.55% while the least increment in oil produced was observed for Case-1A (1.63%) long radius well. This is because, the shorter the arc radius of a well, the higher the mass flow rate. Case-3C is believed to have performed better at 495 s compared to Case-2C at 300 s due to overall shorter measured depth. Hence higher overall liquid produced at longer simulation time.

Sections 4.2.9.1 to 4.2.9.3 discusses proactive cresting control in thick-oil rim reservoir at 495 s using Case-3C ((V_d/H_r = 0.063 as shown in Table 3-1 in Chapter 3), which performed best in terms of oil produced and oil recovery [3701 cm^3 oil produced (Table 4-4), 41.98% oil recovery (Figure 4-15)] as illustrated in Figure 4-12 and cumulative water produced of 1859 cm^3 (Table 4-5) at base cases; lateral length in reservoir (l_r = 0.305 m) and 50 cP oil viscosity. In *Section 4.2.9.1*, Figure 4-17 shows that at higher shut-in times, higher oil recovery and oil produced were observed due to capillarity (wettability) and gravity effects. Increments in oil recovery (1.55%) and oil produced (3.56%) were observed between the best case (Case 6) and base case (Case 1). *Section 4.9.2* showed that the cresting control resulted in lower cumulative water produced. Due to wettability effect, 9.90% reduction in cumulative water produced was realised between the best case (Case 6, at 9000 shut-in time) and worst case (Case 1, at no shut-in time). Due to interruptions in production and reservoir wettability effects, the cumulative liquid produced reduced generally with increase in shut-in times, discussed in *Section 4.2.9.3* and illustrated in Figure 4-19.

Sections 4.3.1 and 4.3.1 to 4.3.5.3 discusses the effect of varying inclined sections of a horizontal well and proactive cresting control in thin-oil rim reservoirs respectively at a simulation time of 210 s. in *Section 4.3.1*, the effect of oil viscosity and lateral length in the reservoir on cumulative oil recovered is similar to that observed in thick-oil rim reservoirs in *Section 4.2.4*). Hence, at a simulation time of 210 s, reduction in oil produced was observed for higher oil viscosity (100 cP). The shorter the well length, the higher the oil withdrawal rate. For this reason, the shorter radii well category performed best. Due to lower oil mobility, higher cumulative water was produced at oil higher oil viscosity in *Section 4.3.2*. Similar results in *Section 4.2.5* were observed. Hence, higher cumulative water produced in terms of lateral lengths in the reservoir, was experienced in the short radii wells category.

Section 4.3.3 shows that water cut depends on the volumes of cumulative water and oil produced. *Section 4.3.4* showed similar trend as described in *Section 4.2.7*. hence, the pressure drop was higher in longer radii wells with time compared to the short and medium radii well categories. The results in *Section 4.3.5.1* demonstrated the ineffectiveness of the proactive cresting control technique in thin-oil rim reservoirs. Limited increase in oil recovery (0.19%) and cumulative oil produced (6.84 cm^3) was observed between the best case (Case-9, at 2700 s shut-in time) and the base case (Case-7 at no shut-in time) as shown

in Table 4-13, due to a shorter oil column thickness. More so, *Section 4.3.5.2* shows that only 1.13% reduction in cumulative water produced was realised, due to the short oil column height and possibly little volumes of available pores spaces for oil displacement by capillarity. Due to the ineffectiveness of the proactive control technique in thin-oil rim reservoirs, Table 4-21 showed that decrement in cumulative liquid produced were as low as 0.21%.

Table 4-22 and 4-23 show summaries of the effect of the variable used in this investigation on oil recovery, cumulative water produced, oil produced and the improvements from his research for thick-oil rim reservoirs and thin-oil rim reservoir respectively.

In this research, improvements in oil recovery, oil produced with reductions in produced water were instigated. Varying the inclined section of the horizontal well in thick-oil rim reservoirs resulted in 6.53% increase in oil recovery and 11.40% reduction in cumulative water produced at 300 s. Higher oil recovery increment of 7.93% and 19.15% reduction in cumulative water produced at 495 s. Increment of 16.29% in oil recovery and 15.14% reduction in produced water was observed in thin-oil rim reservoirs at 210 s simulation time. Improvements in the proactive cresting control technique was limited in oil recovery for both thin- and thick oil-rim reservoirs at 0.19% and 0.7% respectively. However, reductions in cumulative produced water were observed at 9.90% and 1.13% in thick- and thin oil rim reservoirs respectively.

Table 4-22: Summary of EFFECTS of variable used in water and gas cresting investigations in thick-oil rim reservoirs

Variables	Oil produced	Oil recovery	Cumulative water produced
Viscosity (*Section 4.2.4 to 4.2.6*)	Increase in oil viscosity causes a reduction in oil produced up to 1.5 times, half the initial oil viscosity.	Increase in oil viscosity results in decrease in oil recovery up to 1.5 times, half the initial oil viscosity.	Increase in viscosity resulted in increase in cumulative water produced up to 1.5 times, half the initial oil viscosity due to lower oil mobility
Length of lateral section in reservoir (*Section 4.2.4 to 4.2.6*)	Increase in mass flow rate increases with a shorter lateral length in the reservoir. Hence, higher volumes of oil up to 20.29% were produced.	This results in higher oil recovery up to 20.29% because of increase in volumes of oil produced.	Reduction in cumulative produced water was observed at shorter lateral length in reservoir due to the distance between the bottom water inlet point 2 and the perforation of the well by up to 44.36%.
Inclined section of horizontal well (*Section 4.2.1 to 4.2.7*)	Varying the inclined section of the horizontal well increase oil production up to 8.48%.	This resulted in increase in oil recovery up to 8.48%.	Volumetric reduction up to 19.15% in cumulative produced water were observed.
Oil production time (*Section 4.2.8*)	Oil produced increased with increase in simulation time up to 10.55%.	Oil recovery increased with simulation time up to 10.55%.	Although water produced comparison for 300 s and 495 s was not discussed in this study, the increase in water cut (as high as 26.00%) from 300 s to 495 s denotes an increase in cumulative water produced, from Equation 4.1.
Proactive cresting control (*Section 4.2.9.1 to 4.2.9.3*)	Reasonable volumetric increase in oil produced up to 3.56%.	Limited increment in oil recovery up to 1.55%.	Significant reduction in produced water up to 9.90%.

Table 4-23: Summary of EFFECTS of variable used in water and gas cresting investigations in thin-oil rim reservoirs

Variables	Oil produced	Oil recovery	Cumulative water produced
Viscosity (*Section 4.3.1 to 4.3.2*)	Increase in oil viscosity causes a reduction in oil produced up to 1.5 times, half the initial oil viscosity.	Increase in oil viscosity results in decrease in oil recovery up to 1.5 times, half the initial oil viscosity.	Increase in viscosity resulted in increase in cumulative water produced up to 1.5 times, half the initial oil viscosity due to lower oil mobility.
Length of lateral section in reservoir (*Section 4.3.1 and 4.3.2*)	Increase in mass flow rate increases with a shorter lateral length in the reservoir. Hence, higher volumes of oil were produced up to 3.29%.	This results in higher oil recovery because of increase in volumes of oil produced up to 3.29%.	Reduction in cumulative produced water was observed at shorter lateral length in reservoir due to the distance between the bottom water inlet point 2 and the perforation of the well up to 15.25%
Inclined section of horizontal well (*Section 4.3.1 and 4.3.2*)	Varying the inclined section of the horizontal well increase oil production up to 16.28%.	This resulted in increase in oil recovery up to 16.28%.	Volumetric reduction up to 15.14% in cumulative produced water were observed
Proactive cresting control technique (*Section 4.3.4.1 to 4.3.4.3*)	Limited volumetric increase in oil produced up to 0.7%.	Limited increment in oil recovery of up to 0.19%.	Limited reduction in produced water up to 1.13%.

Numerical considerations using CFD and PIV will be discussed in the next Chapter. In CFD modeling, boundary conditions described in Chapter 3, *Section 3.3.1*, reservoir properties described in *Section 3.4.1a* and horizontal well (Case-3C) detailed in Table 3-1 and 3-2 will be implemented. Sensitivity analysis will be performed to ascertain its (CFD) use and validating with an experimental model will be demonstrated.

PIV will be used to determine the velocity of the water cresting at different at different time steps at an initial outlet pressure of -4.351 Psig, using captured water cresting images.

CHAPTER-5

NUMERICAL SIMULATION

5.1 Introduction

5.1.1 Computational Fluid Dynamics (CFD)

CFD is a technique used to simulate phenomena involving heat transfer, chemical reaction, mass transfer, and fluid flow. This is possible by solving mathematical Equations that govern a given phenomenon using numerical algorithms on a computer with appropriate boundary condition. Fluid flow or dynamics can be predicted using CFD when used correctly. CFD provides good and accurate results for visualisation of flow fields. Care must be taken to ensure the CFD is used correctly because improper use can result in quantitative errors, which result from improper specification of boundary conditions and meshes.

In demonstrating validation of experimental results, it is pertinent to apply appropriate boundary conditions and use of specific mathematical models to accurately capture the multiphase flow behaviour in water and gas cresting occurring simultaneously using appropriate experimental data, such as the boundary condition. In order to model water and gas cresting, it is important to understand the technical aspects of the problem and as such apply appropriate information like using the multiphase volume of fluid (VOF) model that can accurately capture interfaces that exist at the Water-Oil and Gas-oil contacts.

5.1.2 Particle Image Velocimetry

Particle Image Velocimetry (PIV) is a method that has been applied in diverse fields for visualisation of flow in fluids. The use of this techniques has been on the high over the past decade due to its non-intrusive investigation of flow fields (Melling, 1997). Velocity measurements in instantaneous 2D and 3D are obtained using the PIV (Jakobsen et al., 1996) where the seeding particles in motion are used to calculate the velocity fields. This method was adopted in this research to study the velocity of the bottom water during water cresting. This was possible by extracting image frames from a video taken for Case-3C at oil viscosity of 50 cP and simulation time of 300 s.

5.2 Overview of Mathematical model of fluid flow and cresting

Navier-stokes Equation describes the behaviour of viscous fluid substances such as air, water or oil. The movement of water, oil and gas during cresting was numerically modeled by applying the physics of flow to Newton's second law. The Navier-stokes Equations for transient state, viscous flow take the form:

Continuity Equation

$$\frac{\partial \rho}{\partial t} + \frac{\partial}{\partial x_i} (\rho u_i) = 0 \tag{5.1}$$

Momentum Equation

$$\frac{\partial}{\partial t} (\rho u_i) + \frac{\partial}{\partial x_j} (\rho u_i u_j) = -\frac{\partial P}{\partial x_i} + \frac{\partial}{\partial x_j} \left[\mu \left(\frac{\partial u_i}{\partial x_j} + \frac{\partial u_j}{\partial x_i} - \frac{2}{3} \partial_{ij} \frac{\partial u_i}{\partial x_i} \right) \right] \tag{5.2}$$

Energy Equation

$$\frac{\partial E}{\partial t} + u_j \frac{\partial E}{\partial x_J} = \frac{q^*}{\rho} + \frac{1}{\rho} \frac{\partial}{\partial x_j} \left(k \frac{\partial T}{\partial x_j} \right) \tag{5.3}$$

Where,

u_i = Averaged velocity components in m/s

ρ = Fluid density in kg/m^3

P = Pressure in N/m^2

μ = Dynamic viscosity in cP

∂_{iJ} = Kronecker delta function (equal to one if $i = j$, else zero)

$\partial/\partial x_i$ = Variation of parameters in X, Y and Z coordinates in m

T = Temperature in ºC

q^* = Heat flux in J/s

t = Time in s

K = Thermal conductivity in W/cm°C

C_p = Specific heat in Nm

Energy $(E) = C_pT$

In the oil and gas industry, multiphase flow simply refers to two or more phases flowing simultaneously, such as water, oil and gas. These materials could have different states, phases (gas, water or oil) or have different chemical properties but in the same state or phase (liquid-liquid system such as water droplets in oil). Therefore, the multiphase VOF method can depict the volume of each phase in a stratified or dispersed mixture with each phase having distinct volume fraction and velocity fields. In the present study, FLUENT-17 was used as the solver for the computational modeling of water and gas cresting. The multiphase VOF was used in this study because it provides a clear and sharp interface between three phases (oil, water and gas) in a stratified arrangement in order of gravity and density differences (sharp interface at the WOC and GOC), through a computational grid.

5.3 Procedure and simulation

The first step for the pre-processor stage was to create a 2D CAD replica of the physical model for the fluid flow domain. The 2D CAD model was similar to the reservoir used earlier in Chapter 3 (shown in Figures 3-1, 3-2, 3-4 and 3-9) and Chapter 4 (Figure 4-1). This geometry was modeled in the Rhinoceros modeling package. The geometry was saved with the extension "STEP" (STandard for the Exchange of Product) model data. The STEP file was then imported into FLUENT that served as both the pre-processor and post-processor.

Meshing of the 2D geometrical model was performed using the ANSYS mesher. In this study, the finite difference method was applied to the imported CAD model. A total of 52162 elements were generated after meshing, with sectional illustration in Figure 5-1. The mesh was checked for quality such as a maximum skewness of 0.5.
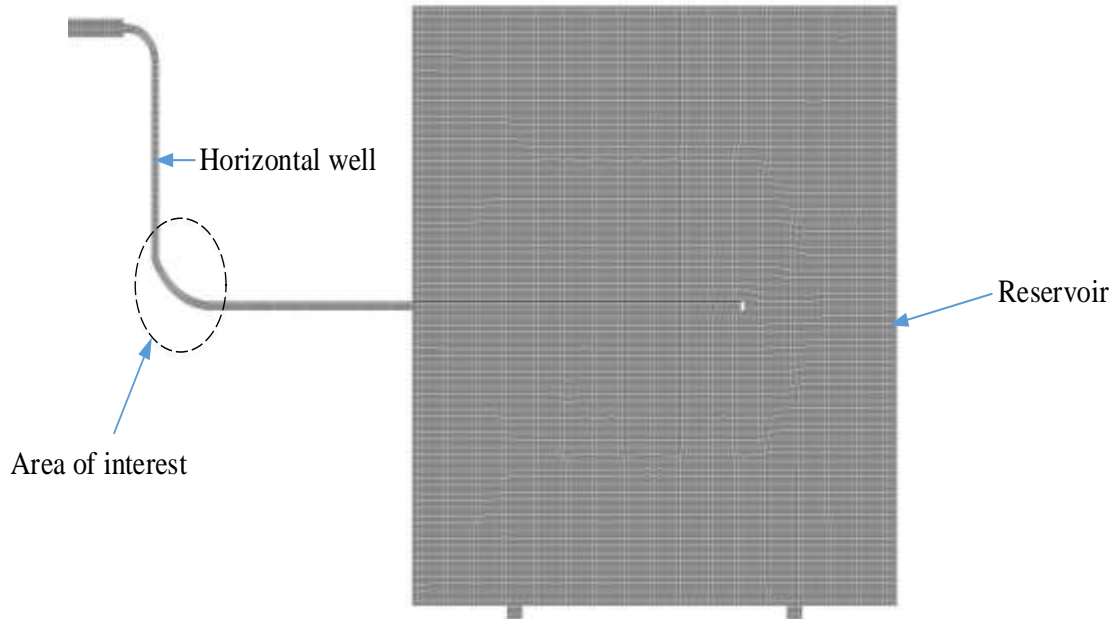
Figure 5-1: Section of mesh used for simulation

Boundary conditions are key aspects to defining realistic boundary conditions in CFD simulations. As shown in Figure 5-2, the water inlet points were defined as water inlet points 1 and 2 while the open top for gas cresting modeling and the reservoir fluids outlets were defined as free surface and pressure outlet respectively. It is important to note that flow of reservoir fluids from the reservoir to the pressure outlet was through the four perforations (two holes per cross section) of the horizontal well, with its horizontal section positioned at 0.225 m (the same position in the experimental apparatus described in Chapter 3, *Section 3.4.2a)* on the y-axis of the reservoir.

The perforation were also positioned on the y-axis and perpendicular to the horizontal section of the well. The dimension of the horizontal well used was Case-3C described in Tables 3-6 and 3-7. Case-3C was the preferred case, having performed best in terms of oil produced at 495 s discussed in Chapter 4, *Section 4.2.1.* boundary conditions from experimental model were used in for higher accuracy validation regardless of the limitation of 2D models. The boundary conditions from the experimental model described in Chapter 3, *Section 3.3.1* and summarised in Tables 5-1 were used while the properties of the oil, water and gas similar to the experimental reservoir model fluid properties in Chapter 3, *Sections 3.3.1a and 3.3.1b*, also summarised in Table 5-2 were defined for numerical computation. The total porosity from the experimental model (19.1%) was used to define the porous media input (viscous resistance, Inertial loss coefficients) for the packed

141

reservoir bed using Ergun's Equation (Equation 5.4 to 5.6) (ANSYS, 2016) with values summarised in Table 5-3. In Table 5-3, Cases 1N and 2N represents total void fractions 1E-3 and 1E-4 respectively, used in Ergun's Equation to derive the viscous resistances and inertia loss coefficients. In Equations 5.4 and 5.6, the mean particle diameter, D_p was assumed to be approximately 0.003m.

Table 5-1: Application of boundary conditions

Boundary conditions	Values from physical model
Free surface	Atmospheric pressure
Water inlet 1	0.015 Kg/s
Water inlet 2	0.015 Kg/s
Pressure outlet	-4.351 Psig

Table 5-2: Properties of reservoir fluids

Fluid type	Density (kg/m^3)	Viscosity (cP)
Water	998	1.00
Oil (Silicone oil)	972	50
Gas (Air) at 14.7 Psi	1.225	1.7894E-2

$$\alpha = \frac{D_p^2}{150} \frac{\varepsilon^3}{(1-\varepsilon)^2} \tag{5.4}$$

$$R_v = 1/\alpha \tag{5.5}$$

$$C_2 = \frac{3.5}{D_p} \tag{5.6}$$

Where,

α = Effective Permeability in D

ε = Total void in fraction

R_v = Viscous resistance in m^{-1}

C_2 = Inertia loss coefficient in m^{-1}

Table 5-3: Porous media inputs

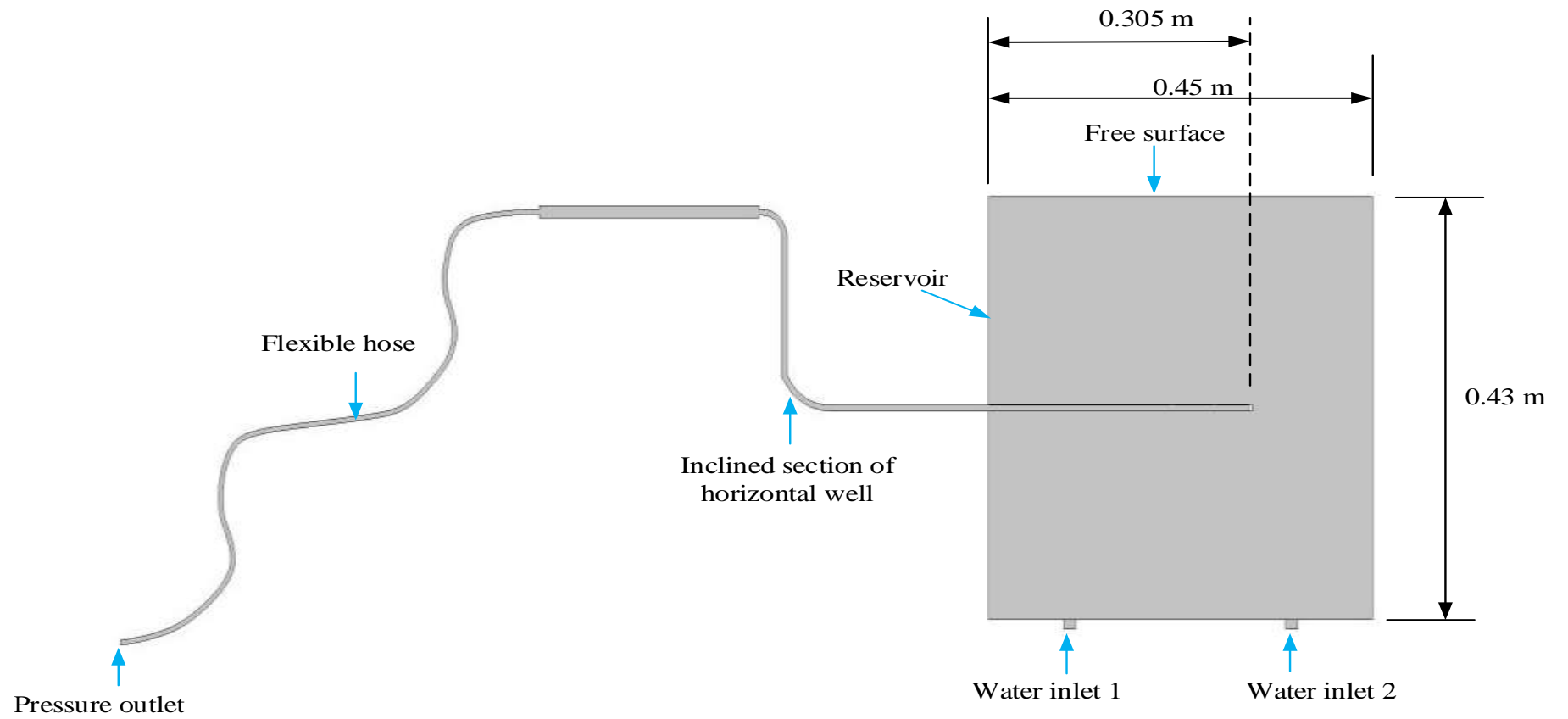| Parameters	Case 1N	Case 2N
Viscous resistance (m^{-1})	1.66E+16	1.67E+19
Inertial loss coefficient (m^{-1})	1.17E+12	1.17E+15

Figure 5-2: 2D CAD model from apparatus design for FLUENT simulation

The pressure base solver was used which is only supported explicitly. This approach was preferred over the density-based approach because it can be used to model mildly compressive, in-compressive and turbulent flows (Djavareshkian and Reza-zadeh, 2006). In this study, the VOF Eulerian multiphase model was used due to its ability to accurately capture the interfaces between 2 or more phases. Hence, was used to capture the WOC and GOC during cresting. The realizable k-ε model was used as the viscous model because it has more superior ability to capture mean flows in complex structures (Osama and Huckaby, 2010) compared to standard k-ε model nor the RNG k-ε model. The simulation was transient with acceleration due to gravity in the y-direction (-9.81 m/s), where the negative sign signifies gravitational pull effect.

In order to mimic the experimental model at static condition, the CAD model was patched into regions to represent the phases, as illustrated in Figure 5-3. In Figure 5-3, the red, blue, and green regions represent the zones patched with oil, gas, and water respectively. This was undertaken using the coordinate of the 2D CAD geometry in the x and y directions in Rhinoceros as illustrated in Table 5-4. The simulation was calculated using 200 maximum iterations per time step with a time step size of 1E-4 s and a Courant number of 0.25.
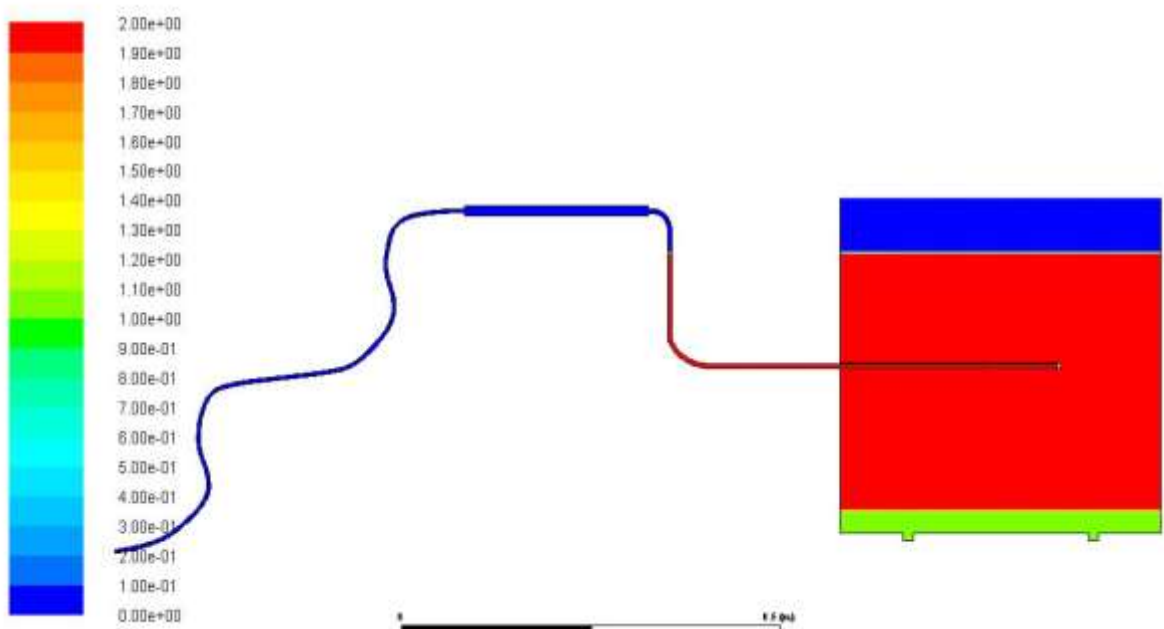
Figure 5-3: Numerical model showing the patched phases at static condition

145

Table 5-4: Patching data in the X and Y axes

Phase 2-water (m)			Phase 3-oil (m)	
X= 0 to 0.45	X= 0 to 1	X= 0 to 0.45	X= -0.25 to 0.45	X= -0.25 to 0.45
Y = 0 to 0.03	Y = 0 to 0.37	Y = 0 to 0.03	Y = 0.03 to 0.34	Y = 0.03 to 0.37

5.3.2 Assumptions

The main assumptions for the CFD model are:

- Total porosity was assumed to be effective porosity, same in each phase zone at static condition for each simulation case.

- No mass transfer between the phases for higher accuracy in tracking the WOC and GOC interfaces as well as the oil mass flow rate during cresting.

- The region from the height of oil in the horizontal well at static condition to the pressure outlet was assumed to be filled with air.

- The effect of effective porosity was altered due to the 2D model limitation.

The flow chart shown in Figure 5-4, summarises the algorithm used in simulating water and gas cresting with limitations that encompasses the pre-processor, solver and the post-processor.

Figure 5-4: FLUENT simulation stages (FLUENT, 2006)

5.4 Particle Image Velocimetry (PIV)

5.4.1 Image extraction, frames generation and processing

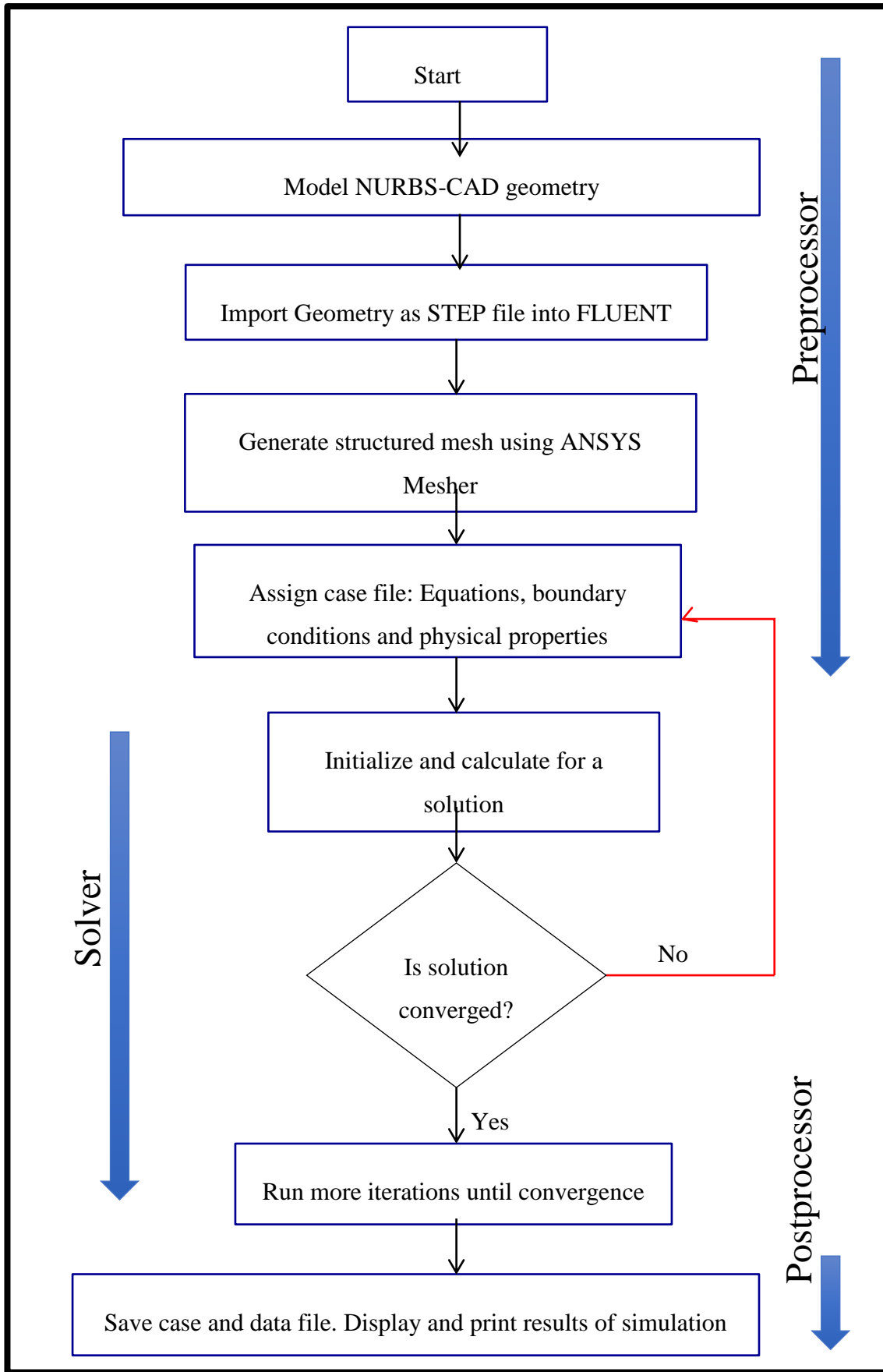In engineering and science, an image can be described as a depiction of subject while image analysis and processing is a combination of the extraction of meaningful data from mainly digital images (Solomon and Breckon, 2010) processing of a series of images or video digitally (Tinku and Ajoy, 2006). The cresting behaviour was captured in video using the 12.1 Mega-Pixels Nikon COOLPIX S9100.

The extraction of images from video was possible using the VLC media player while its processing performed with Dantec's DynamicStudio software. The images were extracted in frames from the cresting video taken. The steps involved in image extraction and frame generation are as follows:

1. The video of interest was transferred to a desktop Personal Computer (PC) with VLC installed.

2. The video was renamed for easy identification and distinction.

3. The VLC media player was opened.

4. The video of interest was opened for double-checking and then paused for further setting applications.

5. Click on "Tools" to access Preferences.

6. In the show settings option, select "All" to access the advanced settings.

7. Expand the Video option and click on "Croppadd".

8. Under the Crop option, pixels to crop from top, bottom, left and rights were inputted.

9. Then click on "Filter" check on video scaling filter and then saved

10. Click on Media then convert/save option.

11. The video to be cropped is then added in the "open media window". In the convert/save drop down, select convert.

12. Click on edit selected profile to access the "video cropping filter" through the video codec and then click on save.

13. Then browse for the directory to save the intended cropped file while renaming the file.

14. After saving the file name, click on start to commence video cropping. The cropped video is the double-checked to see if the video cropping has taken effect. Snapshot (unprocessed image) from video before and after cropping is shown in Figure 5-5.

15. The images were then extracted by taking snapshots (frames) at similar intervals of time and saved in a folder with ".jpg" extension. At total of 9 frames were extracted over 110 seconds. Each folder was then saved in a Universal Serial Bus (USB) stick for future use.
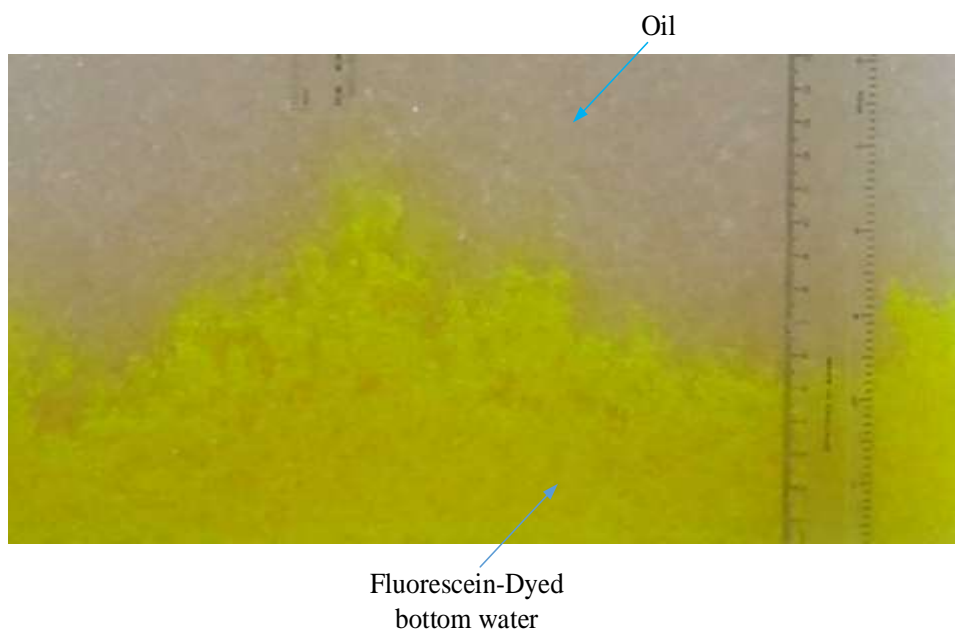

Figure 5-5: Snapshot of unprocessed image

5.4.2 Procedure for PIV analysis

The procedure for PIV analysis is detailed below:

1. The first step was to turn-on the computer that has the PIV software (DynamicStudio) installed.

2. Click on the DynamicStudio 2015a shortcut icon on the desktop and a default database view window will be seen with no active database.

3. A "new database" was created from the file menu. The name and location of the file was specified for the new database.

4. The extracted images were then imported from the file menu ensuring the database of interest is highlighted. The image import wizard facilitated this. The images were first added as single frames. The FlowSenseEO_16M with and edited trigger rate of 100Hz. Then click on finish to finalize the importation.

5. Calibration was performed using one of the images for the software to detect changes in fluid movement with time. To do this, the imported images were duplicated in a closed content list by right clicking on the imported file and choosing the "duplicate" option. The show content list of the duplicated image was enabled and images were deleted, leaving only one for calibration purpose. The duplicated image was then moved to the "new calibration" ensemble. A measure scale factor from point A to B was performed on the calibration image with O as the origin. An absolute distance (actual experimental height of cropped image) of 145 mm was imputed. A calibration method was performed on the calibrated image using the "Multi Camera Calibration".

6. After calibration, the adaptive correlation was used to analyse the flow movement of colored bottom water during cresting under PIV signal. A 16 x 16 pixel was selected for the horizontal and vertical interrogation areas in all cases. The scalar derivatives for each vector were visualized at different time steps by right clicking on the imported images ensemble. The database structure is illustrated in Figure 5-6.
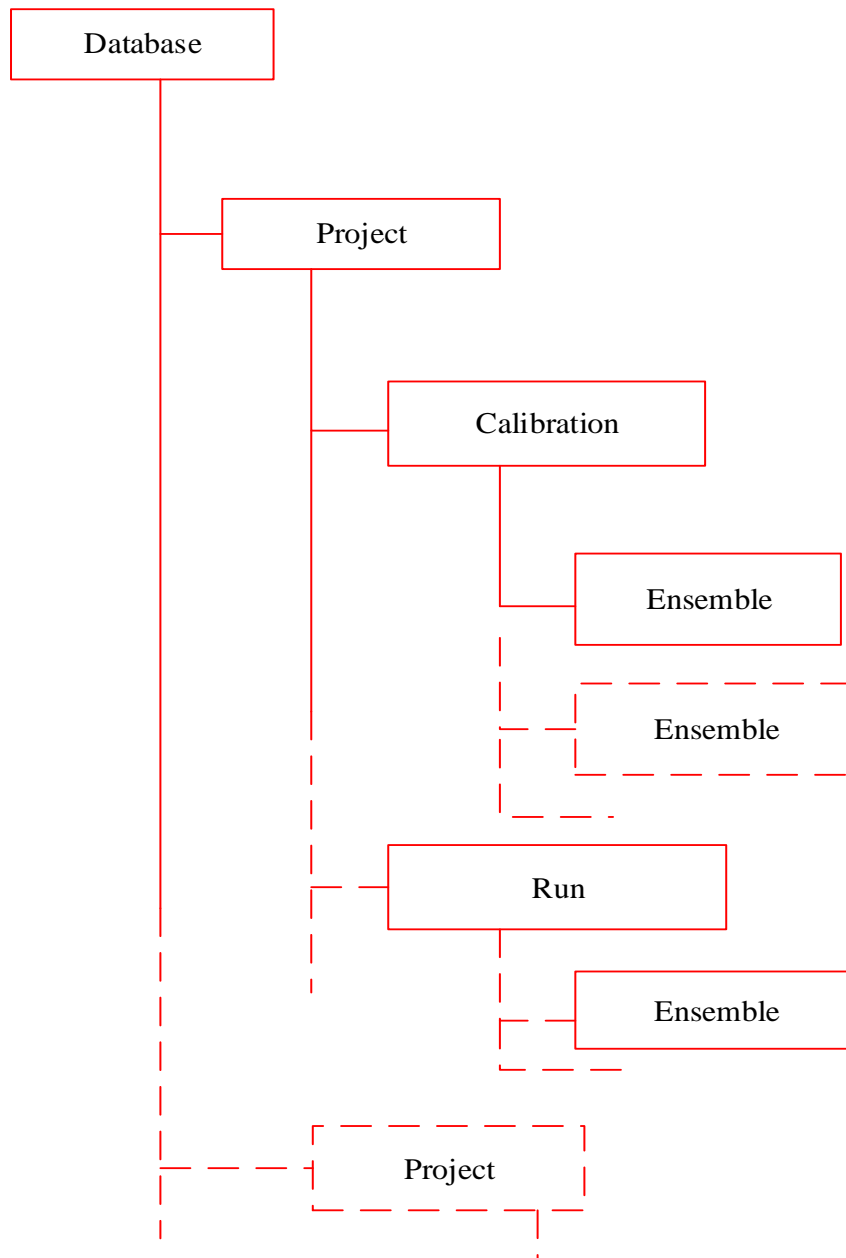
Figure 5-6: Database structure (DantecDynamics, 2015)

7. After analysis, the region of no interest was hidden as illustrated in Figure 5-7, to estimate higher accuracy of the velocity vector during water cresting.
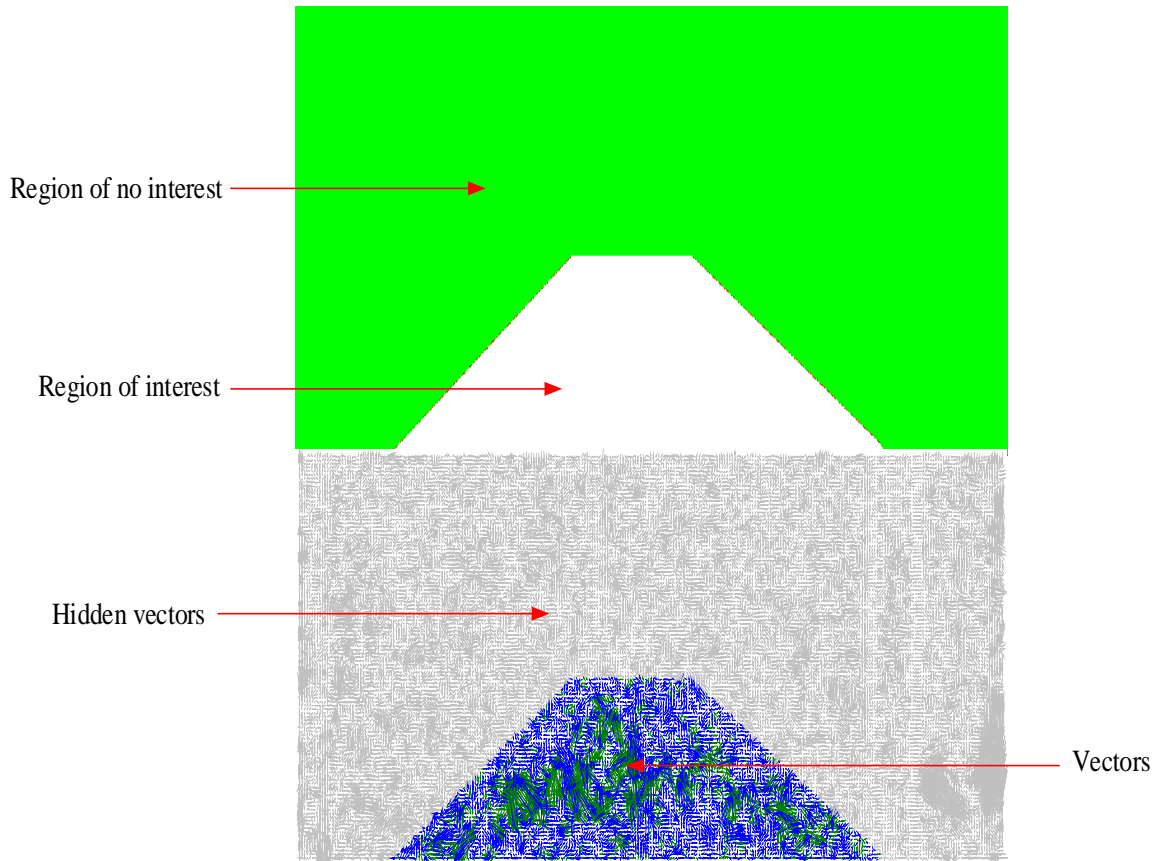
Figure 5-7: Regions of no interest/interest and vectors

8. The numerical result was extracted as ".csv" extension file to be plotted in Microsoft Excel. The results are described in *Section 5.5.2*.

5.5 Results and Discussion

In this section, numerical CFD results are presented to ascertain its cresting applicability and used to validate an experimental model. The velocity of water cresting from captured images was also investigated and discussed. The numerical simulation results for both CFD and PIV are categorized into two major categories shown below:

1) *CFD modeling (Section 5.5.1).*

    i.   CFD model at static and dynamic condition (*Section 5.5.1.1*).

    ii.   Effect of effective porosity on oil production rate (*Section 5.5.1.2*).

    iii.   Effect of production time on WOC and GOC (*Section 5.5.1.3*).

2) *PIV (Section 5.5.2).*

i.   Effect of oil withdrawal time using PIV *(Section 5.5.2.1).*

3) *Comparison of selected case with experimental data (Section 5.5.3).*

i.   CFD and experimental comparison of change in WOC and GOC versus production time *(Section 5.5.3.1).*

ii. CFD and experimental comparison of oil production rate with time *(Section 5.5.3.2).*

5.5.1   CFD modeling

5.5.1.1 CFD model at static and dynamic conditions

Figure 5-8 represents the numerical model (reservoir) at static condition (phases separated in order of their density difference and gravity), while Figure 5-9 represents the numerical model at time (t) > 0 s. The colored regions depict the three reservoir phases: top blue represents the gas cap zone (0.07 m thick), red is the oil zone (0.34 m thick), and bottom blue is the water zone (0.03 m thick). In Figure 5-9, the WOC and GOC are both distorted and crest-like in shape with both apices "highest or lowest geometrical point" of the GOC and WOC interfaces moving towards the perforation zones, which portrays already known cresting knowledge reported by Permadi and Jayadi (2010), Schlumberger (2016).

Figure 5-9 shows the velocity streamlines from the CFD simulation for gas cresting (located at the top half of the reservoir) and water cresting (located at the lower half of the reservoir) occurring simultaneously. The streamlines in Figure 5-10 can be seen to be crest-like movement towards the perforation of the horizontal well.
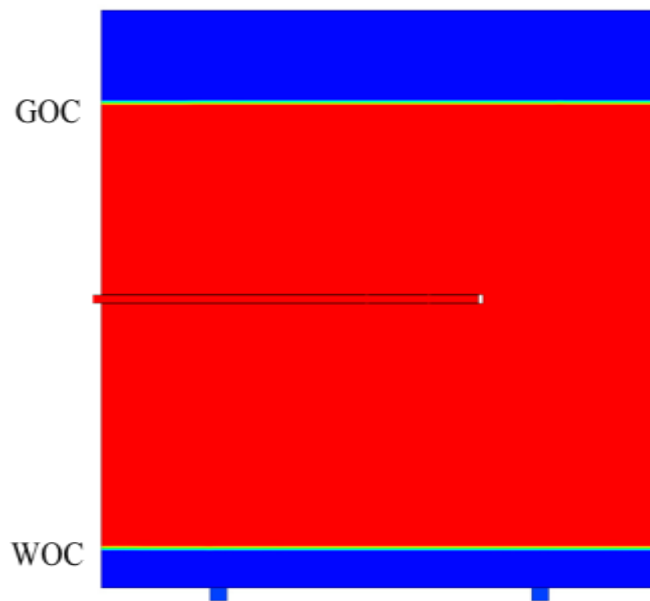
Figure 5-8: Numerical model at static condition
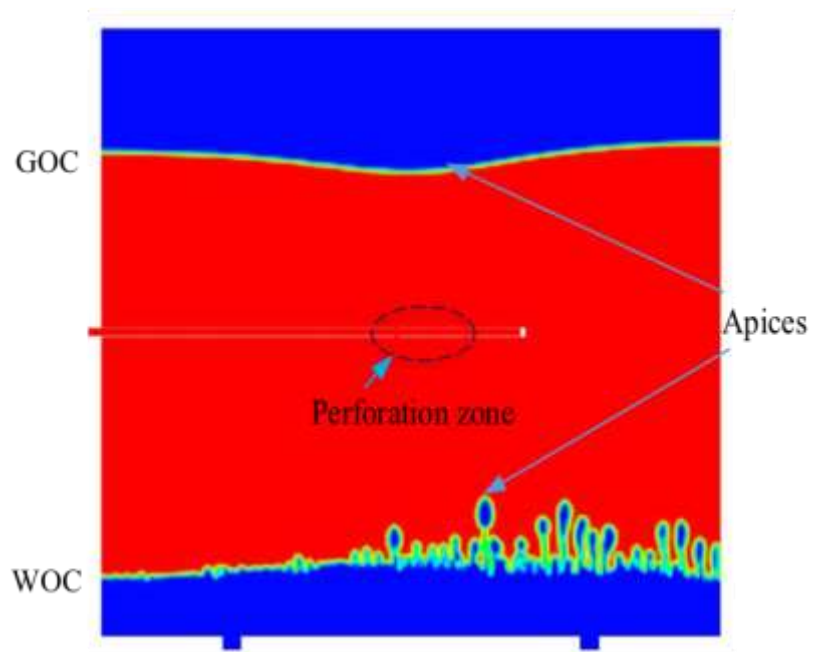
Figure 5-9: Numerical model at t > 0 s
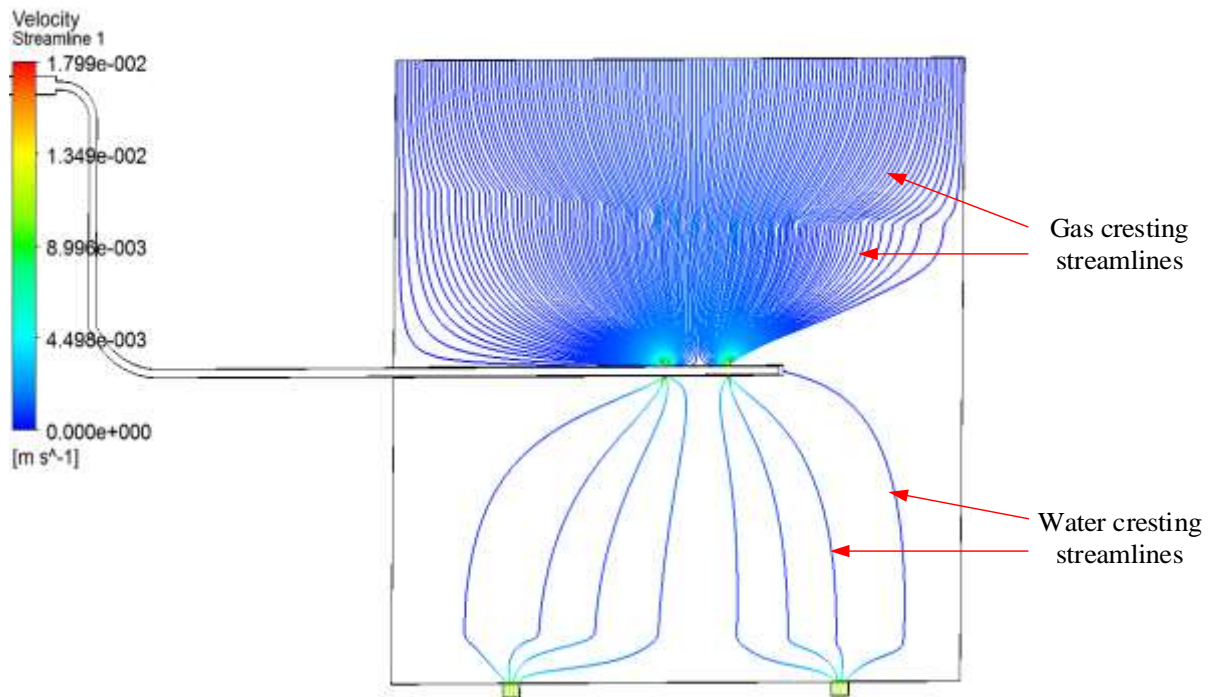
Figure 5-10: Numerical streamlines for water cresting (bottom) and gas cresting (top) occurring simultaneously at effective porosity of 1E-2

5.5.1.2 Effect of effective porosity on oil production rate

Table 5-5 represents the summary of the effect of effective porosity on oil production rate for Cases 1N and 2N at different production time steps, obtained at the outlet boundary. The oil production rate was determined using the function calculator to estimate the oil mass flow rate at the outlet boundary.

Figure 5-11 illustrates a plot of the data shown in Table 5-5. As shown in Figure 5-11, the oil production rate is seen to generally increase gradually with an increase in production time in Cases 1N and 2N. As expected, Figure 5-11 demonstrates that the effective porosity influences oil production rate such that at a lower viscous resistance (a function of void fraction in Ergun's Equation), the oil production rate will be higher. Hence, a reduction in oil production rates of 0.07 and 0.095 Kg/s were observed at 2.5 and 3.5 s respectively when Case 1N is compared to Case 2N.

Table 5-5: Oil production rate for Cases 1N and 2N at different time steps

Time (s)	Well type	0	2.5	3.5
Case 1N (Kg/s)	SR	0	0.274713	0.322148
Case 2N (Kg/s)	SR	0	0.201085	0.227221
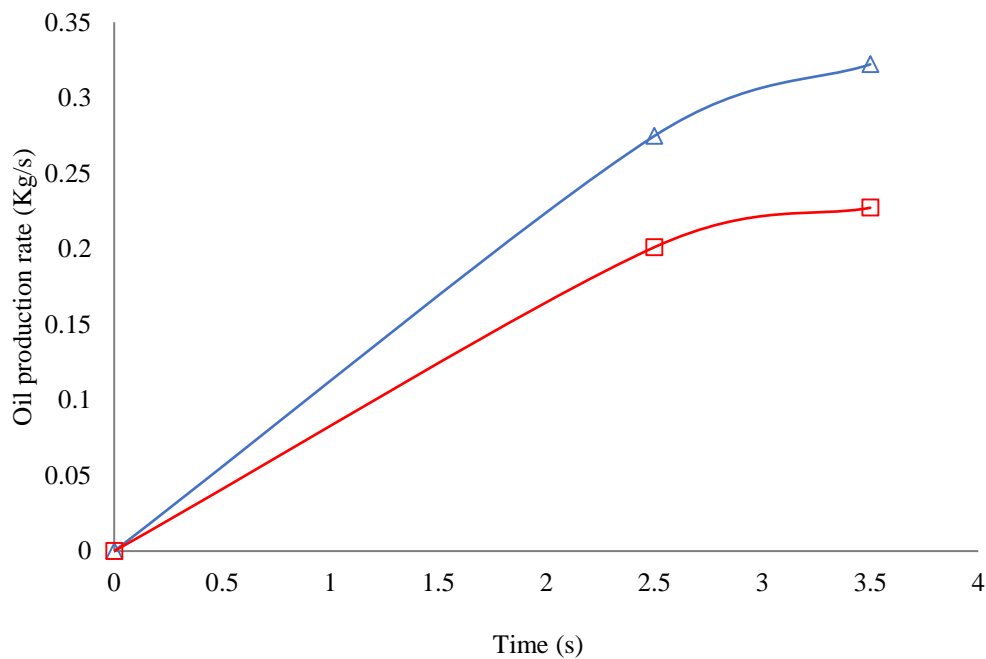
Figure 5-11: Effect of effective porosity on oil production rate at different time steps

5.5.1.3 Effect of production time on WOC and GOC

Production time is another factor that affects the WOC and GOC apices during cresting, depending on the pressure drop. Figure 5-12 illustrates a plane located on the x-z axis for determining the WOC and GOC apices in meters at varying simulation time steps. The data obtained from this procedure are shown in Table 5-6 and represented graphically in Figure 5-13 for Case 2N. As expected, the apices of the WOC (Figure 5-13) and GOC (Figure 5-14) increases steadily with an increase in simulation time towards the perforation of the horizontal well.
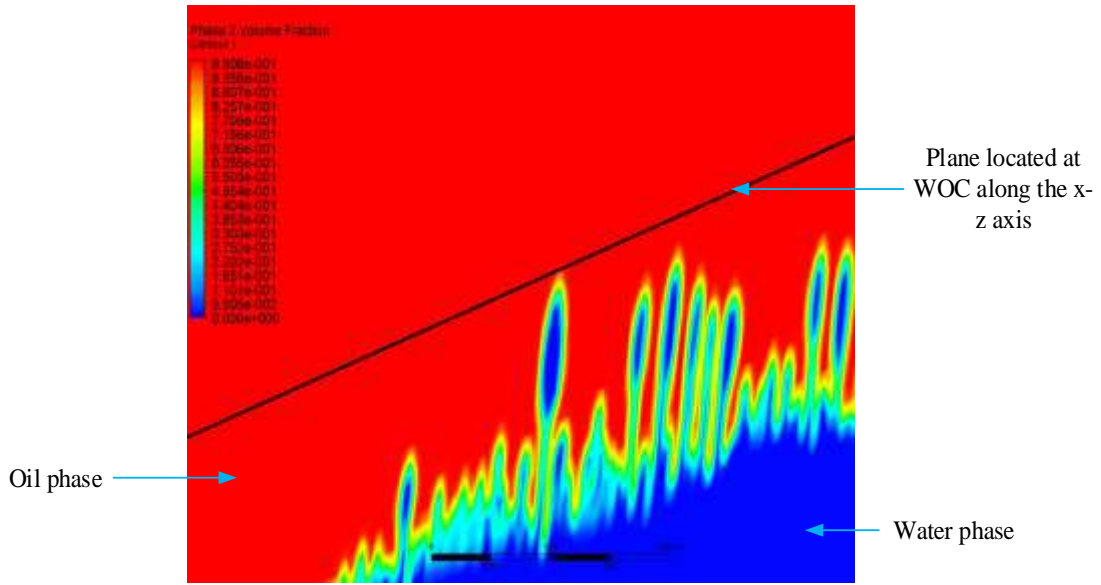
Figure 5-12: Plane located at the x-z axis for determining WOC/GOC apex

Table 5-6: WOC and GOC apices at different simulation time steps

Time (s)	1.5	3.5	4.5
WOC (m)	0.0353541	0.03768	0.0381544
GOC (m)	0.320986	0.284582	0.250045
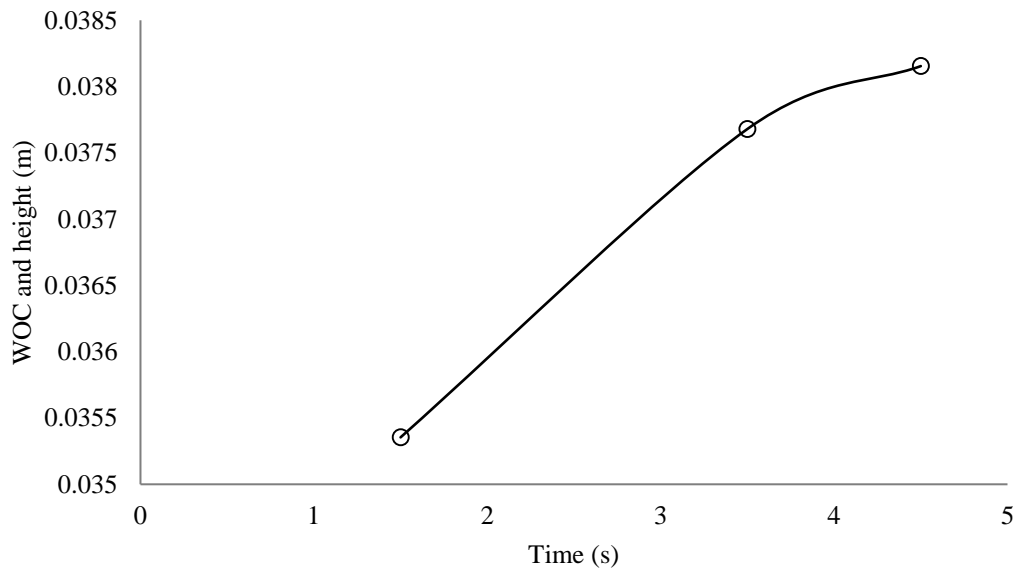
Figure 5-4: Effect of production time on WOC
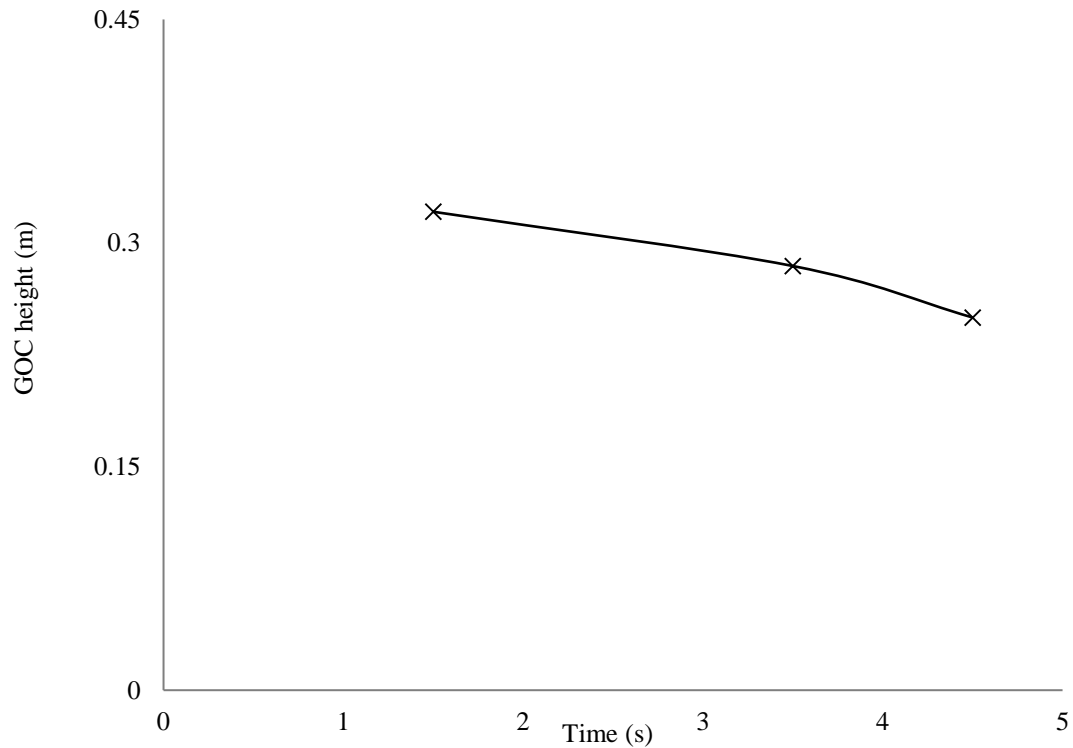
Figure 5-5: Effect of production time on GOC

5.5.2 PIV

5.5.2.1 Effect of oil withdrawal time using PIV

The effect of oil production over time is illustrated in Figures 5-15 and 5-16. Above each figure represents the raw image at different time steps (40 s and 75 s respectively) while the vectors at the different time steps are represented below each figure. From Figures 5-15 and 5-16, the vectors of the processed images can be seen to rise in a crest-like shape depicting a rise in WOC, such that the WOC increases with increase in oil production during water cresting.
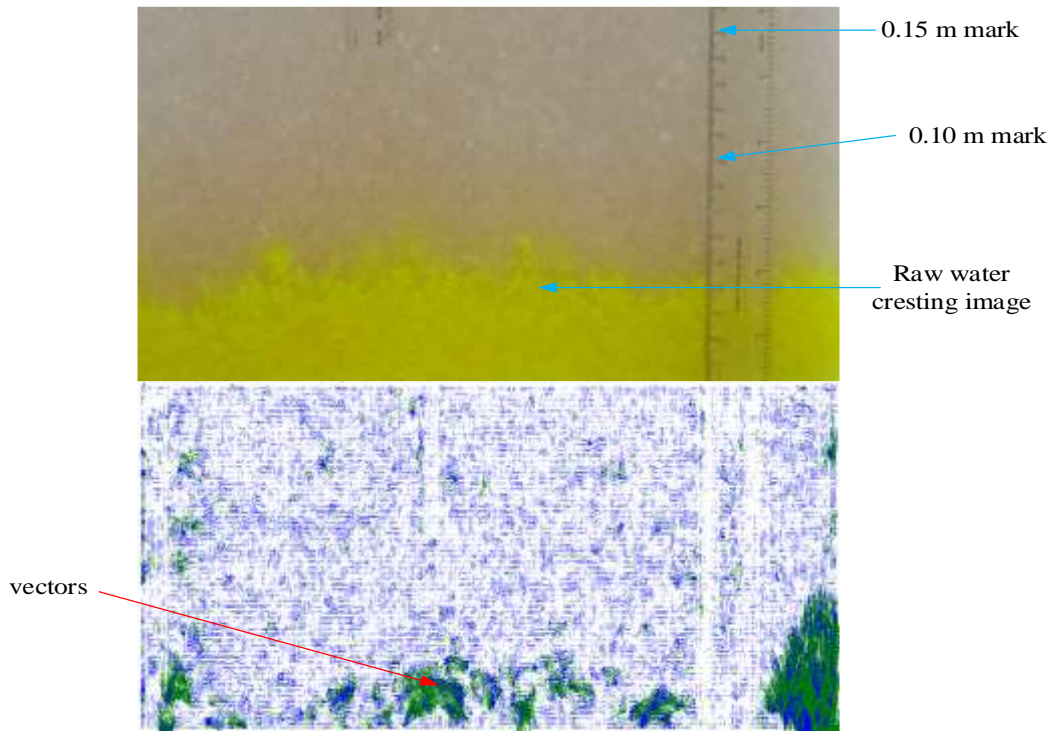
Figure 5-6: Raw image and processed image at 25 s
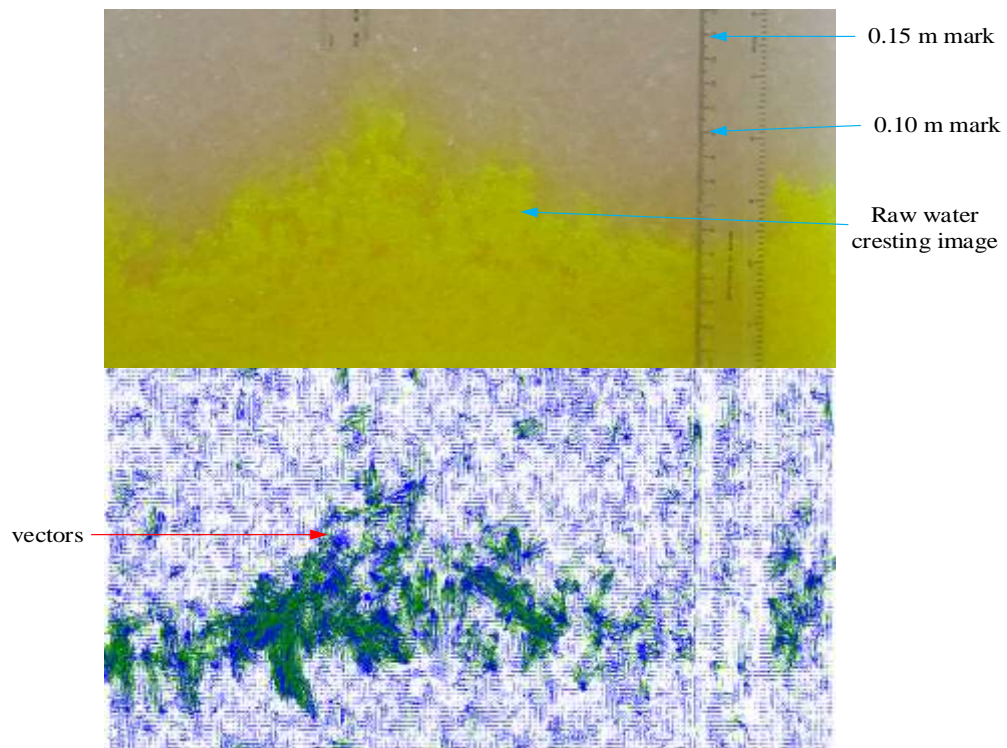
Figure 5-16: Raw image and processed image at 75 s

Table 5-7 illustrates the summary of the averaged velocity at different time steps for Case-3C described in Chapter 3, Tables 3-1 and 3-2. The averaged velocity was estimated by exporting the numerical results for the processed image at 10 s, 40 s, 70 s, and 90 s into Excel, where the generated results were averaged, by dividing the overall sum of numerically generated velocity values by the total number of values.

Figure 5-17 is a representation of the data set in Table 5-7. As shown in Figure 5-17, the velocity of the averaged vectors increase with an increase in oil production with time. The reason for the steady increase in velocity of the WOC with increase in oil withdrawal time is that the closer the WOC is to the perforation at any point in oil production time, the faster the time it takes the effluent (water) to reach the perforation of the well.

Table 5-7: Numerical analysis for velocity vectors for Case-3C at -4.351 Psig outlet pressure

Time (s)	Averaged Velocity (E-15 m/s)
10	0.113
40	0.324
70	0.909
90	2.08
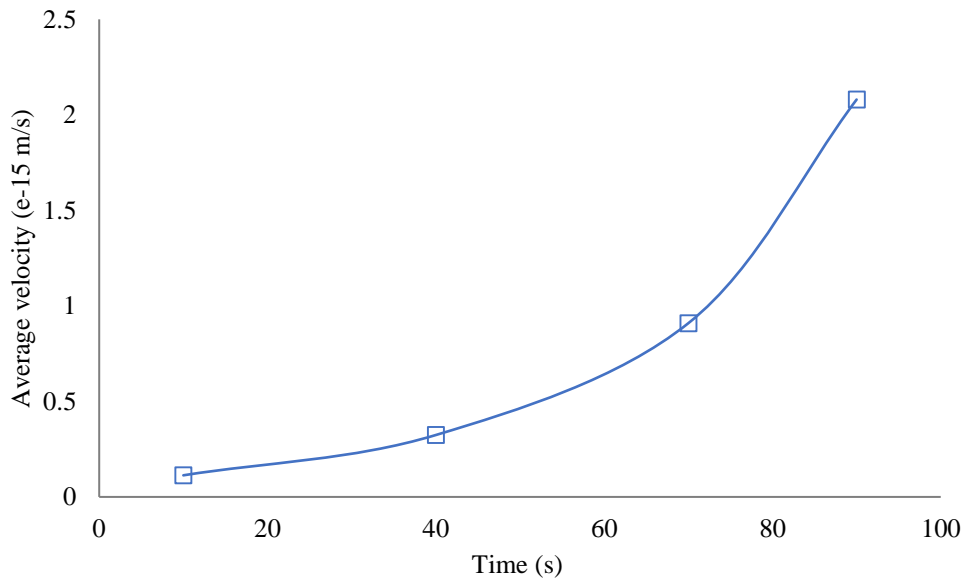
Figure 5-17: Averaged vector velocity versus time

5.5.3   Comparison of selected case of CFD with experimental data

5.5.3.1 CFD and experimental comparison of change in WOC and GOC versus production time

In order to ascertain the accuracy of the 2D numerical model, comparisons were performed with the physical model in terms of oil withdrawal rate as well as the WOC and GOC apex during cresting. Figure 5-18 shows qualitative comparison between the numerical and experimental simulations while Figures 5-19 and 5-20 illustrate the plot of the data represented in Table 5-8. Figure 5-19 represents the comparison of WOC apices while Figure 5-20 represents the comparison of GOC apices between CFD (Case 2N) and Experimental cases. As shown in Figure 5-18, the WOC apices for Cases 3 (CFD) and 4 (Experimental) increased with an increase in production time.

Figure 5-18(a) and (c) represent the CFD model while Figure 5-18(b) and (d) represent the Experimental model. This behaviour is also illustrated in Figures 5-19 and 5-20. However, a steeper trend can be observed in the CFD case, compared to the Experimental case. This high jump in WOC apex is due to the unknown nature and orientation of the interconnected pore spaces in the 2D model, with the WOC height moving only in the vertical direction (y-axis). As such, Figure 5-19 shows that an increase in percentage differences of 4.46% and 4.34% were observed for WOC apices at 2 and 6 s respectively between the CFD and Experimental case.

A similar trend is observed in Figure 5-20, where the GOC apices for the CFD and Experimental cases increased inversely with increase in simulation time. Hence, Figure 5-20 shows that an increase in percentage differences as high as 28.56% was observed for GOC apex at 6 s when compared between the CFD and Experimental case. This high jump in height of the GOC towards the perforation of the well is due to the density of the gas phase and the 2D limitations of the CFD model.
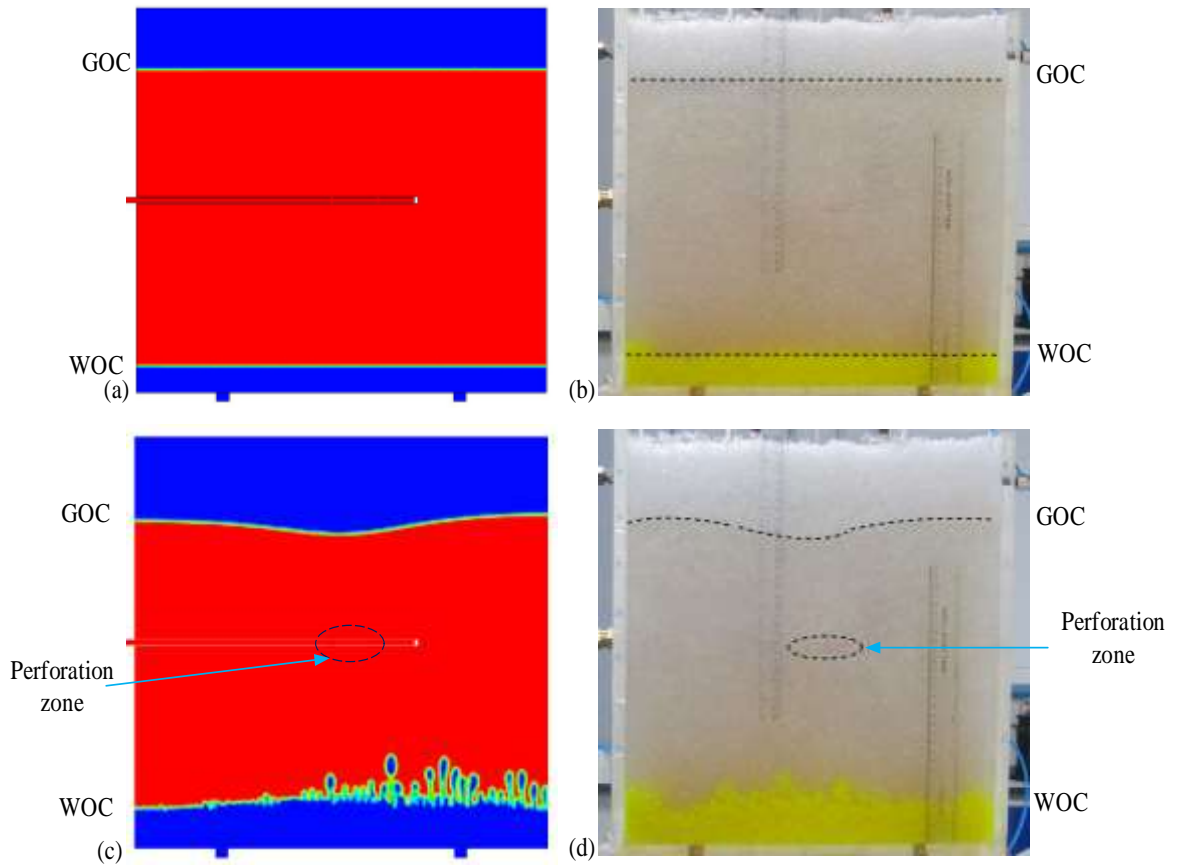
Figure 5-18: Effect of production time on WOC and GOC

Table 5-8: Comparison of WOC and GOC between experimental and numerical simulations

Reservoir fluid contact	CFD			Experiment		
	Time (s)			Time (s)		
	0 (s)	2 (s)	6 (s)	0 (s)	2 (s)	6 (s)
WOC (m)	0.035	0.03768	0.0381544	0.035	0.036	0.0365
GOC (m)	0.37	0.284582	0.250045	0.37	0.365	0.35
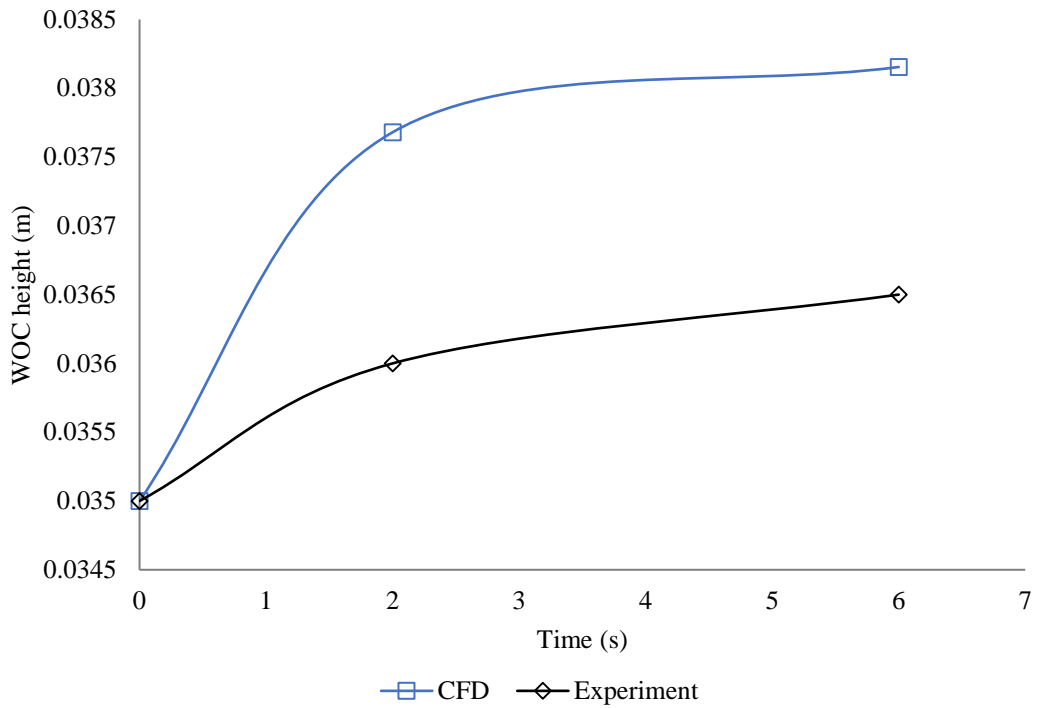
Figure 5-19: WOC versus production time
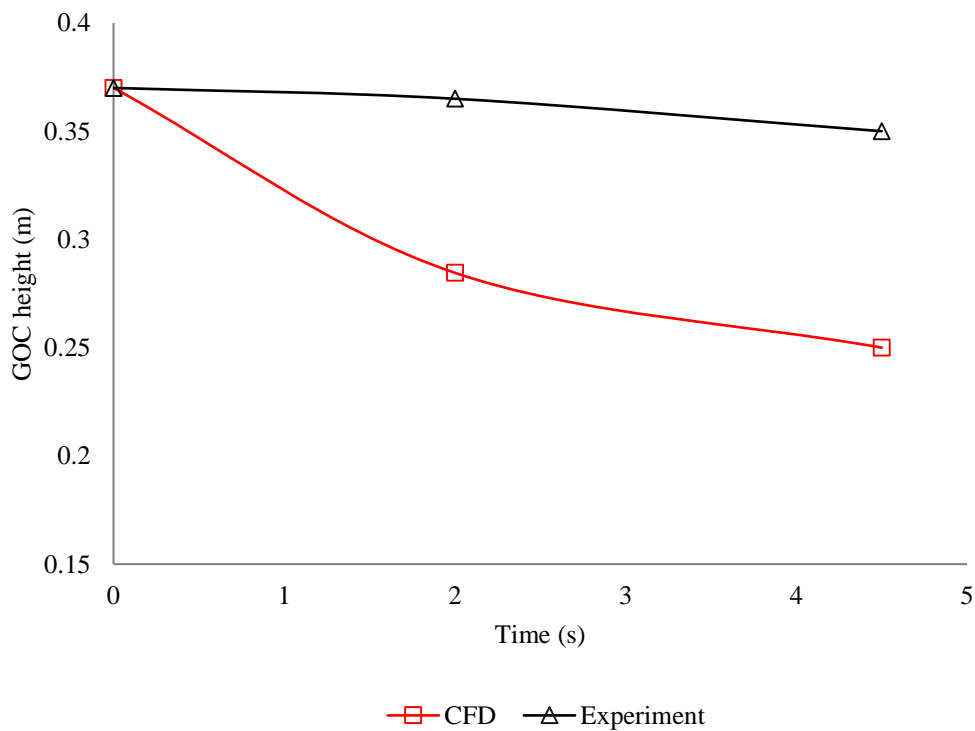
Figure 5-20: GOC versus production time

5.5.3.2 CFD and experimental comparison of oil production rate with time

Table 5-9 shows a comparison of the oil production rate between the numerical and experimental (cumulative oil production rate) simulations from 0-6 s. Figure 5-21 represents

163

the graphical illustration of Table 5-9. As expected, Figure 5-21 show that the oil flow rates for the experimental and CFD cases increased with increase in oil production time. The over predicted oil production rate result of the CFD model from 0-6 s is due to 2D limitations of CFD models such as grain arrangement and packing as well as the comparison method of the Experimental case in cumulative oil production rates. Hence, increments in percentages of 30.51% and 75.06% were observed at 2 and 6 s respectively.

Table 5-9: Comparison of oil flow rate between experimental and numerical simulations

Time (s)	0	2	6
CFD (m)	0	0.00180503	0.00781534
Experiment (m)	0	0.00125426	0.001949
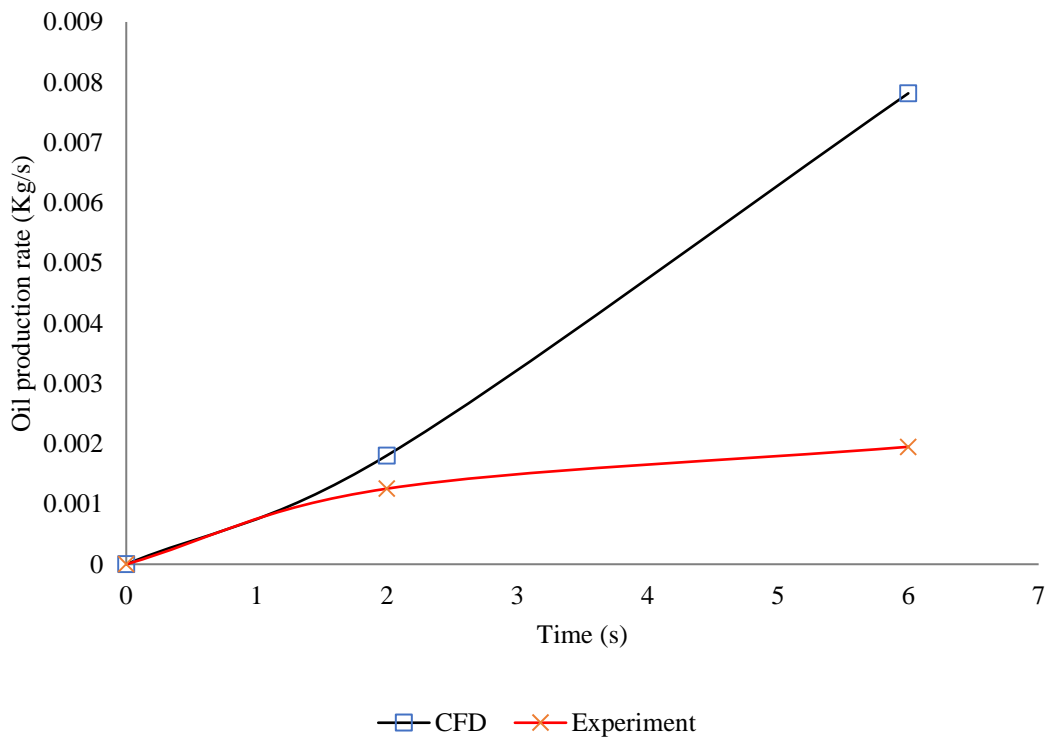
Figure 5-7: Oil production rate versus time

164

5.6 Summary

This Chapter considered numerical simulations using CFD and PIV. The models and approach for numerical simulation was highlighted. The key stages for a complete CFD simulation (pre-processor, solver and postprocessor) was illustrated. FLUENT-17 was used as the solver. The multiphase VOF was used to model a three-phase flow due to a sharp interface between stratified phases. Sensitivity analysis were then performed on the effects of effective porosity on oil production rate and oil production time on WOC and GOC to ascertain its applicability to model cresting problems.

CFD results in *Section 5.5.1.1 to 5.5.1.3* demonstrated the good applicability of CFD in modeling water and gas cresting based on basic oil production and reservoir principles. In *Sections 5.5.1.2 to 5.5.1.3*, the results show that oil production rate increased at lower oil resistance. The WOC and GOC increased with increase in production time.

PIV was used to determine the velocity of vectors at different time step to better understand cresting behaviour. This was possible using extracted images from video taken during cresting, imported and processed using Dantec's DynamicStudio software. From the numerical vector analysis described in *Section 5.5.2.1*, the averaged velocity of the WOC increased with increase in oil withdrawal time due to the proximity of the protruded WOC to the perforation of the well with time.

Section 5.5.3., discusses a comparison of CFD model and the Experimental model, at same oil production time (between 0-6 s). Percentage differences as high as 4.46% and 28.56% were observed in the case of the WOC and GOC comparison *(Section 5.5.3.1)*. This is believed to be due to the nature of flow through the pore spaces, which CFD assumes to be isotropic. *Section 5.5.3.2* shows that the oil production rate increased with increase in production time of 30.51% and 75.06% at 2 and 6 s respectively.

CHAPTER-6

CONCLUSION AND FUTURE WORKS

6.1 Conclusion

In this thesis, a novel experimental procedure was presented for investigating the performance of horizontal wells with varying horizontal and vertical displacements of the inclined section. A novel procedure for cresting control in homogeneous oil reservoirs involving the use of electromagnetically operated valve and effluents breakthrough time was also presented. A rigorous sensitivity analysis was performed involving parameter such as varying lengths of inclined sections, lateral lengths in reservoir and oil viscosity. Numerical models were also considered for cresting investigation and validation using CFD and DynamicStudio softwares. From the results presented it can be concluded that:

- The steepness of the inclined section is important in optimizing the productivity of horizontal wells in oil reservoirs affected by severe water cresting, irrespective of the lateral length in the reservoir.

- The higher the pressure drop, the higher the cumulative water cut due to a higher mass withdrawal rate at any given point in time because the mobility of fluid depends on the pressure drop *(Section 4.2.2).*

- Increased oil recovery efficiency and least water production rate can be achieved using the procedure for varying the inclined section. The performance at the inclined section of a horizontal well depends on the angle of inclination and its vertical displacements. For a given geometry, the higher the angle of inclination, the lower the vertical displacement of the build section due to increasing angles towards the horizontal plane *(Section 3.2.1, Table 3-1)*.

- Using the procedures outlined in this study *(Section 4.2 and 4.3)*, reservoir Engineers can have better understanding as to how production can be effectively optimized in oil reservoirs that are affected by cresting problems. An increment of 6.53% (177.75 cm^3) in oil recovery *(Section 4.2.3)* and 11.40% (258 cm^3) reduction in cumulative

water produced (*Section 4.2.1, Table 4-1*) was achieved at a short simulation time while a 20.14% (356 cm^3) reduction in cumulative water produced *(Section 4.2.5)* and 8.48% (250 cm^3) increase in oil recovery (*Section 4.2.4*) was realized at longer production time for thick-oil rim reservoirs and longer lateral length. Further increases in oil recovery of 3.56% (108.91 cm^3) (*Section 4.2.9.1*) and a reduction in cumulative water produced of 9.9% (183.99 cm^3) (*Section 4.2.9.2)* were observed for thick-oil rim reservoirs using the cresting control procedure, as discussed in this research work. Increment in oil produced of 163 cm^3 *(Section 4.3.1, Table 4-14)* and 134 cm^3 cumulative reduction in produced water *(Section 4.3.2, Table 4-15)* were observed from varying the inclined section of the horizontal well at V_d/H_r equals 0.079 in thin-oil rim reservoirs, at a simulation time of 210 s while a lower oil increment of 6.84 cm^3 *(Section 4.3.5.1)* and cumulative water reduction of 10.98 cm^3 *(Section 4.3.5.2)* were observed when controlled proactively in thin-oil rim reservoirs.

- In general, the shorter the measured depth of horizontal wells, the higher the cumulative water produced, irrespective of oil viscosity. At post breakthrough, the cumulative water produced depends on the measured depth of the horizontal well (*Sections 4.2.5 and 4.3.2*).

- Experimentally, the cumulative water produced and oil recovered for horizontal wells depend on the location of the bottom water injection points *(Sections 4.2.4 to 4.2.6 and 4.3.1 to 4.3.2)*. The further the horizontal displacement from the farthest injection point, the lower the cumulative water produced at the same operating pressure and liquid production time.

- The shape of the water and gas crest depends on the location of the horizontal well perforations and distance of the lateral well length in the reservoir *(Sections 4.2.4 to 4.2.6 and 4.3.1 to 4.3.2)*.

- Short radii wells are recommended for applications in reservoirs with cresting problems *(Sections 4.2 and 4.3).* Shorter radii wells are characterized by higher liquid withdrawal rate; higher volumes of water produced but lower average cumulative water cut.

- Thin-oil rim reservoirs reach incredibly high cumulative water cut values in shorter production time unlike thick column reservoirs at the same operating condition *(Section 4.3.3).* At the same operating condition, reservoir condition and production time, the closer the WOC is to the GOC the higher the cumulative water produced and cumulative water cut.

- The feasibility of the cresting control procedure is believed to depend on reservoir thickness of the oil column, breakthrough time. The longer the shut-in periods the higher the oil recovery and the lower the cumulative water produced due to the longer time required for the pressure drop to supersede the hydrostatic pressure at the WOC. The wider the reservoir sizes the longer the time required for water and gas to recede after shut-in. The GOC level receded almost immediately when compared with WOC due to its relatively low density and viscosity compared to that of water. The thicker the oil column height the more the oil recovered and less the cumulative water produced. The longer the shut-in duration the higher the oil recovered, the lower the cumulative water produced and the lower the cumulative produced liquid *(Sections 4.2.9.1 to 4.2.9.3 and 4.3.4.1 to 4.3.4.3).*

- The CFD analysis demonstrated that the cresting effect depends on oil production rate and effective porosity. The lower the viscous resistance and the higher the oil production rate. The WOC and GOC apices increased with increase in simulation time towards the perforation of the well *(Sections 5.5.1.2 to 5.5.1.3).*

- CFD is a useful simulation tool for cresting prediction and validation of a physical model. However, the over predicted results obtained in terms of validation with the experimental model are due to the isotropic nature of CFD models in terms of flow through porous media (*Section 5.5.3*).

6.2 Future work

Areas for future work are:

1. Investigation of the presented novel procedures in heterogeneous oil reservoirs, water-wet homogeneous and heterogeneous oil reservoirs. The procedures are intended to be applied in both horizontal and multilateral wells.

2. To investigate the behaviour of flow for the reservoir phases (water and oil), by determining their relative permeabilities. It is believed the relative permeability will have effect on the mobility of the oil and water phases in the experimental set up used in this study.

3. Smaller reservoir grain sizes will be investigated in experimental simulations while a 3D CFD model will be considered for higher validation accuracy.

REFERENCES

AAPG 2016a. Drive mechanism and recovery
http://wiki.aapg.org/Drive_mechanisms_and_recovery, accessed September 7,
2016.

AAPG 2016b. Reservoir drive mechanism
http://wiki.aapg.org/Reservoir_drive_mechanisms, accessed September 7, 2016.

Abdallah, W., Buckley, S. J., Carnegie, A., Edwards, J., Herold, B., Fordham, E., Graue,
A., Habashy, T., Seleznev, N., Signer, C., Hussain, H., Montaron, B. & Ziauddin,
M. 2007. Fundamentals of Wettability
https://www.slb.com/~/media/Files/resources/oilfield_review/ors07/sum07/p44_61
.pdf, accessed October 28, 2016.

Aggour, M. A. & Kandil, A. A. 2001. Experimental Study Of Horizontal Well Performance
In Fractured Reservoirs With Bottom-Water Drive. Petroleum Science and
Technology, Vol. 19, pp. 933-947.

Al-Muntasheri, G. A., Sierra, L., Garzon, F. O., Lynn, J. D., & Izquierdo, G. A. 2010. Water
Shut-off with Polymer Gels in A High Temperature Horizontal Gas Well: A Success
Story.

Albonico, P., Bartosek, M., Lockhart, T. P. & Causin, E. 1994. New Polymer Gels for
Reducing Water Production in High-Temperature Reservoirs. Society of Petroleum
Engineers.

Al Zarafi, A. 1993. Breathing New Life Into a Thin Oil Column by Horizontal Drilling.
Society of Petroleum Engineers.

ANSYS 2016. ANSYS 16.1 Help viewer 6.2.3. Adobe, accessed September 17, 2016.

Aulie, T., Asheim, H. & Oudeman, P. 1995. Experimental Investigation of Cresting and
Critical Flow Rate of Horizontal Wells. SPE Advanced Technology series, 3.

Aziz, K., Settari, A., Kaneko, T. & Mungan, N. 1973. Some Practical Aspects Of Coning Simulation. Petroleum Society of Canada.

Balazs, M., Wittmann, G., Vad, J. & Szabo, G. 2009. Experimental modeling of Water and Gas Coning in Horizontal Oil Producing Wells http://www.ara.bme.hu/~szabog/publ/full_text/microCAD_2009_207_leadva.pdf, accessed May 2, 2016.

Beattie, D. R. & Roberts, B. E. 1996. Water Coning in Naturally Fractured Gas Reservoirs. Society of Petroleum Engineers, pp. 605 - 615.

Benamara, A. & Tiab, D. 2001. Gas Coning in Vertical and Horizontal wells, a Numerical Approach. SPE Rocky Mountain Petroleum Technology Conference. Keystone, Colorado: Society of Petroleum Engineers.

Beveridge, S. B., Coats, K. H. & Alexandre, M. T. 1970. Numerical Coning Applications. Petroleum Society of Canada.

Boyun, G. & Lee, R. L. H. 1993. A Simple Approach to Optimization of Completion Interval in Oil/Water Coning Systems.

Brown, K. E. 1984. Technology of Artificial Lift Methods. Penn Well Publi- shing Company, Tulsa, OK.

Carr, T. & Gerlach, P. 2001. Update on Horizontal Drilling in Kansas, Current Status and Case Histories.

Caudle, B. H. & Silberberg, I. H. 1965. Laboratory Models of Oil Reservoirs Produced By Natural Water Drive.

Chen, H. K. 1993. Performance of Horizontal Wells, Safah Field, Oman. Society of Petroleum Engineers.

Chesapeake-Energy 2011. Chesapeake Energy horizontal Drilling method. https://www.youtube.com/watch?v=vvRCYLnVWG8, accessed September 17, 2016.

Choudhary, D. 2011. Directional drilling technology. http://directionaldrilling.blogspot.co.uk/2011/07/types-of-directional-well-profile.html, accessed March 2, 2016.

Coats, K. H., Henderson, J. H. & Modine, A. D. 1970. Numerical Coning Applications. Society of Petroleum Engineers.

Coffin, P. 1993. Horizontal Well Evaluation After 12 Years. Society of Petroleum Engineers. SPE-26618-MS. doi:10.2118/26618-MS.

Curtis , R. 2011. What is horizontal drilling, and how does it differ from vertical drilling? Institute for Energy and Environmental Research of Northeastern Pennsylvania Clearinghouse.

Dai, L. C., You, Q., Yuhong, X., Long, H., Ya, C. & Fulin, Z. 2011. Case Study on Polymer Gel to Control Water Coning for Horizontal Well in Offshore Oilfield. Offshore Technology Conference.

Dantecdynamics 2015. DynamicStudio User's Guide, accessed June 2, 2016.

Djavareshkian, M. H. & Reza-Zadeh, S. 2007. Application of normalized flux in pressure-based algorith. Computers and Fluids. Vol.36 No.7; 1224-1234.

Ehlig-Economides, C. A., Chan, K. S. & Spath, J. B. Production Enhancement Strategies for Strong Bottom Water Drive Reservoirs. Society of Petroleum Engineers.

Ehlig-Economides, C. A., Chan, K. S. & Spath, J. B. 1996. Production Enhancement Strategies for Strong Bottom Water Drive Reservoirs. Society of Petroleum Engineers.

EIA 1993. Drilling Sideways -- A Review of Horizontal Well Technology and Its Domestic Application.

El-Karsani, K. S. M., Al-Muntasheri, G. A. & Hussein, I. A. 2014. Polymer Systems for Water Shutoff and Profile Modification: A Review Over the Last Decade.

Fluent 2006. Fluent user manual 6.3. Adobe, accessed June 2, 2015.

Freeborn, W. R., Russell, B. & Macdonald, A. J. 1990. South Jenner Horizontal Wells A Water Coning Case Study. Petroleum Society of Canada.

Ghahfarokhi, R. B., Green, D. W. & Liang, J.-T. 2006. Simulation of Gelled Polymer Treatments in the Arbuckle Formation, Kansas. Society of Petroleum Engineers.

Graue, D. J. & Filgate, R. A. 1971. A Study of Water Coning in the Kaybob South Beaverhill Lake Field. Society of Petroleum Engineers.

Halliburton 2008. Developing the heavy oil and oil sands assets. http://www.halliburton.com/public/common/Brochures/H06153.pdf, accessed June 12, 2014.

Hatzignatiou, D. G. & Mohamed, F. 1994. Water And Gas Coning In Horizontal And Vertical Wells. Petroleum Society of Canada.

Howard, G. C. & Fast, C. R. 1950. squeeze Cementing Operations. AIME 189, 53-64.

Inikori, S. O. 2002. Numerical study of water coning control with Downhole Water Sink (DWS) well completions in vertical and horizontal wells http://etd.lsu.edu/docs/available/etd-0610102-080619/unrestricted/Inikori_dis.pdf, accessed August 7, 2016.

Jakobsen, M. L., Easson, W. J., Greated, C. A. & Glass, D. H. 1996. Particle image velocimetry: simultaneous two-phase flow measurements. Measurement Science and Technology, 7, 1270.

Jiang, Q. & Butler, R. M. 1998. Experimental And Numerical Modelling of Bottom Water Coning to a Horizontal Well.

Jin, L. & Wojtanowicz, A. K. 2011. Analytical Assessment of Water-free Production in Oil Wells with Downhole Water Loop for Coning Control. Society of Petroleum Engineers.

Jubralla, A. F., Cosgrove, P. & Whyte, S. J. 1995. Horizontal Highlights. Middle East Well Evaluation Review.

Kantzas, A., Burger, D., Pow, M., Cheung, V. & Mourits, F. 1994. Design Strategies For Improved Conformance Using Polymer Gels. Petroleum Society of Canada.

Karp, J. C., LOWE, D. K. & MARUSOV, N. 1962. Horizontal Barriers for Controlling Water Coning. Journal of Petroleum Technology, pp. 783-790.

Khan, A. R. 1970. A Scaled Model Study of Water Coning. Society of Petroleum Engineers.

Kuo, M. C. T. 1983. A Simplified Method for Water Coning Predictions. Society of Petroleum Engineers.

Lakatos, I., Lakatos-Szabo, J., Kosztin, B. & Palasthy, G. 1998. Restriction of Gas Coning by a Novel Gel/ Foam Technique. Society of Petroleum Engineers.

Law, D. S. & Jossy, W. E. 1996. Visualisation Study of Anti-water Coning Process Using Gels. Petroleum Society of Canada.

Leemhuis, A. P., Belfroid, S. & Alberts, G. 2007. Gas Coning Control for Smart Wells. Society of Petroleum Engineers.

Luhning, R. W., Chmilar, M. J. & Anderson, B. S. 1990. The AOSTRA Anti Water Coning Technology (AWACT) Process - From Invention To Commercial Application. Petroleum Society of Canada.

Makinde, F. A., Adefidipe, O. A. & Craig, A. J. 2011. Water Coning in Horizontal Wells: Prediction of Post-Breakthrough Performance. International Journal of Engineering & Technology Vol:.11 No.1.

Melling, A. 1997. Tracer particles and seeding for particle image velocimetry. Measurement Science and Technology, 8, 1406.

Mungan, N. 1979. Laboratory Study of Water Coning In a Layered Model. The Journal of Canadian Petroleum, pp. 66-70.

Murphy, P. J. 1990. Performance of Horizontal Wells in the Helder Field. Society of Petroleum Engineers.

Muskat, M. & Wyckoff, R. D. 1935. An Approximate Theory of Water-coning in Oil Production.

Nurmi, R., Kuchuk, F. J., Cassell, B., Charrdac, J. & Maguet, P. 1995. Horizontal highlights. Middle East Well Evalation Review.

Odeh, A. S. 1986. Reservoir fluid flow and natural drive mechanisms, in IHRDC Video Library for Exploration and Production Specialists, Manual for Module PE502: Boston, MA, IHRDC, pp. 69–120.

Omeke, J. E., Livinus, A., Uche, I. N., Obah, B. & Ekeoma, E. 2010. A Proposed Cone Breakthrough Time Model for Horizontal Wells in Thin Oil Rim Reservoirs. Society of Petroleum Engineers.

Osama, A. M. & Huckaby, E. D. 2010. Simulation of a Swirling Gas-Particle Flow Using Different k-epsilon Models and Particle-Parcel Relationships. Engineering Letters, 18:1, EL_18_1_07

Ozkan, E. & Raghavan, R. 1990. A Breakthrough Time Correlation for Coning Toward Horizontal Wells. Society of Petroleum Engineers.

Papatzacos, P., Herring, T. R., Martinsen, R. & Skjaeveland, S. M. 1991. Cone Breakthrough Time for Horizontal Wells. Society of Petroleum Engineers.

Peng, C. P. & Yeh, N. 1995. Reservoir Engineering Aspects of Horizontal Wells - Application to Oil Reservoirs with Gas or Water Coning Problems. Society of Petroleum Engineers.

Permadi, P. 1996. Fast Horizontal-Well Coning Evaluation Method. Society of Petroleum Engineers.

Permadi, P. & Jayadi, T. 2010. An Improved Water Coning Calculation for Horizontal Wells. Society of Petroleum Engineers.

Permadi, P., Lee, R. L. & Kartoatmodjo, R. S. T. 1995. Behavior of Water Cresting Under Horizontal Wells. Society of Petroleum Engineers.

Permadi, P., Wibowo, W., Alamsyah, Y. & Pratomo, S. W. 1997. Horizontal Well Completion With Stinger for Reducing Water Coning Problems. Society of Petroleum Engineers.

Porturas, F., Vela, I., Pazos, J. & Humbert, O. 2009. Lifting more dry oil by reducing water production with Inflow Control Devices in wells drilled and completed in consolidated reservoirs. Bloque 15, Equador. AAPG. ER Newslette, 4.

Rajan, V. S. V. & Luhning, R. W. 1993. Water Coning Suppression. Petroleum Society of Canada.

Ratterman, G. 2006. Uniform flow profiles improve horizontal wells. Drilling Contractor journal, pp. 34-35.

Recham, R. 2001. Super-Critical Rate Based on Economic Recovery in Water and Gas Coning by Using Vertical and Horizontal Well Performance. Petroleum Society of Canada.

Saad, S. E-D. M., Darwich, T. D. & Asaad, Y. 1995. Water Coning in Fractured Basement Reservoirs. Society of Petroleum Engineers.

Salavatov, T. S. & Ghareeb, A. 2009. Predicting the behaviour of water and gas coning in horizontal wells. Oil and Gas Business.

Samuel, R. & Gao, D. 2007. Horizontal Drilling Engineering - Theory, Methods and Applications.

Schevchenko, E. 2013. Experimental study of water coning phenomenon in perforated pipes, https://brage.bibsys.no/xmlui/handle/11250/235337, accessed August 13, 2015

Schlumberger 2010. ResFlow ICDs in horizontal openhole wells optimize production in thin oil-rim reservoir. http://www.slb.com/~/media/Files/sand_control/case_studies/resflow_malaysia_cs.pdf, accessed May 22, 2016

Schlumberger 2016a. Anisotropy

http://www.glossary.oilfield.slb.com/Terms/a/anisotropy.aspx, accessed September 10, 2016.

Schlumberger 2016b. Buble point

http://www.glossary.oilfield.slb.com/Terms/b/bubble_point.aspx, accessed September 8, 2016.

Schlumberger 2016c. homogeneity.

http://www.glossary.oilfield.slb.com/Terms/h/homogeneity.aspx, accessed April 21, 2016.

Schlumberger 2016d. Reservoir drive mechanisms

http://www.glossary.oilfield.slb.com/Terms/r/reservoir_drive_mechanisms.aspx, accessed September 7, 2016.

Schlumberger 2016 Cresting

http://www.glossary.oilfield.slb.com/en/Terms.aspx?LookIn=term%20name&filter=cresting, accessed May 20, 2016.

Shadizadeh, S. R. & Ghorbani, D. 2001. Investigation of Water/Gas Coning in Natural Fractured Hydrocarbon Reservoirs. Petroleum Society of Canada.

Sherrard, D. W., Brice, B. W. & Macdonald, D. G. 1987. Application of Horizontal Wells at Prudhoe Bay. Society of Petroleum Engineers.

Shirif, E. 2000. Mobility Control by Polymers Under Bottom-Water Conditions, Experimental Approach. Society of Petroleum Engineers.

Shirman, E. I. & Wojtanowicz, A. K. 2000. More Oil Using Downhole Water-Sink Technology: A Feasibility Study. SPE Production & Facilities, pp. 234-240.

Singhal, A. K. 1993. Water And Gas Coning/Cresting - A Technology Overview. Petroleum Society of Canada.

Singhal, A. K. 1996. Water And Gas Coning/ Cresting A Technology Overview. Petroleum Society of Canada.

Smith, C. R. & Pirson, S. J. 1963. Water Coning Control in Oil Wells by Fluid Injection. Society of Petroleum Engineers.

Soengkowo, I. 1969. Model studies of Water Coning in Petroleum Reservoirs with Natural Water Drives.

Solomon, C. J. & Breckon, T. P. 2010. Fundamentals of Digital Image Processing: A Practical Approach with Examples in Matlab. Wiley-Blackwell.

Surguchev, L. M. 1998. Water Shut-Off: Simulation and Laboratory Evaluation. Society of Petroleum Engineers.

Swisher, M. D. & Wojtanowicz, A. K. 1995. New Dual Completion Method Eliminates Bottom Water Coning. Society of Petroleum Engineers.

Symon, K. 1971. Mechanics. Third Edition, Addison-Wesley. ISBN 0-201-07392-7.

Tarek, A. 2001. Reservoir Engineering Handbook. Elsevier; Second Edition; pp. 730, 736.

Thakur, G. C. & Tachuk, A. R. 1974. Retardation Of Water Coning In Oil Wells Using Polymers - A Reservoir Simulation Application. Petroleum Society of Canada.

Thakur, K. A. & Flores, J. 1974. Influence Of Production Rate And Oil Viscosity On Water Coning. Petroleum Society of Canada.

Tinku, A. & Ajoy, K. R. 2006. Image Processing - Principles and Applications. Wiley InterScience.

Umnuayponwiwat, S. & Ozkan, E. 2000. Water and Gas Coning toward Finite-Conductivity Horizontal Wells: Cone Buildup and Breakthrough. Society of Petroleum Engineers.

Van Golf-Racht, T. D. 1994. Water-Coning in a Fractured Reservoir. Society of Petroleum Engineers.

Vasquez, J. E., Jurado, I., Santillan, A. & Hernandez, R. 2006. Organically Crosslinked Polymer System for Water Reduction Treatments in Mexico. Society of Petroleum Engineers.

Verga, F., Viberti, D. & Di Renzo, D. 2005. Are Multilateral Wells Really Effective To Control Water Coning? : Offshore Mediterranean Conference.

Verga, F., Viberti, D. & Ferraro, P. 2007. Prediction Of Water Coning And Water Cresting: Analytical Or Numerical Models? : Offshore Mediterranean Conference.

White, J. L., Goddard, J. E. & Phillips, H. M. 1973. Use of Polymers To Control Water Production in Oil Wells.

Wojtanowicz, A. K., Shirman, E. I. & Kurban, H. 1999. Downhole Water Sink (DWS) Completion Enchance OIL Recovery in Reservoirs with Water Coning Problem. Society of Petroleum Engineers.

Wojtanowicz, A. K., Xu, H. & Bassiouni, Z. A. 1991. Oilwell Coning Control Using Dual Completion With Tailpipe Water Sink. Society of Petroleum Engineers.

Wu, G., Reynolds, K. & Markitell, B. 1995. A Field Study of Horizontal Well Design in Reducing Water Coning. Society of Petroleum Engineers.

Yost, A. B., Overbey, W. K. & Carden, R. S. 1987. Drilling a 2,000-ft Horizontal Well in the Devonian Shale. Society of Petroleum Engineers.

Zaitoun, A., Kohler, N. & Montemurro, M. A. 1992. Control of Water Influx in Heavy-Oil Horizontal Wells by Polymer Treatment. Society of Petroleum Engineers.

Zaitoun, A. & Pichery, T. 2001. A Successful Polymer Treatment For Water Coning Abatement in Gas Storage Reservoir. Society of Petroleum Engineers.

APPENDIX

APPENDIX-A: JOURNAL PUBLICATIONS